

**UNIVERSITY OF SOUTHAMPTON**

FACULTY OF NATURAL AND ENVIRONMENTAL SCIENCES

Ocean and Earth Science

**Nuclear Forensics: Determining the origin of uranium ores and uranium ore concentrates via radiological, elemental and isotopic signatures.**

by

David George Reading

Thesis for the degree of Doctor of Philosophy

May 2016



UNIVERSITY OF SOUTHAMPTON

## **ABSTRACT**

FACULTY OF NATURAL AND ENVIRONMENTAL SCIENCES

Ocean and Earth Sciences

Thesis for the degree of Doctor of Philosophy

### **NUCLEAR FORENSICS: DETERMINING THE ORIGIN OF URANIUM ORE AND URANIUM ORE CONCENTRATES VIA RADIOLOGICAL, ELEMENTAL AND ISOTOPIC SIGNATURES.**

David George Reading

There is increasing demand for the development of rapid and effective analytical tools to support nuclear forensic investigations of seized suspect materials to determine sample origins and ownership. New methods are sometimes simply adapted from other scientific disciplines and can be effectively used to rapidly prepare complex materials for analysis. The adaptation and re-implementation of such techniques for rapid nuclear forensic characterisation is the focus of this thesis with emphasis on geolocating uranium ore concentrates (UOC) whilst preserving as much of the original sample as possible.

A rapid sample solubilisation technique was developed to overcome significant and unpredictable photon self-attenuation observed in U-bearing matrices caused by variable matrix compositions containing dense uranium-bearing particles. The technique enables collection of accurate gamma spectrometric measurements of U-bearing compounds where no photon self-absorption corrections, photon detection efficiency adjustments or sample specific matrix matching are required due to the reproducible and predictable aqueous matrix. The technique was used to prepare and measure 19 UOCs via gamma and alpha spectrometry and the data were statistically analysed by Principal Components Analysis. Half of the UOCs were statistically unique whilst the remaining samples grouped together. The UOCs were re-prepared, re-measured and incorporated into the PCA and plotted in close proximity to the original 3D modelled data. This validates the effectiveness of the procedures to obtain accurate and reliable data and that statistical analysis of the data is able to infer possible sample origins.

A second sample preparation technique was developed and tested using U-bearing samples which allows for 1.5 mg of sample to be formed into a small glass bead after dilution with pure  $\text{MgSiO}_3$  instead of using a specific flux (usually determined with prior knowledge of sample composition) and could over-dilute the sample and introduce contaminants. The glass was prepared using an iridium-strip resistive fusion device and is produced in less than 10 minutes. The resulting homogeneous flux-free bead of glass was then analysed via laser-ablation ICPMS and the rare earth element (REE) patterns were obtained for reference materials and 9 UOCs. The REEs can be used to infer UOC provenance. The patterns were convincingly similar to chondrite normalised reference values and data from chemically purified UOCs and offer a rapid and effective approach to obtaining REE data and other trace element data.



# Table of Contents

<b>Table of Contents .....</b>	<b>i</b>
<b>List of Tables.....</b>	<b>vii</b>
<b>List of Figures .....</b>	<b>xi</b>
<b>DECLARATION OF AUTHORSHIP .....</b>	<b>xv</b>
<b>Acknowledgements .....</b>	<b>xvii</b>
<b>Abbreviations .....</b>	<b>xix</b>
<b>Chapter 1:       Introduction and Background .....</b>	<b>1</b>
1.1   History of Nuclear Forensics and Rationale of this Study.....	1
1.2   The Incident and Trafficking Database (ITDB).....	2
1.3   Uranium and Uranium Ore Concentrate.....	4
1.3.1   Uranium.....	4
1.3.2   Radioactive decay.....	5
1.3.2.1   Alpha decay .....	5
1.3.2.2   Beta decay .....	6
1.3.2.3   Gamma decay .....	6
1.3.2.4   Decay rates, secular equilibrium and decay chains.....	6
1.3.3   Uranium deposits of the world .....	7
1.3.4   Mining .....	13
1.3.5   Milling.....	13
1.3.5.1   Leaching of uranium ore.....	14
1.3.5.2   Concentration and purification .....	16
1.3.5.3   Precipitation and drying of uranium ore concentrate .....	16
1.4   Nuclear Forensic Investigations of uranium ore and uranium ore concentrate ...	18
1.4.1   UOC Isotope Ratios .....	19
1.4.1.1   Uranium .....	19
1.4.1.2   Lead.....	20
1.4.1.3   Strontium .....	21
1.4.1.4   Sulphur.....	21
1.4.1.5   Neodymium .....	21
1.4.2   UOC Impurities and trace elements.....	22
1.4.2.1   Rare earth elements .....	22

1.4.2.2	Anionic and organic.....	22
1.4.2.3	Major elements and trace minerals.....	23
1.4.3	UOC Age or production determination .....	23
1.4.4	UOC Radiological measurements .....	25
1.4.4.1	Alpha spectrometry.....	25
1.4.4.2	Gamma spectrometry .....	25
1.4.5	UOC Structural and morphological measurements.....	25
1.4.5.1	SEM & TEM.....	25
1.4.5.2	Electron microprobe analysis.....	26
1.4.5.3	Raman spectrometry.....	26
1.4.5.4	Infrared spectrometry.....	26
1.4.5.5	XRD .....	26
1.5	Thesis Outline.....	27

## **Chapter 2: A Rapid Dissolution Procedure to Aid Initial Nuclear Forensic**

### **Investigation of Chemically Refractory Compounds and Particles Prior to**

### **Gamma Spectrometry .....29**

Abstract.....	29
2.1 Introduction.....	31
2.2 Methodology .....	37
2.2.1 Instrumentation.....	38
2.2.2 Initial characterisation of CRMs .....	40
2.2.3 Borate fusion for homogenisation .....	40
2.2.4 Understanding the cause of self-attenuation .....	41
2.2.4.1 Bulk density effect.....	41
2.2.4.2 Particle size effect .....	42
2.2.4.3 Monte-Carlo simulations .....	42
2.3 Results & Discussion .....	44
2.3.1 Initial characterisation of CRMs .....	44
2.3.2 Borate fused characterisation of CRMs.....	44
2.3.3 Understanding the cause of self-attenuation .....	47
2.3.3.1 Bulk density effect.....	47
2.3.3.2 Grain size effect .....	48
2.3.3.3 Monte-Carlo simulations .....	49

2.4	Conclusion .....	52
<b>Chapter 3:</b>	<b>Applying multivariate statistics to discriminate uranium ore concentrate geolocations using (radio)chemical data in support of nuclear forensic investigations.....</b>	<b>55</b>
	Abstract .....	55
3.1	Introduction .....	57
3.1.1	Uranium Ore Concentrates .....	60
3.2	Methodology .....	66
3.2.1	Instrumentation .....	66
3.2.2	Initial characterisation of UOCs .....	66
3.2.3	Borate fusion for homogenisation .....	67
3.2.4	Preparation and measurement of <sup>210</sup> Po in UOC via autodeposition .....	67
3.2.5	Principal Components Analysis .....	68
3.3	Results and Discussion .....	70
3.3.1	UOC activity concentration comparison between matrices.....	70
3.3.2	<sup>226</sup> Ra and <sup>210</sup> Pb activity concentrations and their ratio. ....	73
3.3.3	Principal Components Analysis .....	74
3.3.4	Experimental and Statistical Validation. ....	78
3.4	Conclusion .....	81
<b>Chapter 4:</b>	<b>A novel glass bead fusion procedure for nuclear forensics using synthetic enstatite to dissolve uraniferous and other challenging materials prior to LA-ICPMS .....</b>	<b>83</b>
	Abstract .....	83
4.1	Introduction .....	85
4.2	Methodology .....	88
4.2.1	Instrumentation .....	88
4.2.1.1	The Iridium Strip Fusion System .....	88
4.2.1.2	Eagle III $\mu$ XRF probe .....	89
4.2.1.3	LA-ICPMS.....	90
4.2.2	Iridium-strip fusion.....	90

4.2.3	Determining the optimal UOC to silica ratio for fusion .....	91
4.2.4	Geochemical and uranium certified reference materials .....	92
4.3	Results and discussion .....	94
4.3.1	Determining the optimal UOC to silica ratio for fusion .....	94
4.3.2	Laser ablation results .....	96
4.3.2.1	Elemental homogeneity and volatility .....	96
4.3.2.2	Rare earth element patterns.....	99
4.4	Conclusion.....	103

**Chapter 5:        The analysis of rare earth element signatures in uranium ore concentrates as glass beads for laser ablation ICPMS application in nuclear forensics. ....105**

Abstract .....	105
5.1 Introduction .....	107
5.1.1 Rare earth elements .....	107
5.1.2 Measurement of rare earth elements .....	108
5.2 Methodology.....	111
5.2.1 Instrumentation .....	111
5.2.1.1 The iridium-strip electronic device .....	111
5.2.1.2 XRD examination for homogeneity .....	111
5.2.1.3 Laser ablation ICPMS.....	111
5.2.1.4 Solution ICPMS .....	112
5.2.2 Sample preparation for LA-ICPMS .....	112
5.2.3 Chromatographic resin calibration for REE and U separation.....	113
5.2.4 UOC sample preparation for solution ICPMS .....	114
5.2.5 REE and U separation of UOC .....	114
5.3 Results and Discussion .....	115
5.3.1 Resin calibration for REE separation.....	115
5.3.2 XRD examination for homogeneity .....	116
5.3.3 Glass bead LA-ICPMS results and comparisons .....	117
5.3.4 Non-glass bead comparable UOC data .....	121
5.4 Conclusion.....	123

<b>Chapter 6:</b>	<b>Conclusions .....</b>	<b>125</b>
<b>Chapter 7:</b>	<b>Future Work.....</b>	<b>129</b>
7.1	Statistical analysis of radiometric data and REE patterns. ....	129
7.2	Elemental, mineralogical and morphological characterisation .....	129
7.3	Uranium isotopes – Double spike method.....	130
7.4	Further development of techniques to benefit the analysis of late stage nuclear fuel cycle samples .....	131
<b>Appendix A:</b>	<b>Instrumental theory and setup .....</b>	<b>133</b>
A.1:	Gamma spectrometry .....	133
A.2:	ICPMS & LA-ICPMS.....	138
A.2.1	Sample introduction and ion generation.....	138
A.2.2	Ion focusing.....	139
A.2.3	Ion separation using a quadrupole mass filter .....	140
A.2.4	Detection.....	140
A.2.5	Laser-Ablation sample introduction .....	140
<b>Appendix B:</b>	<b>The UOC collection in this study.....</b>	<b>145</b>
<b>Appendix C:</b>	<b>Supplementary data and information for Chapter 3 .....</b>	<b>147</b>
<b>Appendix D:</b>	<b>Supplementary data and information for Chapter 4 .....</b>	<b>151</b>
<b>Appendix E:</b>	<b>Supplementary data and information for Chapter 5 .....</b>	<b>161</b>
<b>Appendix F:</b>	<b>SEM images and elemental mapping of UOCs .....</b>	<b>173</b>
<b>Appendix G:</b>	<b>X-Ray Diffraction .....</b>	<b>183</b>
<b>Appendix H:</b>	<b>Reading D.G., Croudace I.W. &amp; Warwick P.E. (2015). A rapid sample digestion procedure to aid initial nuclear forensic investigations for uranium- bearing ores and concentrates prior to gamma spectrometry. ....</b>	<b>191</b>
<b>Appendix I:</b>	<b>Croudace I.W., Warwick P.E., Reading D.G. &amp; Russell, B.C. (2016). Recent contributions to the rapid screening of radionuclides in emergency responses and nuclear forensics .....</b>	<b>201</b>
<b>Appendix J:</b>	<b>Publications and Conferences .....</b>	<b>225</b>
	<b>List of References .....</b>	<b>227</b>



# List of Tables

<i>Table 1-1: Isotope data for uranium .....</i>	<i>5</i>
<i>Table 1-2: Uranium deposit definitions sorted by global resource contribution .....</i>	<i>8</i>
<i>Table 1-3: Uranium deposit resources, grades, mineralisation association and major uranium minerals .....</i>	<i>10</i>
<i>Table 1-4: Common impurities in uranium ore .....</i>	<i>12</i>
<i>Table 1-5: Comparison between acid and alkali leaching.....</i>	<i>15</i>
<i>Table 1-6: Common chronometers used for determining “model” ages of U samples.....</i>	<i>24</i>
<i>Table 2-1: Selected gamma emitting radionuclides with associated X-radiations where <math>E_{\gamma}</math> = &lt; 200 keV and emission probability &gt; 1%.....</i>	<i>32</i>
<i>Table 2-2: Dissolution methods.....</i>	<i>35</i>
<i>Table 2-3: Certified Reference Materials Data.....</i>	<i>38</i>
<i>Table 3-1: UOC localities, deposit types and mineralogy.....</i>	<i>60</i>
<i>Table 3-2: UOC milling process .....</i>	<i>63</i>
<i>Table 3-3: Components and associated variables used in the PCA.....</i>	<i>75</i>
<i>Table 4-1: CUP-2:MgSiO<sub>3</sub> sample ratios and masses with total SiO<sub>2</sub> percentage.....</i>	<i>92</i>
<i>Table 4-2: Reference materials investigated .....</i>	<i>92</i>
<i>Table 4-3: Percentage standard deviations (%RSD) of the glass beads.....</i>	<i>95</i>
<i>Table 5-1: UOCs investigated in this study.....</i>	<i>110</i>
<i>Table 5-2: Separation scheme for TRU™ resin calibration .....</i>	<i>114</i>
<i>Table A- 1: Laser and ICP-MS operating parameters.....</i>	<i>142</i>
<i>Table A- 2: Isobaric interference correction factors for solution ICPMS .....</i>	<i>143</i>

<i>Table C- 1: UOC gamma spectrometric data prior to fusion (solid matrix). .....</i>	<i>148</i>
<i>Table C- 2: UOC gamma and alpha spectrometric data post fusion (fused matrix). .....</i>	<i>149</i>
<i>Table C- 3: PCA Component Matrix showing weighting of individual variables on each component.....</i>	<i>150</i>
<i>Table C- 4: Variance explained by each component.....</i>	<i>150</i>
<i>Table C- 5: Component scores of each UOC.....</i>	<i>150</i>
<i>Table D- 1: Geological Reference Material AC-E and BE-N concentrations and chondrite normalised data for glass beads.....</i>	<i>152</i>
<i>Table D- 2: Geological Reference Material BHVO-1 and Mica-Fe concentrations and chondrite normalised data for glass beads .....</i>	<i>153</i>
<i>Table D- 3: Geological Reference Material SY-2 and SY-3 concentrations and chondrite normalised data for glass beads.....</i>	<i>154</i>
<i>Table D- 4: Geological Reference Material NOD-A1 and NOD-P1 concentrations and chondrite normalised data for glass beads .....</i>	<i>155</i>
<i>Table D- 5: Uranium Reference Material CUP-1 and BL-5 concentrations and chondrite normalised data for glass beads.....</i>	<i>156</i>
<i>Table D- 6: Uranium Reference Material CUP-2 concentrations and chondrite normalised data for glass beads.....</i>	<i>157</i>
<i>Table E- 1: Cumulative recovery of rare earth elements and uranium from TRU™ resin separation scheme.....</i>	<i>162</i>
<i>Table E- 2: Recovery per fraction of rare earth elements and uranium from TRU™ resin separation scheme.....</i>	<i>163</i>
<i>Table E- 3: Glass bead and solution REE data for UOC Anaconda and Blind River.....</i>	<i>164</i>
<i>Table E- 4: Glass bead and solution REE data for UOC Cotter and Eldorado .....</i>	<i>165</i>
<i>Table E- 5: Glass bead and solution REE data for UOC Faraday and Gunnar.....</i>	<i>166</i>
<i>Table E- 6: Glass bead and solution REE data for UOC Madawaska and North Span.....</i>	<i>167</i>
<i>Table E- 7: Glass bead and solution REE data for UOC Ranger and Rio Algom.....</i>	<i>168</i>

<i>Table E- 8: Solution REE data for UOC Mary Kathleen, Olympic Dam and Rabbit Lake .....</i>	<i>169</i>
<i>Table E- 9: Solution REE data for UOC South Alligator, Chevron Hill and Lucky McGill .....</i>	<i>170</i>
<i>Table E- 10: Solution REE data for Mesa EFI, Mulberry and Queensland .....</i>	<i>171</i>
<i>Table F- 1: General interpretation of UOC using BSE and EDX .....</i>	<i>174</i>
<i>Table G- 1: XRD operating parameters .....</i>	<i>184</i>
<i>Table G- 2: Minor mineral / compound formulae .....</i>	<i>184</i>



# List of Figures

<i>Figure 1-1: Confirmed incidents involving nuclear or radioactive materials reported to the Incident and Trafficking Database between 1993 and 2014. ....</i>	<i>3</i>
<i>Figure 1-2: Uranium production between 2004 and 2014. ....</i>	<i>4</i>
<i>Figure 1-3: The uranium and actinium decay series (Helebrant, 2011) ....</i>	<i>7</i>
<i>Figure 1-4: Generalised structural schematic of a Pachuca tank. ....</i>	<i>15</i>
<i>Figure 1-5: Summary of analytical sequences and methods used for nuclear forensic analysis of nuclear or radioactive suspect materials. ....</i>	<i>19</i>
<i>Figure 2-1: One of eight Canberra HPGe detector with dewar and Cu coated Pb shielding at GAU-Radioanalytical, Southampton, UK. ....</i>	<i>39</i>
<i>Figure 2-2: Expanded schematic of an HPGe detector housing ....</i>	<i>39</i>
<i>Figure 2-3: Activity concentrations for selected radionuclides of both direct and fused CRMs against the expected activity concentration based on certified values. ....</i>	<i>46</i>
<i>Figure 2-4: Bulk density effects on <math>^{210}\text{Pb}</math> &amp; <math>^{234}\text{Th}</math> photon attenuation within certified reference material BL-5 where density is adjusted using cellulose. Data represented as ratio between measured activity concentration and certified activities. ....</i>	<i>47</i>
<i>Figure 2-5: Activity concentrations for pitchblende fractions of varying grain size to assess <math>^{210}\text{Pb}</math> &amp; <math>^{234}\text{Th}</math> photon attenuation. Borate fused activity concentrations of pitchblende given as an average between all grain size fractions. ....</i>	<i>48</i>
<i>Figure 2-6: Geant4 Monte-Carlo simulations for determining the effect that grain size (A) and grain concentration (B) have on the efficiency of low-energy gamma photons (<math>^{210}\text{Pb}</math> and <math>^{234}\text{Th}</math>) originating from a uraninite source. ....</i>	<i>49</i>
<i>Figure 2-7: Geant4 Monte-Carlo simulations to assess the effect on photon origin from differing positions within grains of CRM CUP-1 and CUP-2 and when the emission is from a representative bulk density with no grains present. ....</i>	<i>50</i>
<i>Figure 3-1: QEMSCAN false-colour images for CCRMP certified reference materials CUP-1 (U-ore) and CUP-2 (UOC). ....</i>	<i>59</i>

<i>Figure 3-2: Geographical locations of U mines and milling facilities used to manufacture the UOCs in this study.....</i>	<i>65</i>
<i>Figure 3-3: Measured activity concentrations for <sup>234</sup>Th, <sup>235</sup>U, <sup>234m</sup>Pa, <sup>214</sup>Pb, <sup>228</sup>Ac and <sup>208</sup>Tl from particulate and fused UOC sample matrices.....</i>	<i>72</i>
<i>Figure 3-4: <sup>210</sup>Pb (<sup>210</sup>Po) and <sup>226</sup>Ra (<sup>214</sup>Pb) activity concentration comparisons (top) and their associated ratio (bottom).....</i>	<i>74</i>
<i>Figure 3-5: Three-dimensional Principal Components Analysis results using 3 components with associated component scores (CS) for each UOC. ....</i>	<i>76</i>
<i>Figure 3-6: Three-dimensional Principal Components Analysis results for experimental and statistical validation of techniques. ....</i>	<i>80</i>
<i>Figure 4-1: Schematic of the iridium-strip resistance fusion system .....</i>	<i>89</i>
<i>Figure 4-2: %RSD values of selected elements for 8 geochemical reference materials and NIST calibration glasses. ....</i>	<i>97</i>
<i>Figure 4-3: Resin mounted and laser ablated (circular pits) AC-E and SY-3 where resin interaction is possible due to vesicles and thin edges of glass beads.....</i>	<i>97</i>
<i>Figure 4-4: Ratio of measured element concentration against the GeoReM preferred or consensus values demonstrating element volatilisation of Cu, Pb, Sn and Zn. ....</i>	<i>98</i>
<i>Figure 4-5: Ratio of measured element concentration against the GeoReM preferred of consensus values for the rare earth elements. ....</i>	<i>98</i>
<i>Figure 4-6: Chondrite normalised comparison of REE concentrations from GRM preferred or consensus values and data from laser-ablated glass beads. ....</i>	<i>100</i>
<i>Figure 4-7: Chondrite normalised REE patterns for CCRMP CUP-1 (0.1 wt% U), BL-5 (7.1 wt% U) and CUP-2 (75.4 wt% U) obtained from 2 laser-ablated glass beads. ....</i>	<i>102</i>
<i>Figure 5-1: U breakthrough and capacity curve for TRU™ resin.....</i>	<i>115</i>
<i>Figure 5-2: UOC analogue standard recovery profiles of REE and U using TRU™ resin. ....</i>	<i>116</i>
<i>Figure 5-3: Amorphous XRD data for various UOCs .....</i>	<i>117</i>
<i>Figure 5-4: Glass bead and chemically separated solution REE data with comparable data from Varga et al. 2010b (where available).....</i>	<i>120</i>

<i>Figure 5-5: Solution ICPMS data obtained in this study compared to previous studies where glass beads were below LA-ICPMS detection limits. ....</i>	<i>121</i>
<i>Figure 5-6: Solution ICPMS data which are not comparable to glass beads or previous studies. ....</i>	<i>122</i>
<i>Figure 7-1: Preliminary U isotope ratio data for UOCs relative to natural U CRM-145. ....</i>	<i>131</i>
<i>Figure A- 1: Gamma photon interactions with matter. A) Photoelectric absorption, B) Photoelectric absorption with electron shell rearrangement, C) Compton scattering, D) Pair production. ....</i>	<i>134</i>
<i>Figure A-2: One of eight Canberra HPGe detector with dewar and Cu coated Pb shielding at GAU-Radioanalytical, Southampton, UK.....</i>	<i>137</i>
<i>Figure A-3: Expanded schematic of an HPGe detector housing.....</i>	<i>137</i>
<i>Figure A- 4: Generalised quadrupole ICPMS setup .....</i>	<i>138</i>
<i>Figure A- 5: Ion sampling and focusing through cones and lenses.....</i>	<i>139</i>
<i>Figure A- 6: The X-Series II quadrupole ICPMS at The University of Southampton’s Isotope Geochemistry Mass Spectrometry Facility.....</i>	<i>141</i>
<i>Figure A- 7: The UP-193FX Laser Ablation System at The University of Southampton’s Isotope Geochemistry Mass Spectrometry Facility.....</i>	<i>141</i>
<i>Figure B- 1: Images of UOC Anaconda to Mulberry.....</i>	<i>145</i>
<i>Figure B- 2: Images of UOC North Span to South Alligator.....</i>	<i>146</i>
<i>Figure D- 1: The Iridium strip fusion device.....</i>	<i>158</i>
<i>Figure D- 2: Wet sample loaded on the iridium strip between the two copper terminals.....</i>	<i>158</i>
<i>Figure D- 3: Fused sample on-screen during cooling .....</i>	<i>159</i>
<i>Figure F- 1: The UOCs loaded on SEM stubs with carbon coated adhesive tabs. ....</i>	<i>175</i>
<i>Figure F- 2: SEM BSE Images of UOCs Anaconda, Blind River and Chevron Hill .....</i>	<i>176</i>
<i>Figure F- 3: SEM BSE Images of UOCs Cotter, Eldorado and Faraday.....</i>	<i>177</i>
<i>Figure F- 4: SEM BSE Images of UOCs Gunnar, Lucky McGill and Madawaska .....</i>	<i>178</i>
<i>Figure F- 5: SEM BSE Images for UOCs Mary Kathleen, Mesa EFI and Mulberry.....</i>	<i>179</i>

<i>Figure F- 6: SEM BSE Images for UOCs North Span, Olympic Dam and Queensland.....</i>	<i>180</i>
<i>Figure F- 7: SEM BSE Images for UOCs Rabbit Lake, Ranger and Rio Algom.....</i>	<i>181</i>
<i>Figure F- 8: SEM BSE Images for UOC South Alligator .....</i>	<i>182</i>
<i>Figure G- 1: XRD patterns and identified minerals/compounds for UOCs Anaconda, Blind River, Chevron Hill and Cotter.....</i>	<i>186</i>
<i>Figure G- 2: XRD patterns and identified minerals/compounds for UOCs Eldorado, Faraday, Gunnar and Lucky McGill.....</i>	<i>187</i>
<i>Figure G- 3: XRD patterns and identified minerals/compounds for UOCs Madawaska, Mary Kathleen, Mesa EFI and Mulberry.....</i>	<i>188</i>
<i>Figure G- 4: XRD patterns and identified minerals/compounds for UOCs North Span, Olympic Dam, Queensland and Rabbit Lake.....</i>	<i>189</i>
<i>Figure G- 5: XRD patterns and identified minerals/compounds for UOCs Ranger, Rio Algom, South Alligator and reference material CUP-2 .....</i>	<i>190</i>

## DECLARATION OF AUTHORSHIP

I, DAVID GEORGE READING declare that this thesis and the work presented in it are my own and has been generated by me as the result of my own original research.

NUCLEAR FORENSICS: DETERMINING THE ORIGIN OF URANIUM ORE AND URANIUM ORE CONCENTRATES VIA RADIOLOGICAL, ELEMENTAL AND, ISOTOPIC SIGNATURES.

I confirm that:

1. This work was done wholly or mainly while in candidature for a research degree at this University;
2. Where any part of this thesis has previously been submitted for a degree or any other qualification at this University or any other institution, this has been clearly stated;
3. Where I have consulted the published work of others, this is always clearly attributed;
4. Where I have quoted from the work of others, the source is always given. With the exception of such quotations, this thesis is entirely my own work;
5. I have acknowledged all main sources of help;
6. Where the thesis is based on work done by myself jointly with others, I have made clear exactly what was done by others and what I have contributed myself;
7. [Delete as appropriate] ~~None of this work has been published before submission~~  
[or] Parts of this work have been published as: [please see Appendix J]:

Signed:

Date:



## Acknowledgements

There are many people I would like to thank for their contributions, guidance and support throughout the last four years.

A huge thank you to Ian Croudace and Phil Warwick for not only entrusting this PhD to me but for also providing so much of their time to guide me through what has been at times, a very complex project. Their support, professionally and personally, and their trust in me to run this project was second to none.

Thank you to my family for supporting me throughout and to Kass who has literally lived through the ups and downs of this PhD with me and has always been there no matter what.

Thank you to all those at GAU for your friendly support in all things technical and lab based and for making the main laboratory an enjoyable work environment despite the endless hours working in the fume cupboards.

Thank you to Andy Milton, Matt Cooper, Rex Taylor and Agnes Michalik for all their advice, guidance and data interpretation with all things mass spectrometry or clean lab related. Thank you to Bob Jones and John Ford for their friendly and extended coffee breaks and for regularly reminding me of my almost 9 years at NOCS usually by saying, “Dave, you were here when...”

Thank you to all my fellow PhD students (past and present), office mates over the years and to the Southampton based geologists of 2007/2011. Some truly great memories have been formed with these people and there are too many to name individually but you all have helped me accomplish this PhD.

Finally, thank you to AWE for funding this PhD project.



## Abbreviations

<b>ANOVA</b>	Analysis of Variance
<b>CCRMP</b>	Canadian Certified Reference Materials Project
<b>CRM</b>	Certified Reference Material
<b>Geant4</b>	Geometry and Tracking 4 (Monte Carlo Simulation Package)
<b>GRM</b>	Geological Reference Material
<b>HPGe</b>	High Purity Germanium
<b>HRGS</b>	High Resolution Gamma Spectrometry
<b>IAEA</b>	International Atomic Energy Agency
<b>ITDB</b>	Incident and Trafficking Database
<b>ICPMS</b>	Inductively Coupled Plasma Mass Spectrometry
<b>LA-ICPMS</b>	Laser Ablation Inductively Coupled Plasma Mass Spectrometry
<b>LEGe</b>	Low Energy Germanium
<b>NF-ITWG</b>	Nuclear Forensics International Technical Working Group
<b>NORM</b>	Naturally Occurring Radioactive Material
<b>PCA</b>	Principal Components Analysis
<b>QEMSCAN</b>	Quantitative Evaluation of Minerals via Scanning Electron Microscopy
<b>SEM</b>	Scanning Electron Microscopy
<b>TEM</b>	Transmission Electron Microscopy
<b>UOC</b>	Uranium Ore Concentrate (Yellowcake Uranium)
<b>XRD</b>	X-ray Diffraction
<b>XRF</b>	X-ray Fluorescence



## **Chapter 1: Introduction and Background**

### **1.1 History of Nuclear Forensics and Rationale of this Study**

In 1991, the dissolution of the Soviet Union resulted in Russia, Belarus, Ukraine and Kazakhstan inheriting a nuclear arsenal (Moody et al., 2005). The tight regulations and control that the KGB had over personnel at nuclear facilities and the general safety and security of such facilities and its materials diminished as responsibility was handed over to the newly formed States. Lax security, poor personnel screening and tough economic conditions allowed facility personnel to divert nuclear materials in small quantities on a daily basis, that would be enough to go unnoticed by typical accountancy protocols at nuclear facilities (Zaitseva & Hand, 2003). A kilogram of highly enriched uranium (HEU) in the early 1990's would cost tens of thousands of pounds to produce within a well-established enrichment program and thus the theft and sale of nuclear materials developed (Moody et al., 2005). During 1991, this new phenomenon was being observed in Switzerland and Italy where the first cases of the so-called “nuclear smuggling” were recorded (Mayer et al., 2007). The following years saw a gradual increase in incidents involving nuclear or radioactive materials around central Europe (Wallenius et al., 2006), thus the science of nuclear forensics began to develop and has been discussed in the scientific literature, public policy literature, and popular press (Mayer et al., 2005; May et al., 2006; Talmadge, 2007; Allison, 2008; Brokenshire, 2014).

Nuclear forensics is currently defined as “the examination of nuclear or other radioactive materials or of evidence contaminated with radionuclides in the context of international or national law or nuclear security. The analysis of nuclear or other radioactive material seeks to identify what the materials are, how, when, and where the materials were made, and what were their intended uses” (IAEA, 2015b).

This project was tasked with advancing the field of nuclear forensic science by developing new, and enhancing previous analytical techniques to aid in rapid characterisation of samples to determine possible geographical origins of illicitly recovered uranium ores and uranium ore concentrates (UOC).

## 1.2 The Incident and Trafficking Database (ITDB)

The IAEA (International Atomic Energy Agency) established the *Incident and Trafficking Database (ITDB): Incidents of nuclear and other radioactive material out of regulatory control* in 1995 to record and analyse incidents where nuclear and other radioactive materials had become out of regulatory control (IAEA, 2015a). The database has three main categories:

- 1) Unauthorised possession and related criminal activities that includes the movement of nuclear or radioactive sources with intention to sell, purchase or use such materials.
- 2) Theft or loss of nuclear or radioactive materials from facilities or during transport.
- 3) Unauthorised activities and events such as unauthorised shipment of nuclear or radioactive materials, unauthorised disposals of materials or the detection and/or discovery of uncontrolled sources.

By the end of 2014 the ITDB contained 2,734 confirmed incidents (Figure 1-1) reported by its participating 131 States (IAEA, 2015a). Of these incidents, 86 cases have insufficient information to allocate a category. It should be noted that the total number of incidents between 2012 and 2014 is likely to rise due to a 2-3 year lag time in the reporting procedures. The sudden rise in incidents relating to theft or loss from 2006 is due to a change in reporting procedures and is not indicative of an actual change in frequency of events.

It is important to realise that despite the best of efforts of border controls and the IAEA ITDB, there must be a significant amount of trafficking and smuggling that go undetected and unreported. For example, stolen nuclear materials from within the EU Schengen Area would likely go undetected in transit due to open borders between the participating EU countries. Additionally, detecting low quantities of nuclear material at border controls is difficult due to technological constraints and because nuclear materials can be shielded from radiation detectors and hidden within larger inconspicuous consignments. The ITDB does not account for illegal dumping or un/intentional abandonment of nuclear material or military activities using nuclear materials which could also fall in to the nuclear forensics remit for origin/ownership determination so that appropriate remedial actions can be sanctioned and acted upon by the owner. Examples include the re-entry of space debris or

satellites which contain (wholly or fragments of) on-board nuclear fuel cells (radioisotope thermoelectric generators) which land in unauthorised locations, on foreign soil or international waters; and the use of depleted uranium (DU) as part of armour piercing ordnance in warzones. Identifying the origin and owner from radiological signatures of these materials could aid in determining whom is responsible for remediation of an area which has been affected.

Regardless, the number of incidents being reported to the IAEA is of serious concern and therefore it is crucial for nuclear laboratories to develop accurate, speedy and effective tools for identifying the origins of nuclear materials out of regulatory control. This led to laboratories such as the Lawrence Livermore National Laboratory (USA), the Institute for Transuranium Elements (Germany), and the Atomic Weapons Establishment (UK) expressing interest in forensic investigations to determine the intended use, origin and the potential trafficking route of the illicit nuclear materials. Today, countries from all corners of the world participate in the Nuclear Forensics International Technical Working Group (ITWG) which was originally set up in 1996 by the G-8 (Wacker, 2011; L'annunziata, 2012) and consists of 28 nations and organisations (Smith & Niemeyer, 2004).

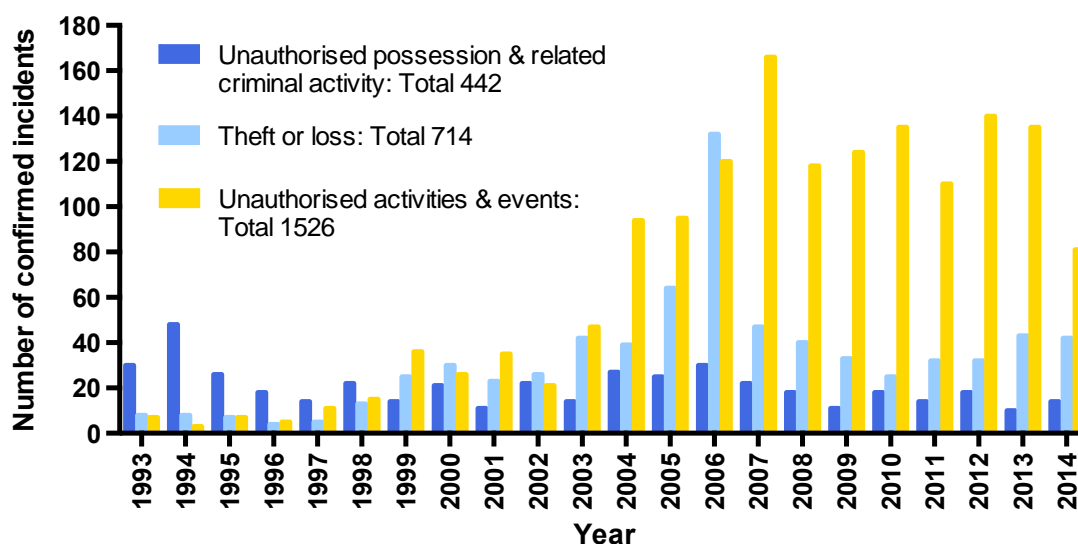


**Figure 1-1: Confirmed incidents involving nuclear or radioactive materials reported to the Incident and Trafficking Database between 1993 and 2014.**

### 1.3 Uranium and Uranium Ore Concentrate

#### 1.3.1 Uranium

Uranium is a primordial radioactive element that is present in low concentrations ~2.8 ppm in the Earth's crust and is mostly required for nuclear power generation, nuclear deterrence, and for research reactors. The requirement for less polluting forms of energy generation has resulted in uranium becoming a highly desired commodity and thus supply routes and ore prospecting has steadily increased to meet demand with major deposits in Kazakhstan now being exploited (Figure 1-2) (World Nuclear Association, 2013, 2015).

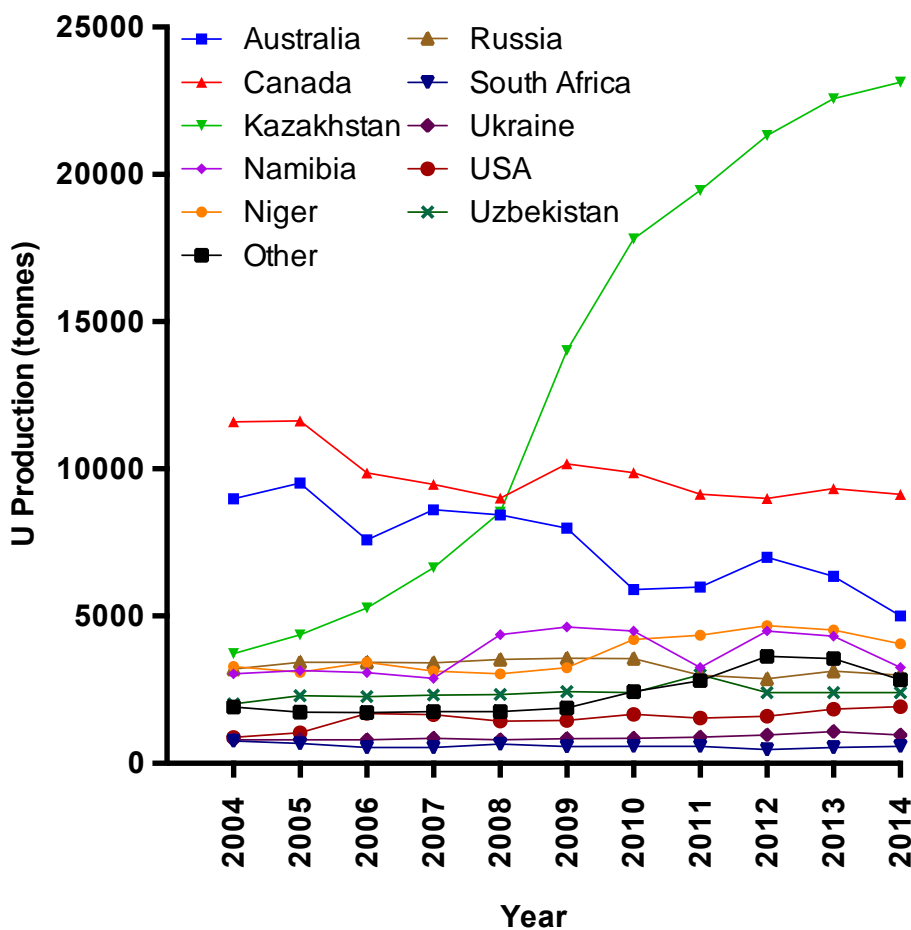


Figure 1-2: *Uranium production between 2004 and 2014.*

Uranium has three main isotopes which are naturally occurring and three anthropogenic isotopes (Table 1-1). Natural uranium ( $^{234}\text{U}$ ,  $^{235}\text{U}$ ,  $^{238}\text{U}$ ) has two natural valence states:  $\text{U}^{6+}$ , which is soluble and mobile under oxidising conditions, and  $\text{U}^{4+}$ , which is insoluble and immobile under reducing conditions. These two valences are intrinsically linked to the U accumulation and grade of global deposits.

**Table 1-1: Isotope data for uranium**

Isotope	Atomic Abundance (%)	Half Life (years)	Specific Activity (Bq/g)
$^{238}\text{U}$	99.275	$4.47 \times 10^9$	$1.245 \times 10^4$
$^{236}\text{U}$	Trace	$23.43 \times 10^6$	$2.39 \times 10^6$
$^{235}\text{U}$	0.72	$7.04 \times 10^8$	$8.001 \times 10^4$
$^{234}\text{U}$	0.0054	$2.46 \times 10^5$	$2.313 \times 10^8$
$^{233}\text{U}$	Trace	$1.6 \times 10^5$	$3.55 \times 10^8$
$^{232}\text{U}$	Trace	70.6	$8.08 \times 10^{11}$

(Berglund & Wieser, 2011; DDEP, 2016)

### 1.3.2 Radioactive decay

Radioactive decay is the spontaneous change within an unstable nucleus of an atom due the nuclei having excess energy. This results in the expulsion of particles or electromagnetic radiation and therefore changing the energy state of the nucleus. Modes of decay are typically alpha, beta and gamma emission where some rarer processes such as spontaneous fission may also occur. Each unstable isotope (radionuclide) will decay with one or more of these modes and will have a characteristic decay half-life. The half-life depends on the amount of excess energy the particular isotope possesses along with the mode of decay and structure of the nucleus.

#### 1.3.2.1 Alpha decay

Alpha ( $\alpha$ ) decay is the preferred mode of decay for heavy nuclei ( $Z > 83$ ) and is characterised by the emission of a single alpha particle. The alpha particle is a  $^4\text{He}$  nucleus ( $^4_2\text{He}^{2+}$ ) containing 2 protons and 2 neutrons resulting in a physical change to the parent isotope where  $Z \rightarrow Z-2$  and  $A \rightarrow A-4$ . An example of alpha decay is that of  $^{238}\text{U}$  to  $^{234}\text{Th}$  ( $^{238}_{92}\text{U} \rightarrow ^{234}_{90}\text{Th} + ^4_2\text{He}$ ).

### 1.3.2.2 Beta decay

Beta ( $\beta$ ) decay is similar to alpha decay where the parent nucleus undergoes a physical change and therefore becomes a different isotope. The unstable nucleus emits an energetic electron ( $\beta^-$  decay) or positron ( $\beta^+$  decay) and a respective antineutrino or neutrino. The process of beta decay allows an unstable atom to obtain a more stable ratio of protons and neutrons.  $\beta^-$  decay generally occurs in neutron-rich nuclei and  $\beta^+$  decay occurs in proton-rich nuclei.

### 1.3.2.3 Gamma decay

Alpha and beta decay will often leave the product nuclide in an excited energy state and is referred to as a nuclear isomer. The isomer will fall to the ground state directly or in steps through the dissipation of energy as gamma ( $\gamma$ ) photons in a process called isomeric transition. The energy associated with each photon emission is the difference between the parent and daughter states with almost negligible loss to recoil energy of the emitting nucleus.

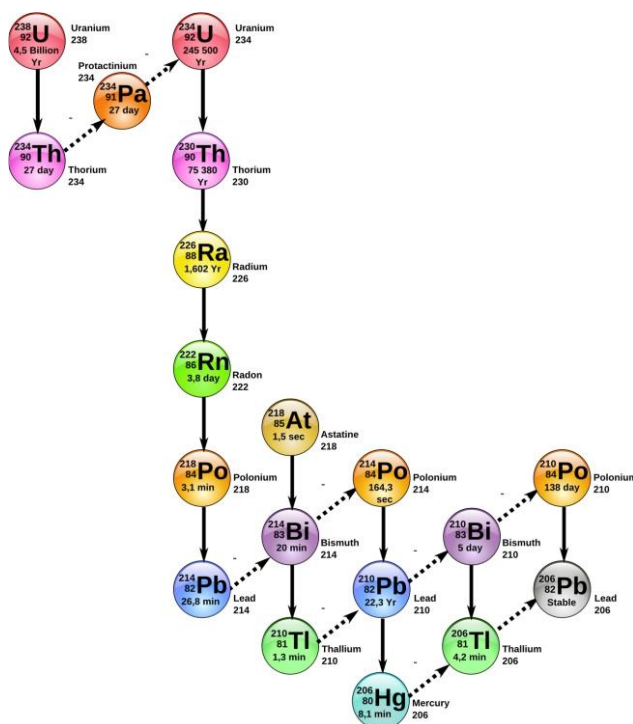
### 1.3.2.4 Decay rates, secular equilibrium and decay chains

A population of identical radionuclides will decay over time ( $t$ ) following an exponential function ( $e^{-\lambda t}$ ) where  $\lambda$  is the decay constant. The time required for half of the original population of radionuclides to decay is the half-life ( $T_{1/2}$ ). The relationship between  $T_{1/2}$  and  $\lambda$  is given as  $T_{1/2} = 0.639 / \lambda$ . From an initial population  $N_0$ , the number of radioactive isotopes present after time ( $N_t$ ) can be demonstrated as follows:  $N_t = N_0 e^{-\lambda t}$ . When calculating the population of a daughter radionuclide, the decay constants of both parent and daughter need to be evaluated as the daughter population is growing according to the decay rate of the parent, but is also decaying according to its own decay constant. When the decay rate and half-life of the parent greatly exceeds that of the daughter, the two radionuclides will eventually be in a state of secular equilibrium as the quantity of daughter radionuclides being produced will equal the rate at which the same radionuclide is decaying. Secular equilibrium is of great importance when studying the uranium decay series as the long lived head of the chain,  $^{238}\text{U}$ , has a half-life of 4.47 billion years and greatly exceeds that of its daughter radionuclides. Therefore, wherever  $^{238}\text{U}$  is present, all

radionuclides to  $^{222}\text{Rn}$  will be present. Radon-222 and its daughters will not necessarily be present at the same quantity to  $^{238}\text{U}$  as gaseous radon can evade the system.

Four decay chains are observed in nature: the uranium series, the actinium series, the thorium series and the neptunium series and each are commonly known simply by the nuclide at the head of the decay chain ( $^{238}\text{U}$ ,  $^{235}\text{U}$ ,  $^{232}\text{Th}$ , and  $^{237}\text{Np}$  respectively). The uranium and actinium series are displayed in Figure 1-3.

Uranium series



Actinium series

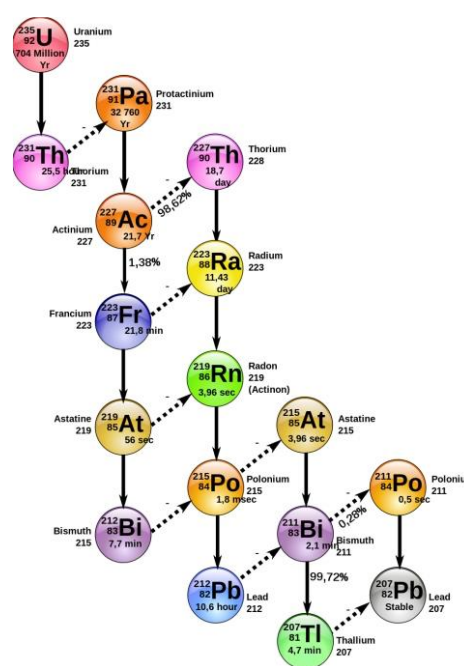


Figure 1-3: The uranium and actinium decay series (Helebrant, 2011)

### 1.3.3 Uranium deposits of the world

The change in uranium mobility along with the propagation conditions and geological setting means that deposits can typically contain up to a few weight percent of uranium and in some rare instances up to 20 Wt% such as the McArthur River deposits of Canada.

Uranium deposits of the world can typically be divided in to fourteen categories based on the geological setting in which the uranium mineralisation occurred (Table 1-2, 1-3 and 1-4 - (Dahlkamp, 1993; Mckay & Mieztis, 2001; Gupta & Singh, 2003; Švedkauskait-Le Gore, 2008; IAEA, 2009; Organisation for Economic Co-Operation and Development et al., 2014)).

Uraninite and pitchblende are both primary minerals and are found in almost all uranium deposits and usually contain Th, Pb and rare earth elements (REE). Uraninite is the macrocrystalline variety of  $\text{UO}_2 + x$ , is usually euhedral and forms in high pressure and temperature metamorphic rock, igneous rock and vein deposits. Pitchblende is the micro- or crypto-crystalline variety with a botryoidal habit and forms in low grade metamorphic rock, metasediments and sandstone (Dahlkamp, 1993; Fritsche & Dahlkamp, 1997). Pitchblende is also almost completely absent of Th whereas uraninite is regularly associated with Th (Fritsche & Dahlkamp, 1997). Despite this, the vast majority of uranium in ore is from hexavalent, secondary minerals such as carnotite (uranium potassium vanadate), autinite (calcium uranyl phosphate), torbenite (copper uranyl phosphate), uranophane (calcium uranium silicate) and brannerite (uranium calcium titanium iron oxide). The majority of U minerals are often associated with other metals and REE and can occasionally be specific to a particular deposit or region.

**Table 1-2: Uranium deposit definitions sorted by global resource contribution**

(compiled from: Dahlkamp, 1993; Gupta & Singh, 2003; Švedkauskait-Le Gore, 2008; IAEA, 2009)

Deposit Type	Typical Occurrence
<b>Unconformity</b>	Proterozoic unconformable contacts with intensely altered metasedimentary basement which is usually faulted and brecciated. Overlaying sandstones are usually undeformed.
<b>Sandstone</b>	Medium to coarse grained sandstone deposits in fluvial or marginal marine environments. Usually interbedded with shale/mudstone causing reducing conditions.
<b>Quartz-Pebble Conglomerate</b>	Overlies unconformable granitic and metamorphic basement.
<b>Vein</b>	Mineralisation occurs when cracks/fractures/breccias are filled by the mineralising fluid. Mostly associated with large granitic systems, batholiths and fault/shear zones.

**Table 1-2 Continued: Uranium deposit definitions sorted by global resource contribution**

<b>Deposit Type</b>	<b>Typical Occurrence</b>
<b>Breccia Complex</b>	Occurs with a granite intrusion exhibiting Fe, K and/or Na metasomatism.
<b>Intrusive</b>	Associated with bodies of alaskite, granite, pegmatite and monzanite.
<b>Surficial</b>	Tertiary to Recent near-surface sediments or soils containing U from intense weathering and erosion of granites.
<b>Collapse Breccia Pipe</b>	Circular, vertical collapse structures filled most commonly with permeable sandstone breccias where mineralisation occurs.
<b>Volcanic</b>	In or near a caldera in acid to intermediate volcanic rock and related to faults and shear zones.
<b>Phosphorite</b>	Marine phosphorite of continental shelf origin. U associated with fine-grained apatite.
<b>Metasomatite</b>	Consist of unevenly disseminated U in structurally deformed rocks that were affected by Na or K metasomatic processes.
<b>Metamorphic</b>	Metasediments and metavolcanics unrelated to granite and where there is no evidence of mineralisation prior to metamorphism.
<b>Lignite beds</b>	Coal seams and immediately adjacent to carbonaceous mud and clay / sandstone beds.
<b>Black shale</b>	Uniformly disseminated U is adsorbed on organic and clay particles in marine organic-rich environments with high levels of pyrite and phosphates.

**Table 1-3: Uranium deposit resources, grades, mineralisation association and major uranium minerals** (compiled from: Dahlkamp, 1993; Gupta & Singh, 2003; Švedkauskait-Le Gore, 2008; IAEA, 2009)

<b>Deposit Type</b>	<b>Global Resource (%)</b>	<b>Typical Grade (U<sub>3</sub>O<sub>8</sub>)</b>	<b>Mineralisation Association *</b>	<b>Major U Minerals</b>
<b>Unconformity</b>	33%	0.3 - 4% But up to 20%	HTR	Pitchblende, Uraninite, Coffinite,
<b>Sandstone</b>	18%	0.05 - 4%	LTR	Uraninite, Coffinite.
<b>Quartz-Pebble Conglomerate</b>	13%	0.015 - 0.15%	NR	Uraninite.
<b>Vein</b>	9%	0.1 - 0.6% But up to 10%	HTR	Pitchblende, Uraninite.
<b>Breccia Complex</b>	<1%	0.04 - 0.08%	HTR	Uraninite.
<b>Intrusive</b>	<1%	0.03 - 0.1%	HTR	Uraninite.
<b>Surficial</b>	<1%	0.06 - 0.07%	Occurs with calcrete	Carnotite.
<b>Collapse Breccia Pipe</b>	<1%	0.3 - 1%	HTR	Pitchblende, Coffinite.
<b>Volcanic</b>	<1%	0.02-0.25%	HTR	Pitchblende.
<b>Phosphorite</b>	<1%	<0.02%	LTR	Syngenetic U in apatite.
<b>Metasomatite</b>	<1%	<0.2%	HTR	Uraninite.
<b>Metamorphic</b>	<1%	<0.2%	HTR	Pitchblende, Uraninite.

**Table 1-3 Continued: Uranium deposit resources, grades, mineralisation association and major uranium minerals**

<b>Deposit Type</b>	<b>Global Resource (%)</b>	<b>Typical Grade (<math>\text{U}_3\text{O}_8</math>)</b>	<b>Mineralisation Association *</b>	<b>Major U Minerals</b>
<b>Lignite beds</b>	<1%	<0.1%	LTR	Organic-U.
<b>Black shale</b>	<1%	<400 ppm	LTR	Disseminated-U.

**\*Mineralisation Association**

**LTR (Low temperature redox):** Mineralisation occurs below the water table where low temperature, oxidised fluids, carrying soluble  $\text{U}^{6+}$  interact with a reducing agent, usually carbonaceous material, sulphides, or hydrocarbons and precipitate U as insoluble  $\text{U}^{4+}$ .

**HTR (High temperature redox):** Similar to low temperature redox, but has higher temperatures. Associated with igneous and metamorphic processes.

**NR (Non-redox sensitive):** Ancient deposits formed from fluvial transport of uraninite during anoxic conditions on Earth (2.3 to 3 Ga).

**Table 1-4: Common impurities in uranium ore** (compiled from Dahlkamp, 1993; Švedkauskait-Le Gore, 2008)

	Element	Ag	Al	As	Au	Ba	Be	Bi	Ca	Cd	Ce	Co	Cr	Cu	Dy	Er	Eu	Fe	Gd	Ge
<b>Deposit Category</b>																				
Unconformity	x			X			X				X		X							
Sandstone			X		X									X				X		
Quartz-Pebble Conglomerate	X		X	X							X	X	X	X	X	X	X		X	
Vein	X			X			X				X		X					X		
Breccia Complex	X			X							X	X		X	X	X	X	X	X	
Intrusive	X			X		X	X							X						
Surficial		X	X		X				X		X			X	X	X	X	X	X	
Collapse Breccia Pipe	X			X								X		X				X		
Volcanic		X	X						X					X				X		
Phosphorite			X								X	X		X	X	X	X		X	
Metasomatite	X			X					X		X			X	X	X	X	X	X	
Metamorphic									X											
Lignite beds			X		X	X				X	X	X	X	X	X	X	X		X	X
Black shale	X		X											X	X					

	Element	Ho	Ir	K	La	Li	Lu	Mg	Mn	Mo	Na	Nb	Nd	Ni	P	Pb	Pd	Pr	Pt
<b>Deposit Category</b>																			
Unconformity										X				X		X			X
Sandstone										X						X	X		
Quartz-Pebble Conglomerate	X	X		X		X							X	X		X		X	X
Vein									X					X		X			
Breccia Complex	X			X		X						X	X					X	
Intrusive					X					X								X	X
Surficial	X			X		X	X	X	X	X	X		X					X	
Collapse Breccia Pipe										X				X		X			
Volcanic					X					X						X			
Phosphorite	X			X		X			X				X			X		X	
Metasomatite	X		X	X		X			X	X	X	X						X	
Metamorphic									X					X		X			
Lignite beds	X			X		X			X				X	X		X		X	
Black shale										X									

	Element	Re	Sb	sc	Se	Si	Sm	Sn	Sr	Tb	Te	Ti	Tm	V	W	Y	Yb	Zn	Zr
<b>Deposit Category</b>																			
Unconformity		X		X							X			X				X	
Sandstone		X		X										X				X	
Quartz-Pebble Conglomerate						X			X			X				X	X	X	X
Vein																		X	
Breccia Complex							X		X			X					X		
Intrusive	X			X	X														
Surficial				X	X	X		X	X		X	X	X	X			X		
Collapse Breccia Pipe		X												X				X	
Volcanic		X					X								X			X	X
Phosphorite			X			X		X	X			X				X	X	X	
Metasomatite						X			X			X					X		
Metamorphic																		X	
Lignite beds	X			X		X			X		X	X	X	X		X	X	X	X
Black shale														X					

### **1.3.4 Mining**

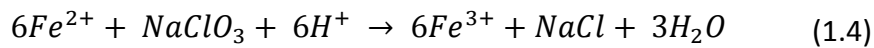
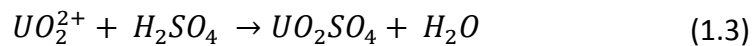
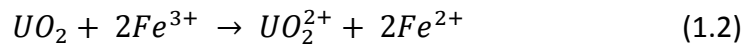
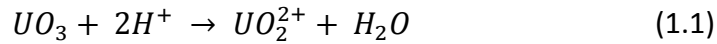
Typically, three uranium ore mining methods are used, open pit, underground and in-situ leaching, and are dependent on the economics, geology, depth and location of the deposit. Open pit mining is typically used when the uranium deposit is near the surface and can be extracted with ease using large excavation equipment or explosives. Underground mining is adopted when the resource is deep underground where removal of the overburden is not economically viable. In-situ leaching is a technique of circulating oxygenated water or leaching-liquor (ammonium carbonate or sulphuric acid) through a porous ore body where the uranium is dissolved and brought back to the surface for treatment.

### **1.3.5 Milling**

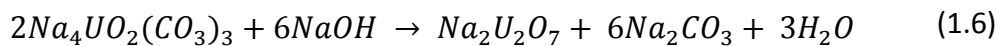
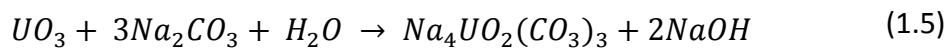
The uranium ore grade is typically <1 wt% U and is therefore purified and concentrated in mills which are normally located near to the ore body. There are instances however where an on-site mill is not viable due to economics and therefore uranium ore is sometimes shipped from smaller mines to a centralised mill and combined with other regional uranium ore feeds. The milling occurs in four main stages, crushing, leaching, concentrating, and precipitation. The final product is known as uranium ore concentrate (UOC) or more colloquially, yellow cake, and generally ranges between 65 and 80 wt% U. All ores require grinding prior to leaching to increase the surface area and thus improve efficiency of the leaching process. Acidic leaching requires particle sizes < 10 mm whereas alkali leaching require < 0.5 mm (Švedkauskait-Le Gore, 2008).

### 1.3.5.1 Leaching of uranium ore

Acidic leaching is completed using sulphuric acid ( $H_2SO_4$ ) and if the uranium is tetravalent, an oxidising agent ( $NaClO_3$  /  $MnO_2$  /  $Fe_2O_3$ ) is required with the aid of ferric iron as a catalyst (Wilson, 1997; Edwards & Oliver, 2000). Optimal conditions for leaching are approximately 12 hours at 40 – 50 °C (Švedkauskait-Le Gore, 2008).



Alkali leaching generally uses  $Na_2CO_3$ ,  $NaHCO_3$  or  $CO_2$  in the circuit and is required when the ore feed contains high carbonate or other acid consuming components. Alkaline leaching is slower than acid leaching but is more selective for uranium dissolution and is due to the formation of a tricarbonat complex. Oxygen is used to convert U(IV) to U(VI) and catalysed by copper sulphate and ammonia. Bicarbonate is used as a buffer to prevent the pH from rising to the point where diuranate would precipitate (Edwards & Oliver, 2000; Gupta & Singh, 2003).



The leaching is usually performed in pachucas which are pneumatic agitation devices that use compressed gas or steam to circulate the pulp around the 15 m diameter and 35 m high vessel (Figure 1-4). The use of pachucas allow for high recovery of uranium within 20 hours if using acid leaching or 100 hours if using alkali leaching when the pulp density is ~50% solids (Gupta & Singh, 2003). The uranium-bearing solutions are separated from leached solids and refractory components using solid-liquid separating devices such as filters or cyclones or flocculants.

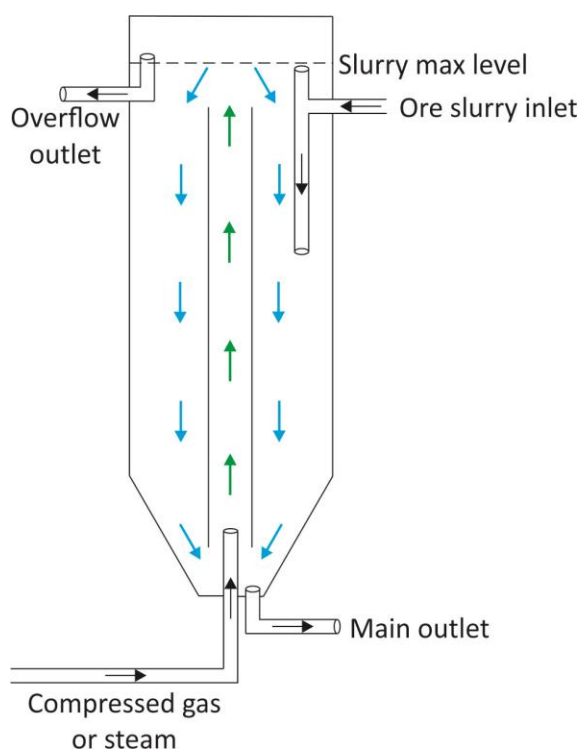


**Figure 1-4: Generalised structural schematic of a Pachuca tank**

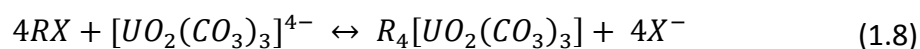
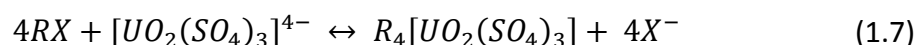
**Table 1-5: Comparison between acid and alkali leaching**

<b>Acid Leaching</b>	<b>Alkali Leaching</b>
U recovery is high	U recovery lower than acid
Suitable for sulphidic and refractory ore	Suitable for high Ca, Mg, carbonate or shale ores.
Expensive – especially for clay-bearing ore	Less expensive as reagents can be recovered
Purification by ion or solvent exchange	Direct precipitation is possible
Effluent neutralisation and disposal is complex	Easy disposal or recycling of effluents
Low leaching of Ra in to solution but high levels of metal easily leached	Ra readily leached
Ore feed can be coarse	Ore feed needs to be ground finely

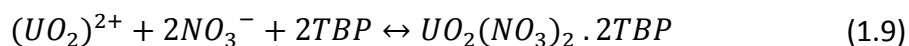
### 1.3.5.2 Concentration and purification

The U solutions contain a complex mixture of cations, anions and impurities. Alkaline leach has high selectivity for U and yields a relatively pure solution, however, acidic leach will contain significant levels of Al, As, Fe, Mg, Mo, Ni, Ti, V, Zr and REE (Wilson, 1997; Edwards & Oliver, 2000; Gupta & Singh, 2003; Švedkauskait-Le Gore, 2008). Moreover, the U concentration in the leachate is still relatively low and therefore further concentration and purification is required and is completed by using ion exchange (IX) and/or solvent exchange (SX).

Ion exchange involves the selective retention of U on anionic or cationic resins and then eluting the U using chloride or nitrate solutions to produce a purified and concentrated solution of U. Elution using sulphate is sometimes preferential as it does not affect the loading of the resin. The main adsorption reactions are given below where R is a fixed ion exchange site (usually a long-chain aliphatic amine), and X is a nitrate or chloride ion present in the resin.



Solvent exchange or liquid-liquid extraction separates compounds based on their relative solubility in two different immiscible liquids where uranium ions complex in to the organic phase. This is completed using solvents such as organophosphate tributyl phosphate (TBP) where the U(VI) is extracted from the strong nitric acid forming a uranium complex ( $UO_2(TBP)_2(NO_3)_2$ ). Weak nitric acid is then added to the organic complex which causes dissociation resulting in free TBP and uranyl nitrate (equation 1.9).



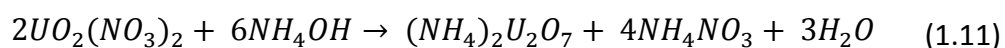
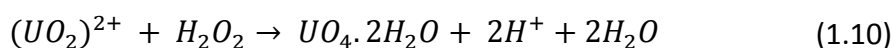
### 1.3.5.3 Precipitation and drying of uranium ore concentrate

The precipitation of uranium from the leach liquors is the most complex part of the uranium milling and processing. The precipitant and the drying and operating conditions are specific to each uranium mill due to the U grade, gangue composition and product specification from the customer. The resulting powdered product is uranium ore concentrate (UOC).

Although colloquially termed as yellowcake, UOC ranges in colour from yellow, orange, brown and dark green and depends on the precipitation technique and which temperature the precipitate has been dried at.

The leach liquor from the alkali circuit is often pure enough to allow for direct precipitation of U using sodium hydroxide in a process which takes less than 12 hours at 50-80°C. Sodium diuranate products from this circuit are usually calcined at ~400 °C to produce UO<sub>2</sub>. When the leach liquor contains significant impurities so that direct precipitation of the uranium cannot occur, lime and/or magnesia are added to produce a gypsum or iron cake which contains a vast majority of the impurities. In most acid based circuits, this would also reduce arsenic and sulphate content (Edwards & Oliver, 2000) and in some mills has also removed aluminium, iron, molybdenum and vanadium (Rowson & Nguyen, 1987).

In acidic circuits, precipitation is achieved with hydrogen peroxide, ammonia, magnesia, magnesium hydroxide or sodium hydroxide (IAEA, 1993; Wilson, 1997; Edwards & Oliver, 2000). Precipitation with hydrogen peroxide is preferred as the other reagents can produce an amorphous and variably composed product containing a mixture of uranates, polyuranates and some impurities (Edwards & Oliver, 2000). The addition of hydrogen peroxide produces uranyl peroxide (equation 1.10) and ammonium hydroxide produces ammonium diuranate (ADU) (equation 1.11). Drying of uranyl peroxide in open-air at ~300 °C produces the bright orange UO<sub>3</sub> where volatile contaminants (water, O, NH<sub>3</sub>, halogens and hydrogen peroxide) are driven off. Higher and more vigorous heating of the uranyl peroxide produces black to dark green U<sub>3</sub>O<sub>8</sub> where U grade could be as high as 98% and where molybdenum and vanadium impurities are virtually eliminated (Edwards & Oliver, 2000). Heating of ADU to 150-200 °C also drives off any volatile contaminants and results in the formation of UO<sub>2</sub>.



## **1.4 Nuclear Forensic Investigations of uranium ore and uranium ore concentrate**

Nuclear forensics is a multidisciplinary science which encompasses many areas of science and technology including radioanalytical chemistry, nuclear and radiochemistry, geochemistry, geology, nuclear and reactor physics, nuclear engineering and processing, material science, statistics and so forth. “Signatures” such as isotopic abundances; major, minor and trace elemental concentrations; and physical and chemical morphology, are all required to attribute illicitly recovered nuclear or other radioactive materials to a source or person. No single “signature” obtained for a sample can successfully identify the origin of a sample. Instead, a combination of the above is adopted to not necessarily determine an exact origin, but rather to eliminate origin possibilities. The sequence and timescales of data acquisition are shown in Figure 1-5. Therefore, it is imperative that new signatures are identified and pre-existing techniques are developed for the discipline, as well as improving and reducing data acquisition times for pre-existing techniques. Throughout the nuclear fuel cycle (NFC), these signatures can be created and destroyed meaning that not all current nuclear forensic approaches can be applied to all stages of the NFC. However, it is possible for signatures to carry through multiple stages of the NFC for example in the conversion of U-ore to UOC where additional process signatures are incorporated. The signatures obtained from repeated measurements of known samples can be incorporated into a nuclear forensic database where future investigated samples can be compared against and the suspect sample’s history and origin can be inferred.

This section describes particular signatures that are key to nuclear forensic investigations with emphasis on uranium ore concentrate characterisation.

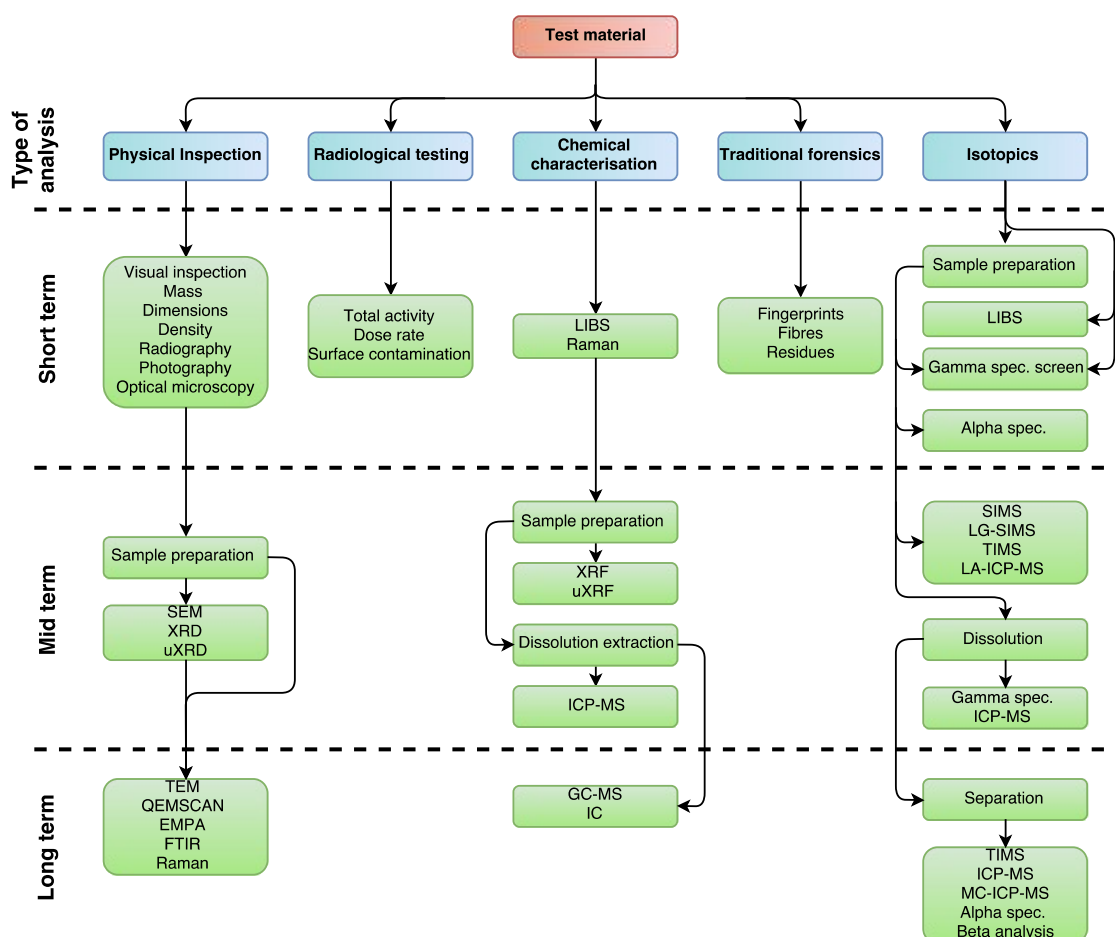


**Figure 1-5: Summary of analytical sequences and methods used for nuclear forensic analysis of nuclear or radioactive suspect materials.**

Short-term: 1 to 7 days, mid-term: 7 to 28 days, long-term 28+ days. *Adapted and extended from (Mayer et al., 2005; Hutcheon et al., 2013; Kristo & Tumey, 2013).*

#### 1.4.1 UOC Isotope Ratios

##### 1.4.1.1 Uranium

Uranium isotopic composition is a critical signature to obtain from U-bearing compounds and can vary greatly depending on the samples provenance in the NFC for example whether a sample is enriched or depleted in  $^{235}\text{U}$ . The isotopic ratio of  $^{238}\text{U}/^{235}\text{U}$  has been widely accepted as 137.88 for many years and until recently has been invariant. More recent studies however have demonstrated that this is not the case as per-mil level variability has been measured in near surface environments (Stirling et al., 2007; Weyer et al., 2008; Richter et al., 2010; Uvarova et al., 2014; Tissot & Dauphas, 2015; Hinojosa et al., 2016)

which has enabled a higher accuracy value of 137.797 for the average terrestrial composition.

The  $^{234}\text{U}/^{238}\text{U}$  and  $^{235}\text{U}/^{238}\text{U}$  can be measured via gamma and alpha spectrometry rapidly but for greater precision and accuracy, mass spectrometry techniques are required (e.g. multi-collector inductively coupled plasma mass spectrometry (MC-ICPMS), thermal ionisation mass spectrometry (TIMS), accelerator mass spectrometry (AMS), or secondary ion mass spectrometry (SIMS)). These ratios have been measured in UOC and the  $^{234}\text{U}/^{238}\text{U}$  ratio has demonstrated the greatest variation between samples and geological deposits as a result of alpha recoil and subsequent leaching of U from the weakened mineral lattice meaning that provenance determination of samples based on U isotopes is possible (Richter et al., 1999; Keegan et al., 2008; Brennecka et al., 2010). The study by Brennecka et al. (2010) demonstrated that the range for  $^{238}\text{U}/^{235}\text{U}$  ratios is 137.792 and 137. These studies do not assess intra-mine variability and the conclusions are based upon limited sample sets. Brennecka et al. (2010) indicates that multiple isotope systems (such as Pb and Sr) would be required to identify the origin of an unknown UOC.

### 1.4.1.2 Lead

Lead has four stable isotopes ( $^{204}\text{Pb}$ ,  $^{206}\text{Pb}$ ,  $^{207}\text{Pb}$  and  $^{208}\text{Pb}$ ) where  $^{204}\text{Pb}$  is the only non-radiogenic isotope as the other three originate from the natural U and Th decay series. Two isotope ratios,  $n(^{207}\text{Pb})/n(^{206}\text{Pb})$  and  $n(^{208}\text{Pb})/n(^{206}\text{Pb})$ , have demonstrated significant variability between mine sites and geological settings due to the age of the deposit and the concentration of the associated parent U and Th (Keegan et al., 2008; Švedkauskait-Le Gore, 2008; Varga et al., 2009; Fahey et al., 2010; Keegan et al., 2014). Additionally, Pb isotopes have been used to distinguish between natural U samples, samples which result from processing activities and those originating from anthropogenic activities (Fahey et al., 2010). Intra-mine variability is assessed in two of the aforementioned studies but there is no general agreement to what extent this occurs. Švedkauskait-Le Gore (2008) demonstrates that samples from the same geolocation appear to have largely similar Pb isotopes and yet Varga et al. (2009) notes that there is significant Pb variability in UOC that have originated from the same mine site as a result of heterogeneous Pb distribution in the ore body and due to the processing effects from chemical separation and dilution with natural Pb. Additionally, it has been noted that uraninite and possibly other uranium

minerals may not be considered stable enough to resist weathering, resulting in loss of Pb (Fahey et al. 2010).

#### **1.4.1.3 Strontium**

Strontium isotopes have been shown to vary over a wide range of samples with different geographic origins (Varga et al., 2009) and is influenced by the age of the deposit and other geological factors such as the abundance of alkali metal-rich minerals (therefore dependent on geological deposit type). The isotope ratio used by Varga et al. (2009) was  $^{87}\text{Sr}/^{86}\text{Sr}$  as  $^{87}\text{Sr}$  fluctuates widely in nature due to the long half-life ( $4.923 \times 10^{10}$  years) of its parent,  $^{87}\text{Rb}$ . Variation within uranium deposits and milling-derived alteration of the isotopic signature is lower than Pb isotopes. Similar types of deposit have similar Sr isotopic composition resulting in the requirement for a multi-variant approach for provenance determination.

#### **1.4.1.4 Sulphur**

The high variation between  $^{34}\text{S}/^{32}\text{S}$  in nature led one study to assess whether the S content of the U-ore feed combined with the introduced S from sulphuric acid during ore leaching could be used for provenance determination of UOCs (Han et al., 2013). The  $\delta^{34}\text{S}$  values (a direct comparison of  $^{34}\text{S}/^{32}\text{S}$  in the sample relative to known standards) demonstrated significant differences between a global set of UOCs.

#### **1.4.1.5 Neodymium**

The isotope ratio of  $^{143}\text{Nd}/^{144}\text{Nd}$  was measured via MC-ICPMS and demonstrated significant variation between UOCs and was dependent on the geological deposit type, the age of the deposit and the Sm/Nd ratio (Krajko et al., 2014). Intra-mine variability was far lower than that observed for Pb or Sr but cannot be used a solitary signature for nuclear forensic purposes due to many samples having comparable Nd isotope ratios.

## **1.4.2 UOC Impurities and trace elements**

### **1.4.2.1 Rare earth elements**

The rare earth elements (REE) consist of the 15 lanthanides plus yttrium and scandium but for the purposes of this study, REE only refers to the lanthanides. The REE concentration pattern in U-ore and UOC is an important signature for nuclear forensic investigations (Varga et al., 2010a, 2010b) as the REE pattern is characteristic of the mineralisation process and the geological deposit (Mercadier et al., 2011). Additionally, there is no fractionation during the uranium milling process in the production of UOC (Varga et al., 2010b) due to REEs having the same oxidation state (3+) with exception to Ce (IV) and Eu (II). The REE pattern is usually chondrite normalised to eliminate the nuclear stability effect (Oddo-Harkins rule – (Oddo, 1914; Harkins, 1917)). The Oddo-Harkins rule stipulates that elements with an even atomic number are more common than elements with an odd atomic number. Odd numbered elements tend to have lower nuclear binding energies and therefore are generally less stable than the even elements.

The REE concentrations have been measured via HR-ICPMS after chemical separation using TRU resin (Varga et al., 2010b, 2010a) and more recently have been measured from laser ablating doped cation exchange resin with reduced isobaric interferences from oxides and hydroxides (Donard et al., 2015) and by Electron Probe Microanalysis (Keatley et al., 2015)

### **1.4.2.2 Anionic and organic**

Anions such as sulphate, chloride, nitrate and fluoride have been investigated in UOCs as potential signatures and were found to be either source related ( $F^-/Cl^-$ ) or process related ( $SO_4^{2-}/Cl^-$ ). The elevated fluorine was found in UOCs produced from phosphate ores which typically contain apatite minerals ( $Ca(PO_4)_3F$ ). Other anionic impurities such as nitrate/chloride and phosphate/chloride demonstrated differences between uranium deposits used for UOC production (Badaut et al., 2009; Keegan et al., 2012). The sulphate/chloride ratio has been used to indicate milling facilities that use sulphuric acid in the leaching of uranium.

Residual organic compounds are present in UOC from the milling process and provide information about the process and solvents used (mostly for SX purification). One study has been conducted to assess the variability and abundance of various organic constituents

between two different UOC production lines by extracting the organic components from the UOC and measuring via GC-MS (Kennedy et al., 2013). The two production lines had very different organic fingerprints and the author suggests that this could be used as an identification tool for nuclear forensics.

#### **1.4.2.3 Major elements and trace minerals**

X-ray fluorescence (XRF) (energy and wave dispersive) have been used to characterise the elemental compositions of bulk materials and UOC where the major element composition is  $> 100 \mu\text{g/g}$  (Keegan et al., 2008). The authors claim the XRF data are comparable with ICPMS data (within 20% uncertainty) but the XRF data was not displayed.

Laser-Induced Breakdown Spectroscopy (LIBS) ionises the surface of a sample and produces a photon emission spectrum where each recorded wavelength peak is characteristic of a particular element. LIBS has been successfully used in the identification of UOC with the aid of Principal Components Analysis (PCA) (Sirven et al., 2009).

#### **1.4.3 UOC Age or production determination**

The age of a suspect sample is a critical piece of information for nuclear forensic investigations. An accurately determined age refers to the time in which the sample was last chemically separated or purified where the progeny isotopes are completely removed from the radioactive parent (usually uranium or plutonium). The subsequent ingrowth of the progeny radionuclides by radioactive decay and the measurement of these progeny radionuclides in relation to the respective parent serves as a chronometer using well understood decay equations (Stanley, 2012; Stanley et al., 2013; Williams & Gaffney, 2011; Williams et al., 2009; Wallenius et al., 2002).

The age determination of uranium or plutonium refers to the “model” age as two primary assumptions are required: 1) the complete separation of progeny radionuclides from the parent was fully achieved at  $t=0$  and 2) a closed system has been maintained in the sample since purification/separation (e.g. no gain or loss of the parent or daughter radionuclides other than that from radioactive decay (Aggarwal, 2016; Keegan et al., 2016)).

The most common chronometer for nuclear forensics is  $^{234}\text{U}/^{230}\text{Th}$  but other chronometers (Table 1-6) are required for concordant “model” ages to improve confidence in the data.

Additionally, the  $^{234}\text{U}/^{230}\text{Th}$  chronometer requires extremely sensitive measurement techniques (e.g. MC-ICPMS) due to the long half-life of  $^{234}\text{U}$  ( $2.46 \times 10^5$  years) and low detection limits of  $^{230}\text{Th}$ . Alpha and gamma spectrometry can be used as a measurement technique for this chronometer also but will be addressed in section 1.4.4.

**Table 1-6: Common chronometers used for determining “model” ages of U samples.**

<b>Chronometer (parent/daughter)</b>	<b>U Application</b>
$^{234}\text{U}/^{230}\text{Th}$	All natural samples containing U
$^{235}\text{U}/^{231}\text{Pa}$	All U samples including DU
$^{232}\text{Th}/^{228}\text{Th}$	All natural samples containing U
$^{234}\text{U}/^{214}\text{Bi}$	All natural samples containing U
$^{238}\text{U}/^{234}\text{Th}$	HEU only
$^{236}\text{U}/^{232}\text{Th}$	Irradiated or reprocessed only

Age determination of UOCs using these approaches is limited due to the high level of impurities (Varga et al., 2011b) and because complete separation of the progeny radionuclides is more difficult to achieve.

#### **1.4.4 UOC Radiological measurements**

##### **1.4.4.1 Alpha spectrometry**

Alpha spectrometry has been used for accurate age determination of HEU using the  $^{234}\text{U}/^{230}\text{Th}$  chronometer and has comparable results to ICPMS methods (Wallenius et al., 2002). Alpha spectrometry has also been used for the determination of  $^{232}\text{U}$ ,  $^{236}\text{U}$  and Pu to determine whether a sample has undergone irradiation or reprocessing (Varga & Surányi, 2009).

##### **1.4.4.2 Gamma spectrometry**

Gamma-ray spectrometry is a non-destructive means of initially characterising illicitly recovered nuclear materials and is the one of the first analytical methods that should be undertaken on suspect materials. Gamma spectrometry provides information on approximate uranium isotopic abundance, indicates the extent of ingrowth of daughter radionuclides in the natural decay series, and whether activation and fission products are present. A couple of studies have also successfully determined the ages of U-bearing materials via high-resolution gamma spectrometry using the  $^{234}\text{U}/^{214}\text{Bi}$  chronometer (Nguyen & Zsigrai, 2006; Nguyen et al., 2009).

#### **1.4.5 UOC Structural and morphological measurements**

##### **1.4.5.1 SEM & TEM**

The Scanning Electron Microscope (SEM) is a valuable tool for nuclear forensic investigations and is the most common means of observing the microstructure and morphology of samples. SEM has been used to make direct comparisons between a previously characterised UOC and an unknown samples (Varga et al., 2011a; Keegan et al., 2014). The SEM can also be used to gain elemental data at micron scale using an electron dispersive X-ray detector.

Transmission Electron Microscopy (TEM) allows for internal structure or morphology of extremely small (micron to nanometre) samples to be analysed. The sample preparation is more delicate and the instrument is more expensive to run than SEM and therefore not widely used in nuclear forensic laboratories.

#### **1.4.5.2 Electron microprobe analysis**

Electron microprobe analysis (EPMA) has been used to measure REE and major elemental concentrations in uranium minerals to demonstrate elemental heterogeneity in a single 3m long uranium vein (Keatley et al. 2015). The detection limit was approximately 100 ppm. The study demonstrated that significant heterogeneity in elemental composition can be observed in a uranium vein demonstrating that care needs to be taken when extrapolating the origins of UOC.

#### **1.4.5.3 Raman spectrometry**

Raman spectra were collected for 89 UOCs and statistically visualised using Principal Components Analysis and Partial Least Square analysis to identify commonalities and differences between the set of UOCs (Ho Mer Lin et al., 2015). This study concluded that it would be possible to assign an unknown UOC to a class based on this statistical representation of the samples for future nuclear forensic investigations.

#### **1.4.5.4 Infrared spectrometry**

Fourier-Transform Infrared spectrometry (FTIR) and Near Infrared spectrometry (NIR) has been applied to UOC studies to identify the type of U compound present and identify any impurities present in the mid-IR spectrum and demonstrates that this technique could be used for future identification of suspect samples (Varga et al., 2011a; Klunder et al., 2013; Plaue et al., 2013).

#### **1.4.5.5 XRD**

X-ray diffraction (XRD) has been used for phase determination of U in UOC samples (Aggarwal, 2016) and also for determining trace minerals and gangue (Reynolds et al., 2010). XRD would also be able to identify chemicals in U-ore and UOC which may be associated to the ore processing.

## 1.5 Thesis Outline

This thesis is comprised of two main sections. Chapters 2 and 3 investigate the use of radiometric spectrometry techniques to accurately characterise uranium-bearing samples and statistically discriminate the results. Gamma spectrometry is regarded as one of the first nuclear forensic measurement techniques to identify the composition of a recovered nuclear specimen. The accurate characterisation of a sample via gamma spectrometry requires knowledge of the physical and chemical properties as well as the assumption that the sample is homogeneous. Chapter 2 assesses the problems of measuring a sample in which no information is available and investigates how photon attenuation occurs in uranium-bearing samples including U-ore and uranium ore concentrate (UOC). Significant attenuation of low to medium energy photons (including minor attenuation of  $^{234\text{m}}\text{Pa}$  – 1001 keV) led to the development of a dissolution procedure using lithium tetraborate flux. The resulting aqueous and homogeneous sample produces a consistent matrix which requires no geometry corrections or sample-specific matrix matching and requires no theoretical corrections to the collected data. This sample preparation procedure was then used to characterise 19 UOCs by gamma and alpha spectrometry (Chapter 3) by using major gamma radionuclides of the three natural decay chains ( $^{238}\text{U}$ ,  $^{235}\text{U}$  and  $^{232}\text{Th}$ ) and the alpha emitting  $^{210}\text{Po}$  as a proxy for  $^{210}\text{Pb}$ . The radiometric data were then statistically analysed by Principal Components Analysis (PCA) to determine whether solitary or groupings of samples in 3-dimensional space could provide trends to identify likely origins of the samples. The PCA was validated by re-preparing six of the UOCs and incorporating the data back in to the original PCA. Half of the UOCs were outliers in the PCA model and therefore had unique radiometric properties. The other half grouped together and shared some similarities such as country of origin.

The second section of this thesis investigates a laser ablation ICPMS sample preparation technique and its application and implications for nuclear forensics. In Chapter 4, the sample preparation technique was tested and validated for UOC and a wide range of geological reference materials. The glass beads were prepared by diluting 1.5 mg of sample with  $\text{MgSiO}_3$  (enstatite) so that the silica content available for glass forming is approximately 50%. This step is critical for production of UOC glass as silica content in UOC is extremely low. A selection of geological and uranium reference materials were also prepared as glass beads and analysed via LA-ICPMS. The glass beads were homogeneous

## Chapter 1

and provided accurate element concentrations compared to certified values despite the low sample mass. The rare earth element (REE) signatures were investigated and matching profiles were obtainable from this technique compared to known values when chondrite normalised. Chapter 5 uses this sample preparation technique to produce two sets of the 19 UOCs as glass beads. The glass beads are then measured for REE in order to obtain a chondrite-normalised signature which has proven in the literature to be a key identifier of a samples geological origin. The REE data obtained from LA-ICPMS was validated by chemically purifying digested UOC using ion exchange chromatography. The solution and laser derived data were complementary to one another demonstrating that the laser ablation technique is a valid tool for determination of REE in UOC.

Finally, Chapter 6 surmises the findings of this thesis and Chapter 7 introduces the future work that is possible from other data collected during this project.

## **Chapter 2: A Rapid Dissolution Procedure to Aid Initial Nuclear Forensic Investigation of Chemically Refractory Compounds and Particles Prior to Gamma Spectrometry**

Reading et al 2015, *Analytica Chimica Acta*, **900**. P1-13 (Featured Article)

### **Abstract**

A rapid and effective preparative procedure has been evaluated for the accurate determination of low-energy (40-200 keV) gamma-emitting radionuclides ( $^{210}\text{Pb}$ ,  $^{234}\text{Th}$ ,  $^{226}\text{Ra}$ ,  $^{235}\text{U}$ ) in uranium ores and uranium ore concentrates (UOCs) using high-resolution gamma ray spectrometry. The measurement of low-energy gamma photons is complicated in heterogeneous samples containing dense, high-mass, mineral phases. Attenuation corrections using mean density estimates result in an underestimation of the activity concentration where dense grains are dispersed within a less dense matrix (analogous to a nugget effect). The current method overcomes these problems using a lithium tetraborate fusion that readily dissolves all components including high-density, self-attenuating minerals/compounds. This is the ideal method for dissolving complex, non-volatile components in soils, rocks, mineral concentrates, and other materials where density reduction is required. This approach avoids the need for theoretical corrections or sample-specific matrix matching. The resulting homogeneous quenched glass produced can be quickly dissolved in nitric acid. The technique has been tested on uranium-bearing Certified Reference Materials and provides accurate activity concentrates compared to the underestimated activity concentration estimates derived from direct measurements of a bulk sample. The procedure offers an attractive solution for initial nuclear forensic studies where complex refractory minerals or matrices exist and is significantly faster, safer and simpler than alternative approaches and produces low-density solutions that can be counted by gamma spectrometry.



## 2.1 Introduction

As of 31<sup>st</sup> December 2013, the IAEA Incident and Trafficking Database (ITDB) contained 2,477 confirmed incidents of illicit trafficking and other unauthorised events involving nuclear and radioactive material outside of regulatory control, reported by 120 participating states dating back to 1993 (IAEA, 2014). In 2013 alone, there were 54 confirmed incidents involving unauthorised possession, criminal activities, theft, or loss of gram quantities of highly enriched uranium or plutonium as well as devices from industrial and medical facilities most commonly containing  $^{192}\text{Ir}$ ,  $^{137}\text{Cs}$  and  $^{241}\text{Am}$ . An additional 93 incidents are reported as unauthorised activities that include the discovery of uncontrolled sources or unauthorised disposals and shipments. These numbers will rise due to a reporting lag time of up to 3 years.

The Nuclear Forensics International Technical Working Group (ITWG), recommends High Resolution Gamma Spectrometry (HRGS) as the initial measurement technique on receipt of unknown, recovered nuclear materials such as uranium ore and uranium ore concentrate (UOC aka yellowcake) enabling rapid characterisation of the uranium content and, if applicable, the degree of isotopic enrichment/depletion (Mayer et al., 2005; Wallenius et al., 2006; Hanlen, 2011; Kristo, 2012; Hutcheon et al., 2013). Development of a database of gamma nuclide signatures for U-ores and UOCs of known provenance would aid in the identification of the origin and history of recovered illicit nuclear materials as part of a nuclear forensics investigation.

For accurate measurements of gamma radioactivity, a matrix-matched calibration standard with the same physical and chemical composition, density, and nuclide distribution as the sample is required to determine the photon detection efficiencies of the gamma detector. For some sample types, such matched calibration standards are unavailable or impractical to prepare resulting in a potential over or under-estimation in photo-peak efficiencies. This is especially critical for U-ores and UOCs where the U phases and other gangue minerals may be heterogeneously distributed with different U minerals having varying densities (e.g. pitchblende =  $8.5 \text{ g cm}^{-3}$ , brannerite =  $5.5 \text{ g cm}^{-3}$ , coffinite =  $5 \text{ g cm}^{-3}$ ). Any low-energy gamma emissions from  $^{238}\text{U}$  and  $^{235}\text{U}$  daughters contained in these dense mineral phases will undergo significant attenuation (Table 2-1).

**Table 2-1: Selected gamma emitting radionuclides with associated X-radiations where  $E_\gamma = < 200$  keV and emission probability  $> 1\%$ .**

Radionuclide	$E_\gamma$ Energy (keV)	Emission Probability (%)
Pb X-ray $K_\alpha$	74.82	59.7
	77.11	100
Pb X-ray $K_\beta$	86.8 - 87.8	34.3
U X-ray $K_\alpha$	89.96	61.8
	93.35	100
U X-ray $K_\beta$	104.82 – 106.31	35.6
Th X-ray $K_\alpha$	92.29	62.14
	95.87	100
Th X-ray $K_\beta$	107.60 – 109.07	35.84
$^{210}\text{Pb}$	46.54	4.25
$^{241}\text{Am}$	59.54	35.92
$^{234}\text{Th}$ ( $^{238}\text{U}$ )	63.30	3.75
	92.38	2.18
	92.80	2.15
$^{231}\text{Th}$	84.21	6.70
	89.95	1.01
$^{228}\text{Th}$	84.37	1.19
$^{235}\text{U}$	109.19	1.66
	143.77	10.94
	163.36	5.08
	185.72	57.00
	202.12	1.08
	205.32	5.02
$^{226}\text{Ra}$	186.21	3.56

There have been two general approaches to produce attenuation correction factors where samples do not match the calibration standards: **experimental** (Cutshall et al., 1983; Kitto, 1991; Venturini & Vanin, 1993; Bolivar et al., 1996; Hussain et al., 1996; San Miguel et al., 2002; McMahon et al., 2004; Długosz-Lisiecka & Bem, 2013) and **theoretical** via Monte-Carlo simulations (Sima & Dovlete, 1997; Jurado Vargas et al., 2002; Pilleyre et al., 2006). The experimental studies mostly focus on environmental sample matrices with emphasis on determining  $^{210}\text{Pb}$  activity concentrations. Cutshall et al., (1983) designed a technique to measure the extent of attenuation through an unknown matrix by making a direct transmission observation of  $^{210}\text{Pb}$ . This method however, required a kilo-Becquerel point source of  $^{210}\text{Pb}$  to be positioned above the sample medium and required two measurements, with and without the source. For laboratories using well-type detectors, a similar technique to Cutshall et al., (1983) would require an axial source to be embedded within the sample, which could be impractical for solid matrices.

The work of Długosz-Lisiecka & Bem, (2013) assumes that  $^{210}\text{Pb}$  is in a state of secular equilibrium with  $^{238}\text{U}$  and uses activity concentrations of other  $^{238}\text{U}$  progeny as a proxy to determine a self-attenuation correction factor for matrices of varying composition. For nuclear forensic characterisation, a state of secular equilibrium cannot be assumed as a sample may have been subjected to milling, processing or enrichment which would alter the extent of equilibrium through the decay chain.

Monte-Carlo simulations require prior knowledge about the sample such as chemical composition, grain size and radionuclide distribution which, along with coding and running the simulation, can be time consuming, delaying the nuclear forensic characterisation programme. Such simulations rely on repeated random sampling to establish an 'expected' behaviour over many events, based upon the rules governing the simulation. Monte-Carlo Transport Codes such as MCNP (Monte-Carlo n-particle) and Geant4 (Geometry and Tracking 4) simulate particle transport through matter, and are utilised for a variety of applications, including high-energy, nuclear and accelerator physics, as well as studies in medical and space science.

The current study focused on developing a procedure to reliably determine low to medium energy gamma-emitting radionuclides in U-bearing samples with no prior knowledge of sample composition. It also planned to avoid using the direct transmission approach to measure the sample mass-attenuation coefficient and to avoid using proxy radionuclides

to assume daughter activity concentrations. To achieve these aims, a rapid method was devised to eliminate or reduce attenuation problems caused by the 'hot-particle effect' and/or high-density matrices.

Borate fusion is well-established as a sample digestion or dissolution method in analytical chemistry and geochemistry and is known to be effective in dissolving minerals and rocks comprising oxides, carbonates, chlorides, sulphates, and phosphates. It can also be applied to organic, sulphidic and even metallic materials if preceded by an oxidation step. An early variant of the procedure used in qualitative analytical chemistry was the classical borax bead procedure (Brush & Penfield, 1898). Borate fusions were extensively used in the geosciences from the 1960's having been introduced as a method in XRF analysis (Claisse, 1957; Claisse & Samson, 1962). In spite of these applications there is no evidence of the method having been applied in radioanalytical chemistry.

Given the beneficial characteristics of borate fusions it is surprising that there were no reported applications in the field of radioanalytical chemistry until the work of Croudace et al., (1997). Prior to that study all reported radioanalytical preparations used a range of less effective, laborious and hazardous methods such as acid attack (HCl, HNO<sub>3</sub>, HF in open or closed vessels), alkali fusion (carbonate, hydroxide, peroxide) or fusion with fluoride followed by K pyrosulfate (Table 2-2).

Table 2-2: Dissolution methods

Digestion method	Silicates	Oxides	Sulphates	Carbonates	Borates	Phosphates	Metals*	Problems / comments	References
Strong mineral acids				X	X		X	Pressure vessels and elevated temperatures may be required. Full recovery of analytes potentially low. Oxidation of sample may be required to prevent volatilisation. Difficult to achieve full U dissolution. Possible volatility issues with: As, Ge, S, Sb, Se.	1
HF / HClO <sub>4</sub> Acid mix	X	X		X	X	X	X	Small sample volumes treatable. HF needs to be removed. Insoluble fluoride precipitates in large sample volumes. Perchlorates potentially explosive. Frequently requires the use of HCl and/or HNO <sub>3</sub> . Possible volatility issues with: As, B, Ge, Sb.	2
HF / H <sub>2</sub> SO <sub>4</sub> Acid mix							X	Small sample volumes treatable. HF needs to be removed. Many evaporation stages.	1
Alkali fluoride with pyrosulfate	X			X				Hazardous and requires treatment with pyrosulfate to remove fluorides. Will attack Pt hardware.	3
NaCO <sub>3</sub> fusion	X			X	X		X	Opens out mineral lattices but requires lengthy treatment. Dissolution of Pt hardware possible. Elevated Pb or Fe(II) will alloy with Pt hardware. Possible volatility issues with: As, Hg, Tl, Se.	4 & 5
NaOH fusion	X			X			X	Opens out mineral lattices but requires lengthy treatment. Dissolution of Pt hardware possible.	6 & 7

**Table 2-2 Continued: Dissolution methods**

Digestion method	Silicates	Oxides	Sulphates	Carbonates	Borates	Phosphates	Metals*	Problems / comments	References
Na <sub>2</sub> O <sub>2</sub> fusion or sinter with acid digestion	X						X	Small sample volumes treatable. Time intensive procedure. Requires use of hot mineral acids. Dissolution of Pt hardware possible. Typical fusion temperature of 250-500 °C. Possible volatility issues with: Au & Ru.	8 - 10
Borate fusion Followed by acid digestion	X	X	X	X			X	Very few issues. Sample size can vary from small to large. Sample:flux ratios from 1:1 upward. Very minor damage potential to Pt hardware. Typical fusion temperature < 1200 °C. Possible volatility issues with: Hg, Pb & Tl.	11 & 12
Flux free fusion & acid digestion	X	X	X	X			X	Small sample volumes treatable. Conducted in non-oxidising atmosphere. Typical fusion temperature > 1300 °C. May require addition of SiO <sub>2</sub> and MgO if silicate poor to help glass formation. Possible volatility issues with: Hg, Pb & Tl.	13 & 14

\* - A prior use of oxidants or nitric acid digestion is required.

1: Bock (1979), 2: Parsa (1992), 3: Sill et al. (1974), 4: Fisher & Kunin (1957), 5: Seim et al. (1957), 6: U.S. Environmental Protection Agency (2014), 7: Smith et al. (1995), 8: Rafter (1950), 9: Enzweiler et al. (1995), 10: Galindo et al. (2007), 11: Croudace et al. (1997), 12: Croudace et al. (1998), 13: Fedorowich et al. (1993) 14: Nehring et al. (2007).

## 2.2 Methodology

Three certified reference materials (CRMs) for uranium (CUP-1, BL-5 and CUP-2, Canadian Certified Reference Materials Project, Ottawa, Canada; Table 2-3) were selected for this study. Detailed mineralogical data and average grain size of each mineral present in CRMs CUP-1 and CUP-2 were obtained via QEMSCAN (Quantitative Evaluation of Minerals via Scanning electron microscopy) (Pirrie et al., 2004; Pirrie & Rollinson, 2011). The CRM BL-5 was not characterised via QEMSCAN as CUP-1 and CUP-2 are regarded as most typical of U-ore and UOC respectively. The CRM CUP-1 consists of grains of U-bearing phases of approximately 18  $\mu\text{m}$  diameter dispersed in a similarly sized less dense matrix containing potassium feldspar, biotite mica, and quartz. CUP-2 consists of homogeneous and discernible uranium-bearing phases with an average grain size of 70  $\mu\text{m}$  dispersed amongst a trace matrix grain size of 25  $\mu\text{m}$  consisting of feldspars, micas, quartz, and gypsum. Each CRM was initially characterised as supplied via HRGS. Sets of experiments were then conducted to understand the cause of self-attenuation observed in U-bearing samples whilst developing a method to overcome this. The CRM BL-5 was diluted with cellulose to reduce sample bulk density, and to assess the effect that U-bearing grain concentration has on the attenuation of low-energy gamma photons. CRM BL-5 was selected due to its elevated U-concentration while demonstrating secular equilibrium through the progeny. A specimen of pitchblende from a deposit known to also contain various copper, tin and iron minerals from Wheal Providence, St. Ives, Cornwall, UK with U concentration of approximately 30% was crushed, ground and separated based on grain size. The pitchblende fractions were analysed to assess the effect that uraninite grain size variation has on photon-attenuation. In addition, a series of Monte-Carlo simulations were performed to computationally simulate the above experiments and to predict differences in photon detection efficiency between the high and low uranium grade CRMs.

**Table 2-3: Certified Reference Materials Data**

	<b>CUP-1</b>	<b>BL-5</b>	<b>CUP-2</b>
References	1	2-4	5
Uranium wt%	0.128	7.09	75.42
Uncertainty $\pm$ wt%	0.002	0.03	0.17
Classification	U-ore	U-ore <sup>a</sup>	UOC
Secular equilibrium	Yes	Yes	No
<sup>238</sup> U (Bq g <sup>-1</sup> ) <sup>b</sup>	15.8 $\pm$ 0.3	876 $\pm$ 3.7	9313 $\pm$ 21
<sup>235</sup> U (Bq g <sup>-1</sup> ) <sup>b</sup>	0.7 $\pm$ 0.01	41 $\pm$ 0.2	434 $\pm$ 1
<sup>226</sup> Ra (Bq g <sup>-1</sup> )	As parent U	866 $\pm$ 21	N/A
<sup>210</sup> Pb (Bq g <sup>-1</sup> )	As parent U	857 $\pm$ 38	N/A

**1: Dalton & Bowman (1986), 2: Faye et al. (1979), 3: Smith & Steger (1983), 4: Smith & Steger, (1984), 5: Dalton & Bowman (1988).**

<sup>a</sup> **BL-5 is described as a “low-grade concentrate” in its certificate.**

<sup>b</sup> **Activity concentration calculated from certified U wt% assuming natural <sup>238</sup>U/<sup>235</sup>U abundances (99.275% and 0.72% respectively).**

### **2.2.1 Instrumentation**

Radionuclide activity concentrations were determined using Canberra 50% N-type HPGe well type gamma-ray spectrometers (Figure 2-1 and 2-2). Gamma spectra were collected using Genie 2000 acquisition software (Canberra Industries, Harwell, UK) and were analysed using Fitzpeaks spectral deconvolving software (JF-Computing, Stanford in the Vale, UK). The spectrometers were previously calibrated using a traceable, mixed nuclide source (NPL, Teddington, UK) with the addition of a <sup>210</sup>Pb solution standard (PTB, Braunschweig, Germany) mixed into a range of different density matrices (cellulose, water, sand, steel and boron and a tin-tungsten ore) to produce a set of efficiency calibrations.



**Figure 2-1: One of eight Canberra HPGe detector with dewar and Cu coated Pb shielding at GAU-Radioanalytical, Southampton, UK**

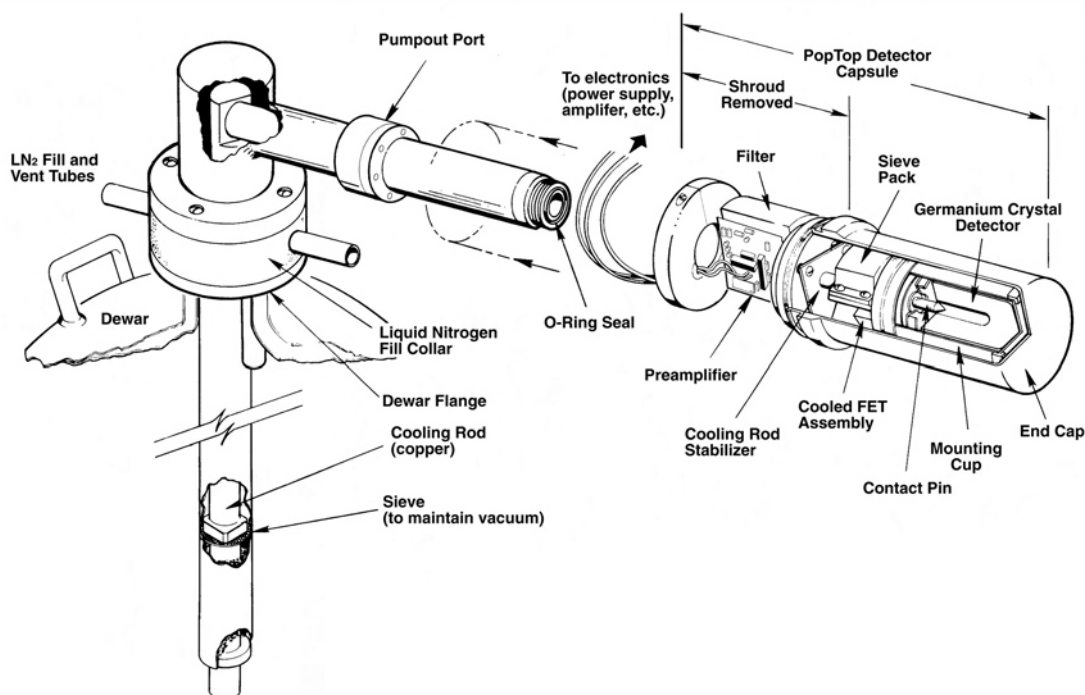


**Figure 2-2: Expanded schematic of an HPGe detector housing**  
(Gilmore & Hemingway, 1995).

All samples were counted for 1 hour as this was found suitable to obtain adequate counting statistics as no improvement in activity uncertainty is achieved by counting beyond this time. The limit of detection values presented in this study are based on the decision limit (or critical level),  $L_c$ , as defined by Currie (1968) which is defined as the signal level above which an observed instrument response may be reliably recognised as “detected”.

### 2.2.2 Initial characterisation of CRMs

All three CRMs were weighed into 20 mL polythene vials (CUP-1 = 28.1 g, BL-5 = 31.6 g, CUP-2 = 34.8 g) and the bulk densities were calculated (1.36, 1.53 and 1.68 g cm<sup>-3</sup> respectively). Apparent photon efficiencies of each measured radionuclide were calculated based on the bulk density of each CRM from the known relationship between photon detection efficiency and sample density acquired from the calibration standards. The samples were characterised for <sup>210</sup>Pb, <sup>234</sup>Th, <sup>226</sup>Ra, <sup>235</sup>U and <sup>234m</sup>Pa activity concentrations where <sup>234</sup>Th is measured as a proxy for the non-gamma-emitting <sup>238</sup>U. The high-energy photon of <sup>234m</sup>Pa (1001 keV) was measured, as the degree of attenuation of this photon should be significantly less than the other radionuclides. Lead-214 and <sup>214</sup>Bi were not assessed due to the potential for disequilibrium between <sup>222</sup>Rn and <sup>226</sup>Ra, due to radon off-gassing. If this is the case, sufficient ingrowth is required for accurate measurements and would not be in the timescales for nuclear forensic investigations.

### 2.2.3 Borate fusion for homogenisation

Approximately 0.6 g of each CRM was heated at 600 °C in air for 3 hours to oxidise the sample to inhibit volatilisation of elements such as Pb due to the high temperature conditions of the fusion procedure (1200 °C) as well as remove any moisture present. An aliquot of 0.5 g of sample was weighed in to a grain stabilised, Pt- 5% Au crucible (Heraeus, Germany) followed by 0.5 g di-lithium tetraborate flux (Fluxana, Germany). The amount of flux used depends on whether the prime purpose is simply to open-out minerals for subsequent acid digestion (low sample:flux of approximately 1:1) or to dissolve the sample in the flux (approximately 1:2). The crucible was agitated briefly to mix the two components. Sodium tetraborate fluxes can be used but requires a higher flux:sample ratio of 2:1 due to higher melt viscosities. The crucible was loaded on to a Vulcan Fusion Machine (Fluxana, Germany) where the sample was heated to 1200 °C and agitated periodically over

a period of 10 minutes. The resulting melt was quenched in 50 mL of Milli-Q water (Millipore, USA). The crucible was placed into the Milli-Q water and acidified with 50 mL of concentrated  $\text{HNO}_3$  to produce approximately 8M acid to digest any residual melt retained in the crucible. After 30 minutes, the Pt crucible was removed and cleaned with Milli-Q water and the rinsings were recovered with the digest. The samples were heated on a hot-plate at 80 °C to reduce the volume to ~30 mL.

The acid digestion of the fused material is comparatively rapid and frequently accompanied by the precipitation of boric acid and silica, which have been shown not to adsorb radionuclides. Each fused sample was vacuum filtered through a Whatman filter No. 540, which supported a Whatman GF-C filter paper. The filter papers were rinsed with 8M  $\text{HNO}_3$  and effectively retained the precipitate resulting in a clear solution being collected. The precipitate was measured via well-type HPGe and planar LEGe gamma spectrometers for 24 hours and contained no detectable radioactivity. The filtered solutions were evaporated to approximately 15 mL, transferred to a 20 mL vial including the washings and made up to 20 mL. The samples were counted immediately to allow determination of  $^{210}\text{Pb}$ ,  $^{234}\text{Th}$ ,  $^{226}\text{Ra}$ ,  $^{235}\text{U}$  and  $^{234\text{m}}\text{Pa}$  activity concentrations. The calibration was made using a mixed gamma efficiency function. During the high temperature fusion process, volatile  $^{222}\text{Rn}$  undergoes degassing and thus the high-energy gamma photons of  $^{214}\text{Pb}$  and  $^{214}\text{Bi}$  would bias low due to their short half-lives (26.9 minutes and 19.8 minutes respectively). It should be noted that if these radionuclides are to be assessed, the samples would need to be sealed to ensure radon retention as secular equilibrium is restored. Therefore,  $^{214}\text{Pb}$  and  $^{214}\text{Bi}$  are not assessed in this study, as the timescales required for accurate measurement would not be typical of a nuclear forensic study.

## **2.2.4 Understanding the cause of self-attenuation**

### **2.2.4.1 Bulk density effect**

Five samples containing CRM BL-5 were weighed into 20 mL polythene vials in increments of 1, 2, 3, 4 and 5 g, filled with cellulose ( $0.6 \text{ g cm}^{-3}$ ), and blended to produce well-mixed samples. The samples were characterised for  $^{210}\text{Pb}$  and  $^{234}\text{Th}$  activity concentrations by gamma spectrometry as these radionuclides would be the most susceptible to minor matrix alterations and associated photon detection efficiency due to their low energy gamma

emissions (Table 2-1). The photon detection efficiencies were calculated based on the bulk density of each homogenised sample (0.68, 0.73, 0.82, 0.89 & 0.97 g cm<sup>-3</sup> respectively).

### **2.2.4.2 Particle size effect**

A specimen of pitchblende was crushed and sieved to produce 5 aliquots of varying grain size range (>250, 250-125, 125-75, 75-63 & >63 µm). Exactly 0.3 g of each size fraction was weighed in to 20 mL polythene vials, filled with acid-washed sand and homogenised. As above, the samples were characterised for <sup>210</sup>Pb and <sup>234</sup>Th activity concentrations. The photon detection efficiencies were calculated as previously described to reflect the bulk density of each sample (~1.5 g cm<sup>-3</sup>). A sample blank consisting of acid-washed sand was analysed and the measured activity was subtracted as a background from the pitchblende and sand samples. To ensure that each particle fraction had equal U mineral distribution, each fraction was fused as described in section 2.2.3. The radionuclide activity across the five fractions were identical within uncertainty demonstrating that each fraction contained equal U mineral concentration.

### **2.2.4.3 Monte-Carlo simulations**

A series of simulations were conducted using the Geant4 platform developed at CERN (Agostinelli et al., 2003), which simulates the movement of particles through matter and is based on the Monte-Carlo N-Particle code from Los Alamos National Laboratory, USA. Monte-Carlo based simulations are based on repeated random sampling to establish the most probabilistic behaviour of particle pathways.

The simulations were designed and conducted to evaluate the effect that grain size and grain concentration/density has on the efficiency of low-energy gamma photons of <sup>210</sup>Pb (46.5 keV) and <sup>234</sup>Th (63.3, 92.4 and 121.8 keV). In both simulations, the emission point was from the centre of dense uraninite grains (8.5 g cm<sup>-3</sup>) dispersed in a less-dense matrix resulting in an average density of 2.6 g cm<sup>-3</sup>. Uraninite was selected as the U mineral in this simulation as it is the densest of all U minerals and would therefore demonstrate the most intense photon attenuation. The grain size simulation used a random number generator to assign 50,000 grain positions of identical grain size within the source volume using grain sizes of 10-80 µm in increments of 10 µm. At each position, a void in the matrix equalling the grain size being modelled was replaced with a uraninite grain. The grain concentration

simulation had grain positions determined in the same way though the grain size was fixed at 100  $\mu\text{m}$ . The concentration of grains ranged from 0 to  $1 \times 10^6$  grains. The simulation with 0 grains, i.e. a homogeneous fluid, had photons originate from within the matrix rather than a dense uraninite grain. Once potential photon positions were determined, a second random number generator was used to determine which position entry was used as an emission point. Photon efficiencies were calculated by firing photons isotropically from one of the randomised positions within the source volume and recording the number of full photopeak energy depositions seen in the modelled HPGe crystal.

Additional simulations were conducted to assess the emission efficiency of photons originating within grains of defined density. Simulations were performed for photon emissions arising from the centre of a grain, randomly throughout a grain, and from a homogeneous medium with no grains present. The simulations used the compositional data acquired from QEMSCAN analyses conducted at The University of Exeter's Camborne School of Mines. The uranium grains were randomly positioned in the bulk volume by removing voids matching the average uranium grain size (CUP-1 = 16  $\mu\text{m}$  and CUP-2 = 70  $\mu\text{m}$ ). Each sample required air to be added to reduce the bulk density to that observed experimentally (CUP-1 = 1.36 and CUP-2 = 1.68  $\text{g cm}^{-3}$ ) due to the lack of pore spaces in the bulk representative volume. To randomly select a non-central emission point from within the spherical uranium grains, a three-dimensional Cartesian coordinate system using a random number generator was used. The simulation involving no grains of uranium used a bulk representative density of all minerals, this time including uranium, and photon generation was selected at random points throughout the entire bulk volume. Each simulation ran for  $1 \times 10^6$  events to minimise statistical uncertainty.

## 2.3 Results & Discussion

### 2.3.1 Initial characterisation of CRMs

The direct measurements of the three reference materials yielded lower than expected activity concentrations (Figure 2-3). The measured  $^{234}\text{Th}$  activity concentrations were 94%, 65% and 7% of the certified activity concentrations for CUP-1, BL-5 and CUP-2 respectively. The extent of the bias is proportional to the uranium content of each sample and the average size of the uranium grains with its supporting matrix. A similar relationship can be observed with  $^{235}\text{U}$  and  $^{210}\text{Pb}$  activity concentrations. Where a certified activity concentration is not available for any measured daughter isotope of uranium, it is assumed that the daughter nuclide activity should be equal to the closest available certified parent nuclide. As CUP-2 is a UOC, daughters of  $^{226}\text{Ra}$  are below the limit of detection (LOD) due to insufficient time for ingrowth following ore processing ( $^{210}\text{Pb} = < 13 \text{ Bq g}^{-1}$  and  $^{226}\text{Ra} = < 19 \text{ Bq g}^{-1}$ ). Protactinium-234m in CUP-1 is also below the LOD ( $< 19 \text{ Bq g}^{-1}$ ) as it is most likely not resolvable from the Compton background due to its low gamma emission yield (0.847%) and low uranium concentration (0.128%). However,  $^{234\text{m}}\text{Pa}$  is detectable in BL-5 and CUP-2 but is not within uncertainty of the expected activity concentration ( $117 \pm 7\%$  and  $92 \pm 7\%$  respectively). This indicates that even high-energy gamma photons cannot be accurately characterised using apparent detection efficiencies based on sample bulk density.

### 2.3.2 Borate fused characterisation of CRMs

The measured activities of fused CRMs using lithium tetraborate are within uncertainty of the activity concentrations expected (as previously discussed) for all measured radionuclides (Figure 2-3). The fusion technique has greatly reduced the matrix effects present in heterogeneous U-bearing samples where grain size, density and concentration can vary. The gamma photons are no longer interacting with such physical properties allowing a vastly improved transmission pathway with reduced attenuation effect. The average activity concentration of all measured radionuclides in the borate fused samples yields U wt% for CUP-1, BL-5 and CUP-2 as  $0.12 \pm 0.02$ ,  $7.24 \pm 0.33$  and  $75.2 \pm 1.8$  respectively which are in agreement with the certified U wt% values (Table 2.2).

Both  $^{235}\text{U}$  and  $^{226}\text{Ra}$  emit  $\sim 186$  keV gamma photons with a yield of 57.0% and 3.6% respectively (DDEP, 2016). The presence of  $^{235}\text{U}$  therefore contributes to the gamma photon peak of  $^{226}\text{Ra}$  and will produce an elevated activity concentration for  $^{226}\text{Ra}$ . Where sufficient  $^{235}\text{U}$  is present, the deconvolving software can correct for the  $^{235}\text{U}$  contribution by using the associated 143.8 keV gamma photon (11% yield). However, if  $^{235}\text{U}$  activity is being attenuated in a complex matrix, the software cannot accurately correct the discrepancy between  $^{226}\text{Ra}$  and  $^{235}\text{U}$ , which results in lower than expected  $^{235}\text{U}$  activity concentrations but accurate (within uncertainty)  $^{226}\text{Ra}$  concentrations. This is observed with CRM BL-5 where  $^{235}\text{U}$  and  $^{226}\text{Ra}$  measured activity concentrations are  $64 \pm 12\%$  and  $113 \pm 17\%$  respectively of the certified activities and are not within uncertainty of one another. The borate fusion technique enables this complication to be overcome without the need for qualitative correction as the attenuation of the gamma photons for  $^{235}\text{U}$  and  $^{226}\text{Ra}$  is greatly reduced allowing for accurate activity concentrations to be measured ( $96 \pm 7\%$  and  $95 \pm 7\%$  respectively). This is important as a qualitative correction could produce an inaccurate  $^{235}\text{U}$  activity concentration if the sample has been enriched in  $^{235}\text{U}$ , does not contain the natural  $^{238}\text{U}/^{235}\text{U}$  ratio, or has been processed whereby  $^{226}\text{Ra}$  would not be expected to be present.

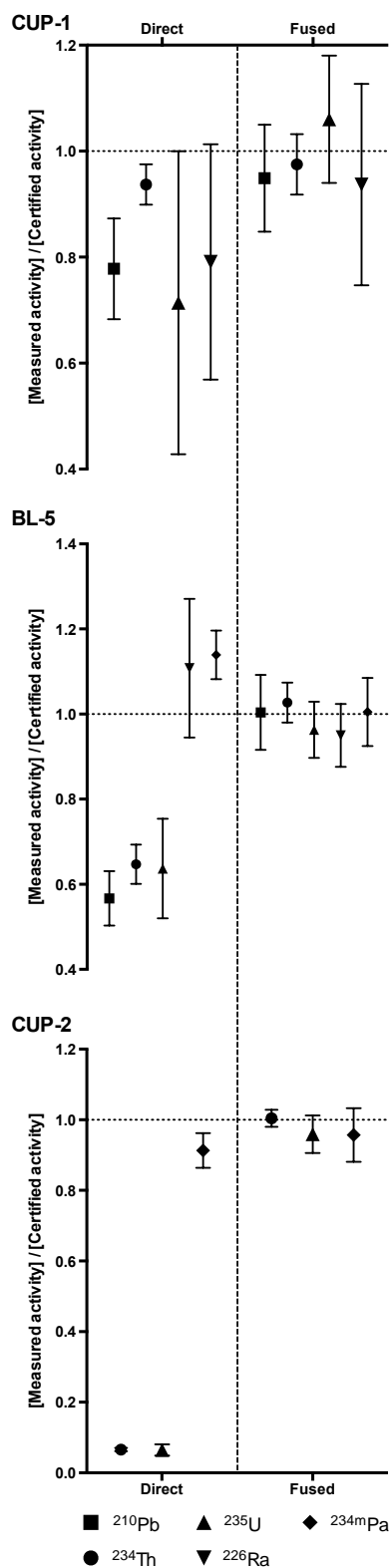


**Figure 2-3: Activity concentrations for selected radionuclides of both direct and fused CRMs against the expected activity concentration based on certified values.**

**\* - Represents LLD value. Uncertainty =  $2\sigma$  and denoted by brackets.**

### 2.3.3 Understanding the cause of self-attenuation

#### 2.3.3.1 Bulk density effect

Reducing the bulk density of CRM BL-5 with cellulose increases the photon detection efficiency of  $^{210}\text{Pb}$  and  $^{234}\text{Th}$  where measured activity concentrations are in better agreement with the certified values compared to those obtained by direct measurements of raw material. The probability of a low-energy photon being detected is increased with lower bulk density materials, as fewer high-density grains of uranium or its matrix will be encountered along the transmission pathway. However, the measured activity concentrations continue to bias low compared to the certified values (Figure 2-4). The bias of  $^{210}\text{Pb}$  and  $^{234}\text{Th}$  improves relative to each other with decreasing bulk density of BL-5. At a bulk density of  $0.97 \text{ g cm}^{-3}$  the two radionuclides are not within uncertainty of one another, but at a bulk density of  $0.68 \text{ g cm}^{-3}$  their activity bias and uncertainties are very similar. This indicates that the degree of attenuation of photons  $> 46.5 \text{ keV}$  in bulk densities  $\leq 0.68 \text{ g cm}^{-3}$  are no longer associated with each other and that another variable, such as grain size, is contributing to the activity bias.

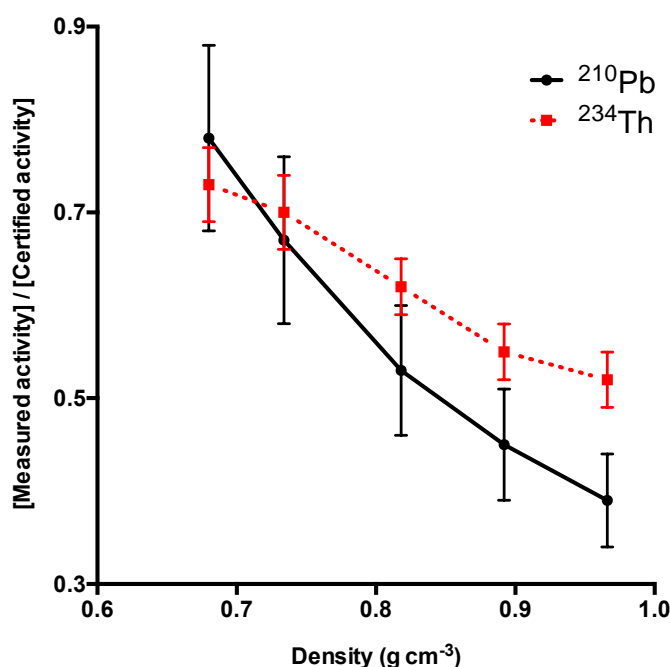


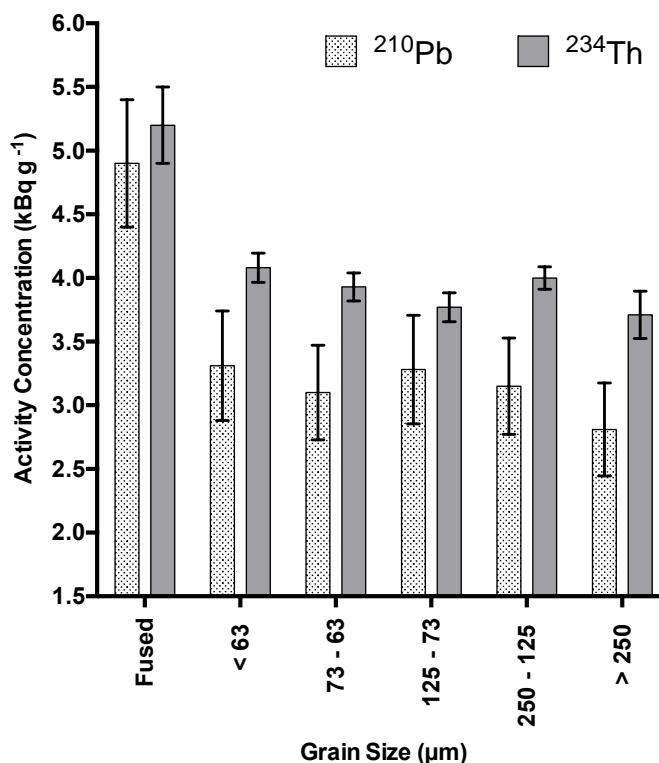
**Figure 2-4: Bulk density effects on  $^{210}\text{Pb}$  &  $^{234}\text{Th}$  photon attenuation within certified reference material BL-5 where density is adjusted using cellulose. Data represented as ratio between measured activity concentration and certified activities.**

**Uncertainty =  $2\sigma$ .**

### 2.3.3.2 Grain size effect

Analysing different grain size ranges from a pitchblende specimen supported in a sand matrix demonstrated that in all but one of the grain size groups,  $^{210}\text{Pb}$  has lower activity concentration, and thus lower photon detection efficiency, than  $^{234}\text{Th}$  (Figure 2-5). This is in spite of the two nuclides being in equilibrium, which was observed when all pitchblende fractions underwent borate fusion to assess compositional variability (average  $^{210}\text{Pb}$  and  $^{234}\text{Th}$  activity concentrations were  $4.9 \pm 0.5$  and  $5.2 \pm 0.3$   $\text{kBq g}^{-1}$  respectively). The activity concentrations of  $^{234}\text{Th}$  are consistent, within uncertainty, across the five fractions. This is also true for  $^{210}\text{Pb}$ . The data demonstrate that both radionuclides bias low from the known activity concentrations where the extent of attenuation for  $^{210}\text{Pb}$  is greater than  $^{234}\text{Th}$ . As the grain size ranges are not uniformly distributed, it is not possible to identify any linear trends between grain size and activity concentration. The data suggests that grain sizes greater than  $63\text{ }\mu\text{m}$  have the same self-attenuating effects on the two radionuclides.

**Figure 2-5: Activity concentrations for pitchblende fractions of varying grain size to assess**



**$^{210}\text{Pb}$  &  $^{234}\text{Th}$  photon attenuation. Borate fused activity concentrations of pitchblende given as an average between all grain size fractions.**

**Uncertainty =  $2\sigma$ .**

### 2.3.3.3 Monte-Carlo simulations

The Geant4 simulation predicted that U-bearing grains below 80  $\mu\text{m}$  do affect the photon efficiency of low-energy gamma photons (Figure 2-6). Unlike the pitchblende grain size experiment, the Geant4 model has uniform grain size distribution and focuses on finer grain sizes. The detection efficiency of 46.5 keV photons originating from 80  $\mu\text{m}$  and 10  $\mu\text{m}$  grains increased from 6% to 14% respectively and the efficiency of the 63.3 keV photons increased from 10% to 15%. The higher energy photons (92.4 and 112.9 keV) demonstrated marginal improvement of  $\sim 2\%$  with the detection efficiency for both photon energies reaching 20%.

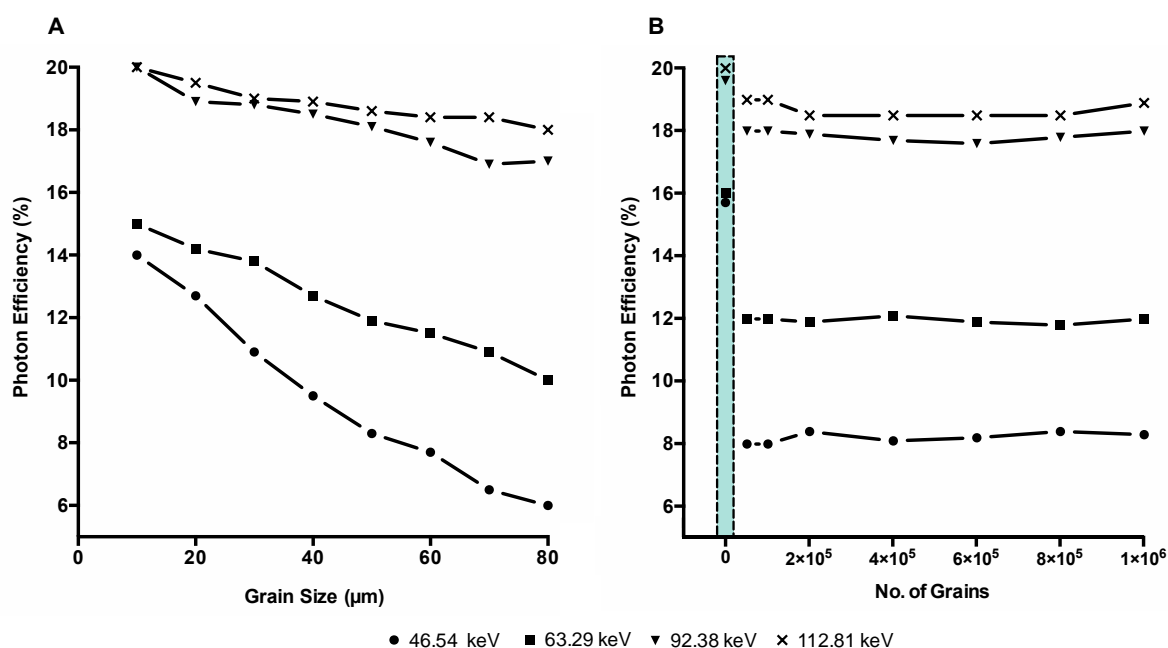


**Figure 2-6: Geant4 Monte-Carlo simulations for determining the effect that grain size (A) and grain concentration (B) have on the efficiency of low-energy gamma photons ( $^{210}\text{Pb}$  and  $^{234}\text{Th}$ ) originating from a uraninite source.**

**Blue shaded region indicates an aqueous sample where no grains are present.**

The detection efficiency arising from randomly positioned photon generations within a uraninite grain is generally higher, albeit only slightly, than the centrally positioned generations (Figure 2-7). The grain size, and hence the distance over which a gamma-photon has to travel through its originating grain, is responsible for this difference. The efficiencies of photons  $\geq 92.4$  keV in both simulations for CRM CUP-1 are identical, indicating that regardless of where the photon is generated, the photon efficiency and

probability of evading the host grain are identical. This is not applicable to CUP-2 as the average grain size is larger than CUP-1 meaning that photons with energies  $\leq 92.4$  keV would not be able to evade or transmit through such grains.

The bulk volume simulation (i.e. photons generated randomly throughout a lower density bulk matrix) demonstrated that photon efficiency is improved in comparison to a grain origination with the greatest difference observed at lower energy. This is to be expected considering that an emission in a bulk representative matrix is likely to have a less dense transmission pathway compared to scattered, heterogeneous dense grains in a similar, but slightly lower density, matrix. The large difference in efficiency observed between the two reference materials is due to differences in mineralogy and grain sizes with particular emphasis on the higher concentration and larger grain size of uranium minerals present in CUP-2.

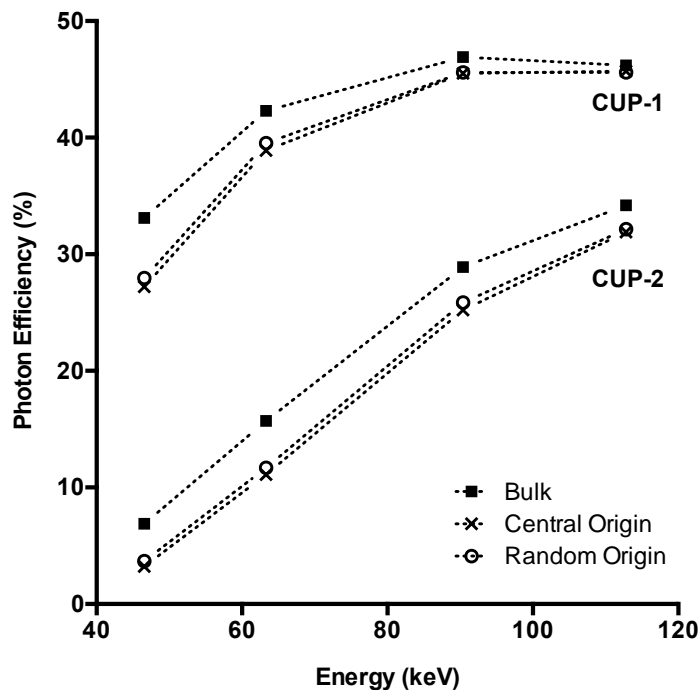


**Figure 2-7: Geant4 Monte-Carlo simulations to assess the effect on photon origin from differing positions within grains of CRM CUP-1 and CUP-2 and when the emission is from a representative bulk density with no grains present.**

The modelled CRMs demonstrate a “nugget effect” that fluctuates based on the abundance and size of uranium grains. This characteristic would be difficult to matrix-match and is the cause of the self-attenuation observed when directly measuring the CRMs.

The experimental and theoretical work performed here demonstrates that the density, size and concentration of uranium-bearing grains has a detrimental effect on the transmission of gamma photons through the heterogeneous sample matrix. This is due to the likelihood of interaction between a photon and a uranium-bearing grain causing attenuation resulting in inaccurate photon detection efficiencies for the matrix. The lithium tetraborate fusion technique produces a homogenous solution where the photon detection efficiencies can be accurately and reliably predicted based on the calibration standards of similar density.

Gamma spectrometry is typically used for initial sample characterisation due to its non-destructive approach to sample measurement thus preserving the sample’s physical form. The borate fusion technique is a destructive technique but requires small sample mass for dissolution and measurement. For most illicitly recovered samples, whether it is a fuel pellet or a powdered UOC, removing such a small mass would not diminish further investigations so long as all physical parameters are recorded prior to fusion including sample dimensions and macro/micro photography. Additionally, the fused sample can be used for further analytical methods such as mass spectrometry without the requirement for further sampling of the parent sample. Both non-destructive and destructive HRGS should be used together as the measurement discrepancy observed between the two approaches could provide information on the matrix composition based on the photon attenuation bias.

## 2.4 Conclusion

The lithium borate fusion technique produces a highly effective and rapid dissolution of virtually any difficult to dissolve material (silicates, oxides, sulphates) as well as dissolving carbonates and halides. This ability makes it very attractive where rapid digestions are required. The fusion process solubilises mineral particles removing the “nugget effects” and increases the detection efficiency of low-energy gamma-emitting nuclides such as  $^{210}\text{Pb}$  and  $^{234}\text{Th}$  in heterogeneous U-bearing samples. The high uranium content of CRM CUP-2 (75 wt% U) had a  $^{234}\text{Th}$  activity concentration of  $7 \pm 1\%$  of the certified value when measured in its solid form using an efficiency correction based on its bulk density. After the borate fusion and digestion technique, the  $^{234}\text{Th}$  concentration was  $100 \pm 2\%$  of the certified value. The three certified reference materials and Monte-Carlo simulations allowed for a “nugget effect” to be observed which is difficult to matrix match and efficiency correct for self-attenuation. The dense uranium-bearing grains are present within a lower bulk density matrix with variable grains sizes causing self-attenuation of low-energy gamma photons. The fusion technique means there is no requirement for sample-specific matrix matching or correcting and combined with rapid sample preparation, offers an attractive, efficient alternative for accurate radiometric characterisation.

The procedure developed could be used to develop a database containing radionuclide activities, U-concentrations,  $^{238}\text{U} : ^{235}\text{U} / ^{238}\text{U} : ^{232}\text{Th}$  ratios, and extent of secular equilibrium for U-ores and uranium ore concentrates of known provenance so that recovered, illicit nuclear materials can be rapidly analysed and compared as part of a nuclear forensic characterisation. The borate fusion technique can be used in other applications where accurate and rapid characterisation of low-energy gamma photons is required, such as accurately measuring  $^{241}\text{Am}$ ,  $^{239}\text{Pu}$  or  $^{241}\text{Pu}$  as part of a nuclear forensic effort or environmental monitoring. Care should be taken with samples potentially containing elements such as Cs and Sr as the borate fusion procedure would cause volatilisation.

Gamma spectrometry is typically used for initial sample characterisation due to its non-destructive approach to sample measurement thus preserving the sample's physical form. The borate fusion technique is a destructive technique but requires low sample mass for dissolution and measurement. For most illicitly recovered samples, whether it is a fuel pellet or powdered UOC, removing such a small mass would not diminish further

investigations so long as all physical parameters are recorded prior to the fusion technique including sample dimensions and macro/microphotography. The borate fused sample, typically <0.5 g but 20 mL in volume can be used for further investigations such as mass spectrometry where no further parent sample is required and no additional sample dissolution procedures such as HF digestion are necessary. For example, 600 soil samples from the Greenham Common Airbase where an alleged nuclear incident took place in 1958 were successfully fused prior to extraction chromatography of U and Pu in preparation for high precision radiometric and mass spectrometric measurements (Croudace et al., 1998; Taylor et al., 1998). The fusion procedure allowed for the samples to be rapidly prepared and measured and enabled results to be published to the public on a rapid project turnaround of months.

The petroleum and mineral processing industries regularly handle materials that contain uranium and thorium in NORM scales and deposits. The accurate determination of the associated low-energy gamma radionuclides is critical for radiological assessment and for appropriately handling and disposing of waste and tailings. Any material that may be affected by a “nugget effect” that requires accurate radiometric characterisation and is not suspected to contain volatile radionuclides would benefit from the borate fusion technique, e.g. the accurate characterisation of hot-particles near nuclear sites such as Dounreay, UK (Dennis et al., 2007) or Chernobyl, Ukraine (Sandalls et al., 1993; Salbu et al., 1994).



## **Chapter 3: Applying multivariate statistics to discriminate uranium ore concentrate geolocations using (radio)chemical data in support of nuclear forensic investigations**

**Reading et al., (Submitted A), Journal of Environmental Radioactivity**

### **Abstract**

The application of Principal Components Analysis (PCA) to U and Th series gamma spectrometry data provides a discriminatory tool to help determine the provenance of illicitly recovered uranium ore concentrates (UOCs). In the present work the PCA is applied to a database of radiometric signatures from 19 historic UOCs from Australia, Canada, and the USA representing many uranium geological deposits. In this study a key process to obtain accurate radiometric data (gamma and alpha) is to digest the U-ores and UOCs using a lithium tetraborate fusion. Six UOCs from the same sample set were analysed 'blind' and compared against the database to identify their geolocation. These UOCs were all accurately linked to their correct geolocations which can aid the forensic laboratory in determining which further analytical techniques should be used to improve the confidence of the particular location.



### 3.1 Introduction

One of the main objectives of nuclear forensic science is to investigate and determine the geographical origin (or geolocation) of illicitly recovered nuclear materials via specific characteristics that are unique to that particular specimen. The necessity and demand for such investigations is amply demonstrated by the existence of IAEA's Incident and Trafficking Database (ITDB) where 257 cases of recovered or discovered nuclear material were reported in 2014 (IAEA, 2015a). Due to the confidentiality and security of the ITDB in protecting IAEA member states' declarations, it is not known how many of these incidents directly involved uranium ore concentrates (UOC). However, a limited number of studies and media reports suggest that in the last decade, several large scale trafficking incidents of UOC have been intercepted including the seizure of 324 kg of UOC in Namibia (NTI, 2012a), the seizure of 170 kg stolen from Rossing Mine (NTI, 2012b; Blake, 2011) and the foiled attempt to sell and transfer 1000 metric tonnes of UOC to Iran (Mutua, 2015). The ability to confidently identify potential geolocations of such recovered samples rapidly and accurately is a key area of interest for nuclear forensic investigations.

This study explores the use of multivariate statistical analysis (Principal Components Analysis, PCA) using radiometric data obtained from uranium ore concentrates (UOC or "yellowcake"). Whilst PCA analysis has traditionally been applied to identify trends and groupings in data, it has rarely been employed as a discriminatory method where statistical comparisons are made between a database of signatures and the unknown to identify a single sample or family of samples (Ho Mer Lin et al., 2015; Keegan et al., 2008; Lin et al., 2015; Robel et al., 2009; Klunder et al., 2013; Švedkauskaitė-LeGore et al., 2008)

Gamma spectrometric data were selected as the investigative signature for the PCA as uranium ore milling causes radioactive disequilibrium in the uranium and thorium decay chains. Many of the associated radionuclides in these chains emit gamma photons on decay enabling observations on the extent of disequilibrium. The disequilibrium is due to the preferential leaching and precipitation of uranium from the ore feed resulting in absent or very low concentrations of other uranium and thorium progeny radionuclides in the final UOC which could be diagnostic of a particular uranium mill. This gamma spectrometric signature consists of data from  $^{234}\text{Th}$ ,  $^{234\text{m}}\text{Pa}$ ,  $^{214}\text{Pb}$ ,  $^{210}\text{Pb}$ ,  $^{235}\text{U}$ ,  $^{228}\text{Ac}$  and  $^{208}\text{Tl}$ .

High-resolution gamma spectrometry (HRGS) is recommended by the nuclear forensics International Technical Working Group as one of the first experimental procedures that should be conducted on receipt of nuclear material for forensics investigations (Wallenius et al., 2014; Hutcheon et al., 2013; Kristo, 2012; Hanlen, 2011; Wallenius et al., 2006; Mayer et al., 2005). Therefore, the use of a statistical technique incorporating data from the first experimental procedure would enhance the investigation by providing the laboratory with an initial geolocation possibility. This information could guide the laboratory to narrow the field of geolocation options.

HRGS is typically used in non-destructive mode and serves to preserve the sample. It can often be applied with few problems when studying homogenised samples, such as uranium fuel pellets since photon detection efficiencies can be adjusted to reflect the uniform sample density. This relationship becomes more difficult to estimate when a sample has a heterogeneous matrix such as uranium ore and UOC which typically consist of higher density uranium-bearing minerals (typically between 5 and 8.5 g cm<sup>-3</sup>) of variable grain size dispersed within lower density mineral phases (e.g. quartz, feldspars, micas, carbonates and iron-oxides; Figure 3-1).

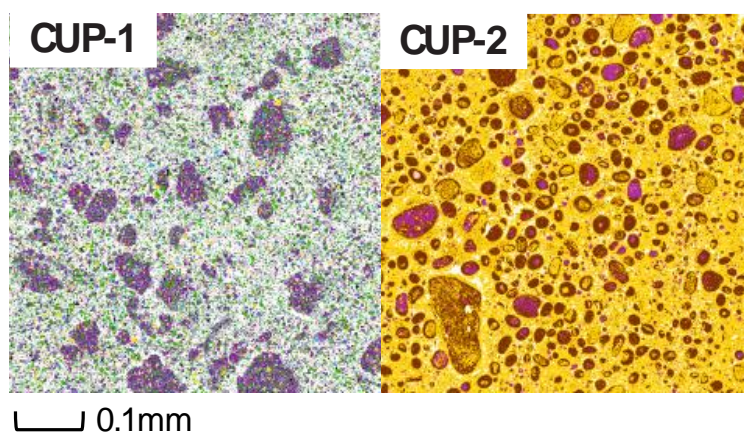
The higher density grains in such heterogeneous matrices cause significant self-attenuation of low to medium energy (<200 keV) gamma photons (<sup>210</sup>Pb, <sup>234</sup>Th, <sup>226</sup>Ra, <sup>235</sup>U) with minor but still significant effects on high energy gamma photon such as <sup>234m</sup>Pa (1001 keV) (Reading et al., 2015).

To accurately characterise U-ore and UOC via HRGS without the requirement for attenuation correction factors as used in environmental samples (Cutshall et al., 1983; Długosz-Lisiecka & Bem, 2013; Pilleyre et al., 2006; Sima & Dovlete, 1997), an effective and rapid preparative procedure was applied using a lithium tetraborate fusion that readily dissolves all components of the sample matrix (Croudace et al., 1998; Reading et al., 2015). The subsequent quenched glass is quickly dissolved in nitric acid resulting in a homogeneous, aqueous sample with significantly reduced self-attenuation effects with a density closer to aqueous calibration standards.

In this study a comparison between the pre- and post-dissolution gamma spectrometric data for a set of UOCs is made. This demonstrates the benefits of using lithium tetraborate fusion to remove particle/density effects in UOCs and uranium ores. The procedure enables

trends and anomalies from the uranium ore feed and milling process to be identified which might otherwise be missed in the traditional HRGS screening of illicitly recovered UOCs. In the traditional sense, samples are measured to ascertain the type of sample such as whether the sample is an ore or UOC based on the low energy emissions of  $^{234}\text{Th}$ . Where significant self-attenuation in a sample occurs, this observation of  $^{234}\text{Th}$  could be grossly underestimated resulting in potential misinterpretation of the overall U concentration thus misidentifying the nature of the sample. This could also have significant impacts on dose estimates for laboratory technicians handling the material. Additionally, the accurate measurement of  $^{210}\text{Pb}$  (46.6 keV) in a UOC may also be able to provide information on the efficiency that a particular mill was operating at based on the extent of  $^{210}\text{Pb}$  ingrowth.

**Figure 3-1: QEMSCAN false-colour images for CCRMP certified reference materials CUP-1**



**(U-ore) and CUP-2 (UOC).**

***CUP-1 agglomerations (purple) are composed of muscovite and biotite mica with silicates. The gangue is composed of feldspars, pyrite, ankerite, apatite and calcite. CUP-2 agglomerations are composed of U-carbonates (pink and brown). The surrounding matrix (yellow) is composed of other U-phases.***

### 3.1.1 Uranium Ore Concentrates

A set of 19 UOCs were supplied by research partners at the Atomic Weapons Establishment (AWE) that represent part of a large, diverse and historical UK collection of samples originally derived from the former BNFL Springfields site (now managed and operated by Westinghouse Electric UK Ltd on the NDA's behalf). This valuable archive was catalogued, rationalised and made available to selected members of the international nuclear forensics community for R&D purposes. The names of the UOCs (derived from sources in Australia, Canada and the USA; Figure 3-2) are given based on the mine site, mill site, or the company responsible for the sample production. Therefore, some similarities could be observed between UOCs as mine/mill sites were sold between companies (for example Faraday and Madawaska – see table 3-1 and 3-2). The ore feeds for each UOC are from a variety of localities and geological settings (Table 3-1 and Figure 3-2) and processing techniques (Table 3-2).

**Table 3-1: UOC localities, deposit types and mineralogy**

UOC Name	Country of origin	Milling Facility	Uranium Deposit Type	Known Uranium Minerals	Other Minerals in Ore Feed
<b>Anaconda</b>	USA	Grants / Bluewater	SSt – Tabular	Coffinite, uraninite,	Calcite, chlorite, ferrosilite, marcasite, pyrite, quartz
<b>Blind River</b>	CAN	Elliot Lake	QPC	Brannerite, coffinite, uraninite	Apatite, cassiterite, garnet, Ilmenite, magnetite, pyrite (5-20%), rutile, titanite, zircon
<b>Chevron Hill</b>	USA	On-site	Sst – Roll front	Autunite, coffinite, uraninite,	Pyrite, marcasite

**Table 3-1: UOC localities, deposit types and mineralogy**

<b>Cotter</b>	USA	Canon City	Sst & vein (3:1)	Coffinite, Pitchblende	Ankerite, pyrite, quartz, minor Cu, Pb, Zn sulphides
<b>Eldorado</b>	CAN	On-site	Vein	Pitchblende, uraninite	Calcite, pyrite, quartz
<b>Faraday<sup>1</sup></b>	CAN	On-site	Intrusive	Uraninite, uranophane, uraniothorite	Amphibole, chalcopyrite, molybdenite, pyroxene, quartz, tourmaline
<b>Gunnar</b>	CAN	On-site	Vein	Pitchblende, uranophane	Chalcopyrite, chlorite, galena, kaolinite, pyrite, quartz
<b>Lucky McGill</b>	USA	On-site	Sst – Roll front	Coffinite, uraninite	Ferrosilite, jordisite, marcasite, pyrite, Mo, Se and V accessory minerals
<b>Mary Kathleen</b>	AUS	On-site	Metamorphic	Uraninite	Albite, allanite, epidote, garnet, K-Fels, REE minerals
<b>Mesa EFI</b>	USA	On-site	Collapse breccia pipe	Coffinite, torbenite, uraninite	Silicate minerals
			Sst	Carnotite	Vanadium minerals
<b>Mulberry</b>	USA	On-site	Phosphate	U recovered from phosphoric acid production	

**Table 3-1 Continued: UOC localities, deposit types and mineralogy**

<b>North Span<sup>2</sup></b>	CAN	On-site / Elliot Lake	QPC	Brannerite, coffinite, uraninite, uranophane, uraniothorite	Chlorite, monazite, pyrite, quartz, sericite
<b>Olympic Dam</b>	AUS	On-site	Haematite Breccia Complex	Brannerite, coffinite, pitchblende	Bornite, chalcocite, chalcopyrite, haematite, quartz, REE minerals
<b>Queensland</b>	AUS	On-site	UR	Autunite, brannerite, coffinite, torbenite, uraninite	Chlorite, Fe-oxides, sericite
<b>Rabbit Lake</b>	CAN	On-site	UR	Pitchblende, uranophane	Dickite, kaolinite, sulphides, vermiculite
<b>Ranger</b>	AUS	On-site	UR	Pitchblende, uraninite,	Chlorite, kaolinite, muscovite, quartz
<b>Rio Algom<sup>3</sup></b>	CAN	Elliot Lake	QPC	Brannerite, coffinite, uraninite, uranophane, uraniothorite	Chlorite, monazite, pyrite, quartz, sericite
<b>South Alligator</b>	AUS	Rockhole Creek	UR	Autunite, pitchblende, uraninite	Au, Pd and Pt minerals

Table 3-2: UOC milling process

UOC Name	Dissolution Process	Extraction Process for U	Precipitation process	Drying	References for Table 3-1 & 3-2
<b>Anaconda</b>	Acid leach with MnO <sub>2</sub>	SX-TA Chloride strip	MgO	Steamed	1
<b>Blind River</b>	H <sub>2</sub> SO <sub>4</sub> acid leach	Fixed bed ion exchange	NH <sub>3</sub>	Calcined 800 °C	2 & 3
<b>Chevron Hill</b>	Acid leach	SX	NH <sub>3</sub>		2 & 4
<b>Cotter</b>	Carbonate leach with O <sub>2</sub>	SX-TA (NH <sub>4</sub> ) <sub>2</sub> SO <sub>4</sub> strip	NH <sub>3</sub>		1 & 2
<b>Eldorado</b>	Carbonate leach with O <sub>2</sub>		NaOH	Steamed	2
<b>Faraday<sup>1</sup></b>	Acid leach with NaClO <sub>3</sub>	IX NaCl strip	MgO		2 & 5
<b>Gunnar</b>					2
<b>Lucky McGill</b>	Acid leach with NaClO <sub>3</sub>	ELUEX	NH <sub>3</sub>		2 & 4
<b>Madawaska<sup>1</sup></b>	Acid leach with NaClO <sub>3</sub>	IX NaCl strip	MgO		2 & 5
<b>Mary Kathleen</b>	Acid leach with MnO <sub>2</sub>	SX-TA NH <sub>3</sub> strip	NH <sub>3</sub>	Calcined	2, 6-8

Table 3-2 Continued: UOC milling process

UOC Name	Dissolution Process	Extraction Process for U	Precipitation process	Drying	References for Table 3-1 & 3-2
<b>Mesa EFI</b>	H <sub>2</sub> SO <sub>4</sub> acid leach with NaClO <sub>3</sub>	SX-TA in kerosene NaCl strip	NH <sub>3</sub>	Calcined at 590 °C	2 & 7
<b>Mulberry</b>	U recovered from phosphoric acid production				
<b>North Span<sup>2</sup></b>					1
<b>Olympic Dam</b>	Acid leach with NaClO <sub>3</sub>	SX-TA in kerosene	NH <sub>3</sub>	Calcined at 750 °C	2, 3, 6, 7 & 9
<b>Queensland</b>	Acid leach with MnO <sub>2</sub>	SX-TA NH <sub>3</sub> strip	NH <sub>3</sub>	Calcined	2 & 8
<b>Rabbit Lake</b>	Acid leach with NaClO <sub>3</sub>	SX-TA (NH <sub>4</sub> ) <sub>2</sub> SO <sub>4</sub> strip	NH <sub>3</sub>	Calcined 650 °C	7 & 9
<b>Ranger</b>	Acid leach with MnO <sub>2</sub>	SX-TA (NH <sub>4</sub> ) <sub>2</sub> SO <sub>4</sub> strip	NH <sub>3</sub>	Calcined	2
<b>Rio Algom<sup>3</sup></b>	H <sub>2</sub> SO <sub>4</sub> acid leach with O <sub>2</sub> .	IX H <sub>2</sub> SO <sub>4</sub> strip	MgO & CaCO <sub>3</sub> or CaO & NH <sub>3</sub>		2 & 7
<b>South Alligator</b>	H <sub>2</sub> SO <sub>4</sub> acid leach.	SX with NaCl	MgO		6 & 8

## Notes for Tables 3-1 and 3-2.

**References:** 1: IAEA, (1976), 2: IAEA, (1980), 3: Dahlkamp, (1993), 4: Albrethson & McGinley (1982), 5: Proulx, (1997) 6: IAEA, (2009), 7: IAEA, (1993), 8: Alfredson, (1980), 9: Edwards & Oliver, (2000)

<sup>1</sup> Faraday and Madawaska are the same mine sites. Faraday operated 1954-1964 and Madawaska operated 1975-1982.

<sup>2</sup> North Span (company) operated many mines that Rio Algom (company) then purchased. Mineralogy for North Span inferred from Rio Algom records.

<sup>3</sup> Rio Algom operated many mines of which Panel, Stanleigh and Quirke mines are the most likely source for this sample.

**QPC** = Quartz-pebble conglomerate; **Sst** = Sandstone; **UR** = Unconformity related;

**SX-TA** = Solvent exchange with tertiary amine; **IX** = Ion exchange; **ELUEX** = Eluate Extraction  
-  $H_2SO_4$  leach with amine extraction in a joint application.

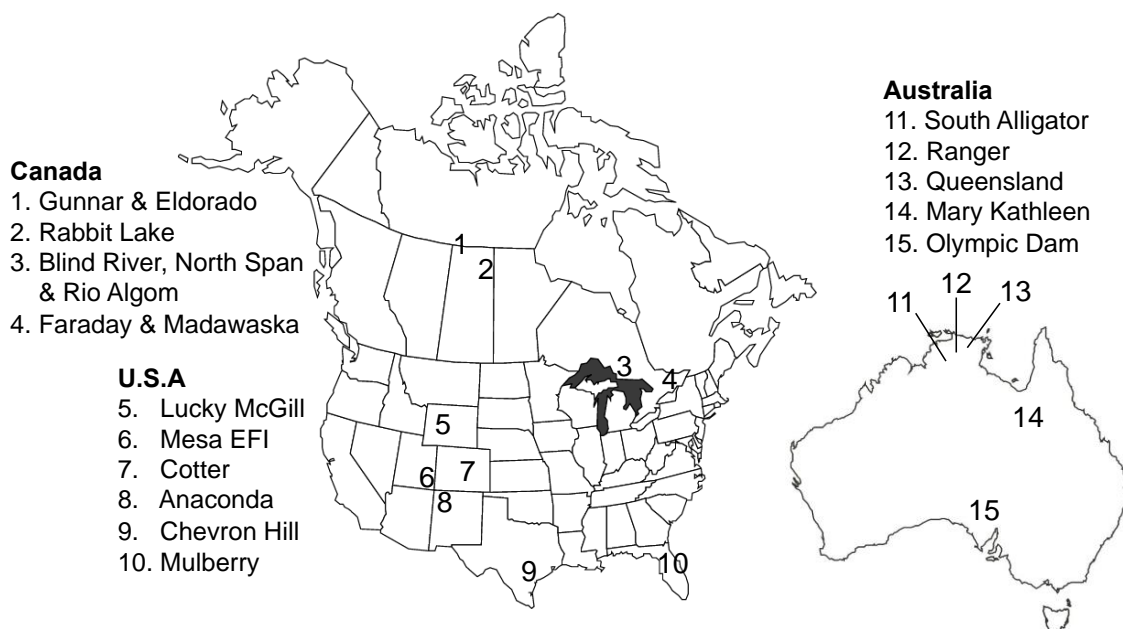


**Figure 3-2: Geographical locations of U mines and milling facilities used to manufacture the UOCs in this study.**

## 3.2 Methodology

### 3.2.1 Instrumentation

Gamma emitting radionuclide activity concentrations were determined using Canberra 50% N-type HPGe well-type spectrometers. The spectra were collected using Genie 2000 acquisition software (Canberra Industries, Harwell, UK) and were analysed using Fitzpeaks spectral deconvolving software (JF-Computing, Stanford in the Vale, UK). The spectrometers were calibrated using spiked radionuclide standards throughout several “density geometries” (matrices of cellulose, water, sand, steel and boron, and a tin-tungsten ore). A mixed nuclide source (NPL, Teddington, UK) and a  $^{210}\text{Pb}$  solution standard (PTB, Braunschweig, Germany) were used. All samples were counted for 1 h as low detection limits and low counting uncertainty (< 6% relative  $^{234}\text{Th}$  fused matrix and < 16% relative  $^{234}\text{Th}$  solid matrix) was achievable in this time.

The  $^{210}\text{Pb}$  activity concentrations were determined via the alpha emitting grand-daughter radionuclide  $^{210}\text{Po}$ , that had been plated onto silver discs (Flynn, 1968) and counted using an Ortec PC alpha spectrometer system fitted with 450 mm<sup>2</sup> Ultra detectors. All measurements were made *in vacuo* for 36 hours. Spectra were acquired using Maestro 7 and analysed by WinPlots 7 (AMETEK, Wokingham, UK).

### 3.2.2 Initial characterisation of UOCs

Approximately 10 g of each UOC was weighed into 20 mL polythene vials and sealed for at least 21 days using Viton rubber discs to prevent loss of radon and to establish secular equilibrium between  $^{226}\text{Ra}$ ,  $^{222}\text{Rn}$  and  $^{214}\text{Pb}$ . The photon efficiency for each measured radionuclide from the UOCs was calculated based on the bulk density of the sample and the known relationship between sample density and photon efficiency acquired from the calibration standards. The samples were characterised for  $^{234}\text{Th}$ ,  $^{234\text{m}}\text{Pa}$ ,  $^{214}\text{Pb}$ ,  $^{210}\text{Pb}$ ,  $^{235}\text{U}$ ,  $^{228}\text{Ac}$  and  $^{208}\text{Tl}$  where  $^{234}\text{Th}$  and  $^{234\text{m}}\text{Pa}$  is measured as a proxy for the non-gamma-emitting  $^{238}\text{U}$ ;  $^{214}\text{Pb}$  (a proxy for  $^{226}\text{Ra}$ ) and  $^{210}\text{Pb}$  was measured to assess the efficiency of the uranium milling, processing and/or contamination; and  $^{228}\text{Ac}$  and  $^{208}\text{Tl}$  are measured as proxies for  $^{232}\text{Th}$ .

### 3.2.3 Borate fusion for homogenisation

Sub-samples of UOC were blended at a 1:1 ratio with di-lithium tetraborate flux (Fluxana, Germany) and fused to  $\sim 1100$  °C with periodic agitation for 5 minutes. The resulting melt was quenched by pouring the melt into a beaker containing 50 mL Milli-Q water (Millipore, USA). After all the glass had settled the excess water was carefully decanted and 8M analytical grade nitric acid (8 M) was then added to digest the sample at 50 °C using a PTFE stirring/hot-plate system. After digestion, any insoluble silica and boric acid (neither of which retained any activity) were removed by vacuum filtration. The sample was heated at 90 °C to reduce the sample volume to  $\sim 15$  mL where it is then transferred to a glass scintillation vial fitted with a Viton rubber disc to retain  $^{222}\text{Rn}$ , topped up to 20 mL with Milli-Q water and measured immediately. A more detailed methodology and rationale for this procedure can be found in Reading et al., (2015). During the fusion process,  $^{222}\text{Rn}$  undergoes degassing and thus causes disequilibrium in activity concentration for the short-lived daughter radionuclides. Therefore, as previously mentioned, the samples were sealed using a Viton disc and re-counted after 21 days. No other UOC originating gamma emitting radionuclides demonstrate volatilisation using this procedure.

During any ore processing  $^{226}\text{Ra}$  progeny are invariably lost. Monitoring for  $^{226}\text{Ra}$  was performed but its low concentration and its single, low yield (3.6%) gamma emission and its interference from  $^{235}\text{U}$  made direct measurement difficult. Instead,  $^{214}\text{Pb}$  measurements are collected as a proxy for  $^{226}\text{Ra}$  once secular equilibrium had been established after 21 days.

### 3.2.4 Preparation and measurement of $^{210}\text{Po}$ in UOC via autodeposition

An aliquot of 150  $\mu\text{L}$  ( $\sim 3\text{--}4$  mg UOC) of each fused solution was evaporated to dryness, spiked with  $^{209}\text{Po}$  ( $0.275\text{ Bq g}^{-1}$ ) as a yield monitor and dried again. The residue was digested with 8 ml of 6M HCl with the addition of 50 ml of Milli-Q Water and  $\sim 1$  g ascorbic acid to prevent any iron present from plating on to a silver planchet (Benoit & Hemond, 1988; Lee et al., 2014). The planchet was covered on one side with PVC tape to limit autodeposition to one side. The planchet was supported by a plastic holder and positioned in the solution, which was covered for 48 hours at 25–30 °C for autodeposition. After this time, the planchet was removed, rinsed, and dried on a warm hotplate at 30 °C. The planchets were measured for 36–48 hours dependent on achieving a  $^{209}\text{Po}$  peak area of at least 2000 counts.

The measured  $^{210}\text{Po}$  (138.4 d) was decay corrected to the autodeposition completion date as  $^{210}\text{Pb}$  is not co-deposited with the  $^{210}\text{Po}$ . As  $^{210}\text{Po}$  is lost during fusion, the measured  $^{210}\text{Po}$  originates solely from ingrowth from  $^{210}\text{Pb}$  since fusion. The measured  $^{210}\text{Po}$  can therefore be used to determine the original  $^{210}\text{Pb}$  activity in the sample. This is achieved by the utilisation of Bateman equations (Equation 3.1) to calculate the initial  $^{210}\text{Pb}$  activity concentration based on the decay corrected  $^{210}\text{Po}$  activity concentration ( $A$ ) and the known decay constants of  $^{210}\text{Pb}$  ( $\lambda_1$ ),  $^{210}\text{Bi}$  ( $\lambda_2$ ) and  $^{210}\text{Po}$  ( $\lambda_3$ ) over a period of time ( $t = 123 \text{ d}$ ) where ingrowth has occurred. The decay and ingrowth calculation allow for accurate  $^{210}\text{Po}$  (and therefore  $^{210}\text{Pb}$ ) activity concentration to be determined for each UOC.

$$^{210}\text{Pb} = \frac{A / \lambda_1 / \lambda_2}{\left( e^{\frac{-\lambda_1 t}{(\lambda_2 - \lambda_1)(\lambda_3 - \lambda_1)}} \right) + \left( e^{\frac{-\lambda_2 t}{(\lambda_1 - \lambda_2)(\lambda_3 - \lambda_2)}} \right) + \left( e^{\frac{-\lambda_3 t}{(\lambda_1 - \lambda_3)(\lambda_2 - \lambda_3)}} \right)} \quad (3.1)$$

### 3.2.5 Principal Components Analysis

Principal Components Analysis was selected as the statistical method of choice as it is a dimensionality reduction technique, whereby the least number of variable combinations, loading on to each component, are determined in order to explain the maximum amount of variance among the UOCs (Jolliffe, 2014; Tabachnick & Fidell, 2013). PCA was selected over other multivariate techniques such as factor analysis, which typically accounts for both variance and covariance (Brown, 2006), due to the nature of the dataset. The variables (radionuclides) in each UOC occur naturally together; therefore they will always correlate strongly so the covariance of the radionuclides does not need to be an area of focus. This study therefore relies on PCA's ability to focus on variance among the samples, which will maximise its potential as a discriminatory technique. Equally, other classification techniques, such as cluster analysis, must be discounted because of the relatively low number of radionuclides measured in the data and the reoccurrence of certain radionuclides across more than one of the significant components.

The PCA in this study was completed using SPSS 21 (IBM). This technique groups related dependent variables (in this case the radionuclides) into a series of components by calculating an eigenvalue for each group of variables (Jolliffe, 2014; Smith, 2002). An eigenvalue is a linear representation of the amount of variance explained by the grouping

of dependent variables which load onto each component. Components may also contain differing numbers of dependent variables subject to the variance explained by each set. Variable groupings with higher eigenvalues will inevitably explain more variance among the samples than groupings with a lower eigenvalue. A data set may contain an infinite number of components which could be used to either group or distinguish the samples, however, for the purposes of the present PCA, only the three components with the highest eigenvalues are selected.

Each UOC in the data set is then assigned 3 component scores (CS) which were calculated based on each of the three components identified as having the highest eigenvalues. The CS for each UOC represent the quantity of each sample's radionuclide activity loaded onto each component, relative to the other samples and the mean value of each radionuclide. These CS values are essentially coordinates (x, y, z) which are used to plot each sample's radiometric properties in three-dimensional space. An Oblimin rotation was applied to the CS in order to visually represent the data in the clearest possible way in three-dimensions.

### 3.3 Results and Discussion

#### 3.3.1 UOC activity concentration comparison between matrices.

The activity concentration discrepancy between the solid and fused gamma spectrometric measurements is proportional to the energy of the gamma emission associated with each radionuclide (Figure 3-3). This bias is most pronounced with  $^{234}\text{Th}$  due to its low energy emissions where the mean measurements from the solid matrix are ~15% that of the fused measurements. Comparatively, the matrix bias for medium energy  $^{235}\text{U}$  is 33% and the high-energy  $^{234\text{m}}\text{Pa}$  is 88% although some samples are within uncertainty of one another. The solid and fused activity concentration discrepancy between  $^{214}\text{Pb}$ ,  $^{228}\text{Ac}$  and  $^{208}\text{Tl}$  is between 60-70%. These discrepancies are a result of photon attenuation within the complex, heterogeneous matrix despite photon detection efficiency adjustments for individual photon energies derived from sample bulk density. The cause, effects and difficulty in applying attenuation corrections to such sample matrices are discussed elsewhere (Reading et al., 2015).

The variation of U grain/agglomeration size and concentration between the UOCs explains why different patterns can be observed between the solid and fused matrices in Figure 3-3; e.g. Lucky McGill – USA demonstrates the highest discrepancy for  $^{234}\text{Th}$ ,  $^{235}\text{U}$  and  $^{234\text{m}}\text{Pa}$  as it most likely contains the largest uranium grains or agglomerations and *vice versa* for Cotter – USA. On visual inspection, Lucky McGill contained a large amount of coarse agglomerations whereas Cotter was more mostly composed of fine powder. See Appendix B for photographs but please note that the photograph for Cotter does not represent the bulk sample – instead it represents the variation in grain size found throughout the container of UOC as supplied from the owner.

A discrepancy is observed between the two matrices for  $^{214}\text{Pb}$  activity concentrations where the bias is proportional to the total  $^{214}\text{Pb}$  present. The UOCs typically have  $< 10 \text{ Bq g}^{-1}$  of  $^{214}\text{Pb}$  with exception to Cotter – USA with  $^{214}\text{Pb}$  activity of  $28 \pm 3 \text{ Bq g}^{-1}$ . Five of the UOCs are below the lower limit of detection (LLD) of  $0.7 \text{ Bq g}^{-1}$ . The presence of  $^{214}\text{Pb}$  is an indicator of the combined inefficiency of uranium ore milling (the removal of  $^{234}\text{U}$  daughter nuclides from the system and thus disrupting the secular equilibrium) and the eventual ingrowth of  $^{234}\text{U}$  daughter radionuclides. These data cannot be used as a chronometer for

the UOC processing date, as an assumption would have to be made that the milling was 100% efficient at removing daughters of  $^{234}\text{U}$ .

Actinium-228 and  $^{208}\text{Tl}$  were detected in all of the Canadian UOCs with exception of Rabbit Lake and was also detected in Cotter – USA indicating that these UOCs, despite undergoing uranium purification, have retained trace amounts of thorium minerals present from the ore feed. The thorium present equates to between  $0.02 \pm 0.01 \text{ wt\% Th}$  (Gunnar and Cotter) and  $1.10 \pm 0.1 \text{ wt\% Th}$  (Madawaska). The difference in activity concentration between  $^{228}\text{Ac}$  and  $^{208}\text{Tl}$  is due to the branching of  $^{208}\text{Tl}$  (36%) and  $^{212}\text{Po}$  (64%) from  $^{212}\text{Bi}$ .

Activity concentrations for  $^{210}\text{Pb}$  (46.6 keV) were not resolvable due to the Compton background and the large peak tailing from the nearby  $^{234}\text{Th}$  photon peak energy of 63.3 keV resulting in a  $^{210}\text{Pb}$  lower limit of detection of  $< 15 \text{ Bq g}^{-1}$ . However, one sample (Cotter – USA) did have a measurable amount of  $^{210}\text{Pb}$  ( $28.5 \pm 2.3 \text{ Bq g}^{-1}$ ) within the fused matrix. The UOCs were measured using a Low Energy Germanium (LEGe) detector as its lower Compton background and improved resolution for low to medium energy photons, compared to HPGe, helped resolve the  $^{210}\text{Pb}$  from the Compton background. As before, only Cotter-USA had resolvable  $^{210}\text{Pb}$  and the remaining samples were all below the LLD ( $< 10 \text{ Bq g}^{-1}$ ).

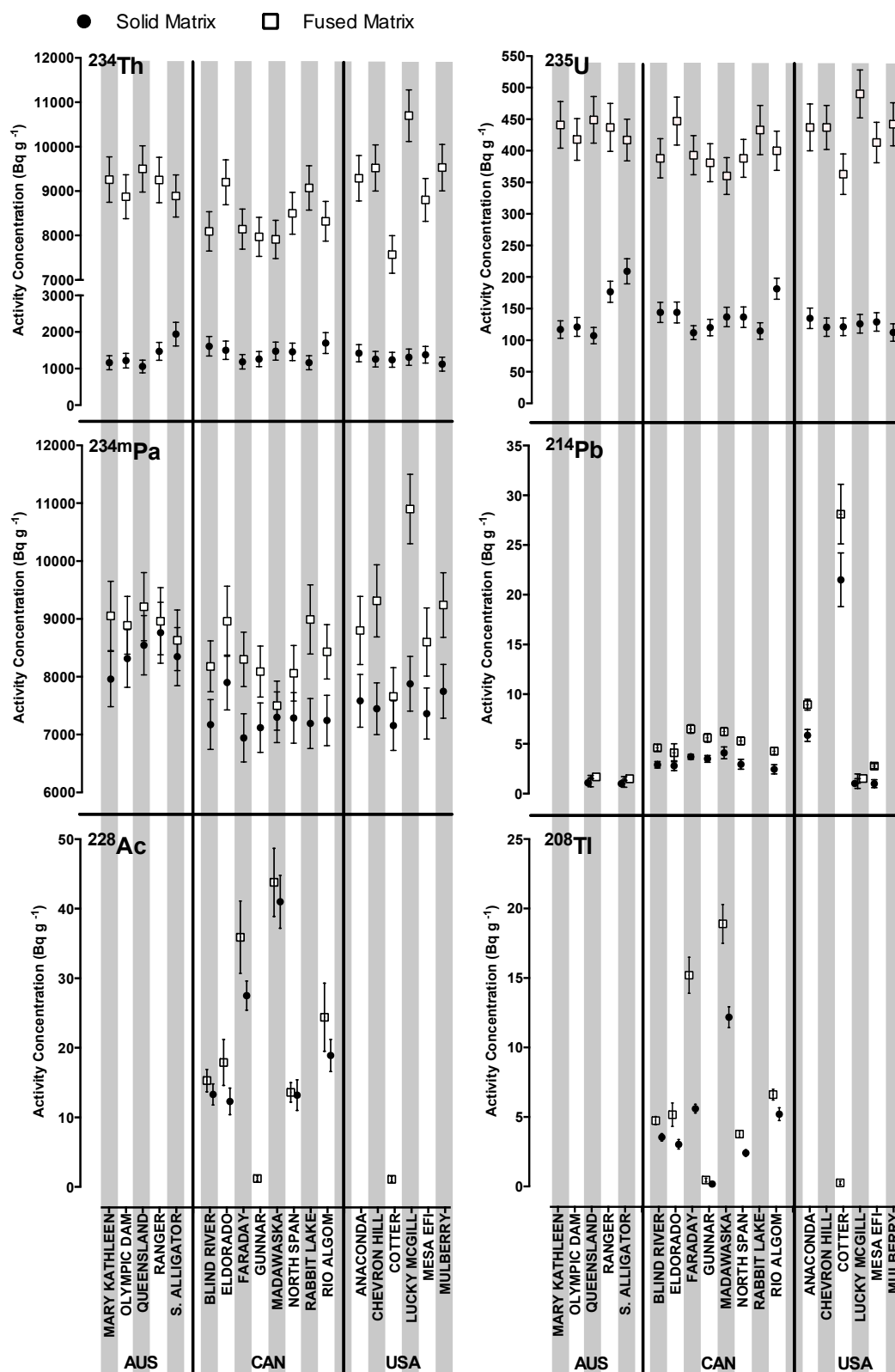


**Figure 3-3: Measured activity concentrations for  $^{234}\text{Th}$ ,  $^{235}\text{U}$ ,  $^{234\text{m}}\text{Pa}$ ,  $^{214}\text{Pb}$ ,  $^{228}\text{Ac}$  and  $^{208}\text{Tl}$  from particulate and fused UOC sample matrices.**

**LLD  $^{214}\text{Pb}$  = < 0.7 Bq g<sup>-1</sup>, LLD  $^{228}\text{Ac}$  = < 0.2 Bq g<sup>-1</sup>, LLD  $^{208}\text{Tl}$  = < 0.1 Bq g<sup>-1</sup>. Uncertainty =  $2\sigma$ .**

### 3.3.2 $^{226}\text{Ra}$ and $^{210}\text{Pb}$ activity concentrations and their ratio.

As  $^{214}\text{Pb}$  activity concentrations were measurable in most of the UOCs via HRGS, it is reasonable to assume that  $^{210}\text{Pb}$  would also be present due to the short half-lives of  $^{214}\text{Bi}$  (26.8 m) and  $^{214}\text{Po}$  (0.16 s). Due to the high LLD for  $^{210}\text{Pb}$  as previously discussed, the grand-daughter radionuclide  $^{210}\text{Po}$  was measured as a proxy using alpha spectrometry.

All of the UOCs had detectable amounts of  $^{210}\text{Po}$  with the exception of Mulberry (Figure 3-4) where the  $^{210}\text{Po}$  LLD =  $< 0.06 \text{ Bq g}^{-1}$  (which is equivalent to  $^{210}\text{Pb}$  LLD =  $0.14 \text{ Bq g}^{-1}$  with 123 d ingrowth). These data were then decay and ingrowth corrected to provide  $^{210}\text{Pb}$  activity concentrations. Where available, the activity concentrations of  $^{226}\text{Ra}$  ( $^{214}\text{Pb}$ ) and  $^{210}\text{Pb}$  ( $^{210}\text{Po}$ ) for all but one sample results in an activity ratio of 1:1 (within uncertainty) demonstrating that there is no discernible disequilibrium between  $^{226}\text{Ra}$  and  $^{210}\text{Pb}$ . The North Span UOC does not have this characteristic due to the  $^{210}\text{Pb}$  activity concentration being three-times greater than  $^{226}\text{Ra}$  (Figure 4). The milling and processing of the North Span UOC may have been less efficient at removing  $^{210}\text{Pb}$  from the uranium series decay products compared to  $^{226}\text{Ra}$  or the sample may have become anthropogenically contaminated after processing. Nevertheless, this unusual characteristic could be a useful diagnostic feature for identifying this particular UOC sample for future identification purposes. The preparation and measurement of  $^{210}\text{Po}$  can be made immediately after fusion as  $^{210}\text{Pb}$  is not affected by the procedure and therefore can act as a suitable proxy radionuclide for  $^{226}\text{Ra}$  and its immediate daughters. A selection of UOCs was treated using acid digest to ensure retention of volatile  $^{210}\text{Po}$  and to demonstrate the validity of the ingrowth and decay corrections for the fused samples. The two digestion approaches (i.e. acid and fusion) produced  $^{210}\text{Po}$  activity concentrations that were in agreement within uncertainty.

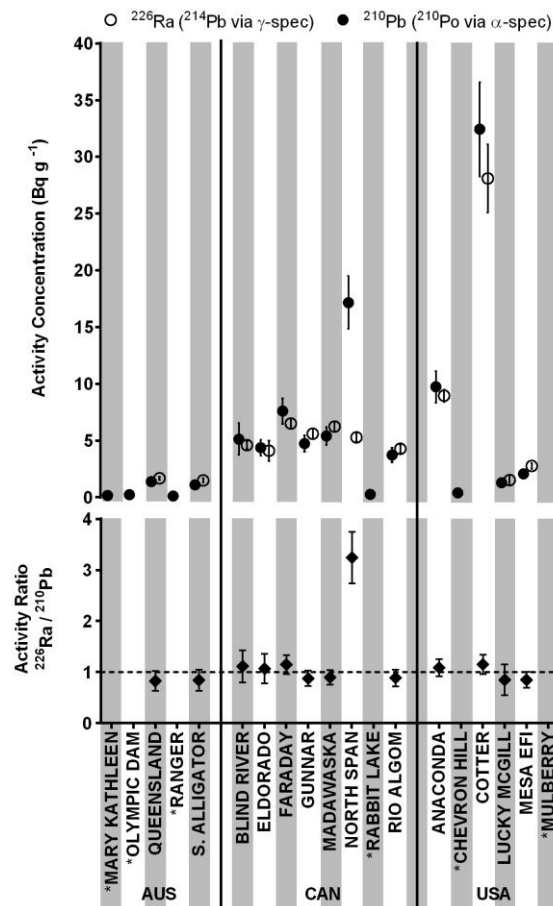


**Figure 3-4:**  $^{210}\text{Pb}$  ( $^{210}\text{Po}$ ) and  $^{226}\text{Ra}$  ( $^{214}\text{Pb}$ ) activity concentration comparisons (top) and their associated ratio (bottom).

\* denotes where ratio is not available due to  $^{226}\text{Ra}$  ( $^{214}\text{Pb}$ ) activity concentration being below the LLD. Uncertainty =  $2\sigma$ .

### 3.3.3 Principal Components Analysis

The components for the PCA were selected in order to explain the maximum amount of variance possible among the UOCs' radionuclide activity concentrations whilst limiting the analysis to only three components (Table 3-3). Lead-214 was removed from the PCA due to the incomplete data which would lower the percentage of variance of each component that it was originally assigned to.

**Table 3-3: Components and associated variables used in the PCA**

Component	Variable Selected	Eigenvalue	% of Variance (cumulative)
1	$^{234}\text{Th}$ , $^{234\text{m}}\text{Pa}$ , $^{235}\text{U}$ , $^{228}\text{Ac}$ , $^{208}\text{Tl}$ , $^{210}\text{Pb}$	4.05	67.46
2	$^{228}\text{Ac}$ , $^{208}\text{Tl}$ , $^{210}\text{Pb}$	1.37	22.80 (90.26)
3	$^{210}\text{Pb}$	0.49	8.20 (98.46)

In the first component, all of the radionuclides are included in the eigenvalue calculation; when analysed as a whole, the inter-relationships of these variables explain 67% of the total variance among the samples. However, as the PCA in this instance is being used as a discriminatory technique, the second and third components include only those radionuclides which vary most significantly from the wider group. Component two includes  $^{228}\text{Ac}$ ,  $^{210}\text{Pb}$  and  $^{208}\text{Tl}$ , which as a group varies most significantly from the wider grouping of radionuclides. The final component contains only  $^{210}\text{Pb}$  due to its high variability among these UOCs. Together, the three components account for 98% of the total variance among the UOCs. The component scores for each UOC and thus their position in three-dimensional space are displayed in Figure 3-5. If the average activity concentration for all radionuclides from all the UOCs was plotted on the PCA in Figure 3-5, the coordinates would be  $x = 0$ ,  $y = 0$ ,  $z = 0$ .

The results of the PCA reveal a central cluster of UOCs, surrounded by a number of outlying samples across all three dimensions shown. Within the cluster, nine of the UOCs share similar CS2 and CS3 values, indicating very little variability among the  $^{232}\text{Th}$  daughters and  $^{210}\text{Pb}$  concentration. Conversely, the outlying UOCs demonstrate a much greater variability in their CS coordinates, indicating major fluctuation of the measured radionuclide concentrations in one or more of the component scores.

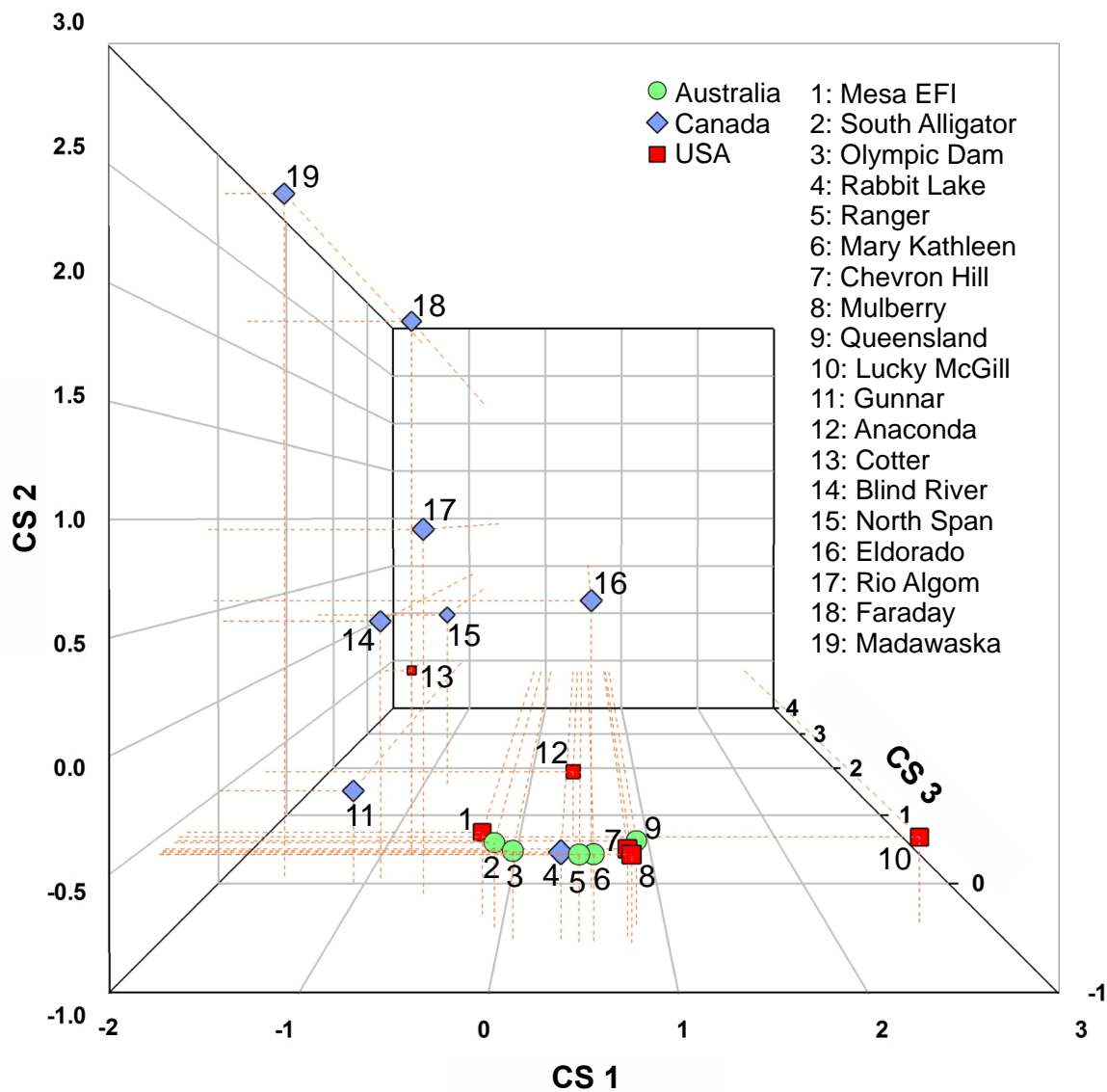


**Figure 3-5: Three-dimensional Principal Components Analysis results using 3 components with associated component scores (CS) for each UOC.**

Although this study only considers a limited number of UOC samples, it is clear that certain trends can be deduced. The Australian UOCs have all clustered in the central group meaning that the samples are all similar radiometrically and in terms of milling efficiency, regardless of the different mill locations and the mineralogy of the ore feed. The Canadian UOCs generally have a lower CS1 value than the central cluster, have highly variable CS2 values and have similar CS3 values to the central cluster with exception to North Span (point 15). The American UOCs generally have a similar CS1 score compared to the central cluster but have two UOCs that are significantly higher (Lucky McGill - point 10) and lower (Cotter – point 13) than this group. The CS2 values are generally low among the American

samples and do not show as much variance as the Canadian UOCs. The CS3 value is again similar to the central cluster but two of the samples have higher values (Anaconda – point 12 and Cotter – point 13).

Regardless of the UOCs geological origin, no trends could be observed between the type of geological deposit and the sample position within the PCA. Similarly, the known mineralogy of the local geology for each ore feed cannot be used to determine the provenance of a UOC. All but two of the Canadian samples exhibit elevated natural thorium activity concentrations suggesting that thorium-bearing minerals are present in these samples (PCA points 14-19) but ore feeds for PCA points 14 (Blind River) and 16 (Eldorado) are not known to contain elevated thorium concentrations. This could be an artefact of mixed ore feeds from various sites around the region so is not diagnostic of the mine site, but instead of the milling site. Similarly, four of the UOCs from the USA (Anaconda, Cotter, Lucky McGill and Mesa EFI) are from a region known for elevated thorium-bearing minerals and yet this is not evident in the PCA. Again, this is not necessarily an indicator of the mine site, but instead of the processing and milling site.

Despite the lack of significant differences in deposit type, mineralogy and known country of origin, the potential of the PCA as a discriminatory tool is still valid.

Although it would be difficult to match an unknown sample to a possible origin if it were to plot in the central cluster, it would allow, with statistical certainty, the laboratory to deduce that the unknown is not similar to any of the outlying positions thus reducing the possibilities of sample origin and *vice versa*. Though the PCA may not be able to indicate the likely origin all potential unknown samples, it could be used to mathematically determine the next best discriminatory technique(s) to deconvolve a group of unknowns based on the HRGS and alpha spectrometric data.

The PCA is unable to incorporate the uncertainty associated with each radionuclide when calculating the component scores associated for each sample as only the mean value is used. This is evident with the Faraday and Madawaska UOCs which are from the same, thorium-rich ore body and mill, where the Faraday site was operated between 1954-1964 and the Madawaska site was operated between 1975-1982 (Proulx, 1997; IAEA, 1980). The two UOCs demonstrate high CS2 values, little variance in CS3 and low CS1 values with respect to the central cluster. The minor difference in CS3 values would indicate that the

milling efficiencies are near identical which is to be expected if the same mill and procedure is being used. The changes observed for CS1 and CS2 however, indicate that the second operational period as Madawaska had a lower U concentration and higher natural thorium concentration indicating a potential change in the ore feed. This may or may not be the case as scrutinising the data from Figure 3-1 would indicate that the two samples have the same uranium and thorium concentration within uncertainty. The two positions of Faraday and Madawaska on the PCA in an ideal situation would be closer together. Despite this, the two samples are significantly different from all of the other UOCs present in the PCA which demonstrates that the samples are most likely not related to any of the other UOCs.

Traditional exploratory statistical techniques such as correlations and analyses of variance (ANOVA) were also considered, but were unable to account for such a complex data set. These methods act by separating only two selected variables for analysis, whilst inter-relationships among the larger set of dependent variables typically cannot be accounted for within complex data sets. Thus, the analysis of such inter-relationships using PCA might be better able to discriminate one UOC from another more so than correlations and ANOVA alone due to its organisation of inter-related variables into a number of components.

### **3.3.4 Experimental and Statistical Validation.**

The robustness and reproducibility of the experimental procedure and statistical approach was validated by re-preparing and re-counting six UOCs, two from each country which demonstrated the most variance based on the original PCA in an attempt to identify whether a large database containing UOC radiological data could be used as a discriminatory and provenance determining tool. The six UOCs were: Cotter, Eldorado, Faraday, Lucky McGill, Queensland and South Alligator. The radiometric data of the six “unknown” samples was added to the pre-existing PCA database and the results are shown in Figure 3-6.

The six “unknown” samples plot close to their original positions as determined in the original PCA indicating that the experimental procedure and statistical approach can be replicated and therefore can be used as a discriminatory tool. Additionally, it demonstrates that not incorporating measurement uncertainty in the component score calculation is not detrimental to the overall analysis in determining where an “unknown” samples plots among previously characterised samples.

For the Canadian and American UOCs, the “unknown” UOCs plot next to the original PCA data indicating that with high amount of certainty, these UOCs can only come from one potential origin. This becomes more complicated for the Australian UOCs where so many UOCs are positioned in close proximity in the central cluster. In this instance, it is unadvisable to attempt to identify an exact origin for the UOC but instead to eliminate which UOCs the “unknown” sample cannot be.

With such a small UOC dataset, it is relatively simple to discriminate between the 19 samples. This will inevitably become more complicated if a larger UOC radiological database was created representing historic and current UOC production. However, as demonstrated with the Australian UOCs, if an “unknown” sample cannot be attributed to a single provenance, it can at least reduce the number of suspected origins greatly. Similarly, if an “unknown” sample plots near a group of UOCs that are known to have highly variable rare earth element (REE) signatures, the laboratory may decide that an investigation in to REE signatures is the best discriminatory method to apply to further discriminate the samples.

The composition of an ore feed will vary over time depending on whether multiple mine sites are being processed simultaneously at a single mill, or whether significant intra-mine compositional variability is possible from large deposits. Adjustment in mill processing techniques to ensure that the quality of product are to the customer’s specification are also factors that need to be taken in to account when applying historic data to unknown suspect materials.

Regardless, the processing technique, parameters and purification efficiency for UOC production will remain consistent for extended periods of time. This results in consistent uranium grade and levels of impurities (daughter radionuclides and other gangue materials) and is diagnostic of the mill during a particular period of operation.

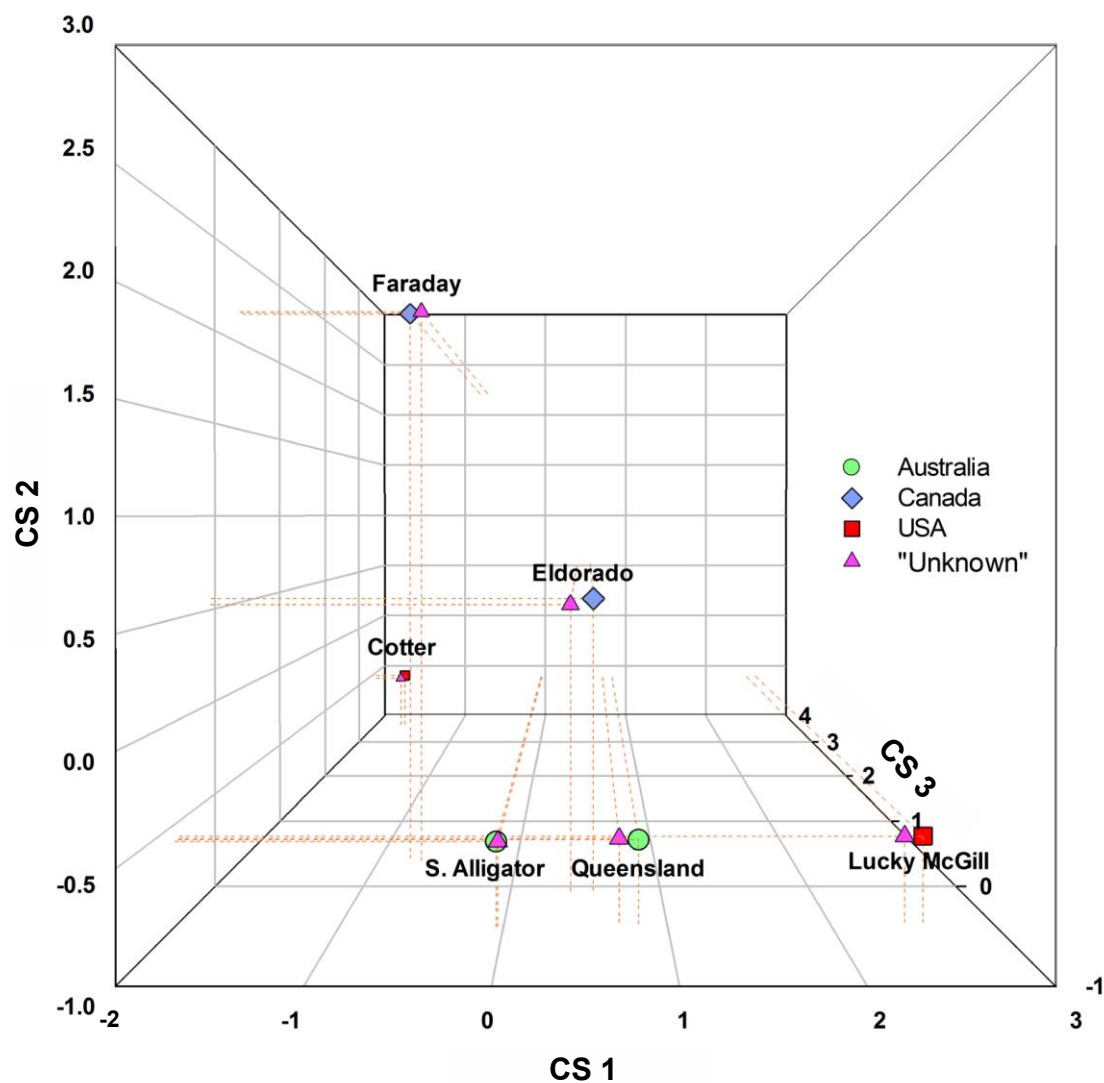


**Figure 3-6: Three-dimensional Principal Components Analysis results for experimental and statistical validation of techniques.**

**CS = component score.**

### 3.4 Conclusion

This study has shown that Principal Component Analysis PCA is a useful nuclear forensic tool that can help indicate the origin of unknown, illicitly recovered UOCs. The study used 19 UOC samples to build a database of radiometric signatures based on gamma and alpha spectrometry. Prior to any applications using gamma spectrometry data it is critical that matrix and absorption effects are adequately compensated for otherwise data accuracy will be diminished. Variable density samples such as U ores and UOCs are particularly susceptible to matrix/particle problems especially significant for radionuclides having only low energy gamma energies. The elimination or reduction of matrix and particle effects can be effectively dealt with using specific digestion methods and in this study a lithium tetraborate fusion is shown to ensure rapid dissolution and accurate data.

The results from the PCA demonstrate that some UOCs group together due to their similar radiometric properties, whereas over 50% of the samples are outliers and are statistically different from one another. Six of these UOCs were re-prepared, measured and scrutinised via PCA in an attempt to validate the experimental and statistical approaches. The “unknown” samples plotted consistently close to their original data points showing that such an experimental and statistical approach can be used for matching an “unknown” sample against known samples within a database for determining the origin of UOCs. This is limited however as the samples represent a single historic moment of the milling facilities processing and ore feed. Temporal examination would need to be conducted to assess how intra-mine and processing variability affects the UOC composition and therefore the robustness of the statistics.

Where an unknown sample plots near a cluster of radiometrically similar samples, the laboratory may be in a better position to determine the next analytical technique required to further constrain the origins of the unknown based on a signature which is known to be different amongst the particular cluster of samples.

For such a technique to be applied for current and future nuclear forensic investigations on illicitly recovered specimens, UOCs representing historic and currently operating uranium mills would need to be profiled for their radiometric properties in order to potentially match a recovered sample in the future.



## **Chapter 4: A novel glass bead fusion procedure for nuclear forensics using synthetic enstatite to dissolve uraniferous and other challenging materials prior to LA-ICPMS**

**Submitted to Analytical Chemistry**

### **Abstract**

There is an increasing demand for rapid and effective analytical tools to support nuclear forensic investigations of seized or suspect materials. New methods are sometimes simply adapted from other scientific disciplines and can effectively be used to rapidly prepare complex materials for subsequent non-destructive analysis. A whole sample fusion method is tested and validated to produce homogeneous, flux-free glass beads of geochemical reference materials (GRMs), uraniferous oxides and uraniferous ore samples prior to the analysis of 14 rare earth elements (REE) via laser ablation ICP-MS. A novelty of the procedure is the production of the glass beads using 9 parts high purity synthetic enstatite ( $\text{MgSiO}_3$ ) as the glass former along with 1 part of sample (with sample masses as small as 1.5 mg). The beads are rapidly prepared (~10 minutes overall time) by fusing the blended mixture on an iridium strip resistance heater in an argon-purged/filled chamber. The chondrite normalised REE patterns subsequently determined by LA-ICPMS are in very good agreement with the reference patterns. The conservation of sample, speed of preparation and suitability for microbeam analysis will make the method attractive for nuclear forensics practitioners and geochemists requiring REE patterns from scarce or valuable samples.



## 4.1 Introduction

Nuclear forensics as a technical discipline has emerged significantly over the last two decades and uses a broad array of advanced analytical procedures to characterise seized or suspect nuclear and related materials (Reading et al., submitted A.; Croudace et al., submitted; Reading et al., 2015; IAEA, 2015b; Hutcheon et al., 2013; Mayer et al., 2013; Stanley et al., 2013; Mayer et al., 2007). The insights gained from such data are used to control suspected trafficking activities, to deter nuclear terrorism and to verify that international nuclear treaties are being upheld. There is an ever-present international threat that nuclear or other radioactive material could be acquired for use in criminal acts. This requires vigilance from the authorities and demands that the radioanalytical community continually develop, refine and improve a range of robust and rapid analytical methods to support the specialist investigative and law enforcement agencies.

**Micro-analytical fusion-with-flux methods:** Many seized materials requiring investigation will be sparingly soluble or insoluble in mineral acids and often heterogeneous. In these cases more specialised fusion methods could be more suitable for producing representative glassy and homogeneous materials for analysis. Analytical approaches for trace elemental analyses such as XRF, ICP-OES and ICPMS, despite having their individual advantages, typically require sample masses >200 mg to reduce detection limits (XRF). Borate fusion (often lithium tetraborate is used as the fluxing agent at high temperature usually above 1100 °C to produce a homogeneous glass or subsequent quenched melt) is also advantageous as a preparation method in ICPMS as acid digestion alone can be unsuitable where resistant minerals exist (e.g. rutile, zircon, chromite) or where boron addition is deemed undesirable. For example, the introduction of Li and B to ICPMS systems (including laser ablation cells) could compromise the analytical work of other researchers (e.g. oceanographers) sharing mass spectrometry facilities whom are interested in ultra-precise boron isotope measurements (Stewart et al., 2015). It is notable that flux based approaches (using lithium borates) though effective also dilute the sample thus increasing detection limits for trace elements (Eggins, 2003; Yu et al., 2003).

**Flux-less fusion techniques:** Creating a glassy compact sample without a flux (flux-free or flux-less) can be advantageous in terms of speed of preparation, homogenisation, conservation of sample and long-term stability (for measurement and archiving). A

possible disadvantage of such flux-less fusions is the volatilisation of some elements, e.g. alkali group metals, Ge, Pb and Sn (Fedorowich et al., 1993; Stoll et al., 2007; Nehring et al., 2007) and elements of interest to the nuclear fuel cycle with low condensation temperatures such as Cs (525 °C), Sr (1190 °C) and I (260 °C) (Lodders, 2003). An early flux-free fusion system was developed by Nicholls (1974) who fused samples (20 mg upward) on an iridium strip in an argon atmosphere to prevent oxidation. Other later designs also used W or Mo as the heating element or performed the fusion in Pt or Mo capsules followed by rapid quenching of the produced glass (Nicholls, 1974; Brown, 1977; Fedorowich et al., 1993; Reid et al., 1999; Kurosawa et al., 2006; Zhu et al., 2013; He et al., 2016). These studies demonstrated that with the correct fusion conditions homogeneous glass beads could be produced and accurately characterised by laser ablation ICPMS for geochemical applications. Where samples are non-siliceous (e.g. oxides, carbonates) it is necessary to add a small quantity of a glass former such as silica to produce a stable glass bead for analysis.

Optimising the fusion conditions (temperature, time and composition) is critical to the homogeneity of the resulting glass bead and ensuring that all components have dissolved effectively. Geological samples rich in Si, Mg, Ca and Fe can be prepared at 1200 °C with fusion times of about 10 seconds whereas samples rich in Al, Si and alkali elements tend to require a longer fusion time and higher temperatures (up to 30 s and 1800 °C) (Nehring et al., 2007; Stoll et al., 2007) to ensure homogenisation of the more viscous Si-rich melts that are produced. The addition of pure MgO has been used by some researchers to improve the fluidity and homogenisation of Si-rich melts (Nehring et al., 2007; Gumann et al., 2003).

**Use of pure synthetic enstatite:** This study has focused on the investigation of silica-poor materials (e.g. uranium ore concentrates (UOC), oxides etc.) and for these it is not possible to form a glassy bead unless glass-forming components are added. In this study it was considered that synthetic enstatite ( $\text{MgSiO}_3$ ) would be an ideal silicate composition capable of dissolving complex materials that would create a glassy bead suitable for subsequent microanalysis. The enstatite was prepared by mixing high purity  $\text{SiO}_2$  and MgO (Specpure™) in molar proportions and the optimal ratio of sample: $\text{MgSiO}_3$  to produce consistent homogeneous glass bead has been investigated. The effectiveness of the overall approach was determined using a set of international geochemical reference samples, two uranium ores, a UOC and two Mn-nodule reference samples.

**REE in nuclear forensics:** It is long established that graphical plots of the lanthanide group elements (or rare earth elements, REEs) can provide powerful insights into genetic processes for materials such as rocks, minerals, ores and processed ores. The plotting of normalised concentrations of La–Lu (logarithmic y-axis) against atomic number is conventionally used by geochemists to visualise REE data. The normalisation involves dividing each REE concentration in a sample by its corresponding value from a chondritic meteorite which serves to remove the well-known saw-tooth abundance distribution (the Oddo-Harkins effect (Oddo, 1914; Harkins, 1917)). UOCs representing processed uraniferous ores, can retain the REE signatures of the ore or the mill from which they were derived because intra-REE variations (chemical fractionation) are expected to be limited during ore milling processes (Varga et al., 2010b). On this basis, REE patterns offer a potentially valuable characteristic that can be used in nuclear forensic investigations (Varga et al., 2010a, 2010b; Mercadier et al., 2011; Keatley et al., 2015) where there will be an interest in the provenance of seized materials. Beyond nuclear forensics, REE patterns are used to infer geochemical associations, formation processes, mineralisation and geological type localities (i.e. geolocation).

Being able to rapidly produce and accurately analyse glass beads for REE from very small samples, particularly using highly sensitive LA-ICPMS, is a potentially powerful investigative technique. The method has so far not been applied in the nuclear forensics field but clearly offers promise over traditional preparative methods where sample is scarce and could, for example, allow potential UOC origin to be inferred. Applications could include the analysis of illicitly recovered UOC which contain almost no silica but which may retain a mineralogical and geochemical memory of the original ore or milling facility. Additionally, this flux-less method of sample preparation and analysis could be extended to the rapid and effective analysis of other geochemical materials which inherently contain low levels of silica such as polymetallic ores and manganese nodules (Abramowski & Stoyanova, 2012) (which can contain 30% Mn and 6% Fe but less than 5% Si).

## **4.2 Methodology**

### **4.2.1 Instrumentation**

#### **4.2.1.1 The Iridium Strip Fusion System**

The design of the fusion device is similar to that described by Fedorowich et al. (1993), but incorporates the addition of a laser pyrometer (CTM-1SF75 650-1800 °C – Micro-Epsilon Messtechnik, Ortenburg, Germany supplied by Impress Sensors and Systems, UK) to provide an accurate digital feedback of the temperature of the Ir-strip. The device was originally designed, constructed and tested by one of the authors (IWC; see Figure 4-1, D-1, D-2 and D-3) and is now available (Raddec International Ltd, Southampton). It consists of a single cylindrical aluminium chamber separated into two sections using a Tufnal® insulating disc that holds two substantial copper electrodes. Aluminium was chosen as the case material to reduce overall weight of the device once an electrical transformer was installed. Holes are drilled in to the lower section of the chamber to allow good airflow around the transformer to prevent overheating. A 4V / 150A transformer supplies the current to the Ir-strip (cut from 0.5mm thick sheet supplied by Heraeus, Germany) via copper terminals which are isolated from the casing. Power to the strip is supplied and controlled using a Eurotherm thyristor circuit (Worthing, UK). Manual heat control is simply made via a 'soft start' potentiometer that provides a rapid and responsive control. A USB microscope with zoom allows effective observation and recording of chamber and Ir-strip fusion conditions. Argon is used to purge the chamber of oxygen and as argon is denser than oxygen, it is introduced at the bottom of the fusion chamber and allowed to escape at the top.

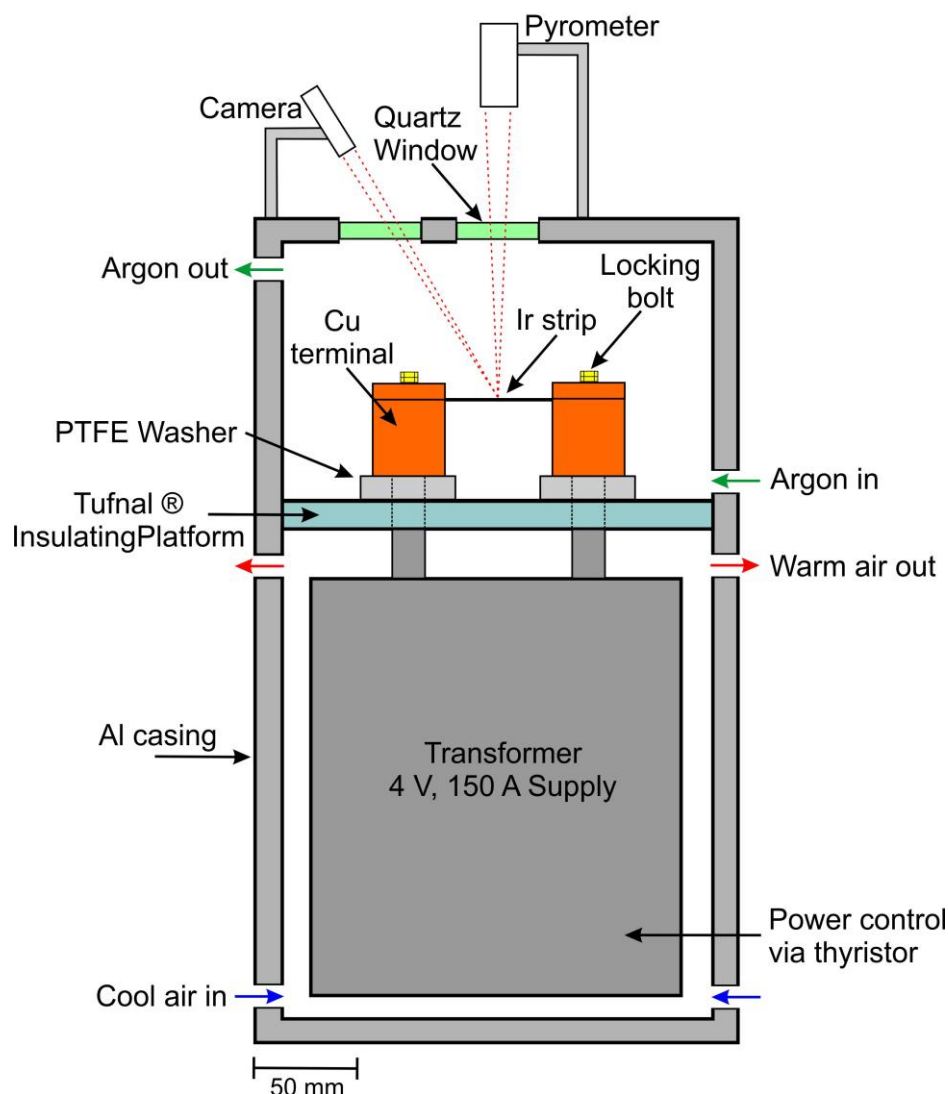


**Figure 4-1: Schematic of the iridium-strip resistance fusion system**

#### 4.2.1.2 Eagle III $\mu$ XRF probe

Glass bead homogeneity was initially assessed using the Eagle III™  $\mu$ XRF microprobe elemental analyser (EDAX Inc®. NJ, USA) which combines an optical microscope and an XRF spectrometer fitted with a 40-300  $\mu$ m Varisport polycapillary waveguide to investigate elemental composition. A Rh X-ray tube operating at 40 kV and 200  $\mu$ A was used for excitation. The Eagle III™ benchtop unit contains a motorised xyz stage to allow for automated elemental sample mapping of Na through to U inclusively. This  $\mu$ XRF unit was used to determine the appropriate blend of UOC to  $\text{SiO}_2$  and MgO to achieve sample

homogeneity prior to any laser ablation measurements due to its ease of setup and rapid analysis.

### 4.2.1.3 LA-ICPMS

The glass beads were ablated using a ESI® New Wave Research™ UP193FX 193 nm solid-state laser ablation system (Fremont, CA, USA) coupled to a Thermo Fisher™ X-Series II Quadrupole ICP-MS (see Appendix A-2 for operating conditions). Instrument calibration, performance and stability was performed using NIST glass standards CRMs 610 and 612 and the elemental concentrations for each CRM were taken from the GeoReM database (Jochum & Enzweiler, 2013; Jochum et al., 2005; Pearce et al., 1997). The relative standard deviation for replicate element concentration measurements of the NIST CRMs were less than 5% with exception to Mg in NIST CRM 610 which was 8%. Each glass bead was measured at a minimum of 40 positions throughout the sample to investigate homogeneity and the following isotopes were measured:  $^{27}\text{Al}$ ,  $^{44}\text{Ca}$ ,  $^{47}\text{Ti}$ ,  $^{55}\text{Mn}$ ,  $^{85}\text{Rb}$ ,  $^{88}\text{Sr}$ ,  $^{90}\text{Zr}$ ,  $^{93}\text{Nb}$ ,  $^{137}\text{Ba}$ ,  $^{139}\text{La}$ ,  $^{140}\text{Ce}$ ,  $^{141}\text{Pr}$ ,  $^{146}\text{Nd}$ ,  $^{147}\text{Sm}$ ,  $^{153}\text{Eu}$ ,  $^{157}\text{Gd}$ ,  $^{159}\text{Tb}$ ,  $^{163}\text{Dy}$ ,  $^{165}\text{Ho}$ ,  $^{166}\text{Er}$ ,  $^{169}\text{Tm}$ ,  $^{172}\text{Yb}$ ,  $^{175}\text{Lu}$ ,  $^{232}\text{Th}$ ,  $^{238}\text{U}$ . Due to the significantly reduced oxide production rates caused by laser ablation and dry plasma, oxide-induced isobaric interferences were not significant.

### 4.2.2 Iridium-strip fusion

Iridium metal strips were prepared by soaking in HF followed by  $\text{HNO}_3$  and Milli-Q® water (Millipore™, USA). Dry samples were loaded onto the centre of the Ir-strip. The sample was dampened with 10  $\mu\text{L}$  of Milli-Q water to form a thick slurry and then dried in air to produce a cake which prevents the sample from vibrating off of the Ir-strip due to the resonance effect of the high current passing through it. The fusion device was closed and argon (BOC Pureshield 99.998% purity) was allowed to flood the chamber for 2 minutes to purge oxygen from the environment to prevent oxidation of the sample. The external pyrometer was positioned so that the point from the laser is next to the gathered sample to allow for accurate temperature determination of the Ir-strip. The current was applied and adjusted to slowly increase the temperature. Once 1500 °C was reached, the sample was allowed to fuse for 1 minute at which point the current was isolated and thus quenches the melt immediately. The Ar was left to flow through the chamber to help with sample and apparatus cooling for 1 minute. The Ir-strip was carefully removed from the chamber and flexed gently to separate the glass bead.

#### 4.2.3 Determining the optimal UOC to silica ratio for fusion

As previously mentioned from other studies, samples with approximately 50%  $\text{SiO}_2$  content should produce homogeneous beads using fusion at  $\sim 1500^\circ\text{C}$  for  $> 10$  s. For samples containing virtually no  $\text{SiO}_2$ , such as UOC, it is imperative that  $\text{SiO}_2$  is added in sufficient quantity to enable the production of the glass bead but not so much that the melt becomes too viscous resulting in heterogeneity. The mass of UOC required must be kept to a minimum but should be sufficient enough that the element/isotope of interest is not below the limit of detection for the measurement technique of choice. Additionally, the final glass bead must have a sufficient surface area (minimum mm diameter) and depth so that multiple ablations can be made from a single sample.

High purity  $\text{SiO}_2$  and  $\text{MgO}$  and CRM CUP-2 (CCRMP) were dried at  $100^\circ\text{C}$  overnight to remove moisture. The  $\text{SiO}_2$  and  $\text{MgO}$  was blended at a 1:1 molar ratio ( $\text{MgSiO}_3$  or enstatite) and then milled to reduce the grain size before being blended with CUP-2 (analogous to a UOC due to its high U content – 75%) at varying ratios whilst maintaining a total sample mass of 15 mg (Table 4-1). This total sample mass was selected as it was found to produce an adequately sized ( $\sim 4$  mm) single glass beads without splitting into two separate and smaller glass beads. The homogeneity and degree of coalescence of the bead was assessed for varying UOC: $\text{MgSiO}_3$  ratios to determine the optimum ratio.

The six resulting glass beads were analysed via  $\mu\text{XRF}$  spectrometry to assess the homogeneity of the three main elements (Mg, Si and U). Each sample was secured on to the x-y-z stage and the sample chamber was put under vacuum. The  $\mu\text{XRF}$  spectrometer was operated in line scan mode for all the glass beads and additional full matrix scans were performed for the 10:90 and 20:80 glass beads.

**Table 4-1: CUP-2:MgSiO<sub>3</sub> sample ratios and masses with total SiO<sub>2</sub> percentage**

Ratio	Total mass (mg)	CUP-2 (mg)	SiO <sub>2</sub> (mg)	MgO (mg)	% SiO <sub>2</sub>
10:90	15	1.5	6.75	6.75	45
20:80	15	3	6	6	40
30:70	15	4.5	5.25	5.25	35
40:60	15	6	4.5	4.5	30
50:50	15	7.5	3.75	3.75	25
60:40	15	9	3	3	20

Uncertainty associated with mass measurement = 0.1%, k=2.

#### 4.2.4 Geochemical and uranium certified reference materials

A variety of geochemical and uranium CRMs (Table 4-2) were prepared as glass beads using the 10:90 sample:MgSiO<sub>3</sub> blend to determine whether such a small amount of reference sample (1.5 mg) diluted synthetic enstatite is sufficient for the accurate and precise measurement of the REEs. The geochemical CRMs were selected due to their differing REE distribution and concentration and as they represent a range of SiO<sub>2</sub> contents. The uranium CRMs were selected due to their range of U and SiO<sub>2</sub> concentrations. CRM CUP-2 is analogous to a typical UOC. A set of MgSiO<sub>3</sub> blanks were also produced to correct for element contaminants associated with the reagents.

The resulting glass beads were mounted in epoxy resin under vacuum and then cut and polished to expose a smooth and flat surface using a similar method to the production of petrographic thin sections. The mounted glass beads were then arranged on to a glass slide so that up to 24 separate samples plus the NIST CRMs could be analysed in one session and without intervention. Approximately 1 mm of space between the mounted glass beads and the edge of the slide was required to ensure sufficient flow of the carrier gas.

**Table 4-2: Reference materials investigated**

<b>Code</b>	<b>Origin</b>	<b>Provider</b>
AC-E	Ailsa Craig Peralkaline Granite – SW Scotland, UK	CRPG IWG-GIT
BE-N	Basalt – Essey-la-Cote, Nancy, France	CRPG IWG-GIT
BHVO-1	Basalt – Hawaii, USA	USGS
BL-5	U-ore (7.1 wt% U) – Beaverlodge, SK, Canada	CCRMP
CUP-1	U-ore (0.1 wt% U) – Schwarzwald, CO, USA	CCRMP
CUP-2	UOC (75.4 wt% U) – Blind River, ON, Canada	CCRMP
Mica-Fe	Biotite Mica-Fe – Massif Central, France	CRPG
NOD-A1	Ferromanganese Nodule – Atlantic Ocean	USGS
NOD-P1	Ferromanganese Nodule – Pacific Ocean	USGS
SY-2	Syenite – ON, Canada	CCRMP
SY-3	Syenite – ON, Canada	CCRMP

### 4.3 Results and discussion

#### 4.3.1 Determining the optimal UOC to silica ratio for fusion

Glass beads with UOC:MgSiO<sub>3</sub> ratios ranging from 10:90 to 60:40 were prepared. For ratios greater than 30:70, the melt was viscous due to the high U content and did not coalesce into a single bead of glass, resulting in a potentially heterogeneous bead. For the two lowest ratio glass beads the melt did coalesce into a single bead (especially for 10:90) and homogenisation was likely to have been achieved.

The six glass beads were mounted in epoxy resin, cut and polished to expose a smooth flat surface and were measured for Mg, Si and U by the  $\mu$ XRF spectrometer to calculate the extent of sample homogeneity as a function of percentage standard deviation (the reproducibility of results) of the count rate. The data were collected using line scan mode for all glasses and full matrix scan mode for the two lowest ratio glass beads (10:90 and 20:80) using a beam size for all measurements was 120  $\mu$ m. The NIST CRM 610 was also characterised to obtain a percentage standard deviation of a truly homogeneous reference material. The measured elements from the NIST 610 CRM include: Na, Mg, Al, Si, Ca, Ti, V, Cr, Mn, Fe, Ni, Cu, Zn, As, Sr, Zr and U where concentrations are all  $\sim$ 450 ppm.

Replicate analyses of NIST CRM 610 (n=50) showed a relative standard deviation of  $\sim$  6% and therefore in this study, any value <10% from a prepared glass bead is considered homogeneous. The line scan results from the glass beads with UOC:MgSiO<sub>3</sub> ratio greater than 30:70 demonstrated that the glasses were heterogeneous (>14 %RSD – Table 4-3). The measurement points were all located towards the centre of the glass bead and avoided any anomalous topographic or surficial features. The line scan results for 10:90 and 20:80 were both <10 %RSD and the entire surface of each glass was measured in matrix mode. The matrix mode analyses demonstrated that the 10:90 and 20:80 glass beads had a percentage standard deviation of 3.26% and 8.98% respectively and are therefore considered homogeneous. The data collected from the edges of the glass were not included in the final calculation.

Replicate analyses of NIST CRM 610 at different points showed a relative standard deviation of about 6% and therefore in this study, any value <10% from a glass bead is considered homogeneous. The line scan results from the glass beads with UOC:MgSiO<sub>3</sub> ratio greater

than 30:70 demonstrated that the glasses were heterogeneous (>14 %RSD – Table 4-4). The measurement points were all located towards the centre of the glass bead and avoided any anomalous topographic or surficial features. The line scan results for 10:90 and 20:80 were both <10 %RSD and the entire surface of each glass was measured in matrix mode. The matrix mode analysis demonstrated that the 10:90 and 20:80 glass beads had a percentage standard deviation of 3.26% and 8.98% respectively and are therefore considered homogeneous. The data collected from the edges of the glass were not included in the final calculation.

**Table 4-3: Percentage standard deviations (%RSD) of the glass beads**

<b>Glass bead – UOC:MgSiO<sub>3</sub></b>	<b>Line or matrix scan (analysis points)</b>	<b>%RSD of count rate</b>
10:90	Line (30) & Matrix (200)	3.26 (matrix)
20:80	Line (30) & Matrix (100)	8.98 (matrix)
30:70	Line (16)	14.65
40:60	Line (16)	17.98
50:50	Line (10)	24.01
60:40	Line (10)	34.25

### **4.3.2 Laser ablation results**

#### **4.3.2.1 Elemental homogeneity and volatility**

The geochemical and uraniferous reference materials were prepared in duplicate as glass beads using the 10:90 sample:MgSiO<sub>3</sub> ratio and were mounted, cut and polished in resin as previously described. The glass beads were analysed using LA-ICPMS to assess the homogeneity and elemental variation using the percentage standard deviation of major elements within the geochemical reference materials (Figure 4-2). The extent of homogeneity was determined from a minimum of 10 groups of 4 ablation spots randomly positioned around the surface of the polished glass bead. Anomalous results due to interaction with resin or vesicles (Figure 4-3), or from poor sample transmission are omitted from the calculation and are identified by the low counts of each measured element in comparison to surrounding ablation spots.

The reproducibility of the data (the percentage standard deviation of each element) is controlled by the sample homogeneity and the measurement uncertainty which is concentration dependent. The NIST 610 and 612 reference glasses are known to be homogeneous and have uniform element concentrations (~450 and 40 ppm respectively). The sample reproducibility for NIST 610 and 612 is 1.5 and 5% respectively, therefore, if a glass bead were to exhibit 5% reproducibility on an element known to be at a concentration of 40 ppm or greater, the glass bead can be said to be truly homogeneous. For element concentration <40 ppm, the reproducibility decreases due to measurement uncertainty and can be clearly observed with NOD-A1 and NOD-P1 where reproducibility of U is 13-15% due to the already low U concentration being diluted further by MgSiO<sub>3</sub>, whereas the Mn reproducibility in the same reference standards is <4% due the exceptionally high concentration of Mn. The glass beads of geochemical reference material in this study are all deemed homogeneous based on the highest concentration elements known to be present and the reproducibility of such elements being less than or equal to 10%. Elemental data that exceed 10% reproducibility typically has a concentration of <10 ppm.

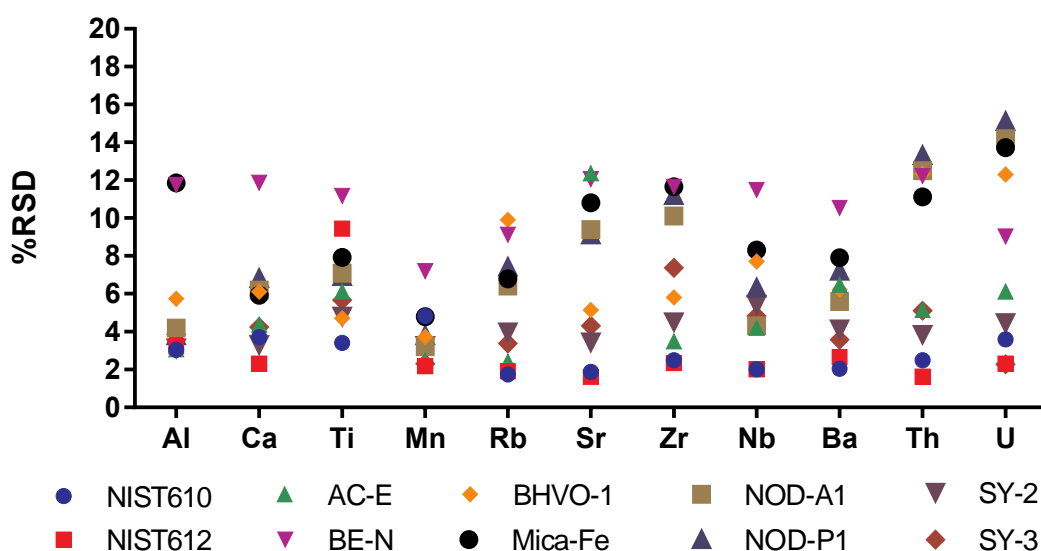


**Figure 4-2: %RSD values of selected elements for 8 geochemical reference materials and NIST calibration glasses.**

**AC-E**



**SY-3**

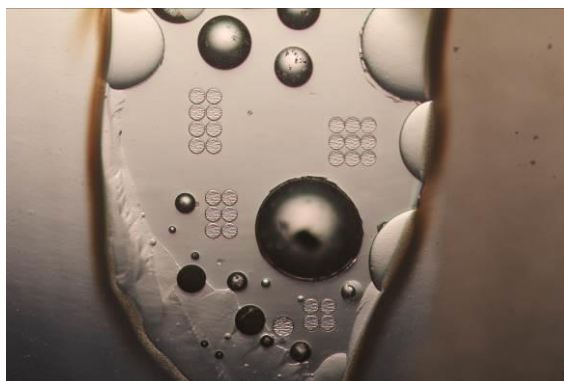


**Figure 4-3: Resin mounted and laser ablated (circular pits) AC-E and SY-3 where resin interaction is possible due to vesicles and thin edges of glass beads.**

Unlike previous studies, these geochemical reference materials have been diluted nine-fold to ensure that a glass can be produced irrespective of the original  $\text{SiO}_2$  concentration. Therefore, the elemental concentrations are far lower than previous studies and higher percentage standard deviation values are calculated due to minor fluctuations in an already low element concentration.

Mean concentrations for Cu, Pb, Sn and Zn were between 0 and 30% of the GeoReM preferred values for SY-2 and SY-3 indicating volatilisation of these elements during fusion (Figure 4-4). Such volatilisation has been previously observed and relates to low condensation temperatures (Nehring et al., 2007; Stoll et al., 2007). The REEs have high condensation temperatures and volatilisation is not observed in the geochemical reference materials (Figure 4-5).

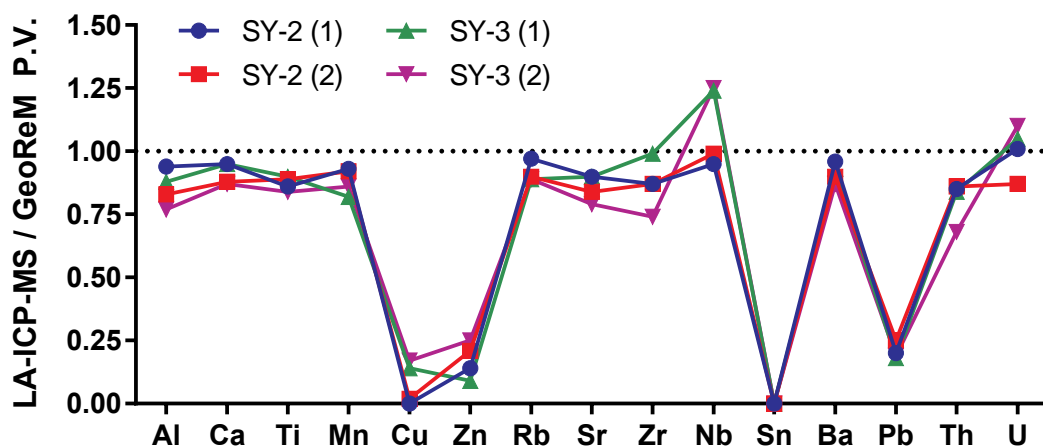


**Figure 4-4:** Ratio of measured element concentration against the GeoReM preferred or consensus values demonstrating element volatilisation of Cu, Pb, Sn and Zn.

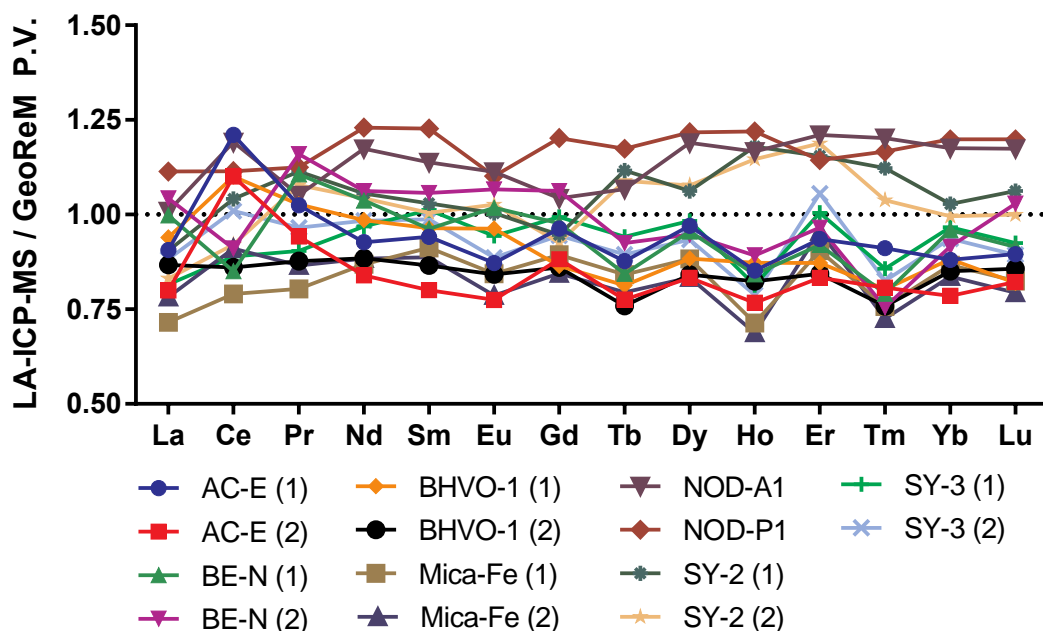


**Figure 4-5:** Ratio of measured element concentration against the GeoReM preferred or consensus values for the rare earth elements.

#### 4.3.2.2 Rare earth element patterns

The REE chondrite normalised (REE/CI) data were determined for each glass bead (Figure 4-6 - Tables available in Appendix D). All glass bead data are averages from at least 40 analysis points and have been blank and dilution corrected. Anomalous results caused by poor sample transmission or from partial interaction with a vesicle or the resin were excluded from the calculation. Reference values are from GeoReM preferred/consensus values and the chondrite normalisation uses the data from Anders and Grevesse (1989).

The chondrite normalised REE data from the glass beads have virtually identical profiles to those based on GeoReM preferred values and demonstrate that despite the low mass of geochemical standard in the final glass bead (< 1.5 mg), accurate REE signatures can be obtained and are well above detection limits for a laser ablation setup coupled to a benchtop ICP-MS. Furthermore, the addition of  $\text{MgSiO}_3$  to this wide range of geochemical reference materials has not caused any anomalous results in the patterns as a result of adjusting the  $\text{SiO}_2$  content to approximately 50%.

Despite some element concentrations not perfectly matching the chondrite normalised GeoReM values, for example the relative Ce enrichment in AC-E, the REE patterns are sufficiently close that the method provides a powerful and rapid analytical tool for applications as demanding as those found in nuclear forensics. The GeoReM values are compiled from datasets using solution ICP-MS methods where chemical separation has been performed to purify the analytical fraction. No chemical separation was performed in this study and yet, REE signatures are near identical to the GeoReM values despite being diluted up to 10 times and measured via LA-ICPMS. This demonstrates that the sample preparation via fusion and analysis via LA-ICPMS is a robust means for collecting accurate rare earth element data.

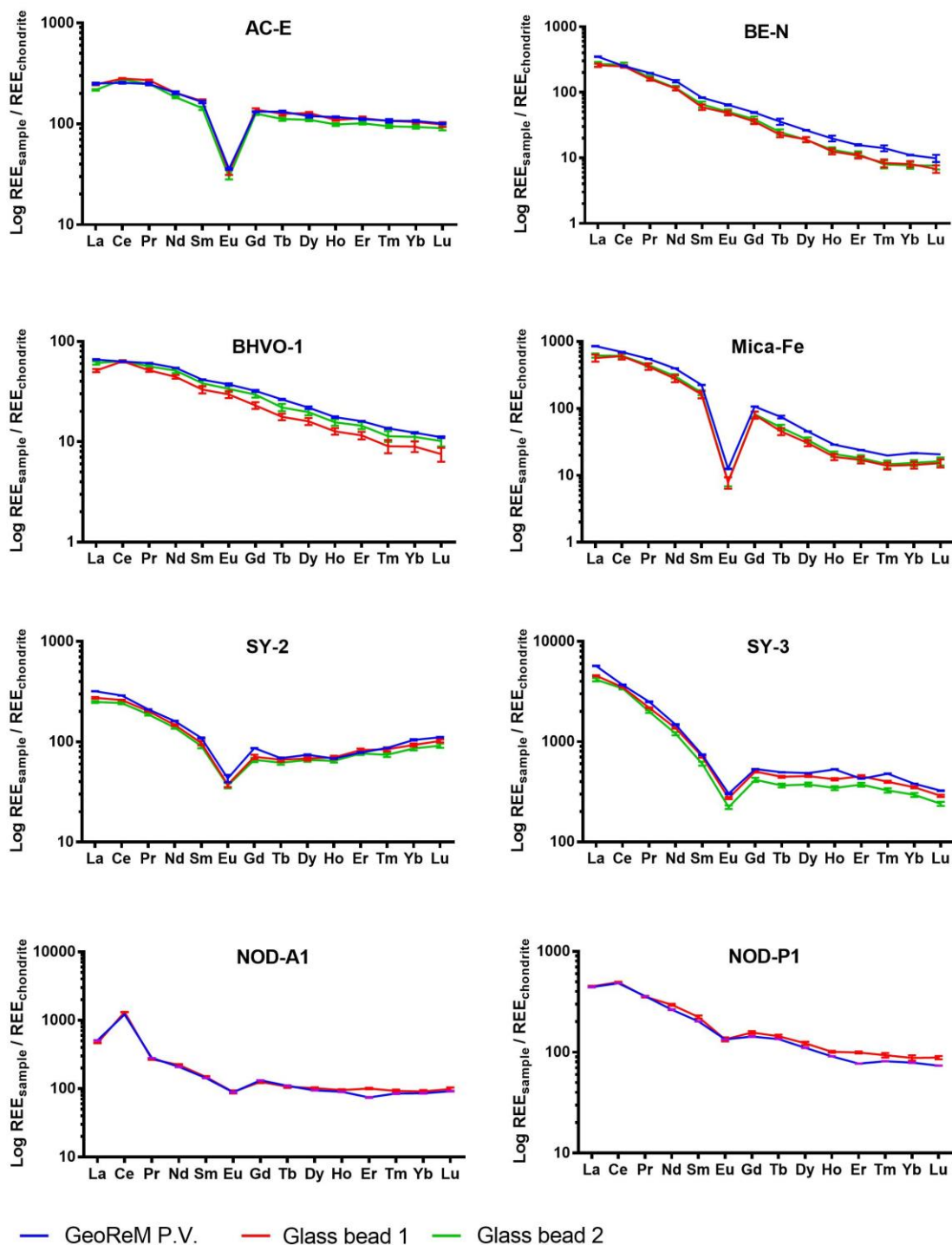


**Figure 4-6: Chondrite normalised comparison of REE concentrations from GRM preferred or consensus values and data from laser-ablated glass beads.**

**Uncertainty calculated from %RSD.**

In a nuclear forensics case, the REE signature of an illicitly recovered specimen of an unknown origin could be compared against a database of known samples in an attempt to identify a geolocation for the sample. Features such as Eu depletion (e.g. AC-E and Mica-Fe), a steady and declining REE concentration (BE-N and BHVO-1) or sharp declining light rare earth concentration relative to the heavier REEs (SY-3) could all be used to identify a possible sample match or geological setting of an unknown specimen.

Three CRMs for U (CUP-1, BL-5 and CUP-2 – Table 4-3) were prepared as glass beads in the same manner as the geochemical reference materials and chondrite normalised (Figure 4-7 – Tables available in Appendix D). No reference values for REEs are available for the U CRMs but the REE patterns for 2 separate glass beads demonstrate near identical profiles and are not dissimilar to the patterns of the geochemical reference materials. The differing magnitude of the signature for CUP-2 is likely due to change in sample transmission between the two glass beads or due to under or over-dilution of the original sample with  $\text{MgSiO}_3$ . No matrix issues are observable in these high U-bearing samples as the signatures are of a similar nature to the geochemical reference materials. This also demonstrates that good coupling with the laser was achievable despite the high U concentration in CUP-2 (75 wt% U).

The required amount of time for sample preparation is typically 10 minutes from diluting a sample with  $\text{MgSiO}_3$  to having the quenched glass bead. At this stage, the glass bead could be loaded immediately in to the sample chamber of the laser and measured. However, the level of human analyst input is greatly increased as each ablation spot would need extra care in positioning to avoid topographical features such as vesicles. In this study, all glass beads (14 GRM + 6 U CRM) were produced in approximately 4 hours and had been mounted in resin, cut and polished within 24 hours. The advantage of ablating polished samples is that the surface is level meaning that constant re-focussing of each ablation spot is not required and it is very easy to identify areas of interest for analysis. Additionally, this large set of samples are loaded in to the sample chamber together meaning that analysis conditions for the samples is consistent and that the laser and ICPMS are able to operate 24/7 without analyst intervention to change samples and re-tune the instruments.

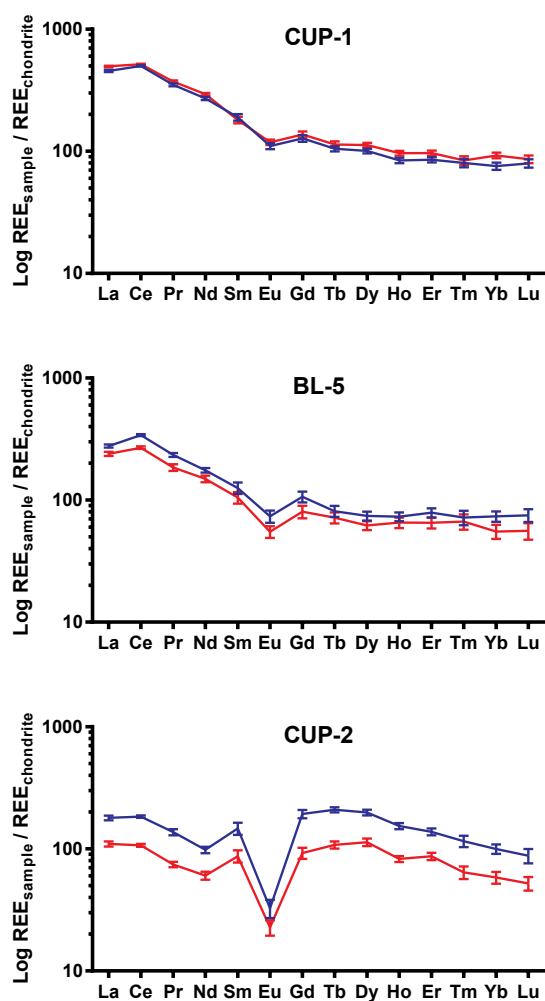


**Figure 4-7: Chondrite normalised REE patterns for CCRMP CUP-1 (0.1 wt% U), BL-5 (7.1 wt% U) and CUP-2 (75.4 wt% U) obtained from 2 laser-ablated glass beads.**

**Uncertainty calculated from %RSD.**

## 4.4 Conclusion

Nuclear forensic studies of difficult to dissolve materials (in acids) such as uranium ore concentrates (UOCs) or uraniferous ores are challenging. A fusion technique that conserves material, is rapid and which produces a robust homogenous glassy sample for subsequent microbeam analysis (e.g. LA-ICPMS) is attractive for nuclear forensics investigations. Low silica bearing samples cannot be fused directly into vitreous beads without a fluxing agent or other glass former. To overcome this problem this study investigated the efficacy of using ultrapure synthetic enstatite ( $\text{MgSiO}_3$ ) to dissolve a range of oxide-rich materials (UOCs, ferromanganese nodules) but also including geochemical reference samples. All samples investigated formed homogeneous glass beads when mixed with synthetic enstatite and then fused on an iridium strip heater at about 1500°C for 1 minute (sample:flux of 1:9). Samples as small as 1.5 mg could be effectively dissolved in the enstatite melt from which the quenched glass bead could be readily recovered for subsequent analysis.

Preparation of a set of geochemical materials (silicates, Mn-nodules and uranium certified standards) provided a set of beads that were analysed using LA-ICPMS and yielded sufficient rare earth element (REE) concentrations for effective analysis. The resulting normalised REE patterns for 8 geochemical reference materials are impressively similar to normalised GeoReM preferred values obtained from chemically separated fractions and measured by solution ICPMS methods. A further improvement in reproducibility could be made by intimately mixing an internal REE standard (thulium) (Croudace & Marshall, 1991) into the enstatite mixture and sacrificing the determination of this one element in unknown samples.

The REE profile obtained from the sample can be compared against a database of known samples in order to identify a geological setting or particular deposit in which a sample has originated in order to benefit nuclear forensic investigations.

The sample preparation and fusion time is typically <10 minutes and many (up to 24 in this study) glass beads can be loaded in the sample chamber of the LA-ICPMS system allowing for unattended, efficient data acquisition.



## **Chapter 5: The analysis of rare earth element signatures in uranium ore concentrates as glass beads for laser ablation ICPMS application in nuclear forensics.**

**Prepared for submission to Analytical Chemistry**

### **Abstract**

A set of uranium ore concentrates (UOCs) are prepared as flux-free glass beads of glass using an iridium strip resistive heater. The glass beads are composed of 1.5 mg UOC and blended at a 1:9 ratio with  $\text{MgSiO}_3$  as this was previously found to be the optimal sample composition to aid the glass forming process. The resulting glass beads of glass are measured for rare earth element signatures via laser ablation ICPMS. Additionally, the UOCs are digested and chemically separated for REE and measured by solution ICPMS to validate the laser derived data. The two sets are comparable and also agree with previously published data. The minimal sample mass and rapid sample preparation time for laser ablation ICPMS could have significant benefits to nuclear forensic investigations as much of the original sample would be retained for other investigations and because data acquisition from sample receipt could be within hours.



## 5.1 Introduction

### 5.1.1 Rare earth elements

The rare earth elements (REE) in this study are 14 lanthanides (La to Lu excluding Pm) although Y and Sc can occasionally be classified in this group. The REE occur in the trivalent form with exception to Ce and Eu. Cerium remains in the trivalent form under anoxic conditions but in oxygenated conditions its solubility decreases and it precipitates as Ce(IV)O<sub>2</sub> causing a positive anomaly relative to the other REEs. Europium however, is trivalent in oxygenated environments but can be present as a divalent ion (2+) in a reducing environment. Additionally due to it having the same charge and ionic radii as Ca<sup>2+</sup>, it can be substituted into plagioclase and other Ca-bearing minerals. Therefore, Eu would be enriched in the plagioclase relative to the other REE but depleted in comparison to the other minerals formed from the magma/mineralising fluids. Additionally, the light rare earth (LREE – La to Gd) can be fractionated from the heavy rare earths (HREE – Dy to Lu) during the formation of minerals such as apatite, garnet, monazite, sphene and zircon (Jarvis, 1988). The geochemical signature of Ce and Eu and the extent of fractionation is preserved so long as no other diagenetic alteration occurs (Mercadier et al., 2011). The fractionation and/or relative enrichment/depletion of Ce or Eu along with the relative elemental concentration of REE present in a sample can act as a forensic tool in identifying a potential geological setting of origin. More importantly, this signature is one of the main diagnostic parameters of uranium ore concentrates (UOC – yellowcake) and combined with other isotopic/elemental/morphological data can aid in the provenance determination of such materials. For example, if the REE signature demonstrated no fractionation or anomaly, the sample would likely originate from a synmetamorphic deposit (Donard et al., 2015) or sandstone derived deposit. A negative Eu anomaly would be diagnostic of a quartz-pebble conglomerate (QPC or placer deposit) (Varga et al., 2010b) due to the REE mineralising fluids interacting with granitic melt or weathered granitic deposits (such as the Blind River / Elliot Lake region of Canada) and therefore from a plagioclase rich source allowing for Eu substitution with Ca (Dahlkamp, 1993; Castor & Hedrick, 2001). Igneous or intrusive deposits will commonly demonstrate LREE enrichment over HREE due to fractionation of HREE in to minerals such as allanite, garnet and pyroxene during partial

melting of the source materials (Lentz, 1996; Oliver et al., 1999; Castor & Hedrick, 2001; Frimmel et al., 2014).

### 5.1.2 Measurement of rare earth elements

The low detection limits and high precision achievable with mass spectrometric techniques such as ICPMS and TIMS are desirable for the measurement of the lanthanides in matrices of a complex nature, such as UOC. However, matrix suppression and instability of signal intensity due to high U concentration in UOC and the formation of polyatomic ions causing isobaric interferences in such matrices can have a detrimental effect on the measurement of REE at low concentration. The polyatomic ions are generally oxides and hydroxides of Ba and low mass lanthanides (e.g.  $^{135}\text{Ba} + ^{16}\text{O}^+ = ^{151}\text{Eu}$  and  $^{147}\text{Sm} + ^{16}\text{O}^+ = ^{163}\text{Dy}$ ) and account for 0.2 to 1.2% of the oxide formed species (Jarvis et al., 1989) but the magnitude of the interference is usually within measurement uncertainty for most geological specimens. Where Ba or LREE is present at an elevated concentration, the oxide contribution can cause significant misinterpretation without adequate corrections.

Chemical separation has been applied to remove the effects caused by elevated U concentration and to also concentrate the lanthanides prior to analysis (Varga et al., 2010a, 2010b). Overcoming spectral interferences can be achieved using doubly charged ions (Jarvis et al., 1989; Jarvis, 1989) or by using higher instrumental mass resolution such as sector field ICPMS (Prohaska et al., 1999; Robinson et al., 1999; Donard et al., 2015) but can result in decreased sensitivity.

The use of laser ablation ICPMS would significantly reduce polyatomic interferences as the sample carrier gas is typically oxygen-free and because the dry plasma results in reduced hydride ion formation. Various studies have shown good agreement of REE concentrations in reference materials measured via LA-ICPMS methods (Fedorowich et al., 1993; Nehring et al., 2007; Stoll et al., 2007; Lach et al., 2013; Reading et al., submitted B) where no major interferences or matrix effects have been observed.

Laser ablation is a highly desirable technique for measuring isotope ratios and elemental concentrations as it is a direct analytical method which usually does not require extensive sample preparation or chemical separation; does not generate aqueous waste at sample preparation or measurement stages; minimises cross-sample contamination; and requires

milligram quantities of sample. The latter is of great importance to nuclear forensic investigations as this is commonly the limiting factor to analyses where sample availability may be low or material may be required for other destructive analytical techniques.

The preparation of fused, flux-free samples of glass using 1.5 mg of sample blended at a 1:9 ratio with  $\text{MgSiO}_3$  has been demonstrated using geological reference materials by Reading et al., (submitted B) and in the previous chapter. This method enables consistently homogeneous glass beads to be produced which are analysed via LA-ICPMS. The glass bead is produced using an iridium strip fusion device where the silica content is at least 50% regardless of the original silica content of the sample due to the addition of  $\text{MgSiO}_3$ . The fusion conditions are 1500 °C for 1 minute and produces homogeneous glass with good reproducibility and agreement for geological reference materials (<10% relative standard deviation).

This study investigates the REE signatures of 19 UOCs obtained from LA-ICPMS analysis of glass beads. The UOCs are also analysed for REE via solution ICPMS following chemical separation in order to validate the laser ablation data. Additionally, where possible, corresponding UOC REE data from other studies are included as a further validation of the laser ablation data and also to demonstrate how REE signatures are comparable between different sample preparation methods and analytical measurement techniques.

The 19 UOCs in this study represent various geological settings, ore feeds and milling techniques from Australia, Canada and The United States (Table 5-1) and are provided by the Atomic Weapons Establishment (AWE), UK. Please see (Reading et al., submitted A) or Chapter 3 for further details.

**Table 5-1: UOCs investigated in this study**

<b>UOC</b>	<b>Country</b>	<b>Milling Facility</b>	<b>Uranium Deposit Type</b>
<b>Anaconda</b>	USA	Grants / Bluewater	SSt – Tabular
<b>Blind River</b>	Canada	Elliot Lake	QPC
<b>Chevron Hill</b>	USA	On-site	Sst – Roll front
<b>Cotter</b>	USA	Canon City	Sst & vein (3:1)
<b>Eldorado</b>	Canada	On-site	Vein
<b>Faraday <sup>1</sup></b>	Canada	On-site	Intrusive
<b>Gunnar</b>	Canada	On-site	Vein
<b>Lucky McGill</b>	USA	On-site	Sst – Roll front
<b>Madawaska <sup>1</sup></b>	Canada	On-site	Intrusive
<b>Mary Kathleen</b>	Australia	On-site	Metamorphic
<b>Mesa EFI</b>	USA	On-site	Collapse breccia pipe or Sst
<b>Mulberry</b>	USA	On-site	Phosphate
<b>North Span</b>	Canada	On-site / Elliot Lake	QPC
<b>Olympic Dam</b>	Australia	On-site	Haematite Breccia Complex
<b>Queensland</b>	Australia	On-site	UR
<b>Rabbit Lake</b>	Canada	On-site	UR
<b>Ranger</b>	Australia	On-site	UR
<b>Rio Algom <sup>2</sup></b>	Canada	Elliot Lake	QPC
<b>South Alligator</b>	Australia	Rockhole Creek	UR

<sup>1</sup>Faraday and Madawaska are the same mine sites. Faraday operated 1954-1964 and Madawaska operated 1975-1982.

<sup>2</sup> Rio Algom operated many mines of which Panel, Stanleigh and Quirke mines are the most likely source for this sample.

QPC = Quartz-pebble conglomerate; Sst = Sandstone; UR = Unconformity related.

## **5.2 Methodology**

### **5.2.1 Instrumentation**

#### **5.2.1.1 The iridium-strip electronic device**

The glass beads in this study were produced using a resistive heating device where a low voltage and high current is passed across an iridium strip resulting in the fusion of a sample loaded on the iridium strip. The device is operated in an argon atmosphere and is manually controlled with the aid of a pyrometer and digital camera (Reading et al. (submitted B) and Chapter 4).

#### **5.2.1.2 XRD examination for homogeneity**

All UOC glass beads suspected to be  $\text{U}_3\text{O}_8$  (melting temperature of 1150 °C) and a selection of other UOCs were analysed via XRD to examine whether the glass was amorphous and therefore truly a glass and homogeneous. The XRD measurements were performed using a Rigaku SmartLab XRD (University of Southampton, UK) instrument fitted with a Cu X-ray tube (45 kV, 200 mA) operating with a 0.3 mm collimator between 5 and 85 degrees  $2\theta$ . Step size was 0.02 degrees  $2\theta$  and step rate was 10 degrees  $2\theta$  / minute. The microscope slides containing the UOC glass beads was loaded on to the xyz stage where an on-board camera was used to focus on the target measurement point. Each bead was measured up to 3 times at different positions.

#### **5.2.1.3 Laser ablation ICPMS**

Laser ablation was performed using a New Wave Research (ESI) UP193FX 193 nm solid-state laser ablation system (Fremont, CA, USA) coupled to a Thermo Fisher X-Series II Quadrupole ICPMS (Appendix A-2). Instrument calibration, performance and stability were performed using NIST CRMs 610, 612 and 614. The percentage standard deviation for replicate element concentration measurements in the NIST CRMs were less than 5% with the exception of Mg in NIST CRM 610 which was 8%. Each UOC glass bead was measured at 10 positions which were randomly selected around the glass bead. Due to the significantly reduced oxide production rates associated with laser ablation and dry plasma, isobaric interferences were not significant. Sample blanks ( $\text{MgSiO}_3$  only) were produced

and subtracted from each UOC measurement to account for contamination from reagents and to correct for instrument background.

#### **5.2.1.4 Solution ICPMS**

Mass spectrometric measurements of solution samples were measured by the X-Series II ICPMS (Appendix A-2). Instrument calibration, performance and stability was performed using an in-house rare earth element standard at varying concentrations ( $\Sigma$ REE ranged from 0.6 to 90 ppb where La = 0.1 to 30 ppb) and from geological rock standards (BHVO-2, BIR-1, JA-2, JB-1a, JB-3 and JGb-1).

Isobaric interference corrections were calculated and applied using isotope ratios of pure Ba, Ce, Pr and Sm metal standards to account for oxide and hydroxide formation (Appendix A-3).

#### **5.2.2 Sample preparation for LA-ICPMS**

Each UOC was dried at 100 °C and blended with MgSiO<sub>3</sub> at a ratio of 1:9 totalling a mass of approximately 15 mg. Subsequent fusion treatment produced a coalesced, homogenous glass bead where the total silica content is 50%. The sample was dampened with 10 µL of Milli-Q water to form a thick slurry and then dried in air to produce a cake which prevents the sample from vibrating off of the Ir-strip due to the resonation effect of the high current passing through it. The fusion device was closed and argon (BOC Pureshield 99.998% purity) allowed to flood the chamber for 2 minutes to purge oxygen from the environment to prevent oxidation of the sample. The pyrometer was adjusted to focus on the centre of the strip and next to the edge of the gathered sample. The current was applied gradually so that the Ir strip slowly reached 1500 °C where it was held for 1 minute for fusion and then quenched immediately by isolating the transformer. The resulting glass bead was carefully flexed off from the Ir strip and then mounted in resin where it was cut and polished to expose a clean and smooth surface. A single glass bead could be produced in ~10 minutes including sufficient cooling time of the apparatus to permit the iridium strip and glass bead could be handled safely.

### 5.2.3 Chromatographic resin calibration for REE and U separation

The TRU™ chromatographic resin (Eichrom, France) has been demonstrated as an efficient and robust material for the separation of REEs from uranic materials (Varga et al., 2010a) and was therefore chosen for this study also. The extraction system is octylphenyl-N,N-diisobutyl carbamoylphosphine oxide (CMPO) dissolved in tri-n-butyl phosphate (TBP) with particle size range 100-150  $\mu\text{m}$ .

The TRU™ resin was tested to calculate the maximum loading and retention of U on the resin prior to breakthrough. This was then used to determine the minimum amount of resin required to support both U and REE from a UOC. A standard containing 500 ppm U was created from a 1000 ppm U ICPMS standard (Spex CertiPrep, NJ, USA) and was supported in a 4M  $\text{HNO}_3$  matrix. The 500 ppm standard was loaded on to the TRU™ resin at 1 mL intervals and the “waste” was collected at each interval. Each collected fraction was diluted 12,500 fold with 3% Suprapur grade  $\text{HNO}_3$  so that the maximum U concentration would not exceed 40 ppb and then measured using the X-Series II ICPMS with In and Re as internal standards. The number of U-free fractions was then used to determine the maximum capacity of U on TRU™ resin prior to breakthrough.

A separation scheme was tested using a UOC analogue to understand the retention and elution curves of REE and U. The UOC analogue had U concentration = 1% and La = 6.5 ppm ( $\Sigma\text{REE} = \sim 20$  ppm) and was prepared using an in-house REE standard and digested analytical grade  $\text{U}_3\text{O}_8$ . The U:REE ratio is equivalent to a UOC with 70% U and 450 ppm La ( $\Sigma\text{REE}$  0.135%). The standard was prepared with these concentrations as previous work has demonstrated that 10 mg of U (approx. 1 wt% U or 13 mg of UOC) allows for reliable REE determination at low concentration (sub ppb) and rarely exceeds La concentration of 450 ppm (Varga et al., 2010b). The separation scheme is described in Table 5-2. Following elution of U with 0.01M  $\text{HNO}_3$ , the column was stripped with 1M  $\text{HNO}_3$ -0.01M HF to remove any residual U and determine the efficiency of the previous eluting stage.

**Table 5-2: Separation scheme for TRU™ resin calibration**

<b>Resin</b>	~0.4 g / ~ 1 mL
<b>Conditioning</b>	10 mL 4M HNO <sub>3</sub>
<b>Load</b>	1 mL of U & REE Std in 4M HNO <sub>3</sub>
<b>Wash</b>	4 x 0.5 mL 4M HNO <sub>3</sub>
<b>REE Elution</b>	25 x 0.5 mL 4M HCl
<b>U Elution</b>	4 x 5 mL 0.01M HNO <sub>3</sub>
<b>U Elution</b>	4 x 5 mL 1M HNO <sub>3</sub> + 0.01M HF

#### 5.2.4 UOC sample preparation for solution ICPMS

All vials, pipette tips and columns were cleaned in 5% HNO<sub>3</sub> for at least 48 hours prior to use. Heavy duty PFA pots with lids (Savillex, USA) were used for sample digestion and were cleaned with conc. HNO<sub>3</sub> at 100 °C before and after use for 24 hours. Each UOC was dried at 100 °C overnight to reduce moisture content. Approximately 20 mg of each UOC was weighed in to a PFA pot and digested and refluxed with 1 mL 40% analytical grade HF (Aristar) and 2 mL 8M analytical grade HNO<sub>3</sub> for 24 hours. The digest was then allowed to evaporate to almost complete dryness before being cooled and rinsed into a plastic scintillation vial using 1mL of 4M HNO<sub>3</sub>.

#### 5.2.5 REE and U separation of UOC

Approximately 2 mL of TRU™ resin was prepared in 8mm plastic columns and topped with a frit. The resin was conditioned with 10 mL 4M HNO<sub>3</sub> and 500 µL of UOC (approximately 10 mg UOC) digest was loaded on to the column and washed with 2 mL 4M HNO<sub>3</sub>. The REE fraction was collected using 7.5 mL 4M HCl and the U fraction was collected with 20 mL 0.01M HNO<sub>3</sub>. The REE fraction was dried down and re-digested in 1 mL 3% analytical grade HNO<sub>3</sub>. A 500 µL aliquot of the digest was diluted ten-fold with 3% HNO<sub>3</sub> and In and Re internal standards were added resulting in 5 ppb in the final solution.

### 5.3 Results and Discussion

#### 5.3.1 Resin calibration for REE separation

Breakthrough of U on TRU™ resin was observed on the 10<sup>th</sup> loading (equivalent to 10 mL) of 500 ppm U in 4M HNO<sub>3</sub> (Figure 5-1). This equates to a working U capacity of 41.7 mg U/g resin. The experiment was repeated and the working U capacity was calculated as 41.2 mg U/g resin.

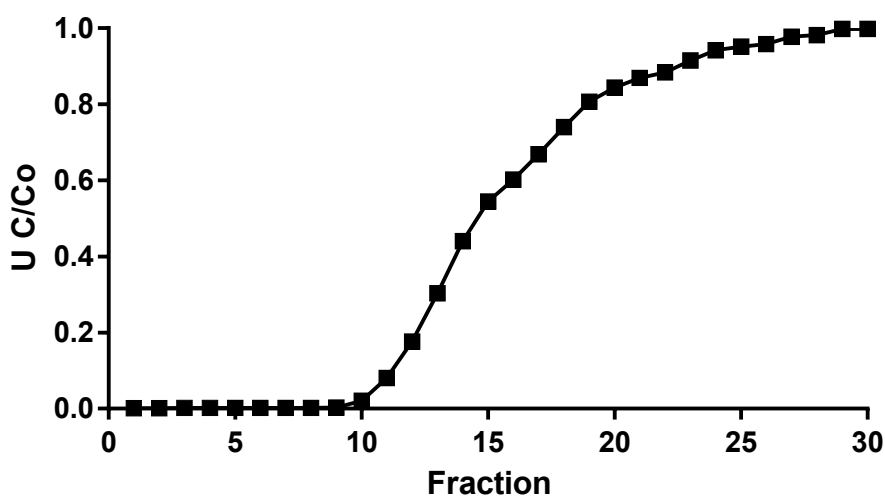


**Figure 5-1: U breakthrough and capacity curve for TRU™ resin.**

The mass of U in the UOC sample used for REE separation is approximately 10 mg therefore the minimal resin required, based on a capacity of 41.2 mg U/g resin, is equal to 0.25 g or 0.7 mL of resin. This does not include the retention capacity required for REE or allowance for any higher concentration U samples so therefore the total resin volume for all UOC separations were approximately 0.4 g / 1 mL.

The REE and U separation curves for the UOC analogue standard demonstrated that the both REE and U can be eluted separately from the TRU™ resin (Figure 5-2). The REE elution was complete by the 14th fraction equating to 7 mL 4M HCl and U was quantitatively retained (with < 0.7% of the U present in the REE fraction). The U elution was complete using 20 mL 0.01M HNO<sub>3</sub>. The final elution stage using HF to strip the resin completely of any remaining elements yielded total REE <1% and U < 1.5% of the loaded sample therefore demonstrating that all analytes are effectively eluted with this scheme.

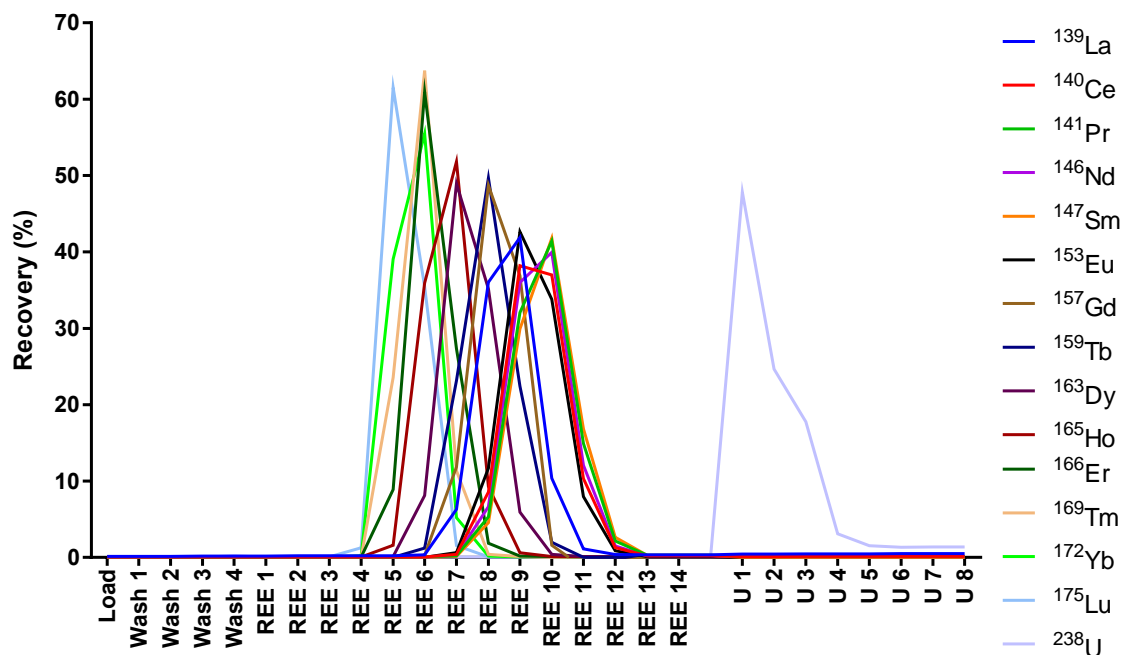
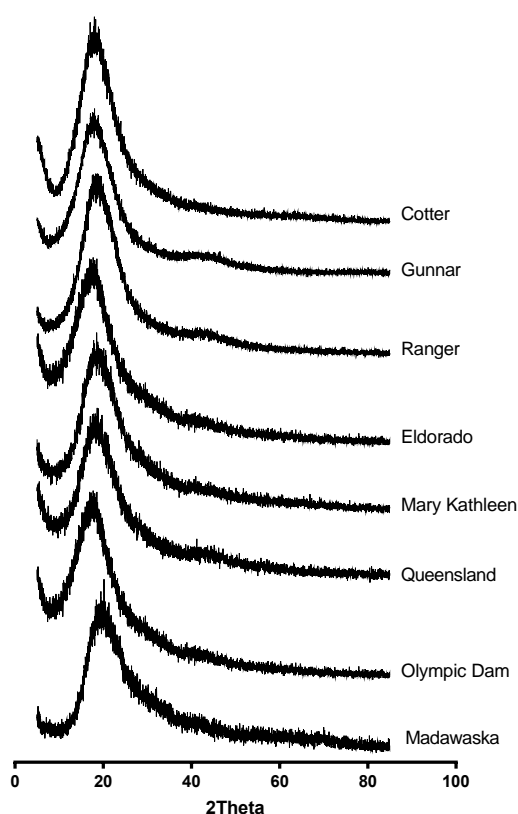


Figure 5-2: UOC analogue standard recovery profiles of REE and U using TRU™ resin.

### 5.3.2 XRD examination for homogeneity

The following UOCs were measured to examine whether the beads were amorphous and therefore can be truly defined as glass and homogeneous samples: Cotter, Eldorado, Gunnar, Madawaska, Mary Kathleen, Olympic Dam, Queensland and Ranger (Figure 5-3). The diffractograms obtained demonstrate that the samples are amorphous with no identifiable peaks associated with crystallographic features. This is evidence for complete melting of all mineralogical phases in the original UOC.



**Figure 5-3: Amorphous XRD data for various UOCs**

### 5.3.3 Glass bead LA-ICPMS results and comparisons

The UOCs were prepared as glass beads in duplicate and mounted, cut and polished on to glass slides ready for LA-ICPMS. The glass beads were analysed at 10 positions randomly scattered around the glass bead. Anomalous results due to poor sample transmission or interaction with a vesicle or resin either at the surface or at depth were removed prior to calculating the average elemental concentration and associated uncertainties from relative standard deviations. The REE concentrations and uncertainty for all data were chondrite normalised using the values of Anders and Grevesse (1989) for comparative purposes. The data from the glass beads were compared to solution measurements from this study and data from other studies where available (Figure 5-4).

Of the 19 UOCs measured via LA-ICPMS, 9 have comparable glass bead and solution REE profiles (Figure 5-4) and the other 10 fall below detection limits of  $\sim 0.2$  ppm of each lanthanide ( $\Sigma \text{REE} < 2.5$  ppm) which equates to  $\sim 2$  ppm ( $\Sigma \text{REE} < 25$  ppm) in the original sample. The Ranger UOC had REE concentrations approaching the detection limit and was

included to demonstrate that although many of the data points were within uncertainty of the solution data (this and previous studies), no discernible shape or observations from the pattern could be deduced due to the level of associated measurement uncertainty. The measurement uncertainty is calculated from the percentage relative standard deviation (%RSD) of each ablation spot and is also an indicator of data reproducibility which is controlled by how homogeneous the sample is and element concentration. The detection limits could be improved by increasing the ablation spot size or total sample in the glass bead to introduce more material to the ICPMS. However, in doing so, this would also increase the amount of U reaching the instrument and potentially contaminating the detector and the quadrupole mass analyser. The spot size used in this study (100  $\mu\text{m}$ ) was adequate to obtain substantial counts (e.g. >200 counts of La and >400 counts of Lu – equivalent to  $\sim 0.2$  ppm) for 9 of the 19 UOCs without concerns of significantly contaminating the instrument. Uranium was not measured to ensure longevity of the detector.

The 9 UOCs above the detection limits have excellent agreement in pattern shape and concentration to the solution data. Glass bead anomalies such as Eu depletion and fractionation between high and low mass REE are the most diagnostic features in the signatures and are all of similar magnitude and distribution as solution measurements (current and previous studies). Variation in concentration is most likely a result of under- or over-dilution of the sample or slightly unfocused ablating causing the spot diameter to increase or decrease relative to the NIST calibration standards.

The REE patterns for the glass beads in Figure 5-4 (except UOC Ranger) are as expected for the known geological setting of the uranium ore feed (see section 5.1 for more information on geological settings for U-deposits). The quartz-pebble conglomerate derived UOCs (Blind River, North Span and Rio Algom) demonstrate the distinct Eu depletion due to the presence of plagioclase and Ca-rich minerals in the deposit causing Eu and Ca substitution. The intrusive deposits (Faraday and Madawaska) are known to be from the same mining area and therefore possibly from the same deposit. These two UOCs are convincingly identical in pattern and concentration and demonstrate the distinctive REE fractionation due to HREE being incorporated in to minerals such as the highly HREE selective allanite. The REE pattern of Anaconda is relatively flat with no clear enrichment or depletion of any one REE, which is characteristic of sandstone deposits. The HREE enrichment observed in

UOC Cotter is typical for alkaline igneous rocks that contain sodium and potassium derived minerals such as alkali pyroxenes and amphiboles that are not commonly found in other rock types. The local geology for UOC Cotter is known to contain Precambrian gneisses and schists, which explains such HREE enrichment. Cotter is also believed to contain sandstone-derived ores in the mill feed which may also explain the relatively flat LREE profile. The blend of ore feeds may also be causing a dilution effect to the HREE enrichment. The vein deposits of Eldorado and Gunnar demonstrate a negative Eu anomaly which could be related to the reducing conditions during the precipitation of uranium oxides (Mercadier et al., 2011). Additionally, it could be a result of interaction with plagioclase-rich country rock as the vein developed causing gradual Eu substitution with Ca along the vein.

Solution ICPMS techniques have complications and considerations with isobaric interferences. The similar REE patterns from laser ablation and solution measurements (which have had isobaric interferences accounted for) of the 9 UOCs (Figure 5-4) demonstrate that this laser ablation technique and setup have negligible polyatomic isobaric interferences.

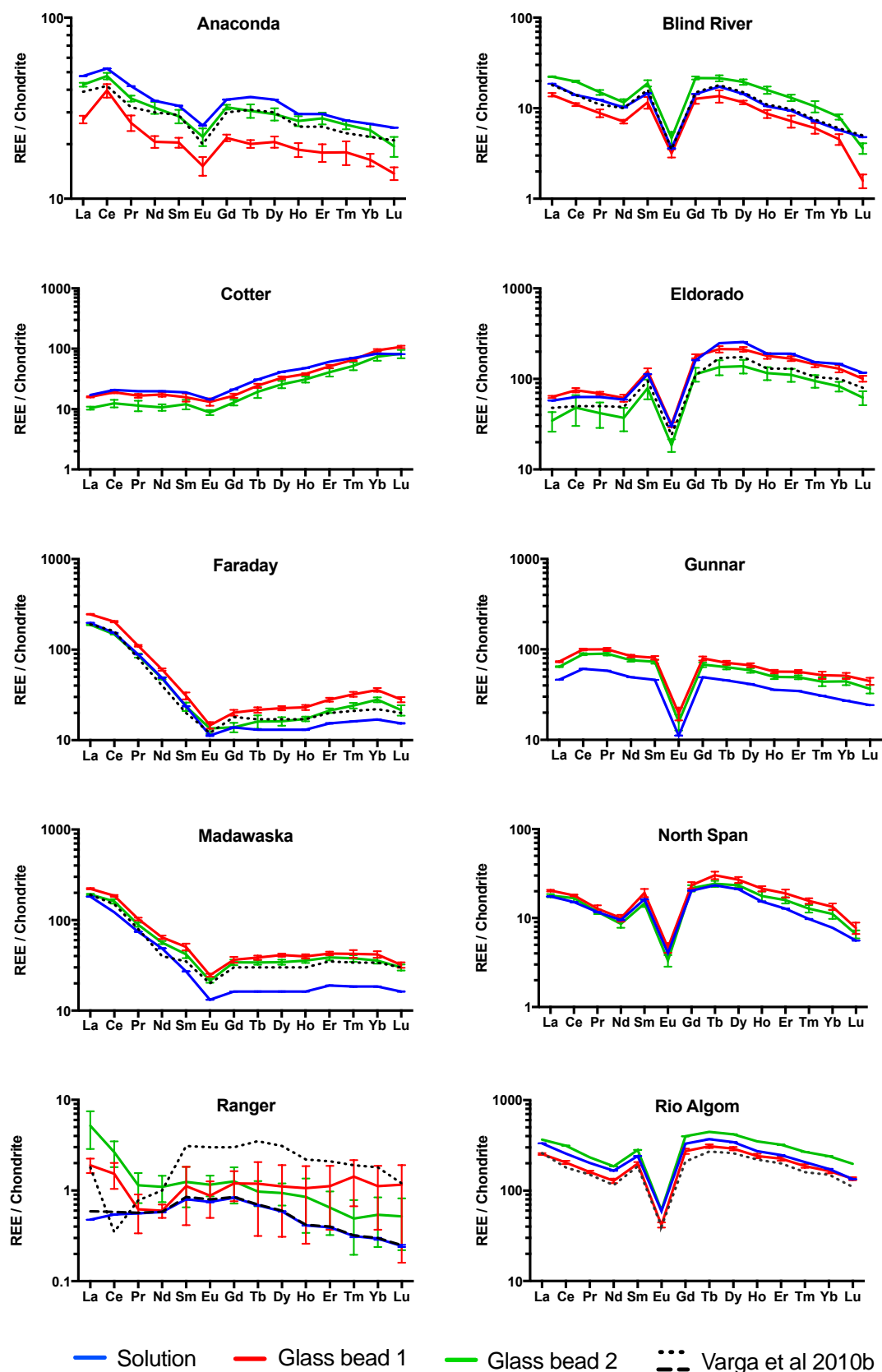


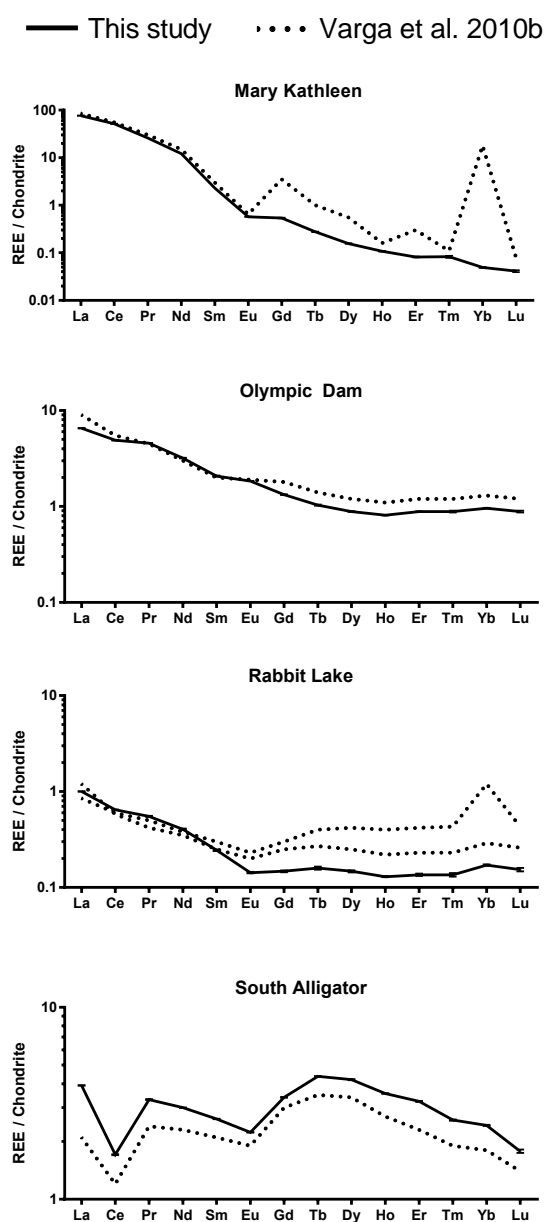
**Figure 5-4: Glass bead and chemically separated solution REE data with comparable data from Varga et al. 2010b (where available).**

Uncertainty calculated from relative standard deviation at  $2\sigma$

### 5.3.4 Non-glass bead comparable UOC data

Of the UOCs which were below the LA-ICPMS detection limits, five had comparable REE normalised patterns to other studies (Figure 5-4 – Ranger and Figure 5-5). In this study the UOC Mary Kathleen has a smoother profile and does not demonstrate the same anomalies (Gd, Er and Yb) as Varga et al. (2010b). Metamorphism and deformation was suggested as the possible reason for these anomalies, but are absent in this study suggesting the previous anomalies could be a sample preparation or contamination artefact.

**Figure 5-5: Solution ICPMS data obtained in this study compared to previous studies**

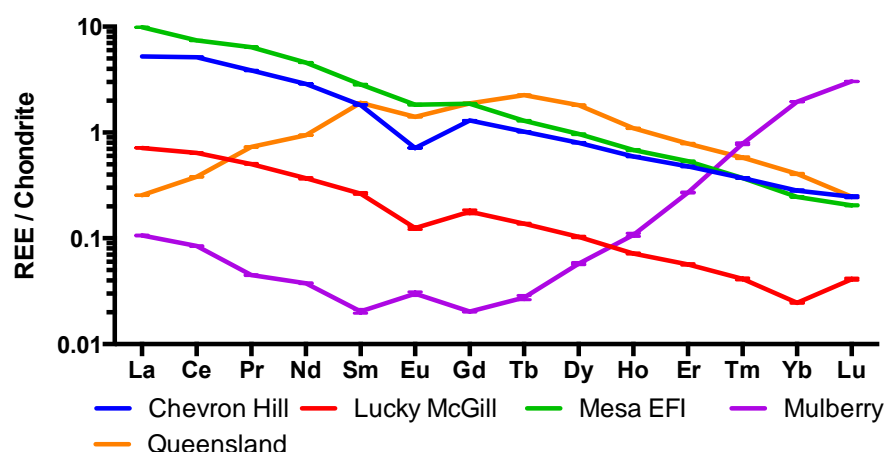


where glass beads were below LA-ICPMS detection limits.

Despite Mary Kathleen having a distinctly different profile, the remaining three UOCs are in very good agreement to previously published data. This demonstrates that despite this study using a less sensitive bench-top ICPMS for solution and laser ablation measurement, excellent comparable data can be gathered to high-resolution ICPMS.

The remaining five UOCs of this study which were below laser ablation detection limits and not comparable to other studies exhibit characteristic features of their geological setting (Figure 5-6). Chevron Hill and Lucky McGill are both of sandstone geological origins and show the same relative depletion of Eu as other sandstone derived samples in this study and Varga et al. (2011b). Mesa EFI is from a collapse breccia deposit and shows no relative enrichment/depletion or fractionation and is similar to Olympic Dam which is also a breccia derived deposit. Mulberry is classified as a phosphorite and is a by-product from phosphoric acid production and shows the same profile of other phosphorite deposits (CAN ESI and USA ESI – Varga et al. (2011b)) with elevated HREE concentration to LREE. Queensland is from an unconformity classified deposit and has the characteristic enriched mid-REE profile to other unconformity deposits in this and previous work with exception to Rabbit Lake which is diagnostic of gneiss rather than uraninite (Fayek & Kyser, 1997).

**Figure 5-6: Solution ICPMS data which are not comparable to glass beads or previous**



studies.

## 5.4 Conclusion

Laser ablated glass beads of flux-free fused glass containing 1.5 mg of uranium ore concentrate have been shown to provide accurate rare earth element patterns compared to chemically separated samples measured by solution ICPMS. Of the 19 UOCs investigated in this study, 10 UOCs measured by LA-IPC-MS resulting in inconclusive data due to detection limits. The other 9 however provided excellent agreement to solution ICPMS data of the same samples and additionally compared well to a previous study which used a higher resolution instrument. Despite half of the samples not yielding usable data from LA-ICPMS, the sample preparation and laser ablation could be extremely beneficial to nuclear forensic investigations. The required mass of UOC is 1.5 mg and a homogeneous glass bead of glass can be produced in less than 10 minutes. It could be argued that 1.5 mg of sample is not representative of a samples composition. However, the glass beads in this study were produced in duplicate from a stock bottle and result in comparable REE signatures and concentrations. This bead can be immediately analysed via LA-ICPMS to provide extremely rapid REE (or other elemental/isotopic) data. Alternatively, a set of glass beads could be mounted in resin, cut and polished and measured without operator intervention such as reloading the ablation chamber between samples or manually focussing each ablation spot. Additionally, this study has used the relatively inexpensive (compared to MC, SF or HR-ICPMS) bench-top ICPMS (X-Series II) and was able to obtain comparable results to a previous study using an Element 2 SF-ICPMS. The laser ablation sample introduction technique greatly reduces polyatomic isobaric interferences and therefore additional corrections, calibrations or calculations are not required.

Due to detection limits for REE analysis, not all UOCs are measurable by LA-ICPMS. However, this is still diagnostic of a samples origin, as in this study's case, if a sample is not measurable, it cannot be from half of the sample set thus narrowing the investigation of sample and/or origin identification. Because the sample preparation and measurement time is extremely rapid, it would not be a hindrance to a nuclear forensic laboratory to then have to process the sample via chemical separation and solution measurements if a sample is not measurable by laser ablation.



## Chapter 6: Conclusions

This thesis has developed new and rapid sample preparatory techniques for the characterisation of uranium ores and uranium ore concentrates (UOC) for nuclear forensic investigations using gamma and alpha spectrometry and laser ablation ICPMS.

The first, lithium tetraborate fusion, was used for complete dissolution of U-bearing samples that contain refractory minerals and produces an aqueous and homogeneous sample with a predictable matrix. The method was developed as U-bearing samples were observed to undergo significant photon attenuation during gamma spectrometric measurements due to the heterogeneous distribution and variable grain size of dense uranium minerals. The fused sample, typically containing < 0.5 g of the original sample in 20 mL solution, can be used for further nuclear forensic investigations including mass spectrometry and alpha spectrometry without the requirement for further destruction of the parent sample and without the use of HF digests. This sample preparation technique allowed for the accurate characterisation of 19 UOCs via gamma and alpha spectrometry. The radiometric data was then statistically analysed using Principal Components Analysis (PCA) to determine whether such data could be used to discriminate between sample origins. The PCA demonstrated that half of the UOC sample set display unique radiometric properties that could be used to identify a possible origin of an unknown sample when compared against a radiometric database of samples. This was examined by re-preparing and re-analysing 6 of the UOCs as unknowns and then incorporating them in to the PCA that contained the original 19 samples. The 6 unknowns all plotted close to their original samples demonstrating that the sample preparation and measurement technique combined with PCA statistical analysis is a valid method to determine possible sample origins. The UOCs that share similar radiometric properties and therefore group together in the PCA still provide crucial information on a potential origin of an unknown, as it demonstrates where a sample cannot have come from. Additionally, if an unknown sample plots among a large group of samples in the PCA, the laboratory may be in a better position to determine the next analytical technique required to further constrain the origins of the unknown based on a signature which is known to be different amongst this particular set of samples. This method of sample preparation and PCA analysis needs validation with modern UOCs from currently operating uranium mills. A suite of UOCs should be collected

from a number of mills over a period of time and then examined via gamma and alpha spectrometry via the lithium borate fusion technique and then analysed via PCA to assess whether such a statistical discriminatory tool can be applied to potential temporally and distally variable end product. Gamma spectrometry is widely accepted amongst the nuclear forensic community as the first measurement technique of an unknown nuclear sample. Previously, this has been to determine whether a sample, for example suspected uranium, is enriched, depleted, natural or reprocessed. Now, with this rapid fusion technique and statistical analysis of gamma spectrometric data, samples could have their provenance determined or options reduced within 2 days of a sample arriving at a nuclear forensic laboratory.

The second sample preparatory method is a flux-free whole-sample fusion procedure that produces glass beads of glass. The homogeneous glass bead can then be measured by laser ablation ICPMS to obtain elemental and isotopic data. The glass bead is composed of a blend of investigatory material and  $\text{MgSiO}_3$  at a 1:9 ratio with a total mass of ~15 mg. This ratio allows for total silica content to be ~50% regardless of the original samples composition so that standardised fusion conditions can be applied to every sample regardless of its composition e.g. UOC which contains little or no silica. A variety of geological reference materials were prepared as glass beads and were shown to be homogeneous from highly reproducible elemental concentration data (<10 %RSD). The rare earth elements (REE) were also measured as the resulting chondrite normalised pattern is indicative of a samples geological origin. The chondrite normalised REE data from the geological reference materials had identical rare earth patterns to the normalised reference values. Glass beads were then produced using the 19 UOCs and the REE were measured. Each UOC was also digested and chemically purified for REE to validate the REE normalised data obtained from laser ablation. The two profiles from each technique had excellent agreement and also compared well to previously published data for REE patterns for some of the UOCs. Due to laser ablation detection limits, not all UOCs were measurable. However, this is still diagnostic of a samples origin as it eliminates all samples that are known to be above the detection limits of 10 ppm for each lanthanide. Glass bead preparation time is approximately 10 minutes and can be analysed immediately via laser ablation. Alternatively a large set of samples can be mounted in resin and polished so that

a smooth and flat surface is exposed for an automated laser ablation run with constant operating conditions and without the requirement for analyst intervention.

The developed techniques in this thesis have been applied to 19 historic UOCs where only a small number of such UOCs are from currently operating uranium mills (Blind River, Mary Kathleen, Olympic Dam and Rabbit Lake). The samples made available for this thesis are not representative of a mill's lifespan and therefore the temporal and distal variability or ore feed(s) and milling technique has not been assessed. The techniques presented in this thesis do demonstrate however that the preparation, measurement, analysis and interpretation are robust to match like-for-like samples. Therefore, if the nuclear forensic community decided to incorporate such investigations into routine analysis and develop a database of radiometric and rare earth element profiles of current UOC production, future cases of illicitly recovered UOC could have their geolocation / mill origin identified. Additionally, both procedures require a small amount of sample and therefore improves the preservation of illicitly recovered samples and also reduces contact dose to the analyst and associated risk of contamination to the laboratory.

The two sample preparation techniques and analyses could significantly improve the speed and efficiency in which nuclear forensic investigations are implemented. After the initial physical characterisation of an illicitly recovered specimen, a small amount (< 1 g) of sample can be prepared for radiometric analysis via the lithium borate fusion technique and for LA-ICPMS as a multiple glass beads. The laboratory can rapidly obtain a plethora of information about the sample in as little as 24 hours of sample receipt. Additionally, the resulting aqueous fraction from lithium borate fusion can be used for mass spectrometric analyses after chemical purification. For example, previous studies have investigated U isotope ratios to determine the presence and possible origins of DU (Boulyga et al., 2001) and whether the age of HEU could be determined (Wallenius et al., 2002). The study by Boulyga et al., (2001) used a combination of concentrated  $\text{HNO}_3$ ,  $\text{HCl}$  and warm  $\text{HF}$  to achieve complete dissolution of soil samples and used  $\text{HNO}_3$ ,  $\text{HCl}$  and  $\text{H}_2\text{SO}_4$  for complete dissolution of metals with various drying and sub-sampling stages. The lithium borate fusion technique would allow for complete sample dissolution without the requirement for strong acid digests. Both studies by Boulyga et al. (2001) and Wallenius et al. (2002) used extraction chromatography techniques to purify their samples prior to mass spectrometric techniques. Lithium borate fusion and the resulting digests offer significant benefits to

future nuclear forensic investigations as the time required for sample preparation would be greatly reduced and the potential contamination from the large amounts of reagents required during sample dissolution would also be limited.

The quenched glass beads produced in this thesis could be used to determine other elemental concentrations and relative ratios to aid in nuclear forensic investigations. Although such data could be obtained via XRF, the detection limits associated with LA-ICPMS are significantly lower when using sample masses of tens of milligrams. The rapidity in which glass beads can be produced could also benefit the mining industry and ore prospecting as samples could be quickly assessed to determine whether a particular deposit/outcrop contains the target mineral based on elemental concentration. This could have significant impact on deep-sea mining where only limited sample can be retrieved from the sea floor.

If the nuclear forensic community were to utilise these rapid methods for initial sample characterisation, the laboratory could be in a better informed position to determine which of the other pre-existing nuclear forensic characterisation techniques would best to deconvolve the origins of the suspect sample.

## **Chapter 7: Future Work**

### **7.1 Statistical analysis of radiometric data and REE patterns.**

The project has demonstrated that the radiometric signatures of 50% of the UOCs in this study can be statistically discriminated from one another where the other 50% share radiometric properties and therefore cannot be easily discriminated (Chapter 3). The addition of the rare earth element (REE) data collected from the UOC glass beads (Chapter 5) into a new or the pre-existing PCA model may be able to better discriminate the radiometrically similar UOCs. A new PCA model encompassing a greater suite of rapidly collected data (and therefore a greater number of sample variables and component loadings) could enhance the initial nuclear forensics profiling of samples where statistically accurate origin determinations could be possible within a matter of days of sample receipt of an illicitly recovered nuclear specimen. Cluster analysis should also be investigated for the REE patterns alone to determine whether correlation can be observed between the REE pattern and the known geological deposit type. It would also be beneficial to obtain UOC from currently operating mills over a period of time to examine temporal variability in the UOC and how it would affect the statistical analyses of future “unknown” samples.

### **7.2 Elemental, mineralogical and morphological characterisation**

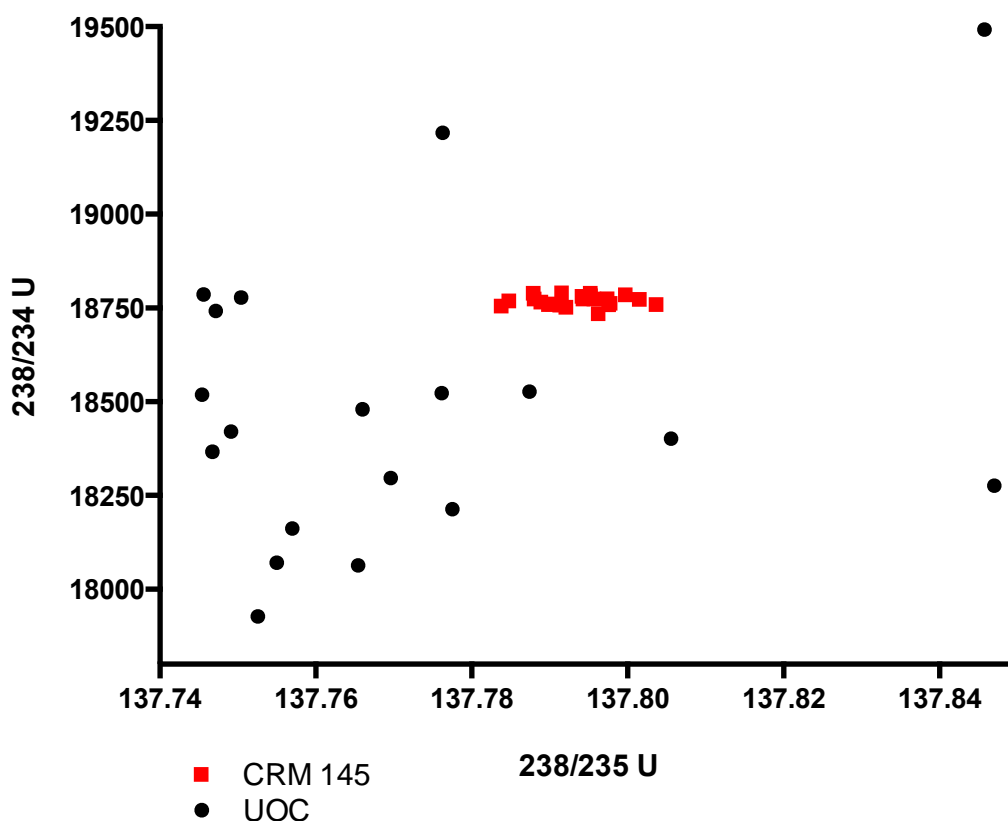
Scanning electron microscopy data (Appendix F) and X-ray diffraction data (Appendix G) have been obtained for all UOCs. The SEM BSE and EDX data provides details of the morphology and grain size with minor elemental identification whilst the XRD provides data on the U phase/compound present and other minor mineralogical/chemical compounds found in each sample. The combination of this data alongside full major and minor X-Ray Fluorescence (XRF) characterisation could yield some interesting results in identifying commonalities between morphology, chemical and elemental composition. For example, is there any evidence for links between a UOC with acicular morphology (SEM) and elemental sulphur/magnesium (SEM & XRF) or ammonia (XRD) from the digestion and precipitation stage of UOC production? The UOCs should be characterised by XRF in bead form as opposed to a pellet to limit the U concentration and subsequent interferences in the XRF spectrometer.

### 7.3 Uranium isotopes – Double spike method

Natural uranium isotopic data ( $^{234}\text{U}$ ,  $^{235}\text{U}$  &  $^{238}\text{U}$ ) has been collected for all UOCs using a Neptune Plus Multi-Collector ICPMS. A double-spike uranium ( $^{233}\text{U}$  &  $^{236}\text{U}$ ) method was used to correct for mass fractionation and instrumental drift. All measurements were completed using Faraday cups and an additional run was completed with a SEM for  $^{234}\text{U}$ . Additionally, as  $^{234}\text{U}$  is the lowest abundant isotope in the samples, a  $10^{12} \Omega$  amplifier was applied to increase the signal. All isotopic data was calibrated and compared against natural U standard CRM 145 (New Brunswick Laboratory, USA). The data is still in the post-experimental processing stage and has not been interpreted (Figure 7-1).

Previous studies in to U fractionation in UOC have used limited sample sets and have also required the samples to be measured twice at two different concentrations to overcome issues with measuring  $^{234}\text{U}$ . The current and unprocessed dataset was collected from a single sample where all 5 isotopes were measured simultaneously due to the advancement in mass spectrometry. It is anticipated that these samples will be re-measured on the same MC-ICPMS in the future as  $10^{13} \Omega$  amplifiers are soon to be installed which will increase instrument sensitivity further enabling cutting edge U isotopic measurements.

It is hoped that once the current data has been processed and confirmed, the U isotopic ratios of  $^{238/235}\text{U}$  and  $^{238/234}\text{U}$  can be incorporated into the growing statistical package that this thesis has implemented.



Depending on the final application of the melt, the sample would either be heated in an oval shaped capsule of suitable size to hold 0.5-1.0 g of sample and equal amount of lithium borate flux where the sample does not need to be coalesced; or it would be a smaller oval shaped capsule with a flattened bottom acting as a reservoir to contain 1.5 mg of sample and synthetic enstatite forming a small glass bead. Investigations would need to be conducted on how best to load and unload the sample from a welded or crimped capsule and whether the capsules could be reused and if so how many times before the capsule failed due to intense internal temperature and pressure conditions.

## **Appendix A: Instrumental theory and setup**

This thesis has used two key instruments to collect data: gamma spectrometers, and an Inductively Coupled Plasma Mass Spectrometer in solution mode and laser ablation mode. Both of these instruments are described here in greater detail with additional information regarding the setup and operating parameters.

### **A.1: Gamma spectrometry**

Gamma spectrometry is the measurement of gamma photons emitted from nuclei which have undergone alpha or beta decay (see section 1.3.2). The nuclei after alpha or beta decay is left in an excited state and will de-excite to a lower energy state by the emission of a gamma photon. Gamma photons cannot be detected directly as they do not cause ionisation or excitation of the detector medium. Therefore, semiconductor detectors are used to measure the gamma photon energy as a function of the number of charge carriers (electrons and holes) mobilised in the detector material which is arranged between two electrodes. The charge carrier mobilisation results in a number of electrons being transferred from the valence band to the conduction band, and an equal number of holes being created in the valence band. The valence band corresponds to outer-shell electrons that are bound to specific lattice sites within the detector. The conduction band represents electrons that are free to migrate through the detector material. The number of electron-hole pairs created by the transfer of energy from the photon to the detector is proportional the intrinsic gamma photon energy. When an electrical field is applied to the semiconductor, the charge carriers are separated and drift to the semiconductor electrodes. The current of the charge carriers is integrated and converted into an electrical signal in a preamplifier. The electrical signals are further processed in a multichannel analyser which converts the analogue signal to a digital value which is proportional to energy of the original gamma photon.

Ideally, a gamma spectrometer would have a response function consisting only of the full photopeak energy only where no continuum or background exists. Unfortunately, this is not the case as gamma photons are able to interact with the detector, the shielding and other gamma photons, electrons and positrons resulting in three key phenomena which

influence the final structure and appearance of the gamma spectrum: photoelectric absorption, Compton scattering, and pair production.

Photoelectric absorption is the interaction of a photon with atomic electron and ejects it with energy equal to the difference between the photon energy and the binding energy of the electron (Figure A-1A). The resulting electron shell vacancy can be filled by capturing a free electron or via electron shell rearrangement resulting in the emission of an X-ray or Auger electron (Figure A-1B).

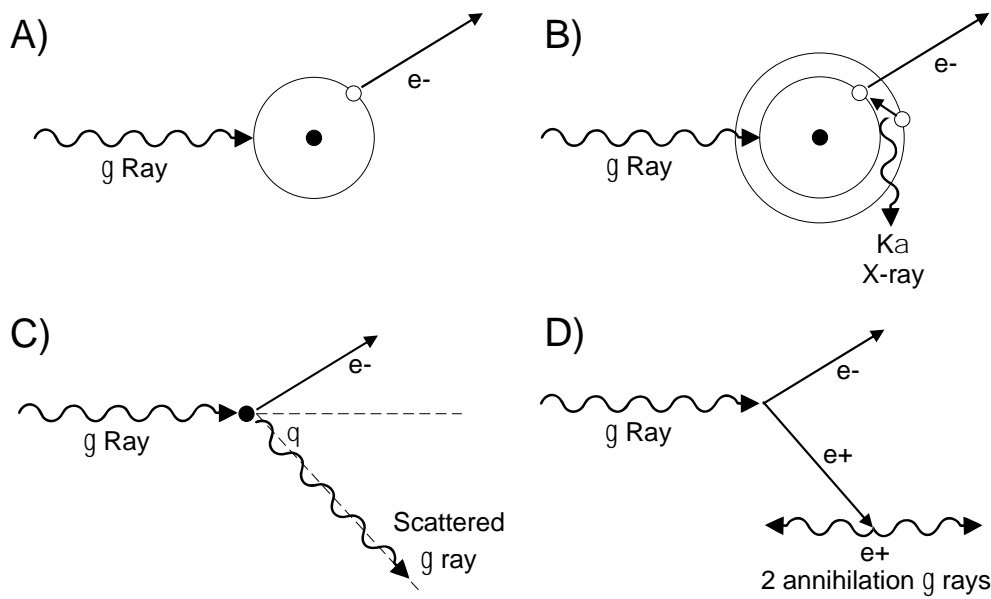


**Figure A- 1: Gamma photon interactions with matter. A) Photoelectric absorption, B) Photoelectric absorption with electron shell rearrangement, C) Compton scattering, D) Pair production.**

Compton scattering is the interaction of an incident photon scattering off from an atomic electron, resulting in a photon with reduced energy and a recoil electron (Figure A-1C). The energy of the incident photon is distributed between the scattered photon and the recoil electron by a relationship dependent on the angle of incidence and is described by equation A.1 where  $E_\gamma$  is the energy of the incident photo,  $m_0c^2$  the rest mass energy of the electron and  $\theta$  the angle through which the interaction occurred. Where  $\theta = 0$ , there is no scattering and the photon energy is unchanged.

$$E'_\gamma = \frac{E_\gamma}{1 + \frac{E_\gamma}{m_0c^2} (1 - \cos \theta)} \quad (\text{A.1})$$

Pair production is the process of a gamma photon turning into an electron-positron pair (Figure A-1D). The incident gamma photon must have energy exceeding the sum of the rest mass energies of an electron and positron ( $2 \times 511 \text{ keV} = 1022 \text{ keV}$ ) for this process to occur. The photon must be in close proximity to a nucleus in order to satisfy conservation of momentum. The resulting positron will eventually interact with one of the omnipresent electrons resulting in electron positron annihilation. Upon annihilation, two 511 keV photons will be released in opposite directions. This process happens almost immediately and will appear to be coincident with the original pair production. When one of the annihilation photons interacts with the detector, a single escape peak at 511 keV is observed on the pulse-height spectrum. Where both annihilation photons interact, a double escape peak is observed at 1022 keV.

Background radiation is always present and needs to be taken into account for all gamma spectrometric measurements. Terrestrial radiation from the natural decay chains ( $^{238}\text{U}$ ,  $^{235}\text{U}$  and  $^{232}\text{Th}$ ) and from  $^{40}\text{K}$  are found in building materials, components of the detector and associated systems and the shielding (with exception to radon) and need to be appropriately quantified so that the contribution from such naturally occurring radiation can be subtracted from the acquired spectrum. Cosmic radiation which is produced in the upper atmosphere also requires background subtraction from an acquired spectrum as standard laboratory Pb shielding cannot prevent the high energy muons or fast neutrons from interacting with the detector. To eliminate this interaction, laboratories are built hundreds of meters underground where the overburden/rock attenuates the high energy cosmic rays.

The shielding of a detector is often lead to prevent gamma photons from reaching the detector. However, lead atoms can become ionised and will emit a characteristic X-ray as a result of electron shell rearrangement. The X-ray's energy is typically between 75 and 85 keV and can be suppressed by including a liner of lower mass metal such as cadmium or tin in the detector shielding. Tin and cadmium also produce characteristic X-rays between 22-30 keV which can also be suppressed by an even lower mass metal such as copper. The radiation from the sample or source in the detector will also interact with the shielding materials which can cause Compton scattering.

The gamma spectrometers used for this thesis are all high-purity germanium (HPGe) well type detectors (see Figure A-2 for the setup of one of the detectors used for this thesis). HPGe detectors are made by highly refining the element germanium and growing it into a crystal. The crystal is then essentially turned into an electronic diode by the addition of positive and negative contacts. The relationship between the energy deposited in the crystal by an incident gamma photon and the current produced is so precise that HPGe detectors can determine gamma energies to better than 0.1%. The major benefit to well type detectors is that the sample is virtually surrounded resulting in a near  $4\pi$  geometry and therefore maximum efficiency.

The HPGe well detectors are calibrated with mixed gamma standards prepared using a commercially-available mixed gamma standard (typically supplied by the National Physical Laboratory, UK) but including other certified radionuclides such as  $^{40}\text{K}$ ,  $^{210}\text{Pb}$  and  $^{226}\text{Ra}$ . The mixed gamma standard are either in solution or typically dispersed through various matrices, producing a generic energy-efficiency calibration covering the energy range 40-1500 keV. The efficiency will be affected by sample density and the amount of sample in the vial and these factors are taken into account in the data processing.

There are two types of counting loss that occur in high resolution gamma spectrometry as a result of the phenomenon of summing – true coincidence summing (cascade summing) and random summing. When these occur they are manifested through the formation of sum peaks – these are more likely to be seen when using well type Ge detectors due to the near  $4\pi$  geometry. Such losses clearly affect the accuracy of data and methods need to be applied to correct for the problem. The detection efficiency of radionuclides with multiple gamma emissions may be reduced by coincidence summing giving a low bias to the results. There are approximately 75 radionuclides such as  $^{60}\text{Co}$ ,  $^{88}\text{Y}$ ,  $^{133}\text{Ba}$ ,  $^{134}\text{Cs}$ ,  $^{152}\text{Eu}$ ,  $^{154}\text{Eu}$  and  $^{214}\text{Bi}$  which are known to exhibit coincidence summing and must be analysed against a certified standard of the specific radionuclide to provide an empirical correction factor which can be applied offline. Random summing is the loss of counts (peak area) when samples have elevated count rates and is independent of energy, sample-to-detector distance and the number of nuclides in the sample. Random summing is correctable with the use of a pulser or a stationary reference source.



**Figure A-2: One of eight Canberra HPGe detector with dewar and Cu coated Pb shielding at GAU-Radioanalytical, Southampton, UK**

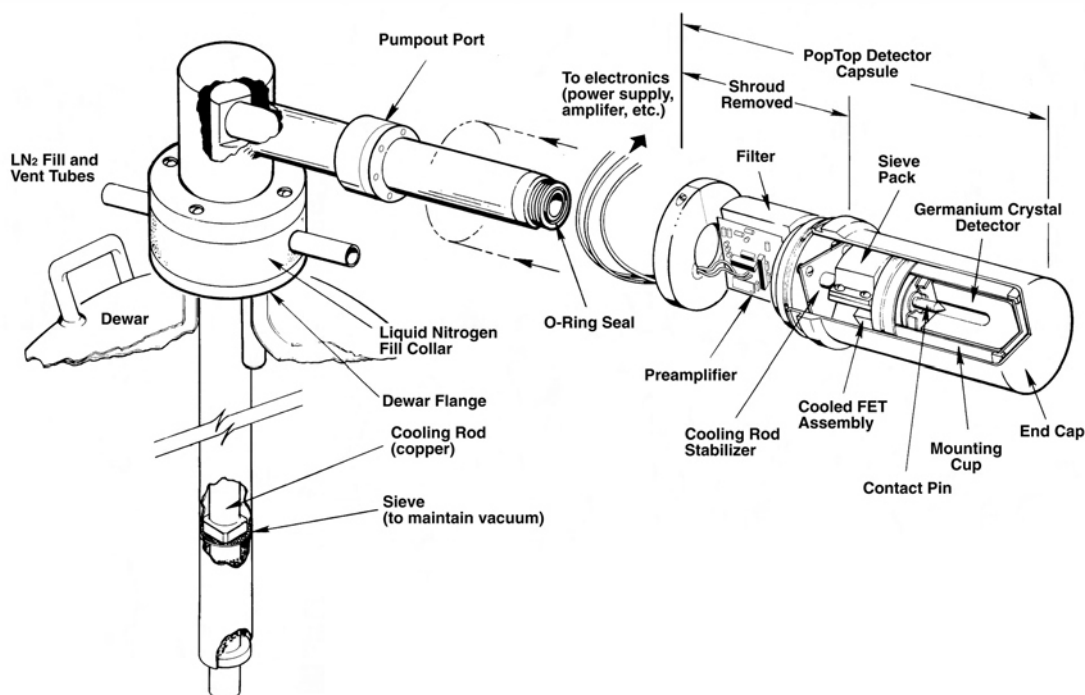


**Figure A-3: Expanded schematic of an HPGe detector housing**  
(Gilmore & Hemingway, 1995).

## A.2: ICPMS & LA-ICPMS

Inductively Coupled Plasma Mass Spectrometry (ICPMS) and Laser Ablation ICP-MS were used for the analysis of REE in glass beads and in chemically purified aqueous fraction. The mass spectrometer in both applications was the X-Series II quadrupole ICPMS (Thermo-Fisher, Germany). The X-Series II features an off-axis high-performance quadrupole mass analyser which provides an extremely high signal-to-noise ratio rivalling that of Sector Field ICPMS. The detector is a discrete dynode electron multiplier, with nine orders of linear dynamic range allowing for the accurate measurement of major and minor concentrations in a single analytical run.

The X-Series II has four basic stages of operation: 1) Sample introduction and ion generation; 2) Ion focusing; 3) Separation of analyte ions using a quadrupole mass filter; 4) Ion detection. Each of these stages will be detailed below.

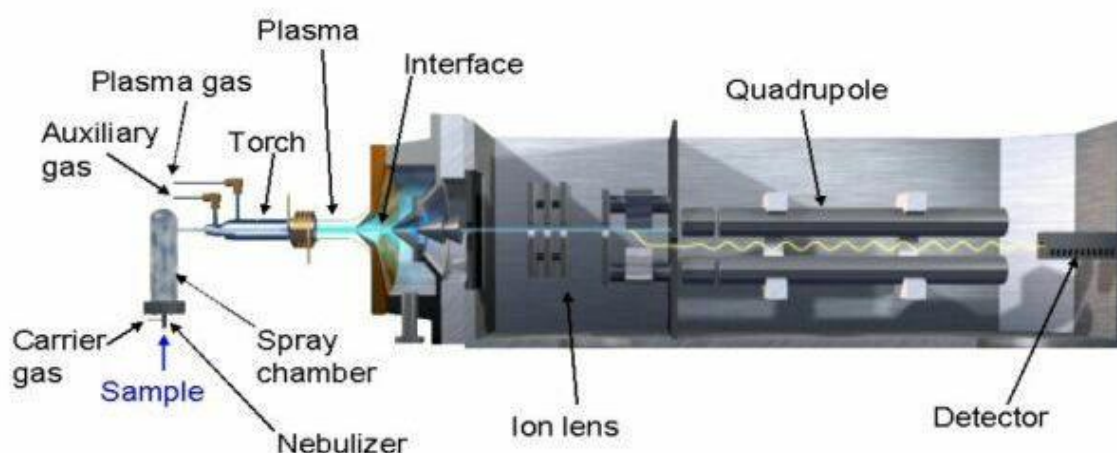


**Figure A- 4: Generalised quadrupole ICPMS setup**

(Image courtesy of Washington University in St. Louis, 2016)

### A.2.1 Sample introduction and ion generation

Samples are loaded onto a Cetac ASX-520 autosampler allowing autonomous and 24 hours operation of the ICPMS. The sample is introduced into argon plasma as a fine aerosol via a peristaltic pump, nebuliser and spray chamber. As the sample enters the plasma (~6000 K), it undergoes desolvation to remove water and solvents and then vaporisation where the sample species are decomposed into their constituent atoms and ionised due to the

collisions with electrons in the plasma. The torch is comprised of three concentric tubes composed of quartz. The outer and middle tube both contain argon where the outer tube is for cooling and sustaining the plasma, while the middle tube helps position the plasma away from the sample injector. The inner tube contains the sample with the nebuliser gas. A radio frequency coil is used to cause collisions between the argon atoms and to stabilise the plasma once ignited.

### A.2.2 Ion focusing

The ions formed in the plasma are extracted through a sample and skimmer cone arrangement. The cones have a current applied causing the ions to accelerate. The sample cone is placed at the tip of the plasma and the ion beam expands into the vacuum behind it where the centre of this expanded beam is pulled through a skimmer cone to the ion transfer system. Ion lenses then focus and optimise the ion transmission to the quadrupole analyser. The X-Series II contains a high efficiency ion guide which incorporates an innovative chicane deflector and off-axis quadrupole.

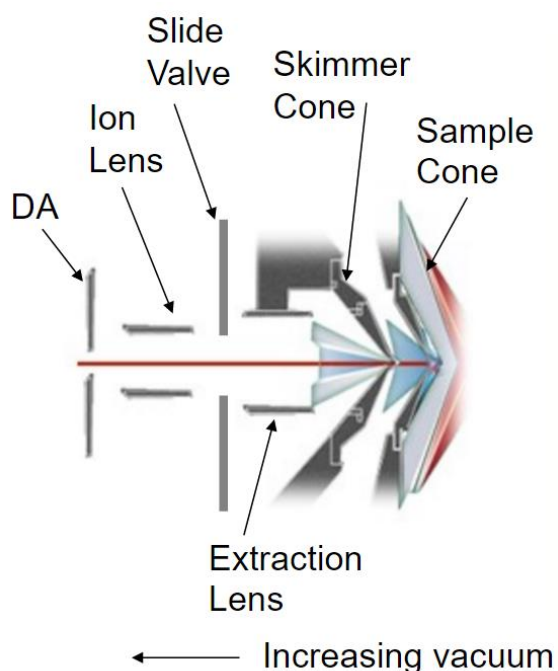


**Figure A- 5: Ion sampling and focusing through cones and lenses**

(Image courtesy of Thermo-Fisher, 2015)

### **A.2.3 Ion separation using a quadrupole mass filter**

The quadrupole consists of four rods mounted equidistantly to each other around the circumference of a circle which separates ions according to their mass to charge ratio. This is accomplished by oscillating RF or DC potentials which are applied to the quadrupole rod pairs. The ions move in a spiral motion down the axis of the quadrupole where the majority of masses are put into an unstable trajectory and are rejected. The ions of interest will have a specific mass to charge ratio and the quadrupole will adjust the frequency / potential between the quadrupole rod pairs in order for the target ions to pass through the quadrupole and reach the detector.

### **A.2.4 Detection**

The X-Series II features a discrete dynode electron multiplier (ion counter) as its detector which is a vacuum-tube structure that multiplies incident charges in a process called secondary emission. Once the desired ions have been isolated, the ion beam reaches the electron multiplier and interacts with one of the dynodes resulting in the release of up to 3 electrons from the surface of the detector. Through successive interactions with the sequential dynodes where each dynode has an electrical potential of 100-200 V greater than the previous, multiplication results in  $10^7 - 10^8$  electrons being collected by a metal anode.

### **A.2.5 Laser-Ablation sample introduction**

A ESI® New Wave Research™ UP193FX 193 nm solid-state laser ablation system (Fremont, CA, USA) was coupled to the X-Series II ICP-MS for the measurement of REE in glass beads. The ablated sample is introduced directly to the X-Series II using He carrier gas and without the requirement for a nebuliser or desolvation. The low wavelength excimer laser (193 nm) allows for reproducible craters where routine precision is 1-3%. The spot size is variable between 5 and 150 µm. The sample holder is on a moveable xyz stage allowing the user to programme a run sequence. The laser and ICPMS software are able to run side by side on the same computer so that triggering of the laser and data collection from the ICPMS are synchronous.



**Figure A- 6: The X-Series II quadrupole ICPMS at The University of Southampton's Isotope Geochemistry Mass Spectrometry Facility**



**Figure A- 7: The UP-193FX Laser Ablation System at The University of Southampton's Isotope Geochemistry Mass Spectrometry Facility**

**Table A- 1: Laser and ICP-MS operating parameters**

X-Series II ICPMS	Laser	Solution
Forward Power (W)	1350	1350
Nebuliser gas flow (L/min <sup>-1</sup> )	0.57	0.86
Auxiliary gas flow (L/min <sup>-1</sup> )	0.8	0.8
Cooling gas flow (L/min <sup>-1</sup> )	13	13
Solution uptake rate (μL/min <sup>-1</sup> )	N/A	~100
Runs and sweeps	1 x 100	4 x 75
Dwell Time (ms)	10	N/A
Sampling cone (mm)	1.0 Ni cone	
Skimmer cone (mm)	0.7 Ni cone	
Resolution	Standard	
Acquisition mode	Time resolved analysis - peak jumping	
Measured isotopes	115In* 137Ba, 139La, 140Ce, 141Pr, 146Nd, 147Sm, 153Eu,	
(* = solution only)	157Gd, 159Tb, 163Dy, 165Ho, 166Er, 169Tm, 172Yb, 175Lu,	
	185Re*, 238U*	
New Wave UP 193 Laser		
Carrier gas flow (He) (L/min <sup>-1</sup> )	1	
Wavelength (nm)	193 Nd:YAG	
Spot size (μm)	100	
Pulse repetition rate (Hz)	5	
Washout between samples (s)	20	

**Table A- 2: Isobaric interference correction factors for solution ICPMS**

Isotope Ratio	Ba	Ce	Pr	Sm
$^{153}\text{Eu} / ^{137}\text{Ba}$	0.00047			
$^{157}\text{Gd} / ^{141}\text{Pr}$			0.00980	
$^{157}\text{Gd} / ^{140}\text{Ce}$		0.00074		
$^{159}\text{Tb} / ^{146}\text{Nd}$			0.00610	
$^{166}\text{Er} / ^{146}\text{Nd}$			0.00301	
$^{163}\text{Dy} / ^{147}\text{Sm}$				0.00170
$^{165}\text{Ho} / ^{147}\text{Sm}$				0.00177
$^{166}\text{Er} / ^{147}\text{Sm}$				0.00114
$^{169}\text{Tm} / ^{153}\text{Eu}$				0.00042
$^{172}\text{Yb} / ^{157}\text{Gd}$				0.00668
$^{175}\text{Lu} / ^{159}\text{Tb}$				0.00552



## Appendix B: The UOC collection in this study

Anaconda - USA	Blind River - CAN	Chevron Hill - USA
		
Cotter – USA	Eldorado – CAN	Faraday – CAN
		
Gunnar – CAN	Lucky McGill – USA	Madawaska - CAN
		
Mary Kathleen – AUS	Mesa EFI – USA	Mulberry – USA
		

**Figure B- 1: Images of UOC Anaconda to Mulberry**





North Span – CAN	Olympic Dam – AUS	Queensland – AUS
		
Rabbit Lake – CAN	Ranger – AUS	Rio Algom – CAN
		
South Alligator – AUS		
		

Figure B- 2: Images of UOC North Span to South Alligator

## **Appendix C:    Supplementary data and information for Chapter 3**

Table C- 1: UOC gamma spectrometric data prior to fusion (solid matrix).

Solid Matrix (Bq/g)												
	<sup>234</sup> Th	±	<sup>235</sup> U	±	<sup>234m</sup> Pa	±	<sup>214</sup> Pb	±	<sup>228</sup> Ac	±	<sup>208</sup> Tl	±
Anaconda	1421	472	134.70	32.40	7583	910	5.86	1.20	-	-	-	-
Blind River	1610	536	144.00	32.00	7174	860	2.90	0.64	13.30	3.00	3.54	0.54
Chevron Hill	1256	424	120.50	29.20	7447	894	-	-	-	-	-	-
Cotter	1241	408	121.20	27.80	7155	858	21.50	5.40	-	-	-	-
Eldorado	1502	500	143.90	32.80	7900	948	2.80	0.98	12.30	3.80	3.03	0.68
Faraday	1185	398	111.90	22.00	6943	834	3.70	0.48	27.50	4.20	5.60	0.64
Gunnar	1259	412	120.00	26.00	7120	854	3.50	0.68	-	-	0.17	0.06
Lucky McGill	1311	442	125.90	29.40	7878	946	1.02	0.98	-	-	-	-
Madawaska	1476	492	136.80	30.80	7301	876	4.10	1.20	41.00	7.60	12.18	1.50
Mary Kathleen	1161	380	116.90	27.80	7961	956	-	-	-	-	-	-
Mesa EFI	1377	456	128.90	29.40	7363	884	1.00	0.80	-	-	-	-
Mulberry	1122	376	112.20	27.60	7748	930	-	-	-	-	-	-
North Span	1458	480	136.50	32.60	7288	874	2.95	1.00	13.20	4.40	2.41	0.46
Olympic Dam	1218	400	121.00	29.80	8316	998	-	-	-	-	-	-
Queensland	1057	348	107.20	26.00	8545	1026	1.09	0.80	-	-	-	-
Rabbit Lake	1161	380	114.60	26.20	7192	864	-	-	-	-	-	-
Ranger	1470	488	176.80	33.60	8761	1052	-	-	-	-	-	-
Rio Algom	1697	568	181.50	33.20	7245	870	2.45	0.94	18.90	4.60	5.20	0.92
South Alligator	1942	644	209.10	39.60	8347	1002	1.00	0.72	-	-	-	-

Table C- 2: UOC gamma and alpha spectrometric data post fusion (fused matrix).

Fused Matrix (Bq/g)														
	<sup>234</sup> Th	±	<sup>235</sup> U	±	<sup>234m</sup> Pa	±	<sup>214</sup> Pb	±	<sup>228</sup> Ac	±	<sup>208</sup> Tl	±	<sup>210</sup> Po	±
Anaconda	9290	1024	437	74	8800	1178	8.95	1.08	-	-	-	-	9.74	2.80
Blind River	8092	884	388	62	8180	880	4.60	0.68	15.30	3.20	4.74	0.60	5.13	2.80
Chevron Hill	9520	1040	437	70	9313	1246	-	-	-	-	-	-	0.39	0.16
Cotter	7570	846	363	64	7660	996	28.10	6.00	1.11	0.80	0.26	0.26	32.44	8.30
Eldorado	9200	1012	447	76	8960	1212	4.10	1.80	17.90	6.60	5.16	1.68	4.38	1.40
Faraday	8144	904	393	62	8300	940	6.50	0.86	35.90	10.40	15.20	2.60	7.60	2.24
Gunnar	7969	884	381	60	8090	880	5.60	0.86	1.20	0.80	0.46	0.28	4.74	1.46
Lucky McGill	10700	1162	490	76	10900	1200	1.52	0.92	-	-	-	-	1.29	0.48
Madawaska	7910	864	360	58	7500	846	6.23	0.82	43.80	5.80	18.90	2.80	5.40	1.58
Mary Kathleen	9260	1024	441	74	9050	1196	-	-	-	-	-	-	0.17	0.06
Mesa EFI	8802	966	413	64	8600	1180	2.76	0.50	-	-	-	-	2.07	0.72
Mulberry	9530	1046	442	68	9240	1116	-	-	-	-	-	-		
North Span	8500	940	388	60	8060	962	5.29	0.80	13.60	2.80	3.77	0.52	17.16	4.64
Olympic Dam	8874	988	418	66	8890	1000	-	-	-	-	-	-	0.24	0.20
Queensland	9500	1040	449	74	9210	1178	1.68	0.30	-	-	-	-	1.39	0.60
Rabbit Lake	9070	1000	433	78	8990	1198	-	-	-	-	-	-	0.26	0.21
Ranger	9250	1024	437	76	8960	1162	-	-	-	-	-	-	0.12	0.10
Rio Algom	8319	896	400	62	8430	940	4.28	0.72	24.40	9.80	6.61	0.78	3.73	1.26
South Alligator	8890	946	417	66	8630	1046	1.50	0.40	-	-	-	-	1.10	0.50

**Table C- 3: PCA Component Matrix showing weighting of individual variables on each component**

	Component Matrix		
	1	2	3
<sup>235</sup> U	0.951	-	-
<sup>234</sup> Th	0.942	-	-
<sup>234m</sup> Pa	0.933	-	-
<sup>228</sup> Ac	-0.732	0.655	-
<sup>208</sup> Tl	-0.722	0.669	-
<sup>210</sup> Po	-0.573	-0.587	0.572

**Table C- 4: Variance explained by each component**

Component	Eigenvalue	% of variance	Cumulative %
1	4.047	67.457	67.457
2	1.368	22.798	90.255
3	0.492	8.203	98.458

**Table C- 5: Component scores of each UOC**

	PCA Component Score		
	1	2	3
Anaconda	0.42016	-0.57022	0.57087
Blind River	-0.8925	0.43828	0.00711
Chevron Hill	0.76056	-0.56202	-0.59368
Cotter	-1.61249	-0.49861	3.46221
Eldorado	0.55298	0.56424	-0.1067
Faraday	-0.76109	2.16318	0.31432
Gunnar	-1.06061	-0.47708	-0.0427
Lucky McGill	2.55425	-0.55755	-0.46684
Madawaska	-1.56311	2.79914	0.03522
Mary Kathleen	0.55999	-0.56888	-0.63521
Mesa EFI	-0.13186	-0.56523	-0.38758
Mulberry	0.78037	-0.5651	-0.64989
North Span	-0.76095	0.2871	1.52778
Olympic Dam	0.08425	-0.56326	-0.61329
Queensland	0.82208	-0.56882	-0.48132
Rabbit Lake	0.36725	-0.56736	-0.61967
Ranger	0.47427	-0.56831	-0.64114
Rio Algom	-0.55468	0.94654	-0.16707
South Alligator	-0.03886	-0.56603	-0.51242

## **Appendix D:   Supplementary data and information for Chapter 4**

Table D- 1: Geological Reference Material AC-E and BE-N concentrations and chondrite normalised data for glass beads

Element	Mass	AC-E (ug g <sup>-1</sup> )						AC-E (CI Normalised)					
		GeoReM		Glass bead 1		Glass bead 2		GeoReM		Glass bead 1		Glass bead 2	
		P.V.	S.D.	Conc.	S.D.	Conc.	S.D.	P.V.	S.D.	REE/CI	S.D.	REE/CI	S.D.
La	139	59.00	1.20	57.71	1.52	50.88	1.74	251.38	5.11	245.87	6.46	216.79	7.41
Ce	140	154.00	3.00	169.92	3.25	166.06	5.18	255.31	4.97	281.70	5.39	275.30	8.58
Pr	141	22.20	0.72	24.19	0.54	22.26	0.85	249.16	8.08	271.44	6.01	249.78	9.55
Nd	146	92.00	3.00	91.82	2.89	83.15	3.68	203.36	6.63	202.95	6.38	183.79	8.14
Sm	147	24.20	0.70	24.73	1.91	21.03	1.69	164.51	4.76	168.15	12.98	142.96	11.51
Eu	153	2.00	0.04	1.87	0.26	1.66	0.17	35.71	0.71	33.45	4.68	29.69	3.04
Gd	157	26.00	0.30	27.15	1.84	24.86	1.58	132.25	1.53	138.11	9.36	126.43	8.03
Tb	159	4.80	0.10	4.57	0.36	4.04	0.29	132.23	2.75	126.03	9.80	111.37	7.88
Dy	163	29.00	1.00	31.06	1.52	26.64	1.66	119.49	4.12	127.96	6.24	109.77	6.83
Ho	165	6.50	0.10	6.08	0.23	5.48	0.37	116.91	1.80	109.37	4.22	98.49	6.67
Er	166	17.70	0.40	18.10	1.31	16.11	0.84	111.39	2.52	113.92	8.24	101.37	5.27
Tm	169	2.60	0.10	2.59	0.20	2.29	0.18	107.44	4.13	106.86	8.12	94.63	7.31
Yb	172	17.40	0.40	16.96	1.10	15.13	1.11	107.08	2.46	104.37	6.80	93.13	6.83
Lu	175	2.45	0.03	2.40	0.26	2.20	0.21	100.82	1.23	98.67	10.69	90.57	8.46

Element	Mass	BE-N (ug g <sup>-1</sup> )						BE-N (CI Normalised)					
		GeoReM		Glass bead 1		Glass bead 2		GeoReM		Glass bead 1		Glass bead 2	
		P.V.	S.D.	Conc.	S.D.	Conc.	S.D.	P.V.	S.D.	REE/CI	S.D.	REE/CI	S.D.
La	139	82.00	2.14	60.69	7.39	60.69	9.72	349.38	9.12	258.59	31.50	270.22	41.40
Ce	140	152.00	3.86	150.40	13.28	160.12	23.08	251.99	6.40	249.34	22.01	265.45	38.27
Pr	141	17.50	0.34	14.15	1.57	14.84	2.28	196.41	3.82	158.85	17.64	166.50	25.63
Nd	146	67.00	5.77	51.40	6.20	52.63	8.08	148.10	12.75	113.62	13.71	116.33	17.85
Sm	147	12.20	0.33	8.76	1.71	9.63	2.04	82.94	2.24	59.53	11.65	65.44	13.87
Eu	153	3.60	0.19	2.70	0.43	2.83	0.51	64.29	3.39	48.30	7.64	50.57	9.15
Gd	157	9.70	0.40	7.07	1.23	7.68	1.48	49.34	2.03	35.94	6.25	39.06	7.51
Tb	159	1.30	0.28	0.82	0.14	0.90	0.18	35.81	7.71	22.56	3.89	24.73	4.97
Dy	163	6.40	0.15	4.64	0.75	4.60	0.82	26.37	0.62	19.11	3.09	18.94	3.37
Ho	165	1.10	0.22	0.70	0.14	0.74	0.13	19.78	3.96	12.58	2.57	13.33	2.31
Er	166	2.50	0.13	1.73	0.33	1.81	0.39	15.73	0.82	10.87	2.10	11.41	2.46
Tm	169	0.34	0.07	0.20	0.06	0.19	0.05	14.05	2.89	8.34	2.29	7.96	2.16
Yb	172	1.80	0.04	1.31	0.28	1.25	0.29	11.08	0.25	8.08	1.74	7.72	1.76
Lu	175	0.24	0.06	0.16	0.04	0.19	0.05	9.88	2.47	6.79	1.78	7.64	1.96

Table D- 2: Geological Reference Material BHVO-1 and Mica-Fe concentrations and chondrite normalised data for glass beads

Element	Mass	BHVO-1 (ug g <sup>-1</sup> )						BHVO-1 (CI Normalised)					
		GeoReM		Glass bead 1		Glass bead 2		GeoReM		Glass bead 1		Glass bead 2	
		P.V.	S.D.	Conc.	S.D.	Conc.	S.D.	P.V.	S.D.	REE/CI	S.D.	REE/CI	S.D.
La	139	15.80	0.30	12.04	0.87	14.31	1.01	67.32	1.28	51.30	3.71	60.96	4.29
Ce	140	37.70	0.70	38.21	1.89	38.36	1.97	62.50	1.16	63.35	3.14	63.60	3.27
Pr	141	5.25	0.09	4.60	0.34	5.05	0.40	58.92	1.01	51.65	3.80	56.66	4.44
Nd	146	24.40	0.30	20.12	1.72	23.17	2.55	53.93	0.66	44.47	3.80	51.21	5.63
Sm	147	6.00	0.10	4.88	0.83	5.64	0.83	40.79	0.68	33.15	5.62	38.36	5.66
Eu	153	2.20	0.10	1.66	0.27	1.89	0.26	39.29	1.79	29.70	4.80	33.68	4.65
Gd	157	6.20	0.30	4.52	0.69	5.81	0.75	31.54	1.53	23.01	3.52	29.55	3.83
Tb	159	0.96	0.03	0.64	0.10	0.80	0.13	26.45	0.83	17.76	2.65	22.05	3.69
Dy	163	5.40	0.30	3.88	0.62	4.79	0.65	22.25	1.24	15.97	2.57	19.74	2.69
Ho	165	1.05	0.04	0.71	0.11	0.87	0.13	18.88	0.72	12.71	1.91	15.65	2.28
Er	166	2.54	0.04	1.84	0.31	2.30	0.35	15.98	0.25	11.57	1.97	14.50	2.23
Tm	169	0.32	0.01	0.22	0.07	0.27	0.07	13.22	0.41	9.05	2.70	11.36	2.76
Yb	172	2.01	0.07	1.46	0.35	1.82	0.34	12.37	0.43	8.97	2.14	11.19	2.11
Lu	175	0.28	0.01	0.18	0.06	0.25	0.06	11.52	0.41	7.53	2.40	10.17	2.33

Element	Mass	Mica-Fe (ug g <sup>-1</sup> )						Mica-Fe (CI Normalised)					
		GeoReM		Glass bead 1		Glass bead 2		GeoReM		Glass bead 1		Glass bead 2	
		P.V.	S.D.	Conc.	S.D.	Conc.	S.D.	P.V.	S.D.	REE/CI	S.D.	REE/CI	S.D.
La	139	216.00	4.00	133.44	32.37	145.21	21.06	920.32	17.04	568.55	137.92	618.71	89.72
Ce	140	480.00	8.00	363.73	78.94	368.23	44.92	795.76	13.26	603.00	130.87	610.46	74.46
Pr	141	48.60	0.30	37.60	8.19	39.70	5.07	545.45	3.37	421.95	91.91	445.55	56.95
Nd	146	179.00	1.00	126.56	30.97	136.82	20.10	395.67	2.21	279.75	68.46	302.44	44.42
Sm	147	32.70	0.30	23.78	5.95	25.37	4.23	222.30	2.04	161.69	40.45	172.44	28.75
Eu	153	1.56	0.01	0.44	0.17	0.45	0.14	27.86	0.18	7.87	3.04	8.10	2.48
Gd	157	21.20	0.30	15.75	3.89	16.08	2.90	107.83	1.53	80.11	19.78	81.81	14.74
Tb	159	2.70	0.25	1.65	0.40	1.88	0.37	74.38	6.89	45.42	11.09	51.82	10.13
Dy	163	10.50	0.10	7.37	1.51	8.19	1.48	43.26	0.41	30.38	6.23	33.75	6.11
Ho	165	1.62	0.01	1.05	0.22	1.15	0.21	29.14	0.18	18.89	4.04	20.73	3.87
Er	166	3.79	0.04	2.71	0.62	2.88	0.61	23.85	0.25	17.03	3.92	18.13	3.83
Tm	169	0.48	0.00	0.34	0.08	0.35	0.10	19.83	0.00	13.93	3.28	14.66	3.95
Yb	172	3.38	0.06	2.33	0.54	2.50	0.52	20.80	0.37	14.32	3.34	15.37	3.18
Lu	175	0.53	0.00	0.37	0.10	0.40	0.11	21.81	0.00	15.25	4.18	16.28	4.36

**Table D- 3: Geological Reference Material SY-2 and SY-3 concentrations and chondrite normalised data for glass beads**

Element	Mass	SY-2 (ug g <sup>-1</sup> )						SY-2 (CI Normalised)					
		GeoReM		Glass bead 1		Glass bead 2		GeoReM		Glass bead 1		Glass bead 2	
		P.V.	S.D.	Conc.	S.D.	Conc.	S.D.	P.V.	S.D.	REE/CI	S.D.	REE/CI	S.D.
La	139	75.00	0.70	58.76	2.53	51.53	2.61	319.56	2.98	250.34	10.80	219.56	11.13
Ce	140	175.00	1.10	157.70	2.55	147.01	7.15	290.12	1.82	261.44	4.23	243.71	11.85
Pr	141	18.80	0.20	18.12	0.64	16.75	0.91	211.00	2.24	203.39	7.17	187.94	10.26
Nd	146	73.00	0.95	66.72	2.89	62.91	3.54	161.36	2.10	147.49	6.39	139.06	7.82
Sm	147	16.10	0.40	14.36	1.48	13.37	1.41	109.45	2.72	97.59	10.07	90.91	9.56
Eu	153	2.42	0.40	2.10	0.25	2.05	0.25	43.21	7.14	37.55	4.40	36.65	4.41
Gd	157	17.00	0.20	13.92	1.39	13.01	1.37	86.47	1.02	70.82	7.06	66.20	6.96
Tb	159	2.50	0.05	2.42	0.24	2.25	0.20	68.87	1.38	66.55	6.72	61.95	5.63
Dy	163	18.00	0.40	16.55	1.40	16.02	1.40	74.17	1.65	68.17	5.75	66.01	5.77
Ho	165	3.80	0.06	3.88	0.31	3.60	0.29	68.35	1.08	69.79	5.58	64.73	5.17
Er	166	12.40	0.30	13.13	0.94	12.17	0.86	78.04	1.89	82.64	5.91	76.61	5.41
Tm	169	2.10	0.02	2.04	0.19	1.80	0.18	86.78	0.83	84.39	7.85	74.41	7.46
Yb	172	17.00	0.60	15.13	1.07	13.98	1.27	104.62	3.69	93.10	6.56	86.05	7.84
Lu	175	2.70	0.04	2.48	0.18	2.23	0.22	111.11	1.65	102.16	7.32	91.76	9.02

Element	Mass	SY-3 (ug g <sup>-1</sup> )						SY-3 (CI Normalised)					
		GeoReM		Glass bead 1		Glass bead 2		GeoReM		Glass bead 1		Glass bead 2	
		P.V.	S.D.	Conc.	S.D.	Conc.	S.D.	P.V.	S.D.	REE/CI	S.D.	REE/CI	S.D.
La	139	1330.00	15.00	1068.79	26.98	977.31	76.98	5666.81	63.91	4553.84	114.94	4164.09	328.00
Ce	140	2230.00	33.00	2115.38	31.22	2054.05	86.79	3696.95	54.71	3506.93	51.76	3405.26	143.88
Pr	141	225.00	4.00	194.26	3.91	177.90	10.66	2525.25	44.89	2180.26	43.88	1996.67	119.64
Nd	146	749.00	14.00	619.45	15.74	544.56	41.01	1655.61	30.95	1369.26	34.78	1203.72	90.65
Sm	147	109.00	2.00	104.69	4.95	88.93	7.80	740.99	13.60	711.72	33.68	604.58	53.00
Eu	153	17.00	0.50	15.36	0.70	12.45	0.98	303.57	8.93	274.30	12.53	222.26	17.44
Gd	157	105.00	1.00	99.29	4.68	81.98	7.87	534.08	5.09	505.02	23.78	416.99	40.01
Tb	159	18.00	0.20	16.23	0.67	13.31	1.16	495.87	5.51	447.24	18.56	366.74	32.05
Dy	163	118.00	1.50	110.49	4.81	91.07	7.96	486.20	6.18	455.26	19.83	375.26	32.80
Ho	165	29.50	0.40	23.50	1.30	19.21	1.80	530.58	7.19	422.71	23.30	345.52	32.31
Er	166	68.00	0.40	71.86	3.50	59.33	5.34	427.94	2.52	452.25	22.03	373.39	33.60
Tm	169	11.60	0.20	9.65	0.46	7.91	0.79	479.34	8.26	398.87	18.91	327.06	32.80
Yb	172	62.00	0.30	57.21	2.85	47.98	4.37	381.54	1.85	352.09	17.51	295.26	26.89
Lu	175	7.90	0.16	7.01	0.35	5.84	0.58	325.10	6.58	288.63	14.58	240.18	23.90

Table D- 4: Geological Reference Material NOD-A1 and NOD-P1 concentrations and chondrite normalised data for glass beads

Element	Mass	NOD-A1 (ug g <sup>-1</sup> )				NOD-A1 (CI Normalised)			
		GeoReM		Glass bead 1		GeoReM		Glass bead 1	
		P.V.	S.D.	Conc.	S.D.	P.V.	S.D.	REE/CI	S.D.
La	139	119.00	2.00	109.09	2.20	507.03	8.52	464.79	9.36
Ce	140	732.00	2.00	792.73	9.79	1213.53	3.32	1314.20	16.23
Pr	141	25.00	0.10	23.90	0.86	280.58	1.12	268.19	9.67
Nd	146	94.00	2.00	100.29	5.86	207.78	4.42	221.69	12.96
Sm	147	21.00	0.10	21.72	1.52	142.76	0.68	147.62	10.34
Eu	153	4.96	0.11	5.02	0.51	88.57	1.96	89.60	9.09
Gd	157	26.00	0.40	24.66	1.91	132.25	2.03	125.45	9.72
Tb	159	4.00	0.07	3.88	0.32	110.19	1.93	106.76	8.72
Dy	163	22.80	0.40	24.66	1.36	93.94	1.65	101.63	5.61
Ho	165	5.00	0.10	5.30	0.30	89.93	1.80	95.34	5.48
Er	166	11.70	0.40	15.94	0.77	73.63	2.52	100.32	4.86
Tm	169	2.05	0.06	2.24	0.21	84.71	2.48	92.38	8.70
Yb	172	13.80	0.40	14.75	1.48	84.92	2.46	90.78	9.12
Lu	175	2.24	0.05	2.39	0.25	92.18	2.06	98.43	10.45

Element	Mass	NOD-P1 (ug g <sup>-1</sup> )				NOD-P1 (CI Normalised)			
		GeoReM		Glass bead 1		GeoReM		Glass bead 1	
		P.V.	S.D.	Conc.	S.D.	P.V.	S.D.	REE/CI	S.D.
La	139	104.00	2.00	105.30	3.64	443.12	8.52	448.66	15.52
Ce	140	294.00	2.00	297.91	7.93	487.40	3.32	493.88	13.14
Pr	141	31.00	0.20	31.70	1.06	347.92	2.24	355.82	11.93
Nd	146	119.50	2.00	133.54	5.85	264.15	4.42	295.19	12.94
Sm	147	29.50	0.30	32.90	2.23	200.54	2.04	223.64	15.17
Eu	153	7.50	0.10	7.51	0.69	133.93	1.79	134.09	12.25
Gd	157	28.20	0.50	30.82	2.02	143.44	2.54	156.76	10.26
Tb	159	4.90	0.02	5.23	0.37	134.99	0.55	144.13	10.30
Dy	163	26.90	0.40	29.77	2.16	110.84	1.65	122.64	8.91
Ho	165	5.07	0.01	5.62	0.26	91.19	0.18	101.07	4.59
Er	166	12.50	0.10	15.80	0.69	78.67	0.63	99.43	4.32
Tm	169	1.90	0.02	2.26	0.23	78.51	0.83	93.48	9.60
Yb	172	12.70	0.20	14.29	1.65	78.15	1.23	87.91	10.14
Lu	175	1.78	0.01	2.15	0.16	73.25	0.41	88.51	6.45

Table D- 5: Uranium Reference Material CUP-1 and BL-5 concentrations and chondrite normalised data for glass beads

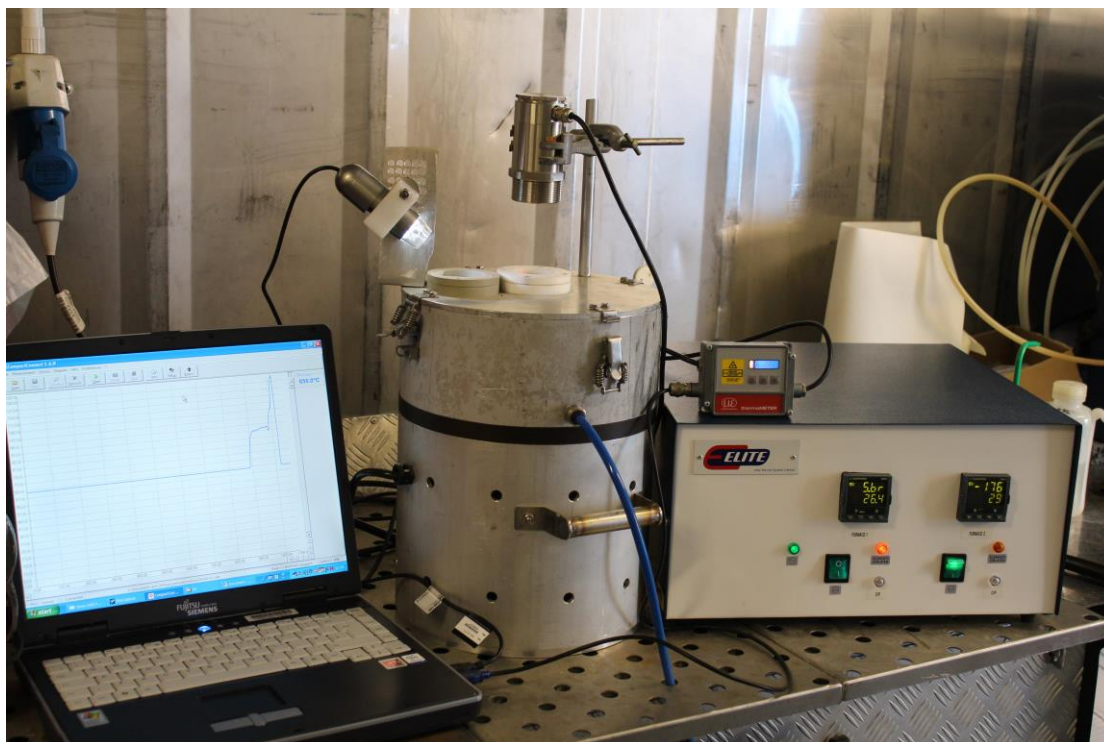
Element	Mass	CUP-1 (ug g <sup>-1</sup> )				CUP-1 (CI Normalised)			
		Glass bead 1		Glass bead 2		Glass bead 1		Glass bead 2	
		Conc.	S.D.	Conc.	S.D.	REE/CI	S.D.	REE/CI	S.D.
La	139	106.71	4.51	116.44	3.02	454.65	19.24	496.12	12.89
Ce	140	302.06	6.47	311.71	5.52	500.77	10.73	516.76	9.15
Pr	141	31.23	1.66	33.23	1.51	350.51	18.66	372.96	16.96
Nd	146	122.49	7.37	132.96	6.18	270.76	16.28	293.89	13.65
Sm	147	27.89	3.38	26.56	3.19	189.60	23.00	180.56	21.68
Eu	153	6.19	0.70	6.63	0.70	110.48	12.45	118.48	12.47
Gd	157	25.07	3.09	26.99	3.17	127.53	15.72	137.30	16.10
Tb	159	3.80	0.37	4.13	0.48	104.73	10.20	113.90	13.30
Dy	163	24.39	2.24	27.30	2.35	100.48	9.22	112.48	9.69
Ho	165	4.69	0.50	5.37	0.48	84.30	8.91	96.54	8.65
Er	166	13.54	1.28	15.37	1.49	85.20	8.04	96.70	9.35
Tm	169	1.94	0.30	2.04	0.33	80.28	12.54	84.38	13.60
Yb	172	12.29	1.71	15.04	1.62	75.64	10.53	92.56	9.95
Lu	175	1.94	0.30	2.09	0.30	79.68	12.22	86.17	12.25

Element	Mass	BL-5 (ug g <sup>-1</sup> )				BL-5 (CI Normalised)			
		Glass bead 1		Glass bead 2		Glass bead 1		Glass bead 2	
		Conc.	S.D.	Conc.	S.D.	REE/CI	S.D.	REE/CI	S.D.
La	139	65.12	3.85	56.17	4.22	277.46	16.41	239.34	17.96
Ce	140	205.29	7.84	162.26	7.93	340.33	12.99	269.00	13.14
Pr	141	20.93	1.53	16.48	2.05	234.92	17.17	184.99	23.04
Nd	146	79.44	6.42	67.58	8.72	175.60	14.18	149.39	19.27
Sm	147	18.50	3.98	15.43	3.37	125.74	27.07	104.89	22.94
Eu	153	4.13	0.94	3.08	0.67	73.69	16.83	55.07	12.05
Gd	157	20.93	4.20	15.81	3.74	106.47	21.34	80.42	19.02
Tb	159	2.95	0.61	2.61	0.53	81.23	16.85	71.86	14.70
Dy	163	18.00	3.04	15.05	2.50	74.17	12.53	62.03	10.30
Ho	165	4.07	0.67	3.63	0.71	73.22	12.05	65.32	12.74
Er	166	12.54	2.16	10.36	2.14	78.94	13.61	65.20	13.45
Tm	169	1.74	0.47	1.62	0.47	72.02	19.50	66.75	19.22
Yb	172	11.96	2.32	9.00	2.36	73.60	14.26	55.36	14.51
Lu	175	1.83	0.44	1.36	0.42	75.21	17.91	56.03	17.12

Table D- 6: Uranium Reference Material CUP-2 concentrations and chondrite normalised data for glass beads

Element	Mass	CUP-2 (ug g <sup>-1</sup> )				CUP-2 (CI Normalised)			
		Glass bead 1		Glass bead 2		Glass bead 1		Glass bead 2	
		Conc.	S.D.	Conc.	S.D.	REE/CI	S.D.	REE/CI	S.D.
La	139	42.10	3.72	25.77	2.50	179.38	15.85	109.79	10.63
Ce	140	110.92	5.21	64.46	3.47	183.88	8.64	106.86	5.75
Pr	141	12.21	1.41	6.63	0.68	136.99	15.82	74.46	7.67
Nd	146	44.43	5.44	27.31	4.11	98.22	12.02	60.37	9.08
Sm	147	21.62	5.02	12.80	2.93	146.94	34.11	87.04	19.94
Eu	153	1.83	0.62	1.27	0.37	32.66	11.13	22.71	6.54
Gd	157	37.97	5.96	18.18	3.81	193.15	30.32	92.45	19.36
Tb	159	7.60	0.74	3.91	0.53	209.39	20.35	107.84	14.65
Dy	163	48.18	5.09	27.47	3.92	198.53	20.97	113.20	16.15
Ho	165	8.55	0.97	4.59	0.50	153.79	17.41	82.61	9.00
Er	166	21.92	2.89	13.81	1.91	137.93	18.21	86.89	12.04
Tm	169	2.79	0.60	1.55	0.37	115.48	24.73	64.25	15.21
Yb	172	16.24	2.88	9.46	2.12	99.95	17.69	58.22	13.05
Lu	175	2.13	0.57	1.27	0.32	87.85	23.59	52.11	13.33



**Figure D- 1: The Iridium strip fusion device**

***General setup – Fusion chamber with camera and pyrometer (centre), PSU and temperature gauge (right), laptop for live temperature data and video camera stream (left).***



**Figure D- 2: Wet sample loaded on the iridium strip between the two copper terminals.**

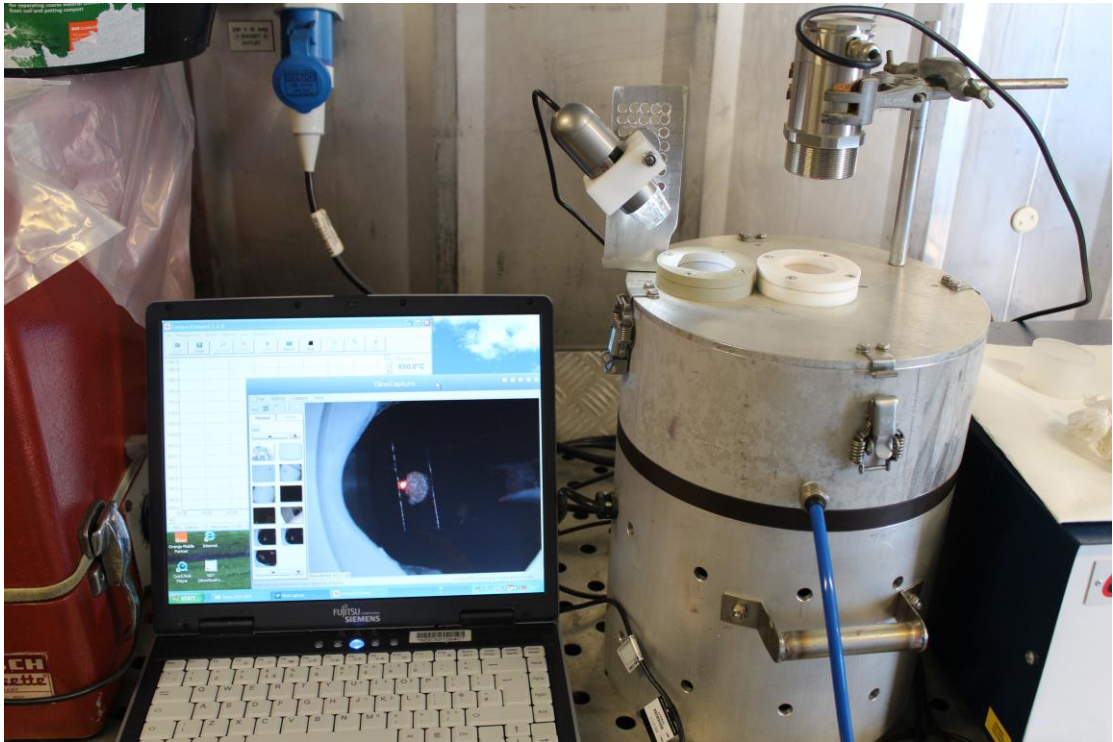


**Figure D- 3: Fused sample on-screen during cooling**

***A fused sample visible on-screen whilst the device is cooling. Red point on-screen is the position of the pyrometer laser.***



## **Appendix E:   Supplementary data and information for Chapter 5**

**Table E- 1: Cumulative recovery or rare earth elements and uranium from TRU™ resin separation scheme**

Cumulative recovery (C/C0)															
Element	Load	Wash 1	Wash 2	Wash 3	Wash 4	REE 1	REE 2	REE 3	REE 4	REE 5	REE 6	REE 7	REE 8	REE 9	REE 10
La	0.14	0.29	0.45	0.62	0.80	0.99	1.19	1.40	1.62	1.86	2.20	8.50	44.53	86.40	96.77
Ce	0.05	0.10	0.15	0.19	0.24	0.29	0.34	0.41	0.47	0.54	0.60	1.02	9.59	47.80	84.80
Pr	0.04	0.08	0.12	0.16	0.22	0.28	0.34	0.40	0.47	0.53	0.61	0.83	6.13	38.19	79.62
Nd	0.03	0.07	0.10	0.14	0.18	0.23	0.27	0.32	0.37	0.42	0.48	0.74	7.40	43.39	83.34
Sm	-	-	-	-	-	-	-	-	-	-	-	0.14	4.70	34.64	76.41
Eu	-	-	-	-	-	-	-	-	-	-	-	0.65	12.32	54.97	88.77
Gd	-	-	-	-	-	0.02	0.04	0.06	0.07	0.09	0.37	12.22	60.95	97.84	99.45
Tb	-	-	-	-	-	-	-	-	-	-	1.24	24.4	74.08	96.50	98.48
Dy	0.03	0.06	0.09	0.12	0.15	0.19	0.22	0.26	0.31	0.42	8.52	57.46	92.64	98.57	98.97
Ho	-	-	0.06	0.11	0.17	0.23	0.28	0.34	0.39	1.97	37.91	89.72	99.02	99.64	99.75
Er	0.03	0.06	0.10	0.13	0.16	0.19	0.23	0.28	0.32	9.21	70.17	97.5	99.37	99.56	99.68
Tm	-	-	-	-	-	-	-	-	-	23.56	87.30	98.66	99.08	99.19	99.19
Yb	0.03	0.06	0.09	0.12	0.14	0.17	0.22	0.26	0.49	39.54	95.02	100.24	100.42	100.50	100.61
Lu	-	-	-	-	-	-	0.08	0.16	1.41	62.92	98.38	99.94	100.02	100.10	100.18
U	-	-	-	-	0.20	0.20	0.20	0.20	0.20	0.30	0.35	0.41	0.46	0.50	0.56

Element	REE 11	REE 12	REE 13	REE 14	U 1	U 2	U 3	U 4	U 5	U 6	U 7	U 8
La	97.91	98.29	98.63	99.04	99.18	99.32	99.52	99.68	99.79	99.88	99.97	100.06
Ce	95.13	96.43	96.65	96.97	98.21	98.34	98.49	98.63	98.78	98.92	99.07	99.23
Pr	94.57	96.74	97.04	97.09	98.68	98.82	98.96	99.11	99.25	99.39	99.55	99.71
Nd	95.42	96.91	97.13	97.21	98.41	98.51	98.61	98.72	98.83	98.95	99.06	99.18
Sm	93.25	95.91	97.00	97.10	98.00	98.00	98.00	98.00	98.00	98.00	98.00	98.00
Eu	96.74	97.61	97.72	97.93	98.59	98.66	98.70	98.81	98.92	99.03	99.13	99.24
Gd	99.45	99.45	99.45	99.45	99.45	99.45	99.45	99.45	99.45	99.45	99.45	99.45
Tb	98.48	98.48	98.48	98.48	98.48	98.48	98.48	98.48	98.48	98.48	98.48	98.48
Dy	99.08	99.16	99.24	99.52	100.24	100.33	100.43	100.52	100.61	100.71	100.80	100.89
Ho	99.86	99.92	99.97	100.04	100.71	100.76	100.82	100.87	100.99	101.10	101.21	101.32
Er	99.76	99.84	99.92	100.12	101.01	101.10	101.20	101.30	101.40	101.49	101.59	101.69
Tm	99.19	99.19	99.19	99.19	99.19	99.19	99.19	99.19	99.19	99.19	99.19	99.19
Yb	100.70	100.77	100.84	100.97	101.83	101.92	102.01	102.09	102.18	102.27	102.37	102.47
Lu	100.25	100.33	100.41	100.61	101.43	101.51	101.58	101.66	101.74	101.82	101.90	101.98
U	0.60	0.65	0.70	0.74	47.83	72.49	90.24	93.36	94.90	96.22	97.57	98.93

Table E- 2: Recovery per fraction of rare earth elements and uranium from TRU™ resin separation scheme

Recovery per fraction (C/C0)															
Element	Load	Wash 1	Wash 2	Wash 3	Wash 4	REE 1	REE 2	REE 3	REE 4	REE 5	REE 6	REE 7	REE 8	REE 9	REE 10
La	0.14	0.15	0.16	0.17	0.18	0.19	0.20	0.21	0.22	0.24	0.34	6.30	36.03	41.87	10.37
Ce	0.05	0.05	0.05	0.04	0.05	0.05	0.05	0.07	0.06	0.07	0.06	0.42	8.57	38.21	37.00
Pr	0.04	0.04	0.04	0.04	0.06	0.06	0.06	0.06	0.07	0.06	0.08	0.22	5.30	32.06	41.43
Nd	0.03	0.04	0.03	0.04	0.04	0.05	0.04	0.05	0.05	0.05	0.06	0.26	6.66	35.99	39.95
Sm	-	-	-	-	-	-	-	-	-	-	-	-	4.56	29.94	41.77
Eu	-	-	-	-	-	-	-	-	-	-	-	-	11.67	42.65	33.80
Gd	-	-	-	-	-	-	0.02	0.02	0.01	0.02	0.28	11.85	48.73	36.89	1.61
Tb	-	-	-	-	-	-	-	-	-	-	-	23.16	49.68	22.42	1.98
Dy	0.03	0.03	0.03	0.03	0.03	0.04	0.03	0.04	0.05	0.11	8.10	48.94	35.18	5.93	0.40
Ho	-	-	-	0.05	0.06	0.06	0.05	0.06	0.05	1.58	35.94	51.81	9.30	0.62	0.11
Er	0.03	0.03	0.04	0.03	0.03	0.03	0.04	0.05	0.04	8.89	60.96	27.33	1.87	0.19	0.12
Tm	-	-	-	-	-	-	-	-	-	-	63.74	11.36	0.42	0.11	
Yb	0.03	0.03	0.03	0.03	0.02	0.03	0.05	0.04	0.23	39.05	55.48	5.22	0.18	0.08	0.11
Lu	-	-	-	-	-	-	-	0.08	1.25	61.51	35.46	1.56	0.08	0.08	0.08
U	-	-	-	-	0.20	-	-	-	-	0.10	0.05	0.06	0.05	0.04	0.06

Element	REE 11	REE 12	REE 13	REE 14	U 1	U 2	U 3	U 4	U 5	U 6	U 7	U 8
La	1.14	0.38	0.34	0.41	0.14	0.14	0.20	0.16	0.11	0.09	0.09	0.09
Ce	10.33	1.30	0.22	0.32	1.24	0.13	0.15	0.14	0.15	0.14	0.15	0.16
Pr	14.95	2.17	0.30	0.05	1.59	0.14	0.14	0.15	0.14	0.14	0.16	0.16
Nd	12.08	1.49	0.22	0.08	1.20	0.10	0.10	0.11	0.11	0.12	0.11	0.12
Sm	16.84	2.66	1.09	0.10	0.90	-	-	-	-	-	-	-
Eu	7.97	0.87	0.11	0.21	0.66	0.07	0.04	0.11	0.11	0.11	0.10	0.11
Gd	-	-	-	-	-	-	-	-	-	-	-	-
Tb	-	-	-	-	-	-	-	-	-	-	-	-
Dy	0.11	0.08	0.08	0.28	0.72	0.09	0.10	0.09	0.09	0.10	0.09	0.09
Ho	0.11	0.06	0.05	0.07	0.67	0.05	0.06	0.05	0.12	0.11	0.11	0.11
Er	0.08	0.08	0.08	0.20	0.89	0.09	0.10	0.10	0.10	0.09	0.10	0.10
Tm	-	-	-	-	-	-	-	-	-	-	-	-
Yb	0.09	0.07	0.07	0.13	0.86	0.09	0.09	0.08	0.09	0.09	0.10	0.10
Lu	0.07	0.08	0.08	0.20	0.82	0.08	0.07	0.08	0.08	0.08	0.08	0.08
U	0.04	0.05	0.05	0.04	47.09	24.66	17.75	3.12	1.54	1.32	1.35	1.36

Table E- 3: Glass bead and solution REE data for UOC Anaconda and Blind River

Anaconda														
Element	Mass	Glass bead 1		Glass bead 2		Solution		Glass bead 1		Glass bead 2		Solution		Varga et al. 2010b
		ppm	S.D.	ppm	S.D.	ppm	S.D.	REE/CI	S.D.	REE/CI	S.D.	REE/CI	S.D.	REE/CI
La	139	6.43	0.30	10.01	0.25	11.17	0.02	27.39	1.29	42.65	1.05	47.60	0.07	39
Ce	140	23.88	2.04	28.73	1.21	31.58	0.06	39.59	3.38	47.63	2.00	52.36	0.10	42
Pr	141	2.34	0.23	3.19	0.12	3.73	0.01	26.23	2.57	35.80	1.35	41.86	0.06	32
Nd	146	9.34	0.70	14.41	1.09	15.73	0.04	20.65	1.54	31.85	2.40	34.76	0.09	30
Sm	147	3.01	0.19	4.19	0.36	4.79	0.01	20.43	1.29	28.52	2.46	32.60	0.09	29
Eu	153	0.85	0.10	1.23	0.14	1.42	0.00	15.19	1.80	21.99	2.48	25.39	0.09	20
Gd	157	4.27	0.18	6.29	0.19	6.93	0.02	21.70	0.91	32.01	0.98	35.25	0.11	30
Tb	159	0.73	0.04	1.11	0.10	1.32	0.00	20.08	0.97	30.56	2.64	36.43	0.06	31
Dy	163	5.00	0.35	7.11	0.55	8.56	0.02	20.60	1.45	29.31	2.26	35.25	0.07	30
Ho	165	1.04	0.09	1.50	0.10	1.63	0.00	18.63	1.64	26.89	1.72	29.38	0.07	25
Er	166	2.86	0.32	4.42	0.33	4.67	0.01	17.98	2.03	27.79	2.07	29.38	0.08	25
Tm	169	0.44	0.07	0.62	0.03	0.65	0.00	18.03	2.72	25.64	1.45	27.03	0.07	23
Yb	172	2.67	0.22	3.88	0.31	4.20	0.01	16.42	1.33	23.90	1.93	25.85	0.03	22
Lu	175	0.34	0.03	0.47	0.06	0.60	0.00	13.80	1.13	19.49	2.47	24.68	0.09	21

Blind River														
Element	Mass	Glass bead 1		Glass bead 2		Solution		Glass bead 1		Glass bead 2		Solution		Varga et al. 2010b
		ppm	S.D.	ppm	S.D.	ppm	S.D.	REE/CI	S.D.	REE/CI	S.D.	REE/CI	S.D.	REE/CI
La	139	3.30	0.15	5.23	0.06	4.37	0.00	14.06	0.62	22.29	0.25	18.61	0.02	18
Ce	140	6.64	0.26	11.94	0.27	8.43	0.01	11.01	0.42	19.80	0.44	13.97	0.01	14
Pr	141	0.79	0.08	1.33	0.08	1.10	0.00	8.84	0.87	14.97	0.90	12.35	0.03	11
Nd	146	3.22	0.15	5.24	0.45	4.61	0.02	7.12	0.34	11.59	0.99	10.20	0.04	10
Sm	147	1.70	0.25	2.78	0.23	2.15	0.01	11.59	1.72	18.87	1.54	14.59	0.05	16
Eu	153	0.15	0.02	0.26	0.05	0.20	0.00	3.18	0.32	4.68	0.81	3.61	0.02	4
Gd	157	2.50	0.29	4.25	0.16	2.83	0.01	12.70	1.50	21.60	0.81	14.38	0.04	15
Tb	159	0.50	0.08	0.78	0.06	0.63	0.00	13.64	2.14	21.47	1.64	17.26	0.07	18
Dy	163	2.81	0.13	4.73	0.32	3.49	0.01	11.60	0.53	19.51	1.34	14.38	0.03	15
Ho	165	0.48	0.05	0.88	0.08	0.59	0.00	8.68	0.89	15.89	1.45	10.55	0.03	11
Er	166	1.14	0.17	2.08	0.17	1.49	0.01	7.19	1.10	13.08	1.06	9.40	0.04	10
Tm	169	0.14	0.02	0.25	0.04	0.17	0.00	6.03	0.81	10.51	1.50	7.19	0.02	8
Yb	172	0.74	0.10	1.30	0.09	0.93	0.00	4.55	0.62	8.01	0.54	5.75	0.03	6
Lu	175	0.03	0.01	0.09	0.01	0.12	0.00	1.58	0.27	3.61	0.48	4.79	0.02	5

Table E- 4: Glass bead and solution REE data for UOC Cotter and Eldorado

Cotter															
Element	Mass	Glass bead 1		Glass bead 2		Solution		Glass bead 1		Glass bead 2		Solution		Varga et al. 2010b	
		ppm	S.D.	ppm	S.D.	ppm	S.D.	REE/CI	S.D.	REE/CI	S.D.	REE/CI	S.D.	REE/CI	
La	139	3.76	0.30	2.26	0.14	4.02	0.01	16.01	0.39	10.41	0.61	17.12	0.02	Not available	
Ce	140	11.48	2.04	7.10	1.08	12.58	0.03	19.03	0.67	12.49	1.79	20.85	0.05		
Pr	141	1.48	0.23	0.94	0.20	1.76	0.00	16.63	1.21	11.46	2.28	19.76	0.05		
Nd	146	7.90	0.70	4.72	0.60	8.96	0.03	17.46	1.37	10.68	1.34	19.80	0.06		
Sm	147	2.31	0.19	1.63	0.32	2.78	0.00	15.70	2.41	12.06	2.17	18.87	0.01		
Eu	153	0.74	0.10	0.47	0.05	0.81	0.00	13.17	1.80	8.79	0.84	14.45	0.01		
Gd	157	3.28	0.18	2.37	0.28	4.16	0.02	16.67	1.33	12.93	1.43	21.17	0.08		
Tb	159	0.89	0.04	0.67	0.15	1.12	0.00	24.41	1.92	19.30	4.00	30.83	0.09		
Dy	163	8.02	0.35	5.93	0.88	10.07	0.03	33.03	1.68	25.85	3.64	41.48	0.11		
Ho	165	2.12	0.09	1.65	0.20	2.66	0.01	38.21	1.25	31.05	3.60	47.86	0.09		
Er	166	8.12	0.32	6.16	1.03	9.72	0.01	51.11	3.12	40.95	6.47	61.16	0.08		
Tm	169	1.59	0.07	1.19	0.19	1.70	0.00	65.89	3.00	52.17	8.06	70.29	0.19		
Yb	172	15.32	0.22	11.63	1.69	13.45	0.04	94.27	4.51	73.76	10.38	82.76	0.25		
Lu	175	2.61	0.03	1.93	0.32	1.97	0.00	107.35	4.49	82.74	13.22	81.23	0.19		

Eldorado															
Element	Mass	Glass bead 1		Glass bead 2		Solution		Glass bead 1		Glass bead 2		Solution		Varga et al. 2010b	
		ppm	S.D.	ppm	S.D.	ppm	S.D.	REE/CI	S.D.	REE/CI	S.D.	REE/CI	S.D.	REE/CI	
La	139	13.91	0.30	6.54	1.97	13.54	0.03	63.24	1.61	34.60	8.41	57.71	0.11	48	
Ce	140	40.70	2.04	23.26	10.80	38.09	0.10	75.17	4.11	48.21	17.90	63.15	0.17	50	
Pr	141	5.60	0.23	3.02	1.17	5.62	0.02	69.17	2.82	41.93	13.14	63.13	0.18	50	
Nd	146	25.73	0.70	13.56	4.85	26.79	0.10	61.47	5.51	37.16	10.72	59.22	0.22	49	
Sm	147	16.65	0.19	9.27	2.86	16.62	0.04	121.73	9.57	79.01	19.41	112.98	0.28	95	
Eu	153	1.66	0.10	0.84	0.17	1.70	0.01	31.28	1.90	18.57	2.96	30.36	0.11	24	
Gd	157	32.29	0.18	17.80	3.90	31.64	0.05	178.26	9.10	112.96	19.83	160.91	0.24	110	
Tb	159	7.19	0.04	3.97	0.92	9.03	0.01	213.13	17.39	135.27	25.22	248.68	0.20	170	
Dy	163	47.94	0.35	27.22	5.83	62.13	0.05	212.42	12.56	138.42	24.01	255.99	0.20	175	
Ho	165	9.40	0.09	5.23	1.05	10.57	0.02	180.09	13.33	115.82	18.92	190.17	0.38	130	
Er	166	24.96	0.32	14.32	2.94	30.22	0.06	167.80	10.44	111.28	18.49	190.17	0.41	130	
Tm	169	3.23	0.07	1.90	0.37	3.72	0.01	144.14	9.48	95.06	15.26	153.60	0.42	105	
Yb	172	19.69	0.22	10.96	1.64	23.77	0.13	129.92	11.90	82.79	10.08	146.28	0.82	100	
Lu	175	2.27	0.03	1.22	0.27	2.84	0.01	100.64	7.66	62.25	11.03	117.03	0.24	80	

Table E- 5: Glass bead and solution REE data for UOC Faraday and Gunnar

Faraday		Glass bead 1		Glass bead 2		Solution		Glass bead 1		Glass bead 2		Solution		Varga et al. 2010b
Element	Mass	ppm	S.D.	ppm	S.D.	ppm	S.D.	REE/CI	S.D.	REE/CI	S.D.	REE/CI	S.D.	REE/CI
La	139	57.68	0.30	44.24	0.66	46.23	0.11	245.76	2.05	188.51	2.80	196.97	0.47	190
Ce	140	122.96	2.04	89.13	0.93	92.33	0.26	203.85	3.98	147.77	1.54	153.06	0.42	160
Pr	141	9.81	0.23	7.67	0.40	7.87	0.01	110.08	2.40	86.04	4.49	88.38	0.13	80
Nd	146	27.28	0.70	21.76	0.67	22.13	0.05	60.29	1.83	48.11	1.48	48.92	0.12	40
Sm	147	4.55	0.19	3.46	0.37	3.49	0.02	30.92	2.72	23.54	2.52	23.69	0.16	20
Eu	153	0.82	0.10	0.75	0.10	0.63	0.01	14.58	1.22	13.45	1.73	11.25	0.14	12
Gd	157	3.96	0.18	2.73	0.33	2.72	0.03	20.15	1.46	13.86	1.65	13.81	0.14	18
Tb	159	0.78	0.04	0.58	0.10	0.47	0.00	21.58	1.48	16.08	2.75	13.04	0.05	17
Dy	163	5.48	0.35	3.92	0.43	3.17	0.01	22.58	1.21	16.17	1.76	13.04	0.04	17
Ho	165	1.28	0.09	0.95	0.05	0.73	0.01	23.00	1.53	17.16	0.98	13.04	0.10	17
Er	166	4.45	0.32	3.37	0.20	2.44	0.02	28.01	1.32	21.19	1.23	15.34	0.10	20
Tm	169	0.78	0.07	0.58	0.04	0.39	0.00	32.09	1.96	24.15	1.71	16.11	0.10	21
Yb	172	5.83	0.22	4.55	0.29	2.74	0.02	35.87	1.72	27.97	1.76	16.88	0.11	22
Lu	175	0.68	0.03	0.52	0.07	0.37	0.00	28.12	1.83	21.47	2.82	15.34	0.12	20

Gunnar		Glass bead 1		Glass bead 2		Solution		Glass bead 1		Glass bead 2		Solution		Varga et al. 2010b
Element	Mass	ppm	S.D.	ppm	S.D.	ppm	S.D.	REE/CI	S.D.	REE/CI	S.D.	REE/CI	S.D.	REE/CI
La	139	17.21	0.30	15.13	0.21	10.87	0.02	73.31	0.88	64.47	0.88	46.32	0.10	Not available
Ce	140	60.31	2.04	53.49	1.37	36.82	0.14	99.99	2.28	88.68	2.28	61.03	0.24	
Pr	141	8.92	0.23	8.01	0.37	5.18	0.01	100.10	4.20	89.90	4.20	58.08	0.16	
Nd	146	38.23	0.70	34.35	1.30	22.30	0.06	84.50	2.87	75.94	2.87	49.29	0.13	
Sm	147	11.91	0.19	10.77	0.54	6.78	0.00	80.97	3.66	73.21	3.66	46.08	0.02	
Eu	153	1.10	0.10	0.89	0.18	0.62	0.00	19.62	3.16	15.89	3.16	11.16	0.03	
Gd	157	15.65	0.18	13.35	0.81	9.67	0.02	79.63	4.11	67.90	4.11	49.21	0.10	
Tb	159	2.59	0.04	2.31	0.13	1.65	0.00	71.24	3.54	63.75	3.54	45.43	0.09	
Dy	163	16.25	0.35	14.24	0.80	10.07	0.03	66.96	3.31	58.67	3.31	41.48	0.12	
Ho	165	3.17	0.09	2.76	0.14	1.99	0.00	56.95	2.56	49.62	2.56	35.77	0.03	
Er	166	9.02	0.32	7.83	0.39	5.51	0.02	56.77	2.44	49.29	2.44	34.68	0.09	
Tm	169	1.26	0.07	1.07	0.12	0.74	0.00	52.06	4.91	44.13	4.91	30.74	0.06	
Yb	172	8.31	0.22	7.21	0.65	4.41	0.01	51.16	3.99	44.36	3.99	27.14	0.04	
Lu	175	1.09	0.03	0.89	0.10	0.59	0.00	44.71	3.98	36.63	3.98	24.20	0.07	

Table E- 6: Glass bead and solution REE data for UOC Madawaska and North Span

Madawaska															
Element	Mass	Glass bead 1		Glass bead 2		Solution		Glass bead 1		Glass bead 2		Solution		Varga et al. 2010b	
		ppm	S.D.	ppm	S.D.	ppm	S.D.	REE/CI	S.D.	REE/CI	S.D.	REE/CI	S.D.	REE/CI	
La	139	52.13	0.30	45.04	0.86	42.71	0.10	222.11	3.92	191.92	3.65	181.98	0.44	190	
Ce	140	111.90	2.04	97.16	5.44	73.72	0.07	185.51	4.06	161.07	9.03	122.22	0.12	150	
Pr	141	9.16	0.23	7.93	0.43	6.63	0.01	102.80	3.46	89.01	4.79	74.35	0.12	80	
Nd	146	29.23	0.70	25.63	0.96	22.07	0.06	64.62	2.80	56.65	2.13	48.77	0.14	40	
Sm	147	7.46	0.19	6.18	0.59	4.00	0.01	50.68	4.29	42.00	4.04	27.19	0.08	35	
Eu	153	1.38	0.10	1.20	0.06	0.74	0.00	24.60	0.95	21.44	1.15	13.21	0.04	20	
Gd	157	7.19	0.18	6.74	0.48	3.19	0.01	36.57	2.76	34.26	2.43	16.25	0.07	30	
Tb	159	1.40	0.04	1.24	0.07	0.59	0.00	38.53	1.97	34.11	2.02	16.25	0.09	30	
Dy	163	9.97	0.35	8.32	0.56	3.94	0.02	41.08	1.67	34.30	2.30	16.25	0.09	30	
Ho	165	2.21	0.09	1.98	0.11	0.90	0.00	39.73	2.18	35.67	1.98	16.25	0.03	30	
Er	166	6.80	0.32	6.16	0.44	3.01	0.01	42.81	1.99	38.74	2.75	18.96	0.09	35	
Tm	169	1.03	0.07	0.92	0.08	0.45	0.00	42.42	4.20	37.81	3.16	18.42	0.09	34	
Yb	172	6.80	0.22	5.79	0.42	2.99	0.02	41.83	3.48	35.62	2.58	18.42	0.11	34	
Lu	175	0.78	0.03	0.73	0.06	0.39	0.00	31.94	2.29	30.02	2.29	16.25	0.12	30	
North Span															
Element	Mass	Glass bead 1		Glass bead 2		Solution		Glass bead 1		Glass bead 2		Solution		Varga et al. 2010b	
		ppm	S.D.	ppm	S.D.	ppm	S.D.	REE/CI	S.D.	REE/CI	S.D.	REE/CI	S.D.	REE/CI	
La	139	4.77	0.30	4.20	0.16	4.12	0.01	20.34	0.44	17.88	0.70	17.55	0.06	Not Available	
Ce	140	10.85	2.04	10.12	0.94	9.14	0.01	17.98	0.38	16.78	1.55	15.15	0.02		
Pr	141	1.14	0.23	1.05	0.06	1.04	0.00	12.74	1.12	11.77	0.71	11.66	0.01		
Nd	146	4.52	0.70	3.88	0.37	4.29	0.01	10.00	0.87	8.58	0.82	9.49	0.02		
Sm	147	2.83	0.19	2.15	0.18	2.39	0.01	19.22	2.01	14.60	1.25	16.26	0.08		
Eu	153	0.24	0.10	0.21	0.03	0.23	0.00	4.64	0.57	3.34	0.49	4.04	0.01		
Gd	157	4.60	0.18	4.25	0.34	3.99	0.01	23.42	1.93	21.64	1.75	20.31	0.04		
Tb	159	1.10	0.04	0.88	0.07	0.85	0.00	30.28	2.86	24.27	1.84	23.28	0.03		
Dy	163	6.55	0.35	5.65	0.27	5.12	0.01	26.98	2.07	23.29	1.13	21.11	0.03		
Ho	165	1.19	0.09	0.98	0.12	0.85	0.00	21.41	1.39	17.69	2.23	15.34	0.06		
Er	166	3.01	0.32	2.52	0.21	2.03	0.00	18.96	1.93	15.87	1.29	12.77	0.03		
Tm	169	0.38	0.07	0.31	0.03	0.24	0.00	15.59	1.13	12.78	1.23	9.75	0.02		
Yb	172	2.18	0.22	1.80	0.22	1.27	0.00	13.43	1.15	11.11	1.32	7.78	0.01		
Lu	175	0.19	0.03	0.16	0.02	0.14	0.00	7.76	1.13	6.59	0.70	5.60	0.03		

Table E- 7: Glass bead and solution REE data for UOC Ranger and Rio Algom

Ranger		Glass bead 1		Glass bead 2		Solution		Glass bead 1		Glass bead 2		Solution		Varga et al. 2010b
Element	Mass	ppm	S.D.	ppm	S.D.	ppm	S.D.	REE/CI	S.D.	REE/CI	S.D.	REE/CI	S.D.	REE/CI
La	139	0.45	0.30	1.21	0.54	0.11	0.00	1.90	0.34	5.17	2.30	0.48	0.00	1.80 & 0.59
Ce	140	0.92	2.04	1.60	0.51	0.33	0.00	1.53	0.49	2.65	0.84	0.54	0.00	0.35 & 0.58
Pr	141	0.06	0.23	0.10	0.04	0.05	0.00	0.62	0.28	1.14	0.41	0.56	0.00	0.78 & 0.57
Nd	146	0.27	0.70	0.50	0.16	0.26	0.00	0.60	0.10	1.10	0.35	0.58	0.01	1.00 & 0.58
Sm	147	0.16	0.19	0.18	0.09	0.12	0.00	1.12	0.70	1.24	0.59	0.80	0.01	3.10 & 0.85
Eu	153	0.05	0.10	0.07	0.02	0.04	0.00	0.88	0.38	1.16	0.30	0.75	0.01	3.00 & 0.80
Gd	157	0.23	0.18	0.25	0.11	0.16	0.00	1.20	0.44	1.26	0.54	0.83	0.01	3.00 & 0.85
Tb	159	0.04	0.04	0.04	0.01	0.02	0.00	1.19	0.87	0.97	0.30	0.69	0.01	3.50 & 0.70
Dy	163	0.27	0.35	0.23	0.06	0.14	0.00	1.11	0.80	0.94	0.26	0.59	0.00	3.10 & 0.60
Ho	165	0.06	0.09	0.05	0.03	0.02	0.00	1.06	0.80	0.85	0.51	0.41	0.00	2.20 & 0.42
Er	166	0.18	0.32	0.10	0.05	0.06	0.00	1.12	0.75	0.65	0.33	0.39	0.00	2.10 & 0.40
Tm	169	0.03	0.07	0.01	0.01	0.01	0.00	1.42	0.75	0.49	0.29	0.31	0.01	1.90 & 0.32
Yb	172	0.18	0.22	0.09	0.05	0.05	0.00	1.12	0.75	0.54	0.30	0.29	0.01	1.80 & 0.30
Lu	175	0.01	0.03	0.01	0.01	0.01	0.00	1.16	0.75	0.52	0.30	0.25	0.01	1.20 & 0.25

Rio Algom		Glass bead 1		Glass bead 2		Solution		Glass bead 1		Glass bead 2		Solution		Varga et al. 2010b
Element	Mass	ppm	S.D.	ppm	S.D.	ppm	S.D.	REE/CI	S.D.	REE/CI	S.D.	REE/CI	S.D.	REE/CI
La	139	53.11	0.30	85.78	0.08	78.31	0.06	253.66	5.51	365.49	0.33	333.66	0.28	260
Ce	140	110.81	2.04	188.92	0.66	154.68	0.06	204.92	8.85	313.19	1.10	256.42	0.10	180
Pr	141	12.81	0.23	20.78	0.01	18.03	0.02	160.58	5.09	233.19	0.10	202.30	0.24	150
Nd	146	52.34	0.70	84.09	0.27	74.98	0.22	128.44	7.35	185.87	0.59	165.75	0.49	115
Sm	147	26.25	0.19	41.42	0.07	35.53	0.09	198.71	8.17	281.58	0.47	241.50	0.63	185
Eu	153	2.10	0.10	3.41	0.00	3.32	0.00	41.80	2.80	60.84	0.01	59.29	0.05	40
Gd	157	48.05	0.18	78.31	0.18	65.02	0.06	272.92	18.36	398.31	0.90	330.72	0.32	210
Tb	159	10.07	0.04	16.17	0.01	13.40	0.02	309.86	14.32	445.46	0.17	369.01	0.43	270
Dy	163	63.49	0.35	101.76	0.23	83.28	0.14	291.41	12.00	419.30	0.96	343.14	0.56	260
Ho	165	12.07	0.09	19.45	0.01	15.16	0.02	241.54	14.04	349.89	0.15	272.66	0.34	220
Er	166	31.90	0.32	51.08	0.07	39.17	0.04	225.21	11.26	321.47	0.46	246.54	0.28	200
Tm	169	4.07	0.07	6.49	0.00	5.01	0.00	186.75	8.87	268.07	0.07	206.82	0.09	160
Yb	172	23.74	0.22	39.09	0.05	28.19	0.05	164.53	9.26	240.58	0.28	173.48	0.31	150
Lu	175	2.98	0.03	4.81	0.00	3.26	0.01	135.12	5.21	197.81	0.03	134.16	0.54	110

Table E- 8: Solution REE data for UOC Mary Kathleen, Olympic Dam and Rabbit Lake

Mary Kathleen						
Element	Mass	Solution		Solution		Varga et al. 2010b
		ppm	S.D.	REE/CI	S.D.	REE/CI
La	139	17.9020	0.0393	76.2761	0.1674	85.00
Ce	140	31.1650	0.0773	51.6661	0.1281	55.00
Pr	141	2.3160	0.0039	25.9933	0.0437	30.00
Nd	146	5.5170	0.0044	12.1950	0.0097	15.00
Sm	147	0.3390	0.0005	2.3046	0.0036	3.00
Eu	153	0.0320	0.0002	0.5714	0.0042	0.65
Gd	157	0.1060	0.0019	0.5392	0.0098	3.50
Tb	159	0.0196	0.0003	0.5392	0.0079	1.00
Dy	163	0.1309	0.0022	0.5392	0.0090	0.55
Ho	165	0.0300	0.0004	0.5392	0.0081	0.16
Er	166	0.1000	0.0020	0.6290	0.0126	0.30
Tm	169	0.0148	0.0008	0.6111	0.0314	0.11
Yb	172	0.0993	0.0023	0.6111	0.0139	18.00
Lu	175	0.0131	0.0006	0.5392	0.0247	0.08

Olympic Dam						
Element	Mass	Solution		Solution		Varga et al. 2010b
		ppm	S.D.	REE/CI	S.D.	REE/CI
La	139	1.5370	0.0044	6.5488	0.0186	9.00
Ce	140	2.9570	0.0053	4.9022	0.0088	5.50
Pr	141	0.4080	0.0010	4.5791	0.0109	4.50
Nd	146	1.4470	0.0063	3.1985	0.0139	3.00
Sm	147	0.3060	0.0027	2.0802	0.0184	2.00
Eu	153	0.1030	0.0003	1.8393	0.0055	1.90
Gd	157	0.2610	0.0027	1.3276	0.0136	1.80
Tb	159	0.0375	0.0004	1.0326	0.0116	1.40
Dy	163	0.2148	0.0017	0.8850	0.0069	1.20
Ho	165	0.0451	0.0002	0.8113	0.0044	1.10
Er	166	0.1406	0.0007	0.8850	0.0042	1.20
Tm	169	0.0214	0.0005	0.8850	0.0192	1.20
Yb	172	0.1558	0.0014	0.9588	0.0084	1.30
Lu	175	0.0215	0.0005	0.8850	0.0188	1.20

Rabbit Lake						
Element	Mass	Solution		Solution		Varga et al. 2010b
		ppm	S.D.	REE/CI	S.D.	REE/CI
La	139	0.2350	0.0011	1.0013	0.0048	1.20 & 0.85
Ce	140	0.3900	0.0018	0.6466	0.0030	0.58 & 0.60
Pr	141	0.0490	0.0006	0.5499	0.0065	0.42 & 0.50
Nd	146	0.1830	0.0028	0.4045	0.0062	0.35 & 0.38
Sm	147	0.0360	0.0007	0.2447	0.0045	0.25 & 0.30
Eu	153	0.0080	0.0001	0.1429	0.0023	0.20 & 0.23
Gd	157	0.0290	0.0006	0.1475	0.0030	0.25 & 0.30
Tb	159	0.0058	0.0002	0.1593	0.0057	0.27 & 0.40
Dy	163	0.0358	0.0009	0.1475	0.0036	0.25 & 0.42
Ho	165	0.0072	0.0001	0.1298	0.0018	0.22 & 0.40
Er	166	0.0216	0.0006	0.1357	0.0035	0.23 & 0.42
Tm	169	0.0033	0.0001	0.1357	0.0055	0.23 & 0.43
Yb	172	0.0278	0.0005	0.1711	0.0031	0.29 & 1.20
Lu	175	0.0037	0.0002	0.1534	0.0066	0.26 & 0.43

Table E- 9: Solution REE data for UOC South Alligator, Chevron Hill and Lucky McGill

South Alligator						
Element	Mass	Solution		Solution		Varga et al. 2010b
		ppm	S.D.	REE/Cl	S.D.	REE/Cl
La	139	0.9200	0.0025	3.9199	0.0109	2.10
Ce	140	1.0310	0.0049	1.7092	0.0082	1.20
Pr	141	0.2950	0.0012	3.3109	0.0134	2.40
Nd	146	1.3590	0.0014	3.0040	0.0032	2.30
Sm	147	0.3860	0.0007	2.6241	0.0046	2.10
Eu	153	0.1250	0.0002	2.2321	0.0043	1.90
Gd	157	0.6680	0.0027	3.3978	0.0137	3.00
Tb	159	0.1586	0.0006	4.3686	0.0153	3.50
Dy	163	1.0210	0.0064	4.2068	0.0263	3.40
Ho	165	0.1979	0.0004	3.5596	0.0073	2.70
Er	166	0.5142	0.0025	3.2360	0.0155	2.30
Tm	169	0.0626	0.0005	2.5888	0.0210	1.90
Yb	172	0.3944	0.0024	2.4270	0.0149	1.80
Lu	175	0.0432	0.0008	1.7798	0.0332	1.40

Chevron Hill					
Element	Mass	Solution		Solution	
		ppm	S.D.	REE/Cl	S.D.
La	139	1.2300	0.0026	5.2407	0.0112
Ce	140	3.1160	0.0145	5.1658	0.0240
Pr	141	0.3440	0.0013	3.8608	0.0140
Nd	146	1.3040	0.0041	2.8824	0.0090
Sm	147	0.2690	0.0012	1.8287	0.0080
Eu	153	0.0400	0.0002	0.7143	0.0041
Gd	157	0.2550	0.0013	1.2971	0.0064
Tb	159	0.0370	0.0001	1.0193	0.0026
Dy	163	0.1940	0.0013	0.7993	0.0055
Ho	165	0.0330	0.0002	0.5935	0.0039
Er	166	0.0760	0.0007	0.4783	0.0042
Tm	169	0.0090	0.0001	0.3719	0.0031
Yb	172	0.0460	0.0007	0.2831	0.0046
Lu	175	0.0060	0.0001	0.2469	0.0055

Lucky McGill					
Element	Mass	Solution		Solution	
		ppm	S.D.	REE/Cl	S.D.
La	139	0.1680	0.0005	0.7158	0.0020
Ce	140	0.3870	0.0009	0.6416	0.0014
Pr	141	0.0450	0.0003	0.5051	0.0038
Nd	146	0.1670	0.0025	0.3691	0.0056
Sm	147	0.0390	0.0007	0.2651	0.0049
Eu	153	0.0070	0.0002	0.1250	0.0032
Gd	157	0.0350	0.0016	0.1780	0.0079
Tb	159	0.0050	0.0001	0.1377	0.0015
Dy	163	0.0250	0.0004	0.1030	0.0017
Ho	165	0.0040	0.0000	0.0719	0.0008
Er	166	0.0090	0.0001	0.0566	0.0009
Tm	169	0.0010	0.0000	0.0413	0.0009
Yb	172	0.0040	0.0001	0.0246	0.0003
Lu	175	0.0010	0.0000	0.0412	0.0010

Table E- 10: Solution REE data for Mesa EFI, Mulberry and Queensland

Mesa EFI					
Element	Mass	Solution		Solution	
		ppm	S.D.	REE/Cl	S.D.
La	139	2.3250	0.0074	9.9063	0.0317
Ce	140	4.4790	0.0112	7.4254	0.0185
Pr	141	0.5730	0.0010	6.4310	0.0108
Nd	146	2.0730	0.0038	4.5822	0.0084
Sm	147	0.4180	0.0031	2.8416	0.0208
Eu	153	0.1030	0.0011	1.8393	0.0205
Gd	157	0.3690	0.0012	1.8769	0.0063
Tb	159	0.0470	0.0003	1.2948	0.0081
Dy	163	0.2350	0.0022	0.9683	0.0091
Ho	165	0.0380	0.0004	0.6835	0.0074
Er	166	0.0850	0.0008	0.5349	0.0049
Tm	169	0.0090	0.0000	0.3719	0.0020
Yb	172	0.0400	0.0003	0.2462	0.0017
Lu	175	0.0050	0.0001	0.2058	0.0022

Mulberry					
Element	Mass	Solution		Solution	
		ppm	S.D.	REE/Cl	S.D.
La	139	0.0250	0.0003	0.1065	0.0011
Ce	140	0.0510	0.0004	0.0845	0.0006
Pr	141	0.0040	0.0000	0.0449	0.0005
Nd	146	0.0170	0.0001	0.0376	0.0003
Sm	147	0.0030	0.0001	0.0204	0.0008
Eu	153	0.0017	0.0001	0.0300	0.0012
Gd	157	0.0040	0.0000	0.0203	0.0002
Tb	159	0.0010	0.0000	0.0275	0.0012
Dy	163	0.0140	0.0003	0.0577	0.0014
Ho	165	0.0060	0.0002	0.1079	0.0035
Er	166	0.0430	0.0004	0.2706	0.0025
Tm	169	0.0190	0.0004	0.7851	0.0154
Yb	172	0.3180	0.0013	1.9569	0.0081
Lu	175	0.0740	0.0003	3.0453	0.0103

Queensland					
Element	Mass	Solution		Solution	
		ppm	S.D.	REE/Cl	S.D.
La	139	0.0600	0.0003	0.2556	0.0012
Ce	140	0.2300	0.0010	0.3813	0.0017
Pr	141	0.0650	0.0005	0.7295	0.0051
Nd	146	0.4270	0.0016	0.9439	0.0035
Sm	147	0.2800	0.0011	1.9035	0.0076
Eu	153	0.0790	0.0007	1.4107	0.0118
Gd	157	0.3720	0.0029	1.8922	0.0149
Tb	159	0.0820	0.0005	2.2590	0.0136
Dy	163	0.4410	0.0019	1.8171	0.0078
Ho	165	0.0610	0.0003	1.0971	0.0063
Er	166	0.1250	0.0007	0.7867	0.0042
Tm	169	0.0140	0.0002	0.5785	0.0099
Yb	172	0.0660	0.0008	0.4062	0.0050
Lu	175	0.0060	0.0001	0.2469	0.0039



## **Appendix F: SEM images and elemental mapping of UOCs**

Scanning Electron Microscopy was used to obtain Backscatter Electron (BSE) and Electron Dispersive X-ray (EDX) data for the 19 UOCs. The data was collected at the National Nuclear Laboratory, Springfields, UK using an FEI Quanta 200F with a field emission gun at 1.25 nm resolution. EDX spectra were collected using a silicon drift detector (150 mm<sup>2</sup>). Spectra was analysed using AZtecEnergy (Oxford Instruments).

**Table F- 1: General interpretation of UOC using BSE and EDX**

<b>Sample Name</b>	<b>Morphology</b>	<b>Minor Elements</b>
<b>Anaconda</b>	Granular, some acicular surface texture	C, N, Na, Mg, Al, Si, S
<b>Blind River</b>	Granular, with assoc. acicular/platelet structured material	C, Na, Mg, Al, Si, S, Ca, Fe
<b>Chevron Hill</b>	Platelet morphology forming rounded agglomerates with covering of fine material	C, Al, S
<b>Cotter</b>	Granular, with assoc. acicular/platelet structured material	C, Na, Mg, Al, Si, S, Fe
<b>Eldorado</b>	Granular, irregular	C, N Al, Si, S, Fe
<b>Faraday</b>	Not clear	C, Na, Mg, Al, Si, S, P, Fe
<b>Gunnar</b>	Not clear	C, Na, Mg, Al, Si, Fe
<b>Lucky McGill</b>	Platelet morphology forming rounded agglomerates	C, Al, S
<b>Madawaska</b>	Granular, frequent platelet/acicular structured material	C, Na, Mg, Al, Si, S, P, Ca, Fe
<b>Mary Kathleen</b>	Not clear	C, S
<b>Mesa EFI</b>	Large agglomerates containing fine acicular/platelet structured material	C, Ma, Al, Si, P, S, Ca
<b>Mulberry</b>	Large agglomerates, some spherical, containing blocky/platelet structure material	C
<b>North Span</b>	Granular, assoc. acicular/platelet structured material	C, Na, Al, Si, S, Ca

Sample Name	Morphology	Minor Elements
Olympic Dam	Granular comprising of clusters of predominantly cubic crystallites	C, S
Queensland	Granular comprising of clusters of predominantly nodular crystallites	C, Al
Rabbit Lake	Acicular morphology forming rounded agglomerates with covering of fines	C, Al, Si, S
Ranger	Granular, with predominantly blocky morphology	C, Na, S
Rio Algom	Granular, with assoc. fine acicular/platelet structured material	C, Mg, Al, Si, S, Ca
South Alligator	Granular, with small rounded agglomerates of platelet structured material	C, Na, Mg, Al, Si, S

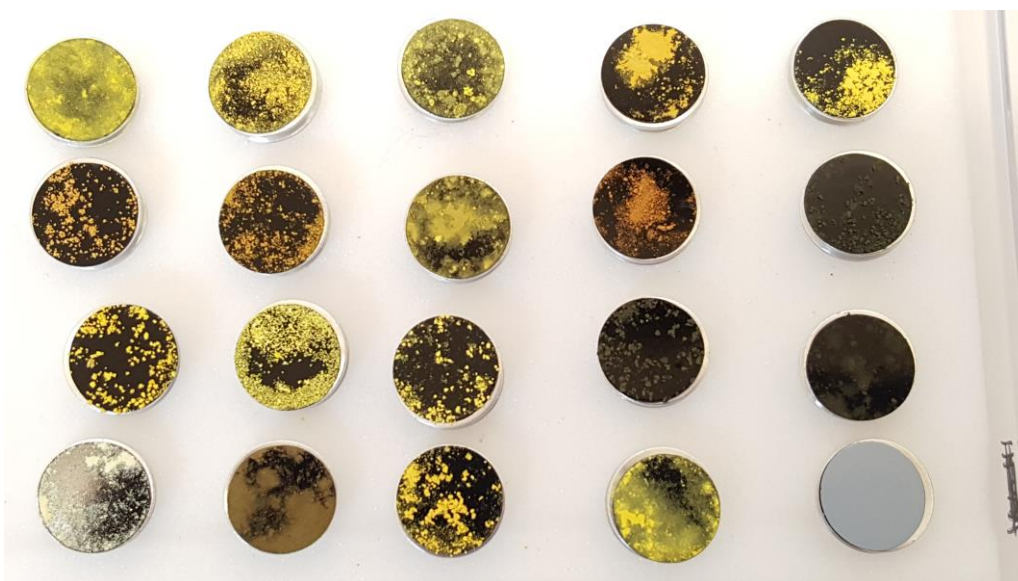


**Figure F- 1: The UOCs loaded on SEM stubs with carbon coated adhesive tabs.**

***The stubs are organised alphabetically from left to right and then top to bottom. The bottom right stub is blank.***

The BSE images for each UOC at varying magnification are presented here. The false colour elemental mapping of all UOCs is available on the enclosed CD-ROM due to loss of colour quality during printing.

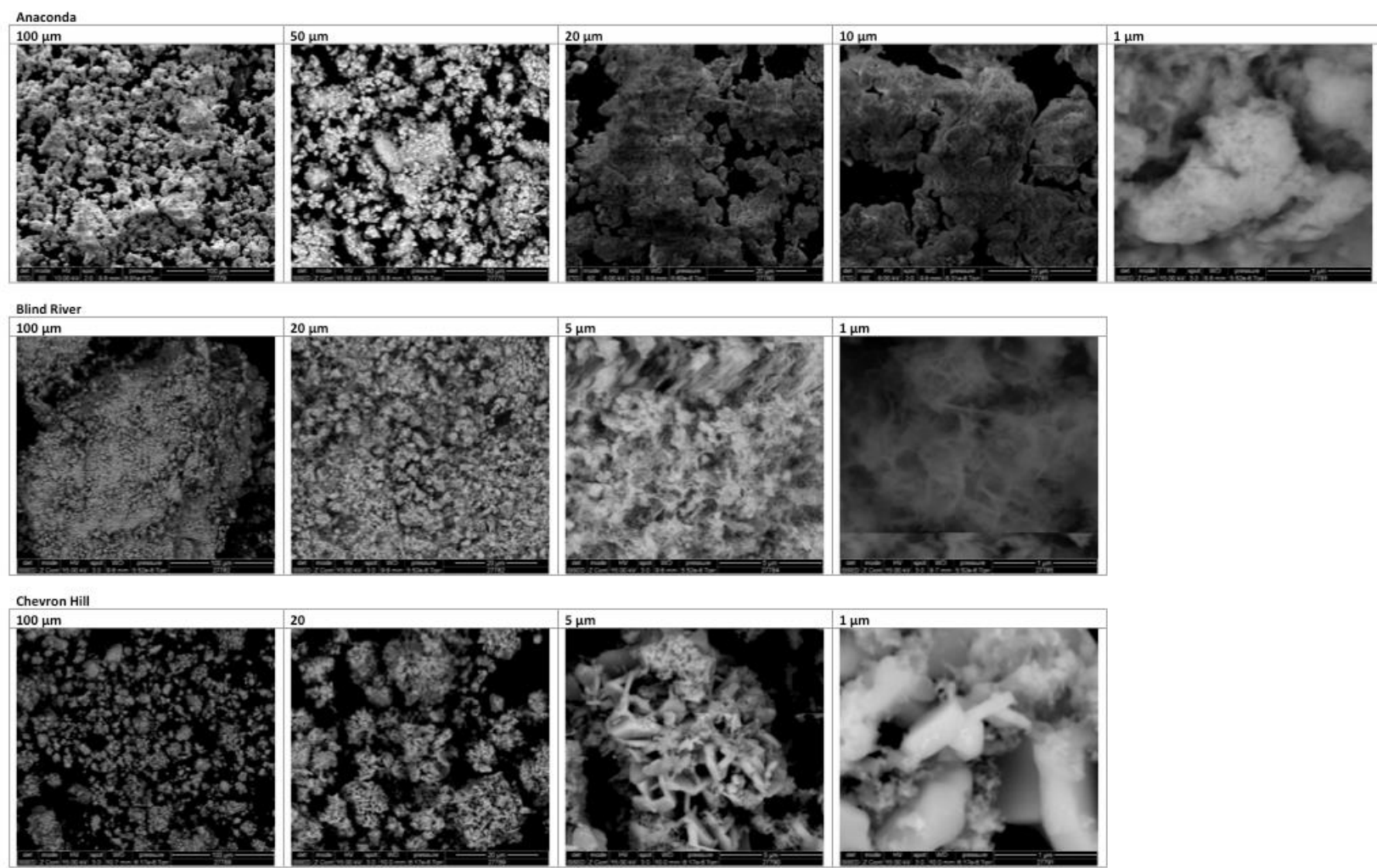
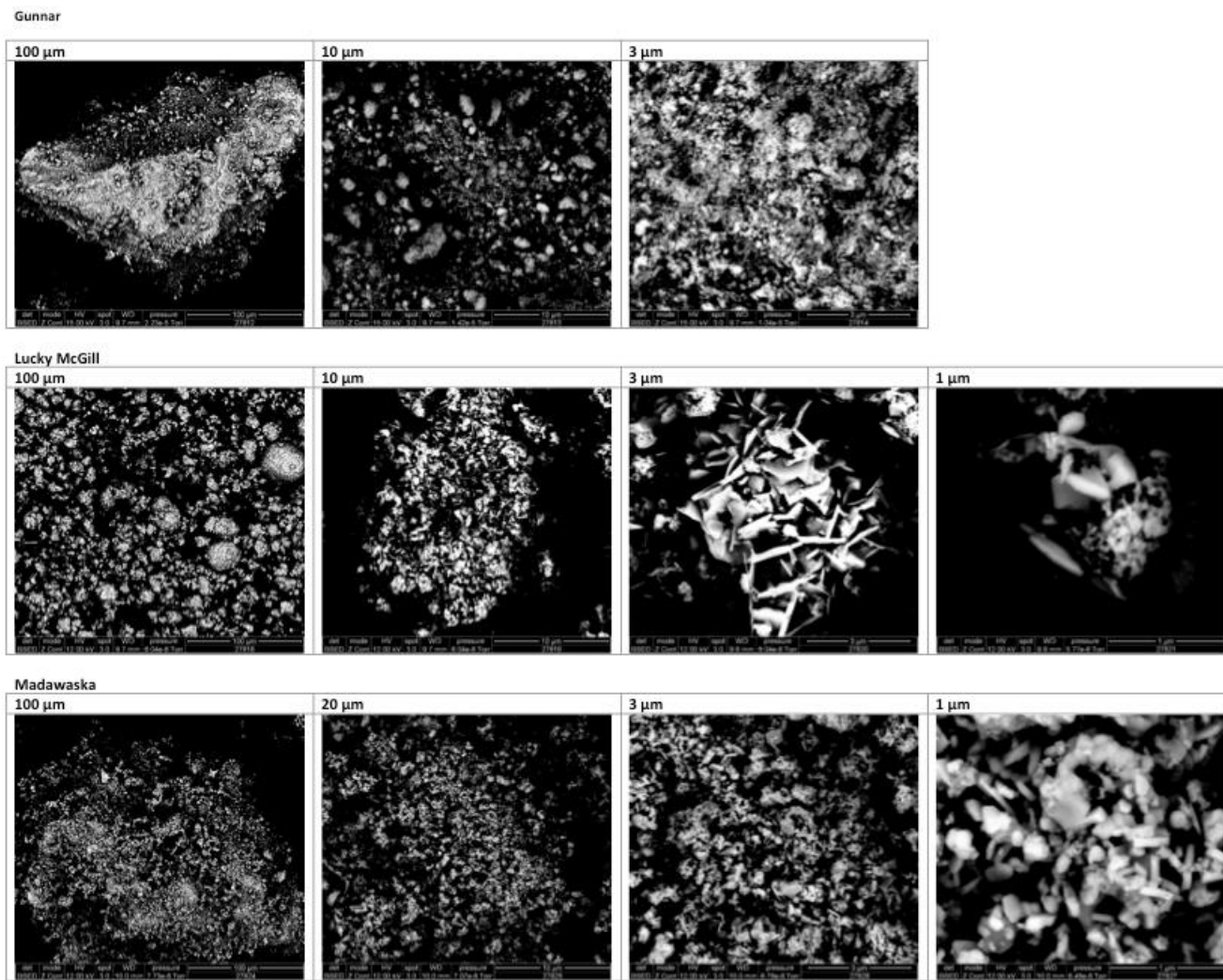


Figure F- 2: SEM BSE Images of UOCs Anaconda, Blind River and Chevron Hill

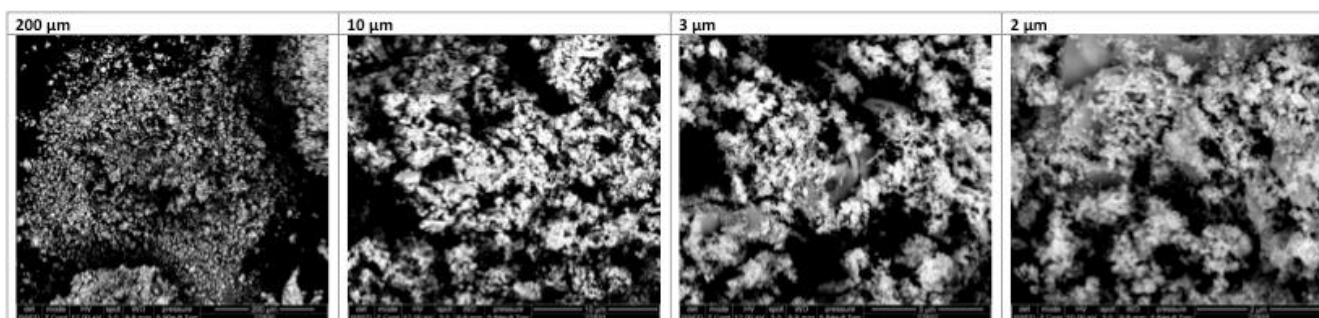


## Appendix F

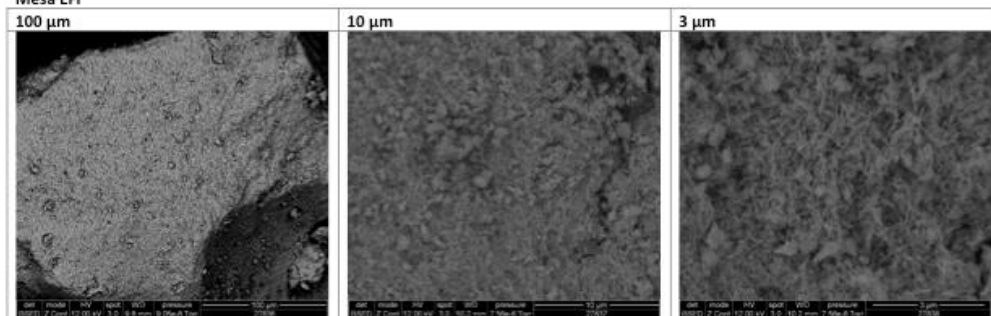


**Figure F- 4: SEM BSE Images of UOCs Gunnar, Lucky McGill and Madawaska**

Mary Kathleen



Mesa EFI



Mulberry

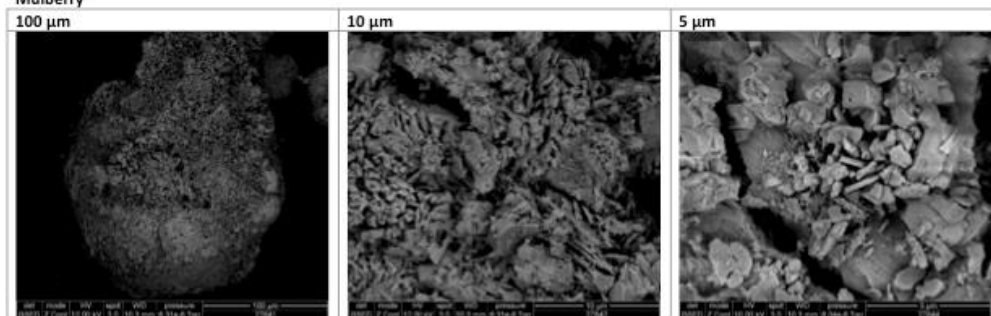
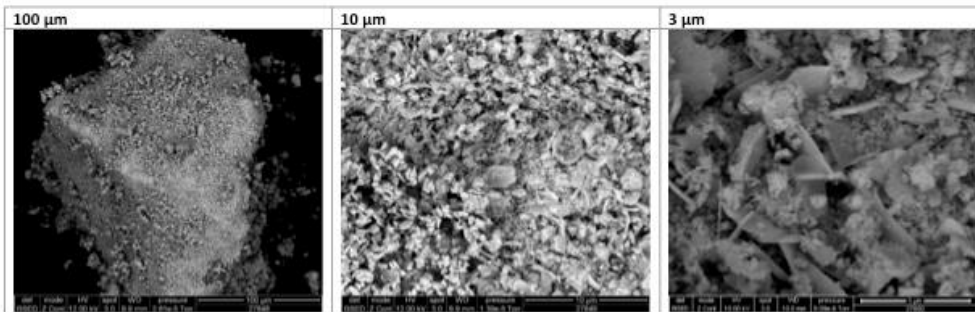


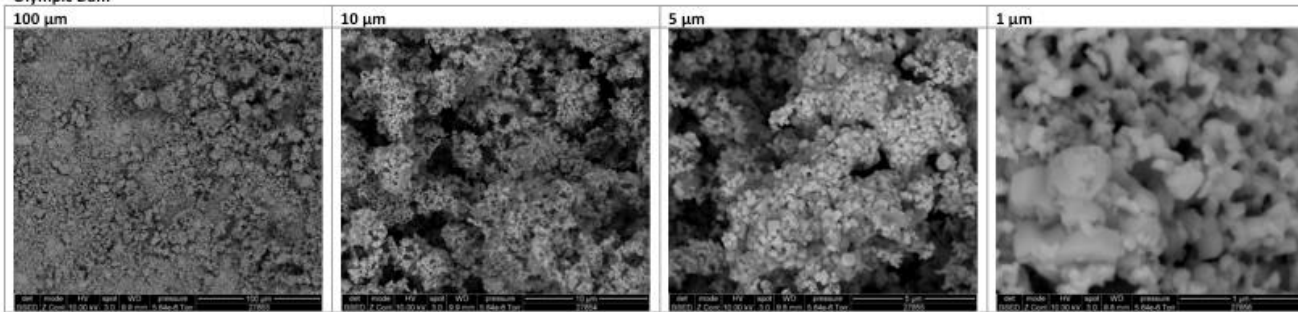
**Figure F- 5: SEM BSE Images for UOCs Mary Kathleen, Mesa EFI and Mulberry**

## Appendix F

North Span



### Olympic Dam



## Queensland

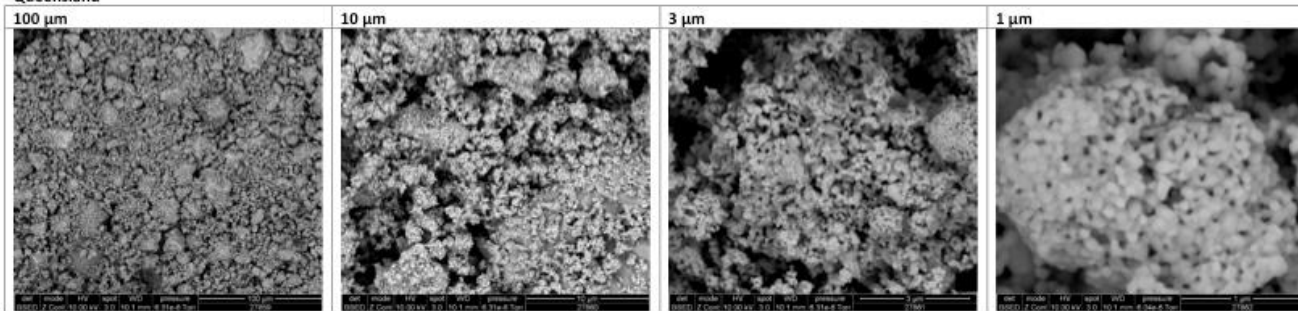
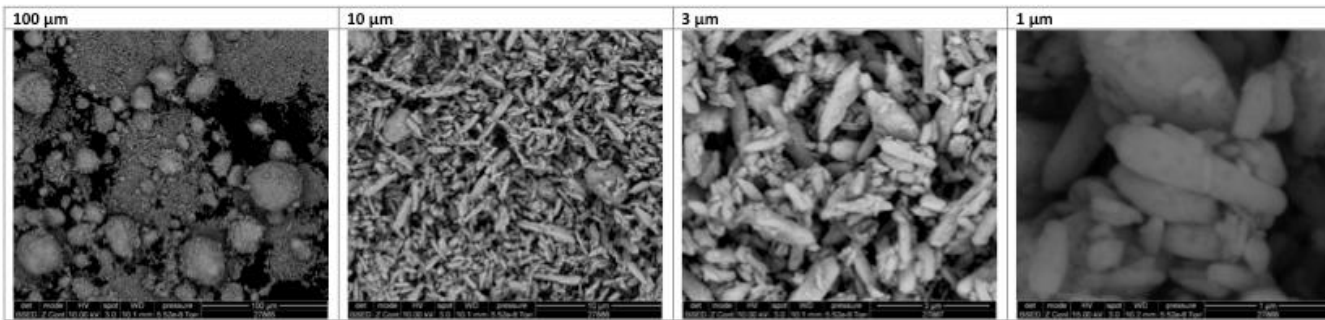
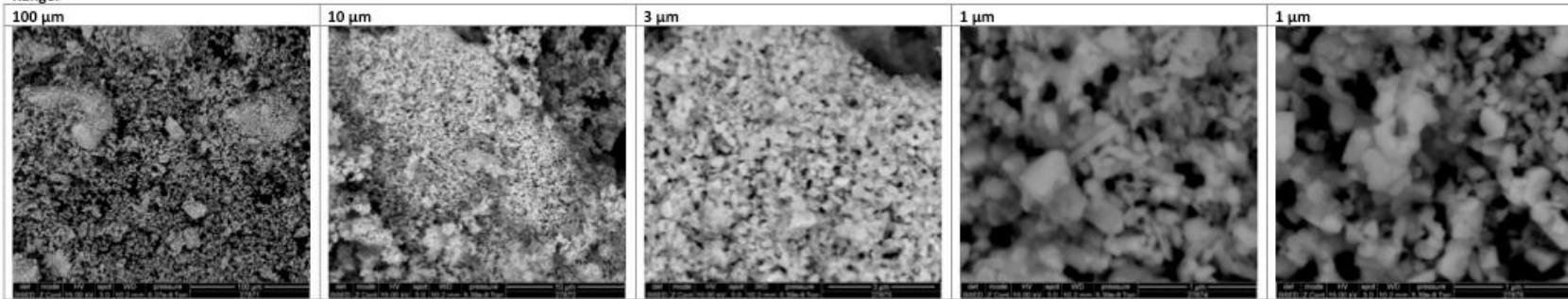


**Figure F- 6: SEM BSE Images for UOCs North Span, Olympic Dam and Queensland**

## Rabbit Lake



Ranger



### Rio Algom

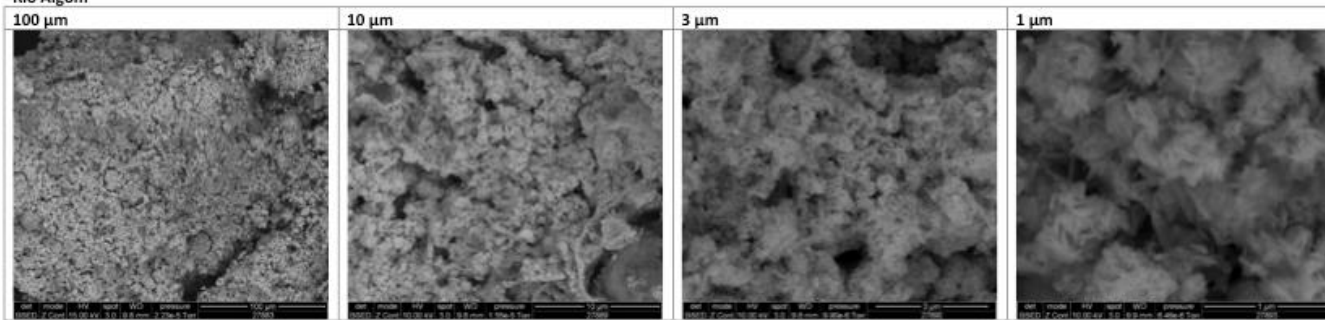


**Figure F- 7: SEM BSE Images for UOCs Rabbit Lake, Ranger and Rio Algom**

## Appendix F

South Alligator

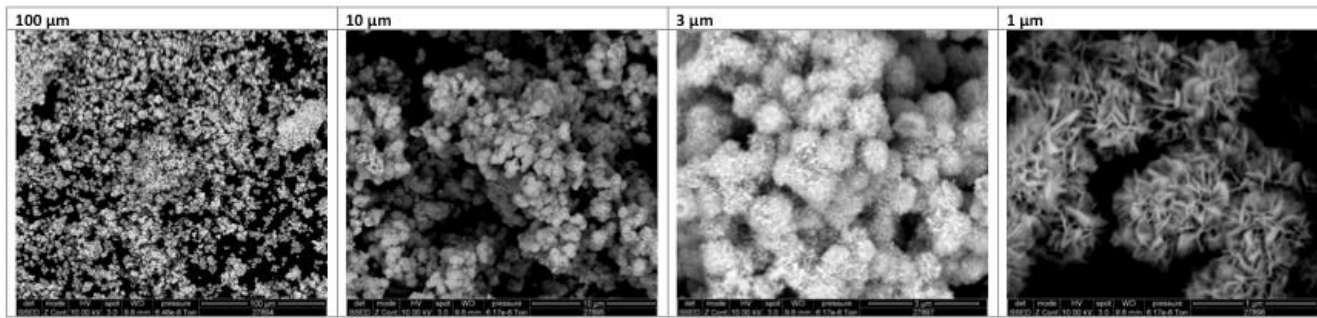


**Figure F- 8: SEM BSE Images for UOC South Alligator**

## **Appendix G: X-Ray Diffraction**

XRD analyses were conducted on the 19 UOCs and also of the UOC analogue CRM CUP-2 using a Panalytical X'Pert Powder XRD (Table F-1).

**Table G- 1: XRD operating parameters**

<b>X-ray source</b>	Cu
<b>K-<math>\alpha</math>1 wavelength</b>	1.54056
<b>K-<math>\alpha</math>2 wavelength</b>	1.54439
<b>Generator voltage (V)</b>	35
<b>Tube current (A)</b>	40
<b>Scan range (2<math>\theta</math>)</b>	2 – 76
<b>Step size (2<math>\theta</math>)</b>	0.02
<b>Time per step (s)</b>	3

Major U-phases were identifiable in samples as well as some other minor U-related minerals. (Table F-2).

**Table G- 2: Minor mineral / compound formulae**

<b>Mineral</b>	<b>Chemical Formula</b>	<b>Compound equivalent</b>
<b>Becquerelite</b>	$\text{Ca}(\text{UO}_2)_6\text{O}_4(\text{OH})_6 \cdot 8\text{H}_2\text{O}$	Uranyl hydroxide
<b>Clarkeite</b>	$\text{Na}(\text{UO}_2)(\text{OH})$	-
<b>Cristobalite</b>	$\text{SiO}_2$	Opal
<b>Jachymovite</b>	$(\text{UO}_2)_8(\text{SO}_4)(\text{OH})_{14} \cdot 13\text{H}_2\text{O}$	-
<b>Metaschoepite</b>	$2\text{UO}_3\text{NH}_3 \cdot 3\text{H}_2\text{O}$	-
<b>Natrozippeite</b>	$\text{Na}_5(\text{UO}_2)_8(\text{SO}_4)_4\text{O}_5(\text{OH})_3 \cdot 12\text{H}_2\text{O}$	Basic uranyl sulphate
<b>Zinczippeite</b>	$\text{Zn}(\text{UO}_2)_2(\text{SO}_4)\text{O}_2 \cdot 3.5\text{H}_2\text{O}$	Basic uranyl sulphate

Becquerelite (or uranyl hydroxide) is typically precipitated in neutral pH where U assay is commonly 80-85% (Hausen, 1998). UOCs that typically contain becquerelite will also contain 2-5% ammonia, alkalis,  $\text{Na}^+$ ,  $\text{K}^+$  and FeO which can be observed with UOC South Alligator where the major U phase is ammonium-bearing.

The zippeite minerals present in UOC have a compound equivalent of basic uranyl sulphate (BUS) and is commonly associated with underground U mines. It is formed in neutral pH and oxidised U liquors and is a major component of high sulphate UOC. The sulphate content can be as much as 10% with small amounts of ammonia (2-5%) and trace FeO (Hausen, 1998).

The presence of sodium, sulphates and carbonates in the major U mineral phase can act as an indicator of the processing history of the sample. For example, Faraday and Madawaska are from the same mine and mill but were produced at two different operational periods. Both diffractograms are amorphous and are noisy due to the poor crystalline nature of the powder sample. The major U phase for Faraday is uranium oxide ammonia hydrate whereas Madawaska is sodium uranyl hydroxide. According to the literature, both samples were produced using acid leaching with  $\text{NaClO}_3$  and precipitated using MgO. The presence of  $\text{NH}_3$  in Faraday is not consistent with the literature and suggests that there could have been an operational change at this particular mill. Nonetheless, the chemical differentiation is an accurate indicator to discriminate the two samples apart considering their ore feed would have been near identical with similar REE profiles and U isotopes.

The Olympic Dam UOC contains cristobalite which is a polymorph of  $\text{SiO}_2$  and has a different crystal structure to the more common quartz. Olympic Dam is situated in a region of Australia (Andamooka, SA) which is world famous for Opal which exhibits similar XRD patterns to cristobalite. The presence of this particular polymorph of  $\text{SiO}_2$  could be a future key identifier for Olympic Dam.

The presence, combination of, and ratio of these major and minor compounds could all have future potential use when combined with other data to discriminate a sample's origin.

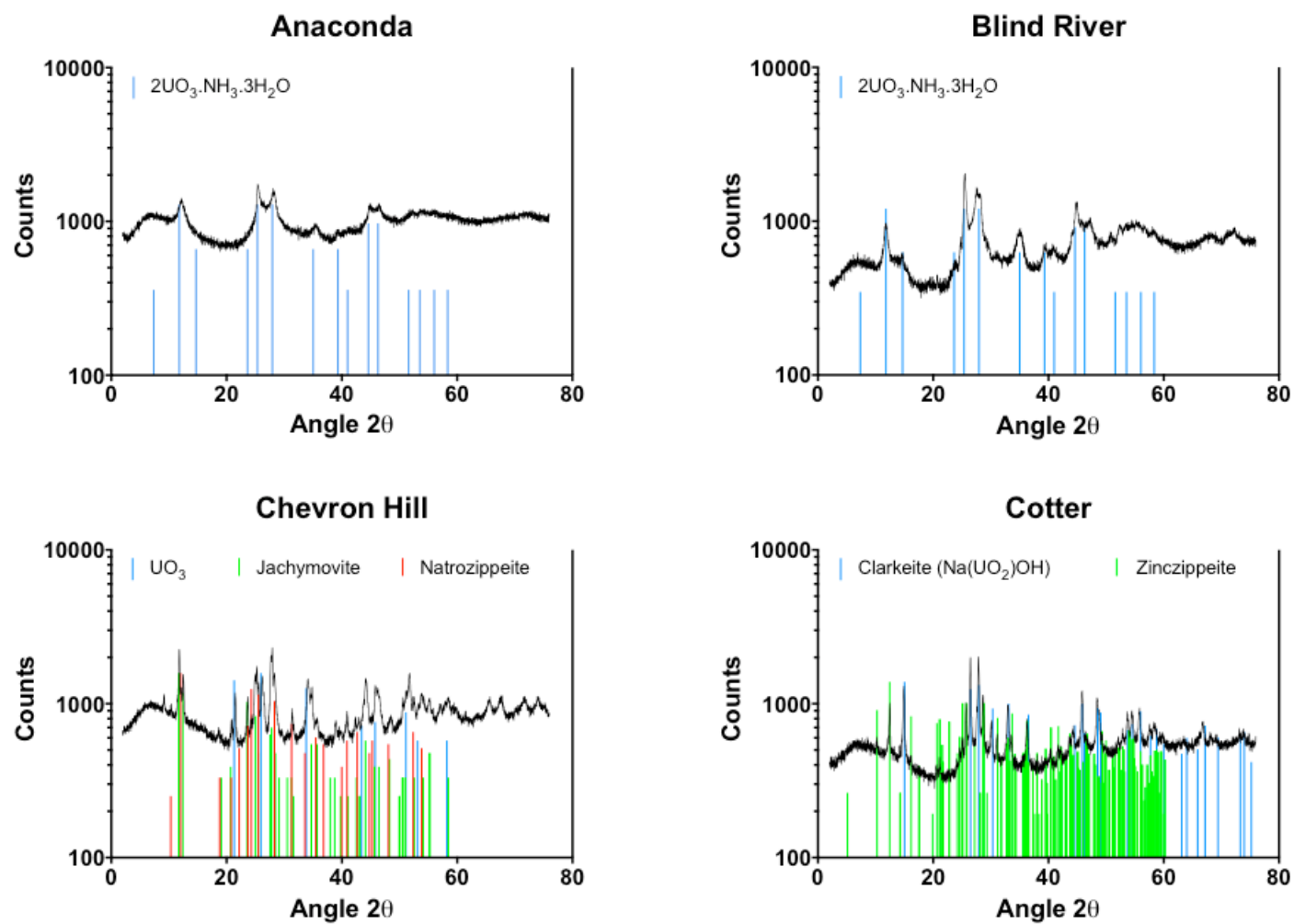


**Figure G- 1: XRD patterns and identified minerals/compounds for UOCs Anaconda, Blind River, Chevron Hill and Cotter**

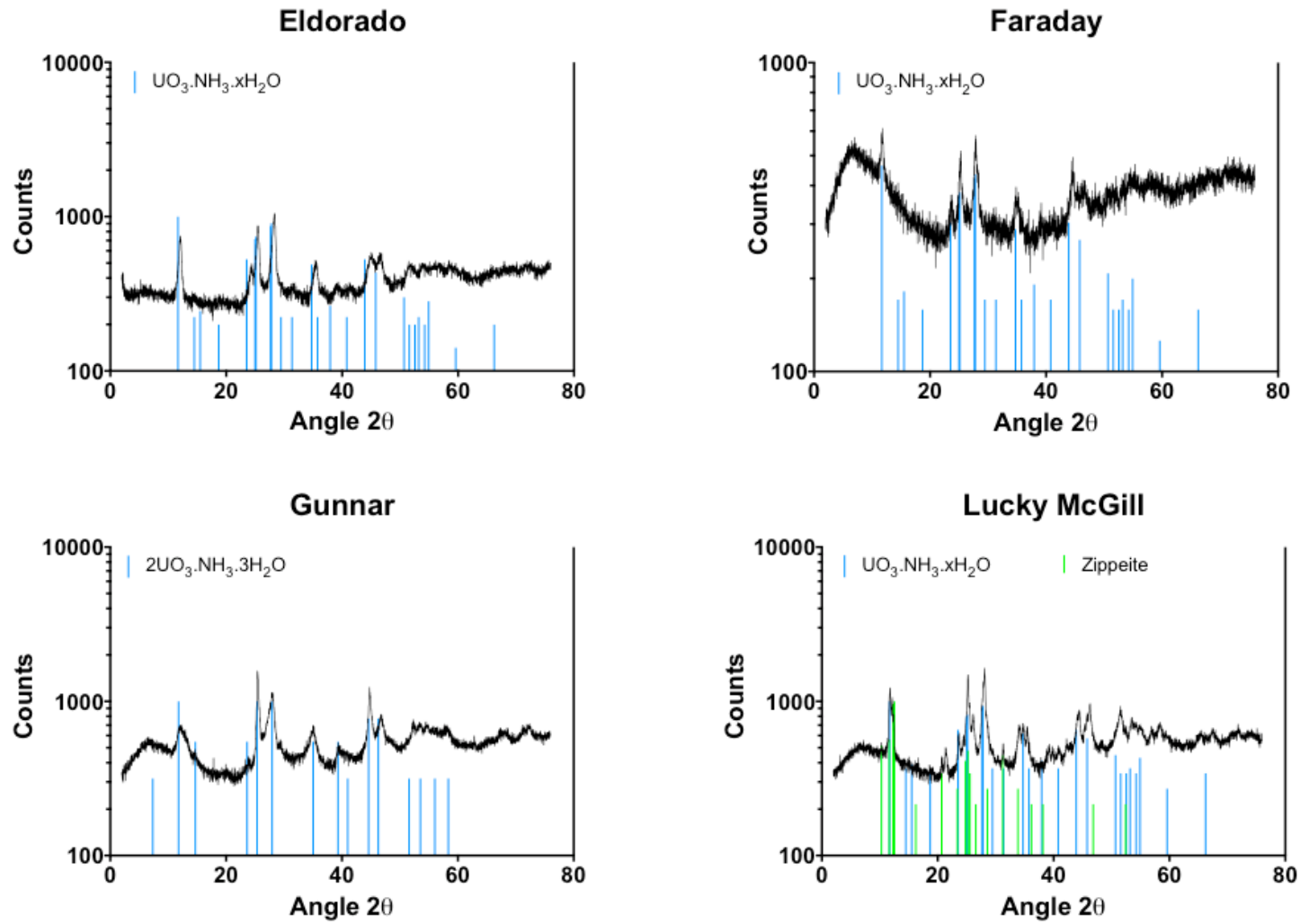


**Figure G- 2: XRD patterns and identified minerals/compounds for UOCs Eldorado, Faraday, Gunnar and Lucky McGill**

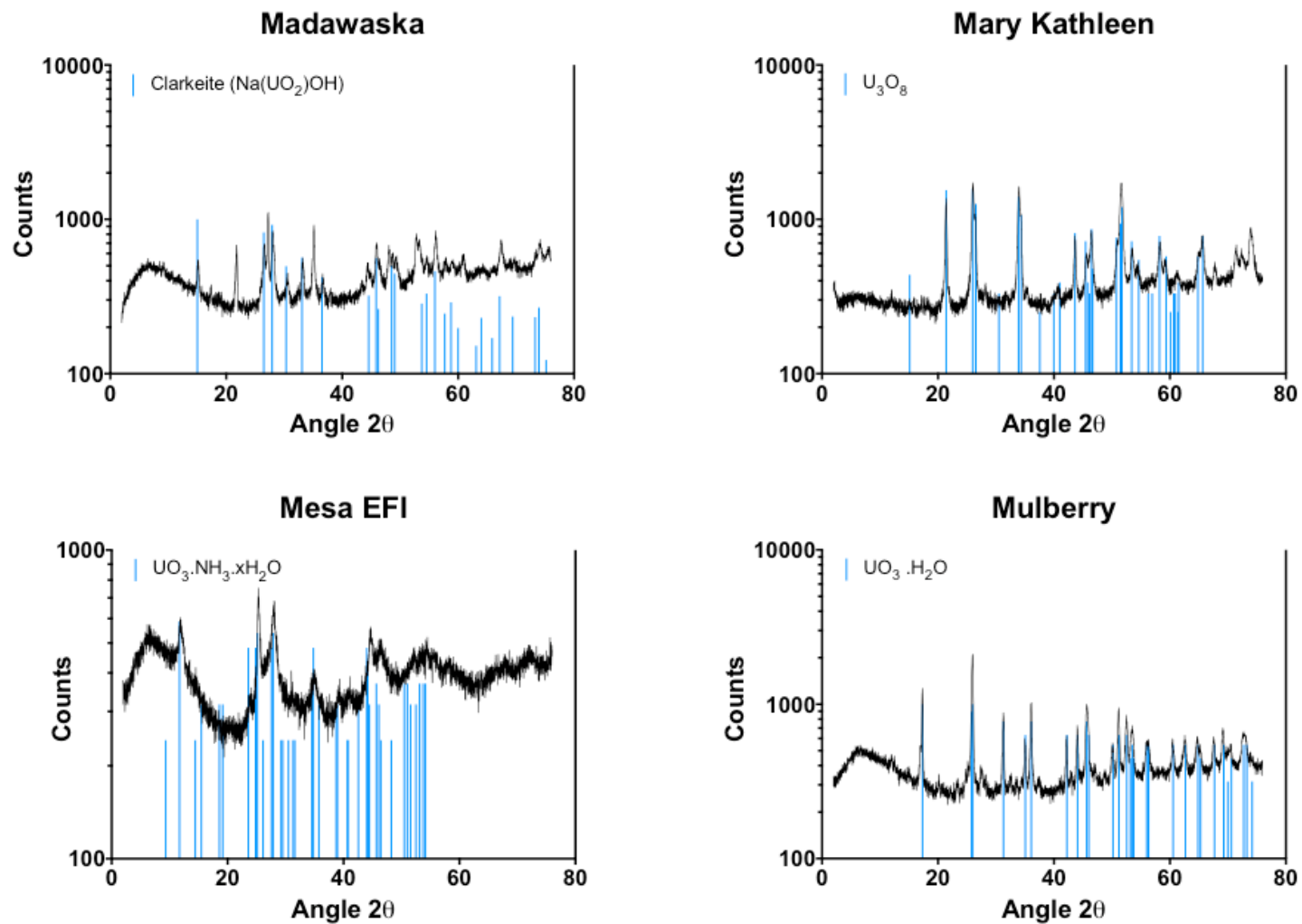


**Figure G- 3: XRD patterns and identified minerals/compounds for UOCs Madawaska, Mary Kathleen, Mesa EFI and Mulberry**

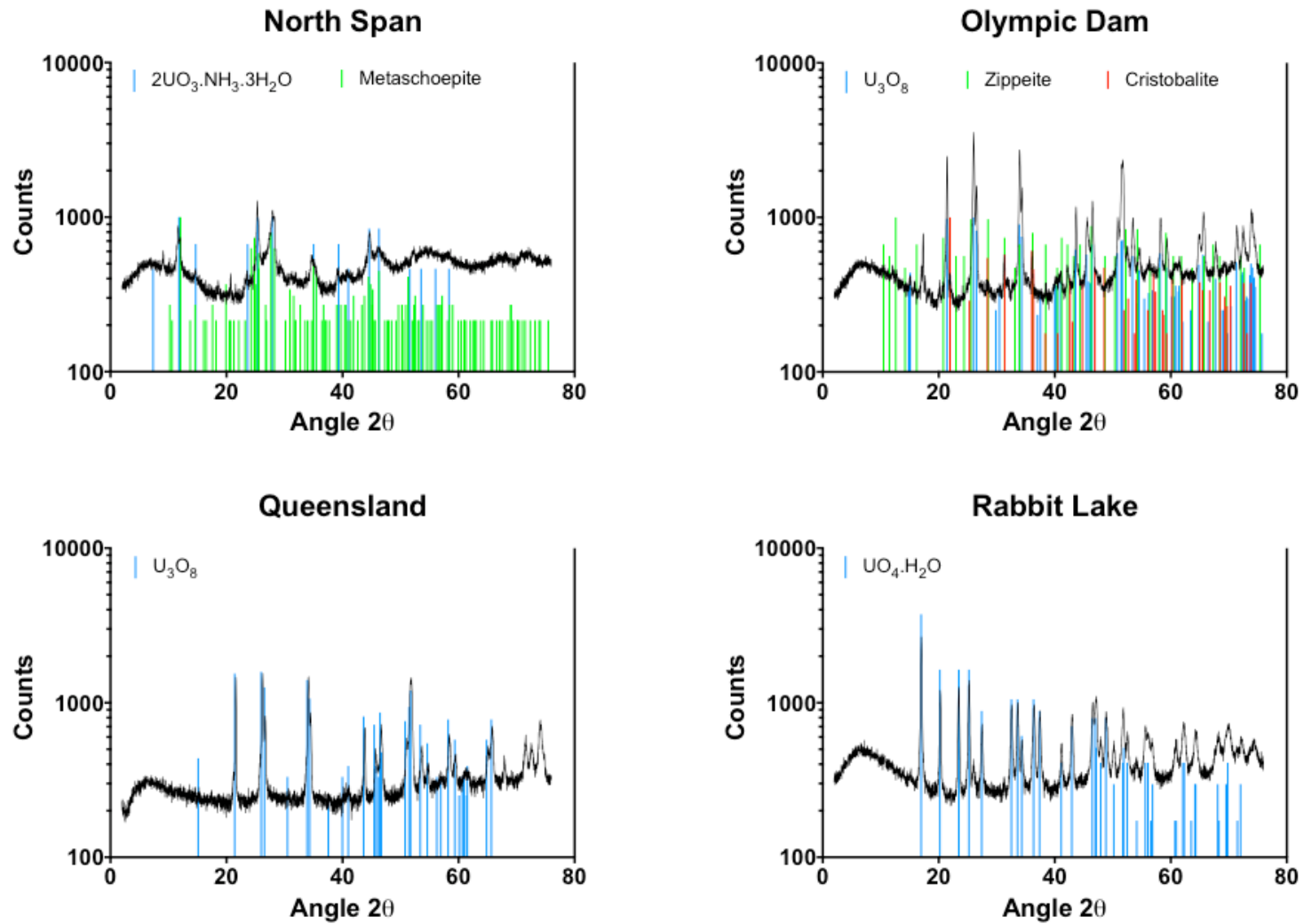


**Figure G- 4: XRD patterns and identified minerals/compounds for UOCs North Span, Olympic Dam, Queensland and Rabbit Lake**

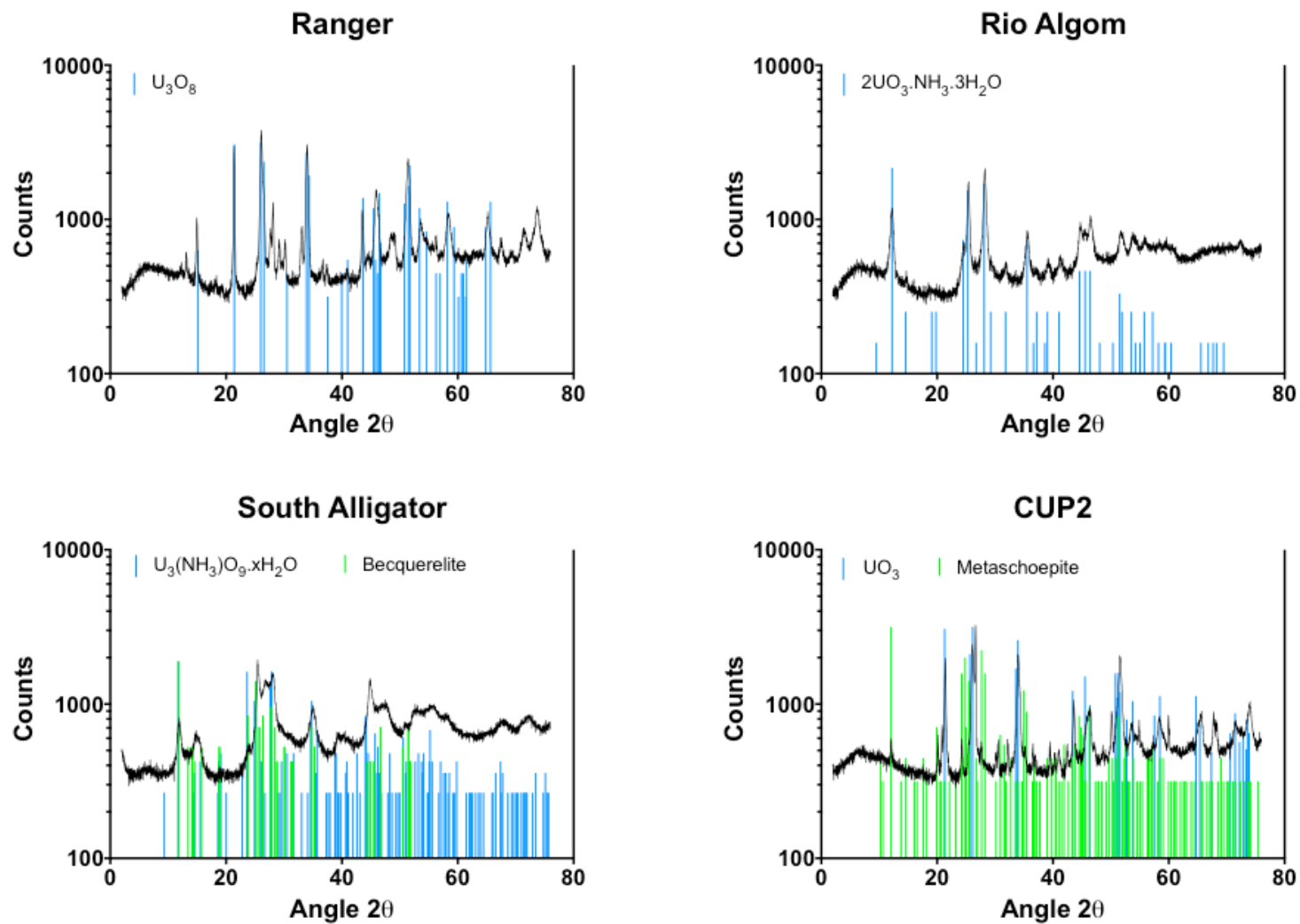


**Figure G- 5: XRD patterns and identified minerals/compounds for UOCs Ranger, Rio Algom, South Alligator and reference material CUP-2**

**Appendix H: Reading D.G., Croudace I.W. & Warwick P.E. (2015). A rapid sample digestion procedure to aid initial nuclear forensic investigations for uranium-bearing ores and concentrates prior to gamma spectrometry.**

European Safeguards Research and Development Association (ESARDA) 37<sup>th</sup> Annual Conference Proceedings. European Commission – Joint Research Centre Technical Report 96321, P599-604





## JRC TECHNICAL REPORT



# ESARDA 37<sup>th</sup> Annual Meeting Proceedings

*2015 Symposium  
19-21 May 2015  
Midland Hotel, Manchester (UK)*

Filippo Sevini  
Editor: Andrea De Luca  
**2015**

Report EUR 27342



European Commission  
Joint Research Centre  
Institute for Transuranium Elements

### Contact information

Filippo Sevini  
Address: Joint Research Centre, ITU Nuclear Security unit, T.P. 800, Via E Fermi 2749, 21027 Ispra, Italy  
E-mail: [filippo.sevini@jrc.ec.europa.eu](mailto:filippo.sevini@jrc.ec.europa.eu)  
Tel.: +39 0332 78 6793

JRC Science Hub  
<https://ec.europa.eu/jrc>

### Legal Notice

This publication is a Technical Report by the Joint Research Centre, the European Commission's in-house science service. It aims to provide evidence-based scientific support to the European policy-making process. The scientific output expressed does not imply a policy position of the European Commission. Neither the European Commission nor any person acting on behalf of the Commission is responsible for the use which might be made of this publication.

All images © European Union 2015

JRC96321

EUR 27342

ISBN 978-92-79-49495-6 (PDF)

ISSN 1831-9424 (online)

doi: 10.2789/099293

Luxembourg: Publications Office of the European Union, 2015

© European Union, 2015

Reproduction is authorised provided the source is acknowledged.

### Abstract

The 37th ESARDA symposium on Safeguards and Nuclear Non-Proliferation was held in Manchester, United Kingdom from 19-21 May, 2015. The Symposium has been preceded by meetings of the ESARDA Working Groups on 18 May 2015. The event has once again been an opportunity for research organisations, safeguards authorities and nuclear plant operators to exchange information on new aspects of international safeguards and non-proliferation, as well as recent developments in nuclear safeguards and non-proliferation related research activities and their implications for the safeguards community. The Proceedings contains the papers (118) submitted according to deadlines.

## A rapid sample digestion procedure to aid initial nuclear forensics investigations for uranium-bearing ores and concentrates prior to gamma spectrometry

**David G. Reading, Ian W. Croudace, Phillip E Warwick**

GAU-Radioanalytical Laboratories, Ocean & Earth Science, University of Southampton, National Oceanography Centre, European Way, Southampton, SO14 3ZH, UK.

E-mail: d.reading@noc.soton.ac.uk

### **Abstract:**

*A rapid and effective preparative procedure has been evaluated for the accurate determination of low-energy (40-200 keV) gamma-emitting radionuclides ( $^{210}\text{Pb}$ ,  $^{234}\text{Th}$ ,  $^{226}\text{Ra}$ ,  $^{235}\text{U}$ ) in uranium ores and uranium ore concentrates (UOCs) using high-resolution gamma ray spectrometry. The measurement of low-energy gamma photons is complicated in heterogeneous samples containing dense, mineral phases. Attenuation corrections using mean density estimates result in an underestimation of the activity concentration where dense grains are dispersed within a less dense matrix (analogous to a nugget effect). The current method overcomes these problems using a lithium tetraborate fusion that readily dissolves all components including high-density, self-attenuating minerals/compounds in a matter of minutes. This is the ideal method for dissolving complex, non-volatile components in soils, rocks, mineral concentrates, and other materials where density reduction is required. This approach avoids the need for theoretical corrections or sample-specific matrix matching. The resulting homogeneous quenched glass produced can be quickly dissolved in nitric acid. The technique has been tested on uranium-bearing Certified Reference Materials and provides accurate activity concentrations compared to the underestimated activity concentration estimates derived from direct measurements of a bulk sample. The procedure offers an attractive solution for initial nuclear forensic studies where complex refractory minerals or matrices exist and is significantly faster, safer and simpler than alternative approaches and produces low-density solutions that can be counted by gamma spectrometry.*

**Keywords:** Borate fusion; photon self-attenuation; heterogeneous matrix.

### **1. Introduction**

The Nuclear Forensics International Technical Working Group recommend high-resolution gamma spectrometry (HRGS) on receipt of unknown, illicitly recovered materials such as uranium ore and uranium ore concentrate (UOC) [1–4]. In addition, the development of a database of gamma nuclide signatures for U-ores and UOCs of known provenance, combined with Principal Components Analysis (PCA) could aid in identifying the origin and history of recovered uranium ores and their concentrates.

The variance in sample matrices from HRGS calibration standards can cause an under or overestimation in photopeak efficiency for the detector due to the self-attenuation of low energy gamma photons within the matrix. Several radionuclides from the uranium and

thorium series have low energy gamma emissions, which could be attenuated (table 1). Previous studies to overcome photon attenuation typically require direct transmission observations with a highly active source [5]; proxy measurements of higher energy gamma photons [6]; or theoretical density corrections derived from modelling photon interactions with the sample matrix [7]. This is not practical for rapid characterisation of recovered illicit materials. Additionally, adjusting the HRGS calibrations based on the relationship between photon efficiency and sample bulk density results in lower than expected activity concentrations. This problem is caused by dense U particles (uraninite =  $8.5 \text{ g cm}^{-3}$ ) of varying size and concentration supported in less dense bulk matrices (typically  $< 2.0 \text{ g cm}^{-3}$ ).

Radionuclide	Energy (keV)	Gamma Yield (%)
<sup>210</sup> Pb	46.5	4.3
<sup>241</sup> Am	59.9	35.9
	63.3	5.3
<sup>234</sup> Th ( <sup>238</sup> U)	92.4	13.7
	92.8	2.5
<sup>231</sup> Th	84.2	6.7
	90.0	1.0
<sup>228</sup> Th	84.4	1.2
	109.2	1.7
	143.8	10.9
<sup>235</sup> U	163.4	5.1
	185.8	57.0
	202.1	1.1
	205.3	5.0
<sup>226</sup> Ra	186.2	3.6

Table 1: Selected gamma emitting radionuclides where energy = < 200 keV and yield = > 1%.

A sample dissolution method using di-lithium tetraborate borate fusion was developed to reduce self-attenuation effects observed in U-bearing compounds to yield accurate activity concentrations from gamma-emitting radionuclides. This method does not require accurate characterisation of the sample prior to measurement, nor does it require any assumptions to be made about the samples composition or history.

mixed nuclide source (NPL, Teddington, UK) with the addition of a <sup>210</sup>Pb solution standard (PTB, Braunschweig, Germany) mixed into a range of difference density matrices (cellulose, water, sand, steel and boron and a tin-tungsten ore) to produce a set of efficiency calibrations.

All samples were counted for one hour, as this was found suitable to obtain adequate counting statistics. The limit of detection values presented are based on the decision limit (or critical level) as defined by Currie [8].

## 2. Instrumentation

Radionuclide activity concentrations were determined with Canberra 50% N-type High Purity Germanium (HPGe) well-type detectors. Gamma spectra were acquired using Genie 2000 acquisition software (Canberra Industries, Harwell, UK) and analysed using Fitzpeaks spectral deconvolving software (JF-Computing, Stanford in the Vale, UK). The spectrometers were previously calibrated using a traceable,

## 3. Methodology

Three certified reference materials for uranium (CUP-1, BL-5 and CUP-2, Canadian Certified Reference Materials Project, Ottawa, Canada; table 2) were selected for this study.

	CUP-1 [9]	BL-5 [10–12]	CUP-2 [13]
Uranium (Wt%)	0.128 ± 0.002	7.09 ± 0.03	75.42 ± 0.17
<sup>238</sup> U (Bq g <sup>-1</sup> ) <sup>a</sup>	15.8 ± 0.3	876 ± 3.7	9313 ± 21
<sup>235</sup> U (Bq g <sup>-1</sup> ) <sup>a</sup>	0.70 ± 0.01	41.0 ± 0.2	434 ± 1
<sup>226</sup> Ra (Bq g <sup>-1</sup> )	As <sup>238</sup> U	866 ± 21	< LOD
<sup>210</sup> Pb (Bq g <sup>-1</sup> )	As <sup>238</sup> U	857 ± 38	< LOD

Table 2: Certified Reference Materials Data. <sup>a</sup> Activity concentration calculated from certified U wt% assuming natural <sup>238</sup>U/<sup>235</sup>U abundances (99.275% and 0.72% respectively).

### 3.1 Initial characterisation of certified reference materials

All three certified reference materials were weighted into 20 mL polythene vials (CUP-1 = 28.1 g, BL-5 = 31.6 g, CUP-2 = 34.8 g) and the bulk densities were determined (1.36, 1.53 and 1.68 g cm<sup>-3</sup> respectively). Apparent photon efficiencies of each measured radionuclide were calculated based on the bulk density of each reference material from the known relationship between photon detection efficiency and calibration standard density. The samples were characterised for <sup>210</sup>Pb, <sup>234</sup>Th, <sup>226</sup>Ra, <sup>235</sup>U and <sup>234m</sup>Pa activity concentrations. Protactinium-234m was measured as its high-energy gamma emissions (1001 keV) should not undergo sufficient photon attenuation in comparison to the lower energy radionuclides. Lead-214 and <sup>214</sup>Bi were not assessed for their extent of attenuation due to the possible disequilibria caused during sample preparation and radon de-gassing.

### 3.2 Lithium borate fusion

Borate fusion is well established as a sample digestion or dissolution method in geochemistry and is known to be effective in dissolving minerals and rocks comprising oxides, carbonates, chlorides, sulphates, sulphides, phosphates and metallic materials. Given the beneficial characteristics of borate fusions as a sample dissolution technique, it is surprising that there were no reported applications in the field or radioanalytical chemistry until the radiometric work of Croudace et al 1998 [14]. Prior to that study all reported radioanalytical preparations used a range of less effective and hazardous acid digestions or laborious alkali fusions.

The three certified reference materials were ignited at 600 °C for 3 hours to oxidise the sample and to inhibit volatilisation of elements such as Pb. An aliquot of 0.5 g of ignited reference material was weighed in to a platinum crucible at a 1:1 ratio with di-lithium tetraborate flux (Fluxana, Germany). The crucible is agitated to mix the two components and fused on a Vulcan Fusion Machine (Fluxana,

Germany) where the sample is heated to 1200 °C and periodically agitated for approximately 10 minutes. The resulting melt is quenched in 50 mL of Milli-Q water and acidified with 50 mL concentrated nitric acid. Any residual material in the platinum crucible is collected and transferred to the digest. The sample is then heated at 80 °C to reduce the sample volume. Boric acid and silica may precipitate which requires filtering. The digest and precipitate is separated with a Whatman GF-C filter paper supported on a Whatman No 540 filter paper using vacuum filtration. The filters papers are then rinsed with 8M HNO<sub>3</sub> and effectively retained the precipitate resulting in a clear solution being collected. The precipitate contained no detectable radioactivity. The filtered solutions are reduced in volume to < 20 mL on a hot plate at 80 °C and then transferred to a 20 mL polythene vial with washing and made up to 20 mL. The samples were counted immediately for the same radionuclides identified above.

## 4. Results

The direct measurements for all three of the certified reference materials yielded low than expected activity concentrations for measured radionuclides (figure 1). The extent of the bias between the measured and certified activity concentrations is proportional to the increasing uranium content in the reference material. This can be observed with <sup>234</sup>Th where the activity concentration is 94%, 65% and 7% of the certified value for CUP-1, BL-5 and CUP-2 respectively. Where a certified activity concentration is not available for one of the measured radionuclides, the closest parent isotope value has been used. Reference material CUP-1 had no measurable <sup>234m</sup>Pa as it was not likely resolvable from the Compton background as the emission yield is very low (0.847%) in a low uranium concentration material (0.128%). Reference material CUP-2 had no measurable <sup>226</sup>Ra or <sup>210</sup>Pb due to the material being a uranium ore concentrate and insufficient time for ingrowth following the ore processing.

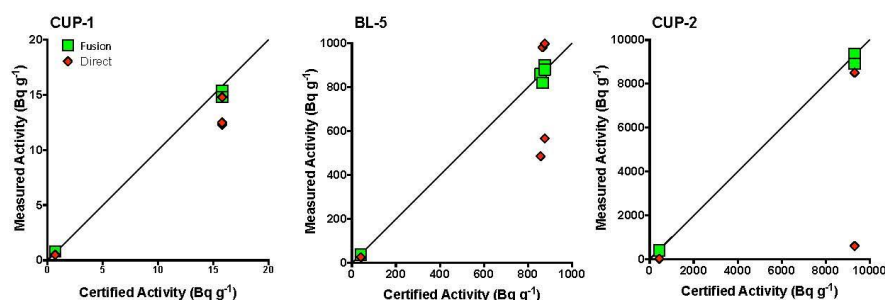


Figure 1: Activity concentrations for selected radionuclides of both solid and fused certified reference materials against the expected activity concentrations based on certified values.

The discrepancy with the direct measurements was identified as being proportional to the uranium concentration and the uranium particle size causing a "hot-particle effect" where the uranium is supported within a less dense bulk matrix. This characteristic would be difficult to matrix-match without significant sample characterisation and is the cause of the self-attenuation observed when directly measuring the certified reference materials.

The measured activities of the reference materials via the lithium borate fusion technique are all within uncertainty of the certified values. The fusion technique significantly reduces any matrix effects present in heterogeneously distributed uranium-bearing samples where grain size, density and concentration can vary. The average uranium weight percentage obtained from the fused materials yields  $0.12 \pm 0.02$ ,  $7.24 \pm 0.33$  and  $75.2 \pm 1.8$  for CUP-1, BL-5 and CUP-2 respectively and are in agreement with certified values (table 2).

Both  $^{235}\text{U}$  and  $^{226}\text{Ra}$  emit  $\sim 186$  keV gamma photons with a yield of 57.0% and 3.6% respectively. The deconvolving software uses lower energy  $^{235}\text{U}$  gamma photons to determine how much of the 186 keV photopeak to assign to each radionuclide as  $^{226}\text{Ra}$  only has one major emission energy. However, if the lower energy gamma photons of  $^{235}\text{U}$  (143.8 keV with 11% yield) are being attenuated then this correction will be inaccurate resulting in lower  $^{235}\text{U}$  and higher  $^{226}\text{Ra}$  activity concentrations. This is observed in certified material BL-5 where  $^{235}\text{U}$  and  $^{226}\text{Ra}$  measured activity concentrations are  $64 \pm 12\%$  and  $113 \pm 17\%$  respectively and are not within uncertainty of one another. Once the reference material was fused, the activities were measured as  $96 \pm 7\%$  and  $95 \pm 7\%$   $^{235}\text{U}$  and  $^{226}\text{Ra}$  respectively. This

is important as a qualitative correction could produce an inaccurate  $^{235}\text{U}$  activity concentration if the sample has been enriched in  $^{235}\text{U}$ , does not contain the natural  $^{238}\text{U}/^{235}\text{U}$  ratio, or has been processed whereby  $^{226}\text{Ra}$  would not be expected to be present.

## 5. Conclusion

The lithium borate fusion technique achieves a highly effective and rapid dissolution of virtually any difficult to dissolve material (silicates, oxides, sulphates) as well as dissolving carbonates and halides. This ability makes it an attractive approach for rapid sample dissolution. The fusion process solubilises mineral particles removing the "hot-particle effects" and increases the detection efficiency of low-energy gamma-emitting nuclides such as  $^{210}\text{Pb}$  and  $^{234}\text{Th}$  in heterogeneous U-bearing samples. The high uranium content of CRM CUP-2 (75 Wt% U) had a  $^{234}\text{Th}$  activity concentration of  $7 \pm 1\%$  of the certified value when measured in its solid form using an efficiency correction based on its bulk density. After the borate fusion and digestion technique, the  $^{234}\text{Th}$  concentration was  $100 \pm 2\%$  of the certified value. The dense uranium-bearing grains are present within a lower bulk density matrix with variable grains sizes causing self-attenuation of low-energy gamma photons. The fusion technique avoids the need for sample-specific matrix matching or correcting and, combined with rapid sample preparation, offers an attractive, efficient alternative for accurate radiometric characterisation.

The procedure developed could be used to develop a database containing radionuclide activities, U-concentrations,  $^{238}\text{U}/^{235}\text{U}$  /  $^{238}\text{U}/^{232}\text{Th}$  ratios, and extent of secular

equilibrium for U-ores and uranium ore concentrates of known provenance so that recovered, illicit nuclear materials can be rapidly analysed and compared as part of a nuclear forensic characterisation.

The borate fusion technique can be used in other applications where accurate and rapid characterisation of low-energy gamma photons is required, such as accurately measuring  $^{241}\text{Am}$ ,  $^{239}\text{Pu}$  or  $^{241}\text{Pu}$  as part of a nuclear forensic effort or environmental monitoring. The technique was used to process and analyse >700 soil samples in only 12 weeks from the Greenham Common Airbase where an alleged nuclear incident took place in 1958. The fused samples underwent extraction chromatography of U and Pu in preparation for high precision radiometric and TIMS measurements [14,15].

Any material that may be affected by a "hot-particle effect" that requires accurate radiometric characterisation would benefit from the borate fusion technique, e.g. the accurate characterisation of hot-particles near nuclear sites such as Dounreay, UK [16] or Chernobyl, Ukraine [17,18]. The petroleum and mineral processing industries also regularly encounter NORM scales and deposits having high densities that contain Ba, Ra, U and Th and thorium. The accurate determination of the associated low-energy gamma radionuclides is critical for radiological assessment and for appropriately handling and disposing of waste and tailings. Such characterisations could also be facilitated using the lithium borate fusion-based technique.

## 6. Acknowledgements

The authors thank Giles Graham, Claire Watt, Nick Bright and AWE Plc. for their support and for funding this PhD project via the AWE Outreach Programme (AWE 30200056).

## 7. References

- [1] I.D. Hutcheon, M.J. Kristo, K.B. Knight, *Nonproliferation Nuclear Forensics*, in: *Uranium - Cradle to Grave*, Winnipeg, 2013: pp. 377–394.
- [2] M.J. Kristo, *Handbook of Radioactivity Analysis*, Third edit, Elsevier, San Diego, 2012.
- [3] R. Hanlen, *Round Robin 3 Exercise After Action and Lessons Learned Report*, PNNL-20079, Pacific Northwest Natl. Lab. U.S. Dep. Energy, Richland, WA. (2011).
- [4] M. Wallenius, K. Mayer, I. Ray, *Nuclear forensic investigations: two case studies*, *Forensic Sci. Int.* 156 (2006) 55–62.
- [5] N.H. Cutshall, I.L. Larsen, C.R. Olsen, *Direct Analysis of  $^{210}\text{Pb}$  in Sediment Samples: Self-Absorption Corrections*, *Nucl. Instruments Methods*. (1983) 309–312.
- [6] M. Diugosz-Lisiecka, H. Bem, *Fast procedure for self-absorption correction for low  $\gamma$  energy radionuclide  $^{210}\text{Pb}$  determination in solid environmental samples*, *J. Radioanal. Nucl. Chem.* 298 (2013) 495–499.
- [7] T. Pilleyre, S. Sanzelle, D. Miallier, J. Fain, F. Courtine, *Theoretical and experimental estimation of self-attenuation corrections in determination of  $^{210}\text{Pb}$  by gamma-spectrometry with well Ge detector*, *Radiat. Meas.* 41 (2006) 323–329.
- [8] L.A. Currie, *Limits for Qualitative Detection and Quantitative Determination. Application to Radiochemistry*, *Anal. Chem.* 40 (1968) 586–593.
- [9] J.L. Dalton, W.S. Bowman, *Report CCRMP 86-2E - CUP-1: A Certified Uranium Reference Ore*, 1986.
- [10] G.H. Faye, W.S. Bowman, W.S. Sutarno, *Report 79-4 Uranium Ore BL-5 - A Certified Reference Material*, 1979.
- [11] C.W. Smith, H.F. Steger, *Report 84-11e - Lead-210 in Certified Uranium Reference Ores DL-1a, BL-4a, DH-1a and BL-5*, 1984.
- [12] C.W. Smith, H.F. Steger, *Radium-226 in Certified Uranium Reference Ores DL-1a, BL-4a, DH-1a and BL-5*, 1983.
- [13] J.L. Dalton, W.S. Bowman, *Report 88-3E CUP-2: A Certified Uranium Ore Concentrate*, 1988.

- [14] I. Croudace, P. Warwick, R. Taylor, S. Dee, *Rapid procedure for plutonium and uranium determination in soils using a borate fusion followed by ion-exchange and extraction chromatography*, Anal. Chim. Acta. 371 (1998) 217–225.
- [15] R.N. Taylor, I.W. Croudace, P.E. Warwick, S.J. Dee, *Precise and rapid determination of  $^{238}\text{U}$  and  $^{235}\text{U}$  and uranium concentration in soil samples using thermal ionisation mass spectrometry*, Chem. Geol. (1998).
- [16] F. Dennis, G. Morgan, F. Henderson, *Dounreay hot particles: the story so far*, J. Radiol. Prot. 27 (2007) A3–11.
- [17] F.J. Sandalls, M.G. Segal, N. Victorova, *Hot Particles from Chernobyl: A Review*, J. Environ. Radioact. 18 (1993) 5–22.
- [18] B. Salbu, T. Krekling, D.H. Oughton, V.A. Kashparov, T.L. Brand, J.P. Day, *Hot Particles in Accidental Releases From Chernobyl and Windscale Nuclear Installations*, Analyst. 119 (1994) 125–130.

## **Appendix I: Croudace I.W., Warwick P.E., Reading D.G. & Russell, B.C. (2016). Recent contributions to the rapid screening of radionuclides in emergency responses and nuclear forensics**

Accepted paper with Trends in Analytical Chemistry (TrAC).

### **Abstract**

The ability to efficiently identify potential radiological threats or actual radioactive assaults on society and the environment demands a sophisticated and dedicated infrastructure comprising specialised personnel, mobile and fixed laboratories and advanced analytical instrumentation. Most developed countries have such systems but ensuring a long-term and resilient capability is recognised as a perennial challenge. National government laboratories specialising in nuclear forensics play a key role in maintaining capability but these organisations continue to benefit significantly from interdisciplinary and innovative contributions derived from universities and other research institutions. This review provides an insight into the range of technologies used and also provides a broad overview of applied techniques and instrumentation that contribute to rapid screening and analysis in the context of nuclear forensics and radiological emergencies.

**Keywords:** Homeland security, nuclear forensics, radiological emergencies, rapid radioanalytical methods, radioanalytical skills gaps, universities as motivators

### **Highlights:**

1. A general overview of current Investigative methods used in nuclear forensics and emergency responses is presented along with a range of new rapid methods.
2. Borate fusion is presented as a valuable tool for rapidly dissolving complex samples with one key application being the elimination of matrix absorption effects that can compromise gamma ray spectrometry data.
3. A novel, rapid liquid scintillation method is presented that uses multiple quench corrections to allow rapid screening and identification of alpha and beta contaminated water and other samples in emergency situations
4. A review of mass spectrometric methods shows their impact on rapid and precise isotopic analysis in the context of nuclear forensics and emergency situations



## I-1. Introduction

There is an international threat of nuclear or other radioactive material being used in criminal acts [1,2]. This requires the radioanalytical community to continually develop or improve a range of robust and rapid analytical methods to support investigative and law enforcement agencies. This paper presents a limited review of commonly used methods and some relatively recent approaches that offer practical benefits and enhancements in sensitivity, speed and accuracy in the context of nuclear forensics and radiological emergencies.

Recent non-nuclear acts committed by terrorists have demonstrated their global organisational ability and several countries are justly concerned that radiological acts could follow. That there is an illicit demand for nuclear or other radioactive materials is known by the authorities from attempts to sell such materials [3,4]. The number of successful transactions is imprecisely known and therefore it is difficult to accurately characterize the 'illicit nuclear market'. Many trafficking incidents are considered amateurish in nature and lacking in planning, resourcing and technical proficiency. There are, however, a few significant cases that are better organised and resourced and involved perpetrators with a track record in trafficking nuclear/radioactive material.

The IAEA has promoted the message that the responsibility for nuclear security matters lies with each member state but that guidance and best practice could be coordinated [5]. It also considers that the identification and inhibition of threats can be most effective through member co-operation and the implementation and development of sophisticated systems. One aspect of this is the IAEA's Incident and Trafficking Database (ITDB) that was originally established in 1995, and which records incidents of illicit trafficking and other unauthorised activities and events involving nuclear and other radioactive material outside regulatory control. Up to the end of 2014, the ITDB contained a total of 2734 confirmed incidents reported by participating States [1]. Of these, 442 incidents involved unauthorised possession and related criminal activities, 714 incidents involved reported theft or loss and 1526 incidents involved other unauthorised activities and events. In the remaining 86 cases, a category could not be assigned due to insufficient reported information.

Nuclear forensics as a technical discipline has been emerging for over two decades [6] and is concerned with characterising various nuclear materials and interpreting the resulting data. It uses a broad array of advanced physical, chemical and isotopic procedures to characterise sampled or seized nuclear and related materials (Figure H-1). The insights gained are used to control suspected trafficking activities, to deter nuclear terrorism and to verify that international treaties (e.g. Non-Proliferation Treaty) are being upheld.

Many of the methods used in nuclear forensics can also be profitably employed during the tracking of intentional or unintentional releases of nuclear or radioactive materials into the environment. For example, deliberate contamination of drinking water supplies with radioactive substances would be likely to have significant health, social, and economic

impacts. This scenario was addressed in a recent multidisciplinary EU-funded study (SecurEau 2008-12) that focused on developing rapid methods for potential CBRN attacks (chemical, biological, or radioactive or nuclear) on water supplies. One of the most rapid of the radiometric methods developed and discussed later involved a novel Liquid Scintillation technique that applied spectral analysis to identify pure beta and alpha emitters in waters, biofilms and pipeline deposits within one hour [7,8].

The ability to reliably monitor and identify illegal activities [e.g. those involving fissionable materials (pre-detonation and post-detonation) and radiological emergencies] requires constant vigilance, effective globally distributed monitoring systems (e.g. CTBTO), specialist national laboratories, innovative investigative approaches and a cohort of highly skilled specialists. Within the last 20 years a gamut of techniques and systematic investigative approaches has been developed by the nuclear forensic communities [9–13]. Regulatory and nuclear forensic agencies not only require sensitive, accurate and precise analytical techniques to undertake their work effectively, but also a supply of suitably skilled specialists working in well-funded centres [14]. As argued by the National Research Council Committee on Nuclear Forensics (2010) [15], without suitable and sustained support, there is a danger of developing a skills/capability gap (Box I-1) that would impact on resilience and the ability to be adequately prepared for radiological threats. Expertise and training offered by well-equipped universities and other research institutions (e.g. those specialising in geochemistry, isotope geochemistry, radioanalytical chemistry etc.) can play a short-term mitigating role in filling these gaps.

For both emergency response and nuclear forensics investigations, comprehensive physical, chemical and radiological characterisation of materials are required to inform emergency response strategies, assess risk and provide evidence for subsequent investigations. Generally, characterisation of any material will be staged and will commence with rapid non-destructive, non-contact, testing followed by more time-consuming in-depth studies typically involving destructive testing of sub-samples (Figure I-1). The requirement for robust and complex datasets to be produced in a time-constrained manner places unique demands on the sample preparation, separation and measurement approaches required for the in-depth characterisation stages. This review provides a general insight into laboratory-based radioanalytical procedures used in nuclear forensic and emergency situations. It also presents a number of recent analytical procedures developed by our group that contribute to the speed of analysis at key stages in the characterisation process.

BOX I-1: Adapted from *Nuclear Forensics: A capability at risk* [15].

Likely expanded growth of nuclear technologies and subsequent illegal access to materials (e.g. through conflicts) adds to the risk of unauthorized activities and demands a sustained support for nuclear security infrastructure and nuclear forensics as summarized below.

### **The status quo in 2010**

Organization in the NF field is insufficiently focused and inhibits development of a strategic consensus

Sustainability – in many countries NF capabilities developed in Government laboratories based on nuclear weapons programs that are in a state of decline.

Workforce skills and Infrastructure are in decline and key facilities are old and are not up to modern standards.

Procedures and Tools – many current NF techniques were developed to carry out Cold War missions and do not reflect current technical capabilities.

### **Recommendations**

1. Streamline organizational structures, align authority and responsibility, develop and issue documents.
2. Issue coordinated and integrated implementation plans to improve national NF program capabilities.
3. Build and maintain effective NF workforces at national laboratories and through collaborations with universities and other organizations.
4. Adapt NF to the challenges of real emergency situations, including, for example, conducting more realistic exercises that are unannounced and that challenge regulations and procedures followed in the normal work environment, and implementing lessons learned.
5. National laboratories should optimize procedures and equipment through R&D to meet program requirements. Modelling and simulation should play an increased role in research, development, and planning.
6. The NF community should develop standards and procedures that are rooted in the same underlying principles that guide modern forensic science.
7. Homeland Security agencies should devise and implement plans that enable access to relevant information in databases including classified and proprietary databases—for NF missions.
8. Establish international sharing of information and best practice, subject to safeguards.

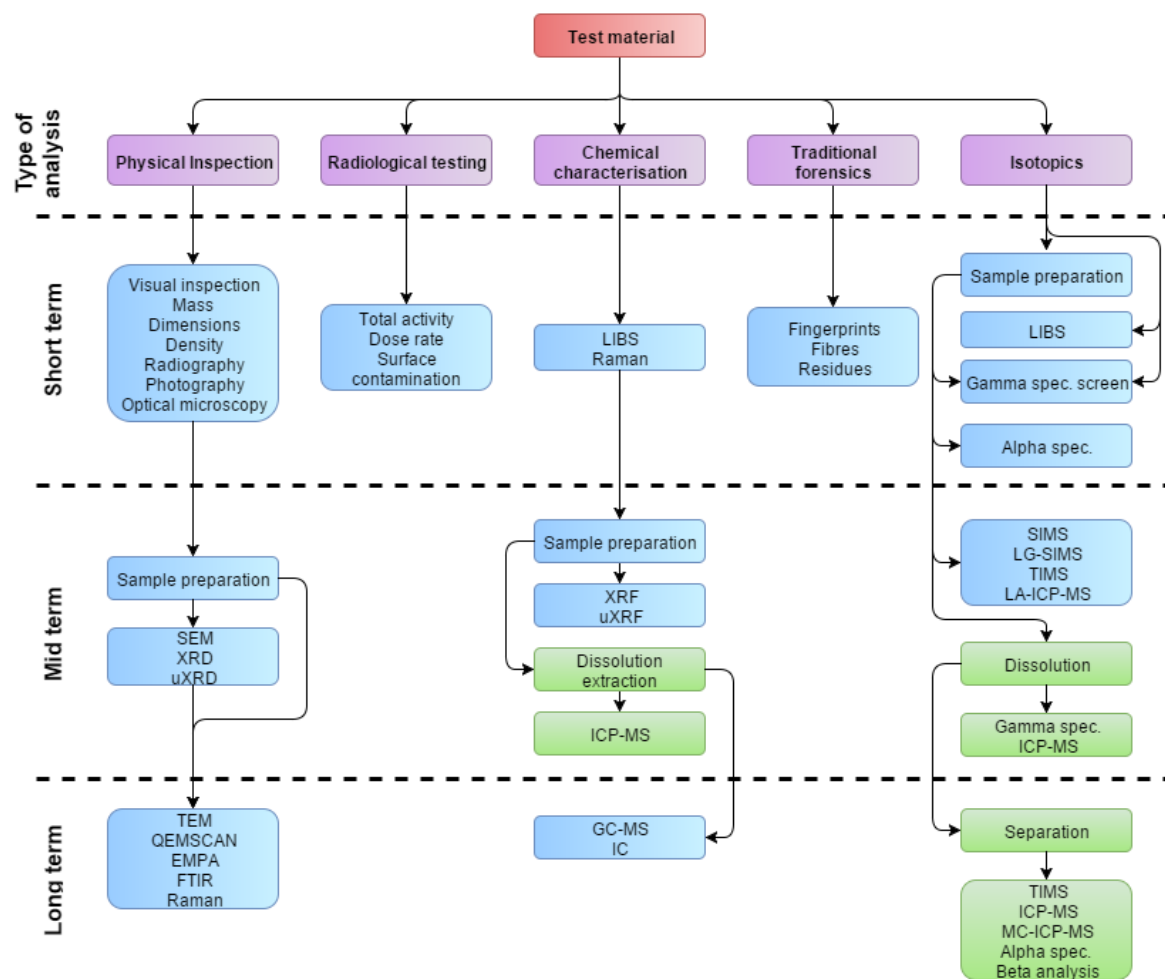


**Figure I-1:** Summary of analytical sequences and methods used when investigating nuclear / radioactive suspect materials in the context of nuclear forensics or emergencies. Techniques shown in green coloured boxes are the focus of this paper. Adapted and further developed from Hutcheon et al 2013 and Mayer et al 2005 [16,17]

## **I-2. Rapid and quantitative methods for digesting solid samples**

Suspicious seized solid samples of security concern usually need to be dissolved after initial non-destructive investigation and prior to more sensitive and targeted analysis (e.g. mass spectrometry). A range of possible dissolution methods exist (Table I-1). The choice will be guided by early compositional information gathered about the suspect material. Some materials will dissolve easily or with persistence in mineral acid media and may benefit from microwave-induced heating in closed PTFE or PFA vessels. Other samples such as silicates, oxides, phosphates and sulphates in soils, sediment, rocks and minerals can be resistant to acid digestion procedures and will succumb following a fusion approach where 'minerals' are opened-out. Perhaps the most effective and attractive of the fusion methods is borate fusion where most minerals readily dissolve when blended with a flux and heated (Box I-2 and Table I-2).

Borate fusion, using lithium borates, was first established in the late 1960s [18] as a means of fusing natural and industrial materials for subsequent XRF analysis. Expansion in the use of the procedure accompanied the development of automated wavelength dispersive X-ray fluorescence spectrometry (WDXRF) and contributed to a general advance in major and trace element geochemistry (e.g. through analysis of numerous samples collected from the International Ocean Drilling Project). It was quickly recognised that most geological rocks and minerals could be readily dissolved in lithium borate fluxes, using either platinum or graphite crucibles. The resulting homogeneous glasses could be measured directly for 50 or more elements by WDXRF analysis. With the advent of inductively coupled plasma spectrometry (ICP-OES and ICPMS), lithium borate fusions were also used to dissolve samples and the melts were poured directly into dilute acid or water to rapidly fragment the quenched glass. Fragmentation enhanced the speed of subsequent acid dissolution and allowed measurement using ICP instruments. Another approach was to apply laser ablation directly to the borate glass disk to acquire chemical information, even down to low trace element concentrations [19]

**Table I-1: Sample digestion methods available for suspect materials.**

Digestion method	Problems / comments	Silicates	Oxides	Sulphates	Carbonates	Borates	Phosphates	Metals *	References
Borate fusion +/- acid digestion	Flexible method with no problems. Effectively digests all materials and is ideal for many elemental and isotopic analysis purposes. High purity lithium borate fluxes used to ensure low analytical blanks. Sample size can vary from 0.1-10 g. Sample:flux ratios from 1:1 upward. Pt-Au crucibles used which are easily cleaned. Typical fusion temperature < 1000-1200 °C.. Possible volatility issues with: Hg, Pb Po & Tl.	X	X	X	X			X	[20]
Flux free fusion +/- acid digestion	Small sample volumes treatable. Conducted in inert Ar atmosphere. Typical fusion temperature > 1300 °C. May require addition of SiO <sub>2</sub> and MgO if silicate poor to help glass formation. Possible volatility issues with Hg, Pb & Tl.	X	X	X	X			X	[21]
HCl, HNO <sub>3</sub>	Microwave digestion, heating in PTFE or PFA pressure vessels may be effective. Full recovery of analytes potentially low. Oxidation of sample may be required to prevent volatilisation. Difficult to achieve full dissolution. Possible volatility issues with: As, Ge, Po, S, Sb, Se, Tc.				X	X		X	[22]
HF / HClO <sub>4</sub> Acid mix	Only small sample masses readily treatable. HF needs to be removed prior to analysis. Insoluble fluoride precipitates in large sample volumes. Perchlorates potentially explosive. Frequently requires the use of HCl and/or HNO <sub>3</sub> . Possible volatility issues with: As, B, Ge, Po, Sb, Tc.	X	X		X	X	X	X	[23]
HF / H <sub>2</sub> SO <sub>4</sub> Acid mix	Small sample volumes treatable. HF needs to be removed prior to analysis. Many evaporation stages.							X	[22]
Alkali fluoride with pyrosulfate	Hazardous as HF produced; requires treatment with pyrosulfate to remove fluorides. Will attack Pt hardware.	X			X				[24]
NaCO <sub>3</sub> fusion	Opens out mineral lattices but requires lengthy treatment. Dissolution of Pt hardware possible. Elevated Pb or Fe(II) will alloy with Pt hardware. Possible volatility issues with: As, Hg, Po, Tc, Tl, Se.	X			X	X		X	[25]
NaOH fusion	Opens out mineral lattices but requires lengthy post fusion treatment. Dissolution of Pt hardware possible.	X			X			X	[26]
Na <sub>2</sub> O <sub>2</sub> fusion or sinter with acid digestion	Attack of Pt hardware possible. Typical fusion temperature of 250-500 °C. Small sample volumes treatable. Time intensive procedure to dissolve the alkaline fusion cake. Possible volatility issues with Au & Ru.	X						X	[27]

### **BOX I-2: Borate fusion**

**Tools:** Pt-Au crucibles are most frequently used and although initially expensive they are very long-lived and can be used to process several hundred samples before requiring refurbishment or re-manufacture. Graphite crucibles are less costly and can be used effectively for 20 or more fusions.

**Heating:** Electrical furnace or gas burner systems (e.g. propane-oxygen) are used to heat fusion mixtures to approximately 1000 C.

**Borates:** For reasons of chemical purity lithium metaborate and lithium tetraborate are most commonly used. Originally developed for the XRF market these are now also widely applied to ICP-OES or ICP-M.

**Sample: flux:** Mixtures used can vary from 1:2 upward and generally produce a homogeneous melt/glass.

**Effectiveness:** Borate fusions will dissolve virtually any sample within 5-10 minutes. Otherwise intractable minor or accessory minerals are readily rendered soluble following a borate fusion. The majority of chemical elements are retained during the fusion procedure except some volatile elements. The melt can be cast onto a Pt-Au plate to produce a homogeneous glass or it can be cast into water or dilute acid and dissolved within 1-2 hours using stirring or ultrasonic disaggregation.

Manufacturer of fusion device	Models	Heating method and no. of samples processed per batch		Acid digestion capability
		Gas	Electric	
Claisse Canada	LeNeo, TheOx Eagon 2,M4	1-6	1-6	Yes
Breitlander Germany	Autofluxer 2 Autofluxer 4	2 4	na	Yes
Equilab	<b>Fi</b> induction heating <b>F2</b> induction heating	na	1-2	Yes
Fluxana Germany	Vulcan (XRF/ICP/AES)	1-6	1-6	Yes
Herzog Germany	HAG-M-HF Induction heating	na	1	No
Initiative Scientific Australia	Beadmaster-4 QP PF	na	1-4 2, 4, 6, 12 5, 10, 15	Yes
Spex Katanax Canada	K1 K2 X-600	na	1 1- 6 1-6	Yes
XRF Scientific Australia	Phoenix II xrFuse-2 xrFuse-6	1-6	1-6	Yes

**na – not available as an option.**

Given the beneficial characteristics of borate fusion (speed, safety and ability to dissolve a broad range of materials) and its established use in the geochemical field, it is surprising that it was not applied in radioanalytical chemistry until the work by Croudace and co-workers in 1996 [20]. A likely reason is that most radioanalytical practitioners were chemists who traditionally used classical solution methods (acids, bases) or alkali carbonate or fluoride fluxes to digest samples, both of which were non-ideal. The first reported routine application of borate fusion in radioanalytical sample preparation related to a 1996 research project that demanded high precision and rapid isotopic analysis of U and Pu. The ability to digest, chemically purify and measure 800 soil and QC samples by mass spectrometry within a 3-month period is a testament to the effectiveness of borate fusion. This was a complex and high public profile investigation of an alleged nuclear weapon incident (Feb 1958) at the former USAF airbase at Greenham Common near Newbury in the UK. It was alleged that the ground had become contaminated and a broad ranging soil sampling program was established to assess the veracity of the claims. Prior to this work, radioanalytical specialists would traditionally have used one or more sample digestion approaches to extract U and Pu (and other elements with radioactive species) from soils. The traditional methods were slow and often potentially hazardous using hydrofluoric acid attacks or fusions with alkali fluorides, carbonates and peroxides. The 1996 study demonstrated the impressive benefits of using borate fusion in the rapid digestion of solid materials. Subsequently the lithium tetraborate method has been routinely used by the originators in routine environmental radioactivity and nuclear forensic investigations [28–34].

### **I-3. Overcoming matrix attenuation in gamma spectrometric measurements**

Upon discovery or seizure of illicitly trafficked nuclear materials, the unknown specimen should be measured via gamma spectrometry within 24-hours to gain a rapid but preliminary understanding of the radiological composition and concentration. The measurement of low energy gamma photons (40-200 keV) in potentially heterogeneous sample matrices containing high-density particles, such as uranium ore concentrate (UOC or yellowcake), can result in under or overestimated activity concentrations. This is because of photon self-attenuation and the inability to correctly adjust photon detection efficiencies based on sample mean density as a result of the heterogeneous sample matrix. For U-ore and UOC, dense U-bearing minerals of variable grain size are supported within a lighter bulk matrix comprising trace minerals and/or chemical residues (analogous to a nugget effect) [33]. The extent of photon attenuation observed in reference materials is proportional to the grain size and concentration of the dense U phases. With high grain size and concentration, the probability of a transmitting photon undergoing attenuation within such a grain is increased. Other experimental [35–38] and theoretical [39–41] approaches have successfully been applied to overcome or correct for photon attenuation but they are not applicable to nuclear forensic investigations and highly heterogeneous matrices due to impracticalities, assumptions or time consuming requirements.

Lithium tetraborate flux was used to rapidly and efficiently dissolve and digest a set of complex and heterogeneous compounds resulting in an aqueous sample with a predictable and consistent geometry / density identical to aqueous calibration standards [33]. This procedure removes the requirement for attenuation correction factors deduced from direct transmission style experiments and no proxy radionuclides are used. Additionally, no prior knowledge about the chemical, physical and radiological composition of the sample is required. To demonstrate the importance of this technique, three certified reference materials (CRMs) for U, CUP-1 (0.128 wt% U), BL-5 (7.09 wt% U) and CUP-2 (75.42 wt% U) were characterised in their as supplied form (direct measurement) and after lithium borate fusion (fused measurement) using HPGe well-type gamma spectrometers (Figure I-2). The total sample used was 0.5 g and was found to be adequate for the measurement of low U concentration samples such as ores. Where UOC or high radioactivity samples are suspected, lower sample mass could be used but the associated uncertainty would increase. The entire procedure is extremely rapid as the preparation requires approximately 20 h and the measurement time is 1 h.

Direct measurement of the low-grade U-ore reference material CUP-1 gives  $^{210}\text{Pb}$  and  $^{234}\text{Th}$  activity concentration of  $78 \pm 10\%$  and  $94 \pm 10\%$  respectively of its certified value. The higher energy  $^{235}\text{U}$  and  $^{226}\text{Ra}$  measured activity concentrations agree with certified values within uncertainty. In the fused form, measured  $^{210}\text{Pb}$  and  $^{234}\text{Th}$  are  $95 \pm 10\%$  and  $98 \pm 8\%$  respectively of the certified value. For the UOC analogue CUP-2, the directly measured  $^{234}\text{Th}$  activity concentration is  $7 \pm 1\%$  of the certified activity concentration whereas after fusion, this value is  $100 \pm 2\%$  of the certified value. Additionally, directly measured  $^{234\text{m}}\text{Pa}$  (1001 keV) in CUP-2 was  $91 \pm 5\%$  of the certified value indicating that even high-energy gamma photons are being measurably attenuated.

Gamma spectrometry is used in nuclear forensic analysis as offers a non-destructive capability thereby preserving the recovered sample for other testing. Although the borate fusion procedure is a destructive technique, the sample mass required is very small resulting in the majority of the sample being preserved for future analyses and requirements. Additionally, the resulting fused sample can be used for mass spectrometric / radiochemical measurements without the requirement of further sub-sampling and digestion thus increasing the speed in which other analytical techniques can be implemented as part of the nuclear forensics characterisation.

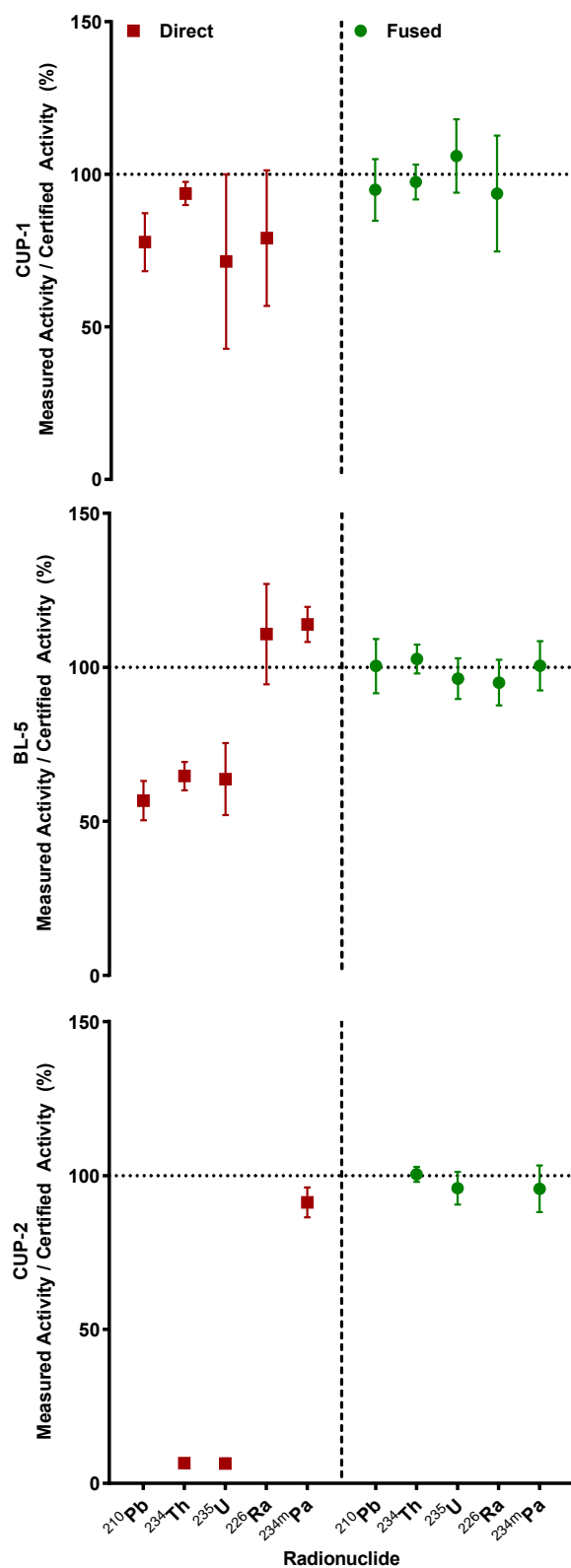


**Figure I-2:** Activity concentrations for natural uranium radionuclides of direct and fused reference materials using certified activities. Missing data are due to activity concentrations being below LOD. Uncertainty =  $2\sigma$ . Adapted from Reading et al. 2015 [33].

#### **I-4. Rapid radionuclide screening including identification and quantification**

Following an actual or suspected assault on a water supply, rapid identification and quantification of contaminants is critical to assessing the risk to the public and remediation actions required. The EU Framework 7 project – Secureau [7] considered CBRN assaults on drinking water supplies. As part of this programme, our group was tasked with the development of rapid techniques for the identification and quantification of radionuclide contaminants. Such a screening technique must be capable of detecting alpha and beta emitting radionuclides and must be sensitive to low energy beta emitters. Most techniques used for routine analysis of radionuclides in drinking waters either are incapable of detecting alpha, high energy beta and low energy beta emitting radionuclides or do not provide spectrometric information necessary for radionuclide identification. Liquid scintillation analysis (LSA) was identified as the only radiometric technique capable of fulfilling this role. The technique exhibits detection efficiencies approaching 100% for alpha and high energy beta emitting radionuclides and good efficiencies even for low energy beta emitters such as  $^3\text{H}$  (18.6 keV) and  $^{14}\text{C}$  (156 keV). Alpha and beta emissions can be distinguished if required using pulse shape analysis techniques. In addition liquid scintillation analysis provides spectrometric information that is critical for radionuclide identification.

Radionuclide identification by LSA is complicated by the effect of quenching on peak position. Theoretically, the maximum energy of emission ( $E_{\text{max}}$ ) is diagnostic of the nuclide present. However, quenching effectively shifts the beta spectrum to lower energies, with the degree of quench being dependent on the sample composition. To overcome this, a multiple quench correction approach was developed to permit radionuclide identification irrespective of quench conditions [8]. Two quench parameters, the internal quench parameter (which is dependent on emission energy and quench level) and the external quench parameter (which is dependent on quench level only), were measured along with the sample activity. The quench parameters were combined to provide a factor that is related only to emission energy and is independent of quench. This factor was then used to determine the decay energy of the emission and hence the identity of the radionuclide present. Once the decay energy is known, the measured sample count rates can be corrected for detection efficiency to provide activity estimates. An additional factor, termed the peak shape factor was developed to measure the asymmetry of the peak and to distinguish between alpha and beta emitting radionuclides as well as providing an indication of the presence of multiple radionuclides (Figure I-3). Internal quench parameters ( $\text{SQPI}(x)$ ) are determined from the sample spectrum and are quoted in terms of the spectrum channel number below which a defined percentage area ( $x$ ) of the spectrum lies. The peak shape factor (PSF) is the ratio of the SQPI values calculated for 95% of the spectrum and 50% of the spectrum ( $\text{PSF} = \text{SQPI}(95)/\text{SQPI}(50)$ ). Deconvolving of alpha and beta emitting radionuclides can be achieved using other approaches but this requires specific signal processing capability that is not available on all commercial liquid scintillation counters and which is also dependent on quench.

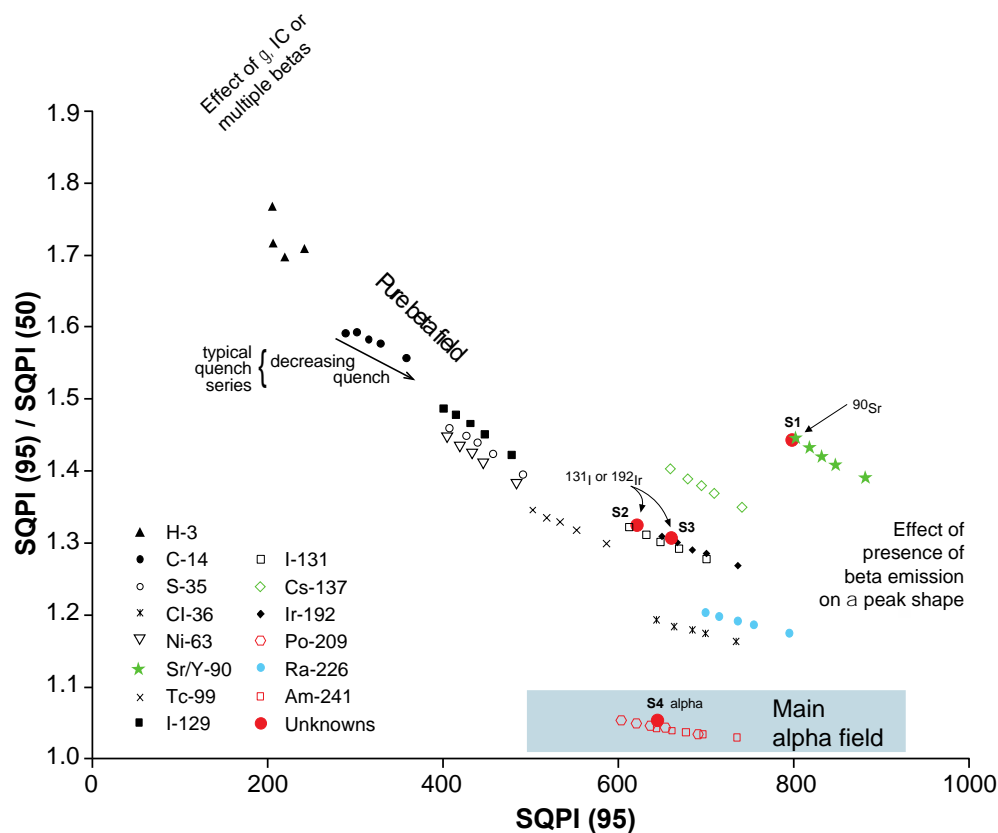


**Figure I-3:** Identification of radionuclides using a peak shape factor (SQPI(95)/SQPI(50)). S1 – S4 represents test samples spiked with an unknown radionuclide that are superimposed on standards data. The radionuclide present in each sample was identified by its position on the plot along with data from the combined internal / external quench ratio. Reproduced with permission from Warwick et al, 2013 [8], Copyright 2013, American Chemical Society.

The novel approach was demonstrated to be effective at identifying and quantifying radionuclides in a range of drinking waters with [Ca+Mg] ranging from 0 - 230 mg L<sup>-1</sup>. The approach is rapid, providing data within 60 minutes of sample receipt and is capable of quantifying alpha and beta emitting radionuclides down to at least 10% of the emergency drinking water action levels. The approach was also demonstrated as effective for the screening of radionuclide contamination in Fe-rich (up to 64 wt % Fe), Mn-rich (5.7 wt % Mn and 42 wt % Fe) and CO<sub>3</sub><sup>2-</sup>-rich (35 wt % Ca) pipeline scales. Both developments relate to advances in data processing rather than instrumental development and can therefore be implemented using existing, commercially-available hardware.

## H-5. Analyte separation techniques

Chemical separation of the analyte from the bulk matrix and potential interferences is critical to alpha spectrometric and beta radionuclide analysis as well as for mass spectrometric determination of radionuclides. Traditionally, such separations have been achieved using solvent extraction, precipitation or ion-exchange based techniques. Extraction chromatographic materials potentially offer more specific separation whilst retaining the benefits associated with chromatographic separation. Development of novel extraction chromatographic materials has permitted targeted separation of the analyte, simplifying separation schemes and reducing analysis times. A range of extractants including simple complexants, ion-selective macrocyclic complexants (e.g. crown ethers, cryptands, calixarenes), chelating agents and liquid ion exchangers have been used. In general, materials are based on an extractant / solvent coated onto an inert support although covalent bonding of the extractant to the support has also been reported. Commercially-available resins have been developed for the targeted purification of Ni, Sr, Sn, Pb, Tc, lanthanides and actinides and have been utilised in safeguards / nuclear forensics applications [42–49]. Higginson et al (2015) [50] reported the development and characterisation of a soft N-donor ligand extractant for the separation of  $^{241}\text{Am}$  from matrix elements including rare earth elements, specifically for nuclear forensics applications. Our group has developed and characterised extraction chromatographic materials based on ketones (DIBK) for the isolation of  $^{55}\text{Fe}$  [51], amines for the separation of  $^{99}\text{Tc}$  [52] and calixarene-based materials for the isolation of  $^{135}\text{Cs}$  prior to ICPMS measurement [53]. In all cases high specificity for the target analyte was demonstrated. For  $^{135}\text{Cs}$ , the calixarene (Bob-CalixC6) was used to effectively separate  $^{135}\text{Cs}$  from the isobaric interference  $^{135}\text{Ba}$  (6.59% natural abundance), achieving separation factors > 2500. Caesium was eluted from the column in 0.05M  $\text{HNO}_3$ . This acid strength can be aspirated directly into an ICPMS, avoiding the need for further evaporation of the sample prior to ICPMS, reducing analysis times and eliminating the potential for contamination. Direct assay of the analyte adsorbed onto an extractant has been applied for the measurement of rare earth elements in U ore concentrates by LA-ICPMS [54]. Combining the extraction chromatographic functionality with scintillant detection into a single solid-phase material offers further simplification of the analytical scheme, reduction in analysis times and potential reduction in waste generation.

## I-6. Mass spectrometric developments for rapid screening of radionuclides

Measurement of a number of radionuclides by radiometric techniques is extremely challenging and labour-intensive, and in some cases may not be possible. The advances in mass spectrometric techniques (particularly ICPMS) has increased the number of nuclides detectable and in many cases the sensitivities achievable, expanding measurement capabilities in the field of nuclear forensics. Initially, ICPMS focussed on detection of single longer lived radionuclides where the low specific activities favoured an atom-counting

technique e.g.  $^{238}\text{U}$ ,  $^{234}\text{Th}$ ,  $^{99}\text{Tc}$ , and  $^{237}\text{Np}$ . As the technique has advanced, the capabilities have expanded to include the detection of long lived, low abundance radionuclides including  $^{93}\text{Zr}$ ,  $^{135}\text{Cs}$  and  $^{59}\text{Ni}$ ; quantification of shorter-lived radionuclides such as  $^{90}\text{Sr}$ , significantly reducing the analytical time for such analyses [55]; and measurement of isotopic ratios e.g.  $^{135}\text{Cs}/^{137}\text{Cs}$  [56,58],  $^{239}\text{Pu}/^{240}\text{Pu}$  [58]  $^{236}\text{U}/^{238}\text{U}$  [59], and  $^{127}\text{I}/^{129}\text{I}$  [60,61]. This has significant implications in the field of nuclear forensics, enabling the user to determine the source of nuclear contamination.

ICPMS offers a significantly reduced measurement time and higher sample throughput compared to alpha and beta counting techniques for longer-lived radionuclides, with a count time of several minutes per sample. Following sample digestion, ICPMS can be used as a rapid screening technique to determine the bulk sample composition and identify radionuclides of interest. Following chemical separation, multiple radionuclides can be determined within a single sample run. A major consideration is the extent of interference removal required, primarily the elimination of isobaric, polyatomic and tailing interferences. The instrumental setup will influence the extent of chemical separation required prior to sample introduction, and the sensitivity and detection limits achievable (Table I-2). The flexibility of sample introduction has led to significant advances in radionuclide measurement capabilities by ICPMS. A number of variables must be considered including the sample uptake rate, instrumental sensitivity, hydride and oxide formation rate, and the efficiency of sample washout to avoid cross-contamination.

Quadrupole instruments without a collision or reaction cell have limited ability to remove interferences, and are reliant on chemical separation and/or sample introduction-based separation to remove interferences. An example of a recent instrumental development in quadrupole ICPMS is the Agilent 7900 with an Ultra High Matrix Introduction (UHMI) system that allows direct analysis of sample with up to 25 % TDS, potentially reducing the sample preparation time required prior to analysis. Alternatively, the Agilent 8800 Triple Quad ICPMS/MS (ICP-QQQ) consists of a quadrupole positioned either side of a collision-reaction cell (termed the octopole reaction system, ORS), which leads to greater control over the ions entering the cell compared to previous generation reaction cell instruments, and improves the abundance sensitivity to a theoretical value of 10<sup>-14</sup>. This setup has been proven to be advantageous to measurement of several isotopic ratios, including  $^{135}\text{Cs}/^{137}\text{Cs}$  [56],  $^{129}\text{I}/^{127}\text{I}$  [61], and  $^{236}\text{U}/^{238}\text{U}$  [59].

**Table I-2: Summary of key features of ICPMS and alternative mass spectrometric techniques**

<b>Instrument stage</b>	<b>Strengths</b>	<b>Potential problems</b>
<b>ICP-MS sample introduction</b>		
Solution nebulisation	<ul style="list-style-type: none"> <li>• Straightforward and potential for low sample uptake rates</li> </ul>	<ul style="list-style-type: none"> <li>• Higher oxide and hydride formation rates, and lower introduction efficiencies compared to other techniques</li> </ul>
Desolvating sample introduction	<ul style="list-style-type: none"> <li>• Reduced hydride and oxide formation</li> <li>• High introduction efficiency</li> </ul>	<ul style="list-style-type: none"> <li>• Long washout times</li> <li>• High cost compared to solution nebulisation</li> </ul>
Laser ablation	<ul style="list-style-type: none"> <li>• Low sample uptake</li> <li>• No sample preparation prior to introduction</li> <li>• Low oxide and hydride formation compared to solution nebulisation</li> </ul>	<ul style="list-style-type: none"> <li>• Lower sensitivity than solution nebulisation</li> <li>• Heterogeneous sample leads to inaccurate measurement</li> </ul>
Cold plasma	<ul style="list-style-type: none"> <li>• Rapid compared to offline chemical separation</li> </ul>	<ul style="list-style-type: none"> <li>• Increased vulnerability to matrix effects, necessitating chemical separation prior to measurement</li> </ul>
Glow discharge Capillary electrophoresis Electro thermal vaporisation	<ul style="list-style-type: none"> <li>• High sample introduction efficiency</li> <li>• Reduced sample preparation</li> </ul>	<ul style="list-style-type: none"> <li>• Prior separation required for complex sample matrices</li> </ul>
<b>ICP-MS instrument design</b>		
<b>Quadrupole</b>	<ul style="list-style-type: none"> <li>• Robust</li> <li>• Straightforward preparation</li> </ul>	<ul style="list-style-type: none"> <li>• Lack of instrument-based separation</li> <li>• Inferior instrument detection limit</li> </ul>
<b>Collision cell</b> (Thermo iCap-Q)	<ul style="list-style-type: none"> <li>• Polyatomic interference removal</li> </ul>	<ul style="list-style-type: none"> <li>• No isobaric interference removal</li> </ul>
<b>Dynamic Reaction Cell</b> (Perkin Elmer NexION)	<ul style="list-style-type: none"> <li>• Isobaric interference removal</li> </ul>	<ul style="list-style-type: none"> <li>• Higher LOD than ICP-SFMS</li> <li>• Potential for polyatomic interference formation in the cell</li> </ul>
<b>Triple quadrupole (MS/MS)</b> (Agilent 8800)	<ul style="list-style-type: none"> <li>• Improved cell chemistry control</li> </ul>	<ul style="list-style-type: none"> <li>• Higher LOD than ICP-SFMS</li> <li>• Lower instrumental sensitivity and instrument LOD than ICP-SFMS</li> </ul>
<b>Sector field (single detector)</b> (Thermo Element 2, 2XR) (Nu Attom) (Spectro MS)	<ul style="list-style-type: none"> <li>• High abundance sensitivity</li> <li>• High instrument sensitivity</li> <li>• Low detection limits</li> </ul>	<ul style="list-style-type: none"> <li>• Extensive chemical separation required prior to sample introduction</li> </ul>
<b>Sector field (multi-collector)</b> (Thermo Neptune plus) (Nu Plasma II)	<ul style="list-style-type: none"> <li>• High accuracy isotope ratio measurements</li> </ul>	<ul style="list-style-type: none"> <li>• Extensive chemical separation required prior to sample introduction</li> </ul>
<b>Alternative measurement techniques</b>		
TIMS	<ul style="list-style-type: none"> <li>• Widely applied to radionuclide measurement, particularly precise isotope ratio measurements</li> </ul>	<ul style="list-style-type: none"> <li>• ICP-MS now more widely applied due to its high ionisation efficiency</li> </ul>
RIMS and AMS	<ul style="list-style-type: none"> <li>• High sensitivity</li> </ul>	<ul style="list-style-type: none"> <li>• Longer sample preparation</li> <li>• Time consuming sample preparation</li> <li>• Lack of commercial instrument availability</li> <li>• High instrument cost</li> </ul>

Sector field instruments have limited ability to remove interferences, as even at high resolution the majority of isobaric and polyatomic interferences cannot be resolved. Operating at medium or high resolution reduces the instrument sensitivity, but has been proven to improve the detection limit because of the enhancement in abundance sensitivity and polyatomic interference removal [55,62,63]. Generally, radionuclide measurements by sector field measurements (such as the Thermo Scientific Element 2XR) are performed in low resolution mode and combined with extensive chemical separation and efficient sample introduction to achieve very high sensitivity and detection limits in the fg/g range [32,53,58,64]. Further to this, multi-collector instruments are fitted with multiple detectors, which increases beam usage efficiency compared to single collector instruments, as there is no need to cycle a number of small ion beams through a single detector [65,66]. This enables highly accurate measurement of isotopic ratios ( $\sim 0.001\%$ ) [65,66]. In order to achieve accurate isotopic ratio values, the instrumental mass bias and response of each detector must be monitored, most commonly by measuring a standard of known isotope ratio and determining a mass bias factor, using an element with a similar mass and ionisation efficiency to the nuclide of interest.

Thermal ionisation mass spectrometry (TIMS) is a realistic alternative to ICPMS and has some benefits (high source stability leading to high precision measurements) but also has some negative features (longer filament preparation time, filament burnout). The TIMS technique was well established before the advent of ICPMS but is undoubtedly being progressively replaced by double focussing, sector field plasma-based methods. Accelerator mass spectrometry (AMS) and resonance ionisation mass spectrometry (RIMS) are both highly sensitive techniques that offer superior sensitivity to ICPMS. They have a place in nuclear forensics but exist in fewer highly specialised and expensive facilities. They are likely to be used if readily available or in otherwise exceptional circumstances.

## **I-7. Conclusion**

The ability to investigate radioactivity assaults requires a broad and multi-disciplinary technical capability that includes appropriately skilled personnel, a range of instrumental and analytical approaches and laboratory infrastructure (mobile and fixed). International co-operation is also a key requirement to ensure the spread of good practice and to share know-how given a limited pool of talent. Building greater resilience within the nuclear forensics and radioanalytical sector is largely stimulated within the existing national laboratories. However, as is shown in this review, other organisations like universities with specialisms in radioanalytical science, geochemistry, photonics and mass spectrometry can also play a beneficial role. As demonstrated, such centres of excellence frequently contribute innovative analytical solutions and skilled scientists that are fit for the nuclear forensics community.

## Acknowledgements

The lead authors are grateful to the EU for funding the SecurEau Project (FP7/2007-2011) grant agreement No. 217976) which led to some of the information contained in this review. They also acknowledge AWE Plc and the UK Nuclear Decommissioning Authority for funding the PhD research projects of DGR and BCR respectively that contributed to some of the information contained herein.

## H-8. References

- [1] IAEA, IAEA Incident and Trafficking Database ( ITDB ), Vienna, Austria, 2015.  
<http://www-ns.iaea.org/downloads/security/itdb-fact-sheet.pdf>.
- [2] IAEA, Illicit Nuclear Trafficking: Collective Experience and the Way Forward, IAEA, Edinburgh, UK, 2008.
- [3] D. Butler, V. Ghirda, AP INVESTIGATION: Nuclear black market seeks IS extremists, Assoc. Press. (2015).  
<http://bigstory.ap.org/article/9f77a17c001f4cf3baeb28990b0d92eb/ap-investigation-nuclear-smugglers-sought-terrorist-buyers>.
- [4] M. Nichols, Iraq tells U.N. that “terrorist groups” seized nuclear materials, Reuters Online. (2014). <http://www.reuters.com/article/us-iraq-security-nuclear-idUSKBN0FE2KT20140709>.
- [5] IAEA, Nuclear Security Plan 2014-2017, Vienna, 2013.
- [6] K. Moody, I. Hutcheon, P. Grant, Nuclear Forensic Analysis, Taylor & Francis, Boca Raton, FL, 2005.
- [7] SECUREAU, Security and decontamination of drinking water distribution systems following a deliberate contamination, Project 217976, EU, FP7-SECURITY, 2013.
- [8] P.E. Warwick, I.W. Croudace, Identification and quantification of radionuclides in contaminated drinking waters and pipeline deposits, *Anal. Chem.* 85 (2013) 8166.
- [9] M.J. Kristo, S.J. Tumey, The state of nuclear forensics, *Nucl. Instruments Methods Phys. Res. Sect. B Beam Interact. with Mater. Atoms.* 294 (2013) 656–661.
- [10] Z. Varga, A. Nicholl, M. Wallenius, K. Mayer, Development and validation of a methodology for uranium radiochronometry reference material preparation., *Anal. Chim. Acta.* 718 (2012) 25–31.
- [11] F.E. Stanley, A.M. Stalcup, H.B. Spitz, A brief introduction to analytical methods in nuclear forensics, *J. Radioanal. Nucl. Chem.* 295 (2013) 1385–1393.
- [12] M. May, Nuclear Forensics - Role, State of the Art, and Program Needs, AAAS, Washington D.C., 2012.
- [13] M. Wallenius, K. Mayer, Age determination of plutonium material in nuclear forensics by thermal ionisation mass spectrometry., *Fresenius. J. Anal. Chem.* 366 (2000) 234–8. <http://www.ncbi.nlm.nih.gov/pubmed/11225665>.
- [14] K. Mayer, Expand nuclear forensics, *Nature.* 503 (2013) 461–462.

- [15] Committee on Nuclear Forensics; National Research Council, Nuclear Forensics: A Capability at Risk (Abbreviated Version), 2010.
- [16] I.D. Hutcheon, M.J. Kristo, K.B. Knight, Nonproliferation Nuclear Forensics, in: Uranium - Cradle to Grave, Winnipeg, 2013: pp. 377–394.
- [17] K. Mayer, M. Wallenius, I. Ray, Nuclear forensics - a methodology providing clues on the origin of illicitly trafficked nuclear materials., *Analyst*. 130 (2005) 433–41.
- [18] F. Claisse, Accurate XRF Analysis Without Internal Standard, Norelco Report. III. 4 (1957) 3–19, 95–106.
- [19] S.M. Eggins, Laser ablation ICPMS analysis of geological materials prepared as lithium borate glasses, *Geostand. Newsl.* 27 (2003) 147–162.
- [20] I. Croudace, P. Warwick, R. Taylor, S. Dee, Rapid procedure for plutonium and uranium determination in soils using a borate fusion followed by ion-exchange and extraction chromatography, *Anal. Chim. Acta*. 371 (1998) 217–225.
- [21] J.S. Fedorowich, J.P. Richards, J.C. Jain, R. Kerrich, J. Fan, A rapid method for REE and trace-element analysis using laser sampling ICPMS on direct fusion whole-rock glasses, *Chem. Geol.* 106 (1993) 229–249.
- [22] R. Bock, A Handbook of Decomposition Methods in Analytical Chemistry, International Textbook Company Limited, London, 1979.
- [23] B. Parsa, A Sequential radiochemical procedure for isotopic analysis of uranium and thorium in soil, *J. Radioanal. Nucl. Chem.* 157 (1992) 65–73.
- [24] C.W. Sill, K.W. Puphal, F.D. Hindman, Simultaneous determination of alpha-emitting nuclides of radium through californium in soil, *Anal. Chem.* 46 (1974) 1725–1737.
- [25] S. Fisher, R. Kunin, Use of Ion Exchange Resins for Determination of Uranium in Ores and Solutions, *Anal. Chem.* 29 (1957) 400–402.
- [26] U.S. Environmental Protection Agency, Rapid Method for Sodium Hydroxide / Sodium Peroxide Fusion of Radioisotope Thermoelectric Generator Materials in Water and Air Filter Matrices Prior to Plutonium Analyses for Environmental Remediation Following Radiological Incidents, 2014.
- [27] C. Galindo, L. Mougin, A. Nourreddine, An improved radiochemical separation of uranium and thorium in environmental samples involving peroxide fusion., *Appl. Radiat. Isot.* 65 (2007) 9–16.
- [28] R.N. Taylor, I.W. Croudace, P.E. Warwick, S.J. Dee, Precise and rapid determination of  $^{238}\text{U}$ ,  $^{235}\text{U}$  and uranium concentration in soil samples using thermal ionisation mass spectrometry, *Chem. Geol.* (1998).
- [29] I.W. Croudace, P.E. Warwick, R.N. Taylor, A.B. Cundy, Investigation of an alleged nuclear incident at Greenham Common Airbase using TI-mass spectrometric measurements of uranium isotopes, *Environ. Sci. Technol.* 34 (2000) 4496–4503.

- [30] I.W. Croudace, T. Warneke, P.E. Warwick, R.N. Taylor, J.A. Milton, High precision Pu isotope ratio measurements using MC-ICPMS, in: P.E. Warwick (Ed.), *Environ. Radiochem. Anal. II, Spec. Publ. 291*, Royal Society of Chemistry, 2003.
- [31] I.W. Croudace, P.E. Warwick, R.C. Greenwood, A novel approach for the rapid decomposition of Actinide resin and its application to measurement of uranium and plutonium in natural waters., *Anal. Chim. Acta.* 577 (2006) 111–8.
- [32] B.C. Russell, I.W. Croudace, P.E. Warwick, J.A. Milton, Determination of Precise  $^{135}\text{Cs}/^{137}\text{Cs}$  Ratio in Environmental Samples Using Sector Field Inductively Coupled Plasma Mass Spectrometry, *Anal. Chem.* (2014).
- [33] D.G. Reading, I.W. Croudace, P.E. Warwick, R. Britton, A Rapid Dissolution Procedure to Aid Initial Nuclear Forensics Investigations of Chemically Refractory Compounds and Particles Prior to Gamma Spectrometry, *Anal. Chim. Acta.* 900 (2015) 1–9.
- [34] D.G. Reading, I.W. Croudace, P.E. Warwick, K.A. Cigliana, Applying multivariate statistics to discriminate uranium ore concentrate geolocations using (radio)chemical data in support of nuclear forensic investigations, *J. Environ. Radioact.* (2016).
- [35] N.H. Cutshall, I.L. Larsen, C.R. Olsen, Direct Analysis of  $^{210}\text{Pb}$  in Sediment Samples: Self-Absorption Corrections, *Nucl. Instruments Methods.* (1983) 309–312.
- [36] E.G. San Miguel, J.P. Perez-Moreno, J.P. Bolivar, R. Garcia-Tenorio, J.E. Martin,  $^{210}\text{Pb}$  determination by gamma spectrometry in voluminal samples ( cylindrical geometry ), *Nucl. Instruments Methods Phys. Res. Sect. A Accel. Spectrometers, Detect. Assoc. Equip.* 493 (2002) 111–120.
- [37] C.A. McMahon, M.F. Fegan, J. Wong, S.C. Long, T.P. Ryan, P.A. Colgan, Determination of self-absorption corrections for gamma analysis of environmental samples: comparing gamma-absorption curves and spiked matrix-matched samples., *Appl. Radiat. Isot.* 60 (2004) 571–7.
- [38] M. Długosz-Lisiecka, H. Bem, Fast procedure for self-absorption correction for low  $\gamma$  energy radionuclide  $^{210}\text{Pb}$  determination in solid environmental samples, *J. Radioanal. Nucl. Chem.* 298 (2013) 495–499.
- [39] O. Sima, C. Dovlete, Matrix Effects in the Activity Measurement of Environmental Samples Implementation of Specific Corrections in a Gamma-ray Spectrometry Analysis Program, *Appl. Radiat. Isot.* 48 (1997) 59–69.
- [40] M. Jurado Vargas, A. Fernández Timón, N. Cornejo Díaz, D. Perez Sánchez, Monte Carlo simulation of the self-absorption corrections for natural samples in gamma-ray spectrometry., *Appl. Radiat. Isot.* 57 (2002) 893–8.  
<http://www.ncbi.nlm.nih.gov/pubmed/12406634>.
- [41] T. Pilleyre, S. Sanzelle, D. Miallier, J. Faïn, F. Courtine, Theoretical and experimental estimation of self-attenuation corrections in determination of  $^{210}\text{Pb}$  by  $\gamma$ -spectrometry with well Ge detector, *Radiat. Meas.* 41 (2006) 323–329.

- [42] Y. Kuno, D. Donohue, P. Doherty, R. Lafolie, M. Kohl, Development and Improvement of Analytical Techniques for U / Pu / Np / Am / Cm At the Safeguards Analytical Laboratory. Report IAEA-SM-367/5/06., Vienna, 2006.
- [43] Z. Varga, M. Wallenius, K. Mayer, E. Keegan, S. Millet, Application of lead and strontium isotope ratio measurements for the origin assessment of uranium ore concentrates., *Anal. Chem.* 81 (2009) 8327–34.
- [44] Z. Varga, R. Katona, Z. Stefánka, M. Wallenius, K. Mayer, A. Nicholl, Determination of rare-earth elements in uranium-bearing materials by inductively coupled plasma mass spectrometry., *Talanta*. 80 (2010) 1744–9.
- [45] J.N.W. Brown, J.D. Robertson, J.D. Brockman, Measurement of U and Pu isotope ratios in hair and nail samples using extraction chromatography and multi-collector inductively coupled plasma mass spectrometry, *Talanta*. 129 (2014) 481–485..
- [46] E. Keegan, M.J. Kristo, M. Colella, M. Robel, R. Williams, R. Lindvall, et al., Nuclear forensic analysis of an unknown uranium ore concentrate sample seized in a criminal investigation in Australia, *Forensic Sci. Int.* 240 (2014) 111–121.
- [47] J. Krajko, Z. Varga, E. Yalcintas, M. Wallenius, K. Mayer, Application of neodymium isotope ratio measurements for the origin assessment of uranium ore concentrates, *Talanta*. 129 (2014) 499–504.
- [48] H. Kurosaki, J.R. Cadieux, S.B. Clark, An alternative method for chronometric determinations involving curium, *J. Anal. At. Spectrom.* 29 (2014) 2419–2423.
- [49] A. Roman, Characterization and Optimization of Extraction Chromatography Resins for Rapid Separations for Safeguard and Nuclear Forensics Purposes, University of Nevada, Las Vegas, USA, 2014.
- [50] M.A. Higginson, O.J. Marsden, P. Thompson, F.R. Livens, S.L. Heath, Separation of americium from complex radioactive mixtures using a BTPPhen extraction chromatography resin, *React. Funct. Polym.* 91-92 (2015) 93–99.
- [51] P.E. Warwick, I.W. Croudace, Isolation and quantification of <sup>55</sup>Fe and <sup>63</sup>Ni in reactor effluents using extraction chromatography and liquid scintillation analysis, *Anal. Chim. Acta*. 567 (2006) 277–285.
- [52] P.E. Warwick, I.W. Croudace, A.G. Howard, Solid-Phase Extraction of Technetium - Amine Complexes onto C 18 Silica and Its Application to the Isolation of <sup>99</sup>Tc, 72 (2000) 3960–3963.
- [53] B.C. Russell, P.E. Warwick, I.W. Croudace, Calixarene-based Extraction Chromatographic Separation of <sup>135</sup>Cs and <sup>137</sup>Cs in Environmental and Waste Samples Prior to Sector Field ICPMS Analysis, *Anal. Chem.* 86 (2014) 11890–11896.
- [54] S. Asai, A. Limbeck, LA-ICPMS of rare earth elements concentrated in cation-exchange resin particles for origin attribution of uranium ore concentrate, *Talanta*. 135 (2015) 41–49.

- [55] A.P. Vonderheide, M. V. Zoriy, A. V. Izmer, C. Pickhardt, J. a. Caruso, P. Ostapczuk, et al., Determination of  $^{90}\text{Sr}$  at ultratrace levels in urine by ICPMS, *J. Anal. At. Spectrom.* 19 (2004) 675.
- [56] J. Zheng, W. Bu, K. Tagami, Y. Shikamori, K. Nakano, S. Uchida, et al., Determination of  $^{135}\text{Cs}$  and  $^{135}\text{Cs}/^{137}\text{Cs}$  atomic ratio in environmental samples by combining ammonium molybdophosphate (AMP)-selective Cs adsorption and ion-exchange chromatographic separation to triple-quadrupole inductively coupled plasma-mass spectrometry, *Anal. Chem.* 86 (2014) 7103–10.
- [57] B.C. Russell, I.W. Croudace, P.E. Warwick, Determination of  $^{135}\text{Cs}$  and  $^{137}\text{Cs}$  in environmental samples: A review, *Anal. Chim. Acta.* 890 (2015) 7–20.
- [58] J. Zheng, Evaluation of a new sector-field ICPMS with Jet Interface for ultra-trace determination of Pu isotopes : from femtogram to attogram levels Evaluation of a new sector-field ICPMS with Jet Interface for ultra-trace determination of Pu isotopes : from femt, (2015).
- [59] M. Tanimizu, N. Sugiyama, E. Ponzevera, G. Bayon, Determination of ultra-low  $^{236}\text{U}/^{238}\text{U}$  isotope ratios by tandem quadrupole ICPMS/MS, *J. Anal. At. Spectrom.* 28 (2013) 1372.
- [60] Ž. Ežerinskis, A. Spolaor, T. Kirchgeorg, G. Cozzi, P. Vallenga, H.A. Kjær, et al., Determination of  $^{129}\text{I}$  in Arctic snow by a novel analytical approach using IC-ICP-SFMS, *J. Anal. At. Spectrom.* 29 (2014) 1827–1834.
- [61] J. Zheng, H. Takata, K. Tagami, T. Aono, K. Fujita, S. Uchida, Rapid determination of total iodine in Japanese coastal seawater using SF-ICPMS, *Microchem. J.* 100 (2012) 42–47.
- [62] M. V. Zoriy, C. Pickhardt, P. Ostapczuk, R. Hille, J.S. Becker, Determination of Pu in urine at ultratrace level by sector field inductively coupled plasma mass spectrometry, *Int. J. Mass Spectrom.* 232 (2004) 217–224.
- [63] G. Sharabi, B. Lazar, Y. Kolodny, N. Teplyakov, L. Halicz, High precision determination of  $^{228}\text{Ra}$  and  $^{228}\text{Ra}/^{226}\text{Ra}$  isotope ratio in natural waters by MC-ICPMS, *Int. J. Mass Spectrom.* 294 (2010) 112–115..
- [64] C.S. Kim, C.K. Kim, K.J. Lee, Simultaneous analysis of  $^{237}\text{Np}$  and Pu isotopes in environmental samples by ICP-SF-MS coupled with automated sequential injection system, *J. Anal. At. Spectrom.* 19 (2004) 743–750.
- [65] R.N. Taylor, T. Warneke, J.A. Milton, I.W. Croudace, P.E. Warwick, R.W. Nesbitt, Multiple ion counting determination of plutonium isotope ratios using multi-collector ICPMS, *J. Anal. At. Spectrom.* 18 (2003) 480–484.
- [66] M.E. Wieser, J.B. Schwieters, The development of multiple collector mass spectrometry for isotope ratio measurements, *Int. J. Mass Spectrom.* 242 (2005) 97–115.



## Appendix J: Publications and Conferences

**Reading, D.G., Croudace, I.W., Warwick, P.E. & Britton, R. (2015)**

A rapid dissolution procedure to aid initial nuclear forensics investigations of chemically refractory compounds and particles prior to gamma spectrometry.

*Analytica Chimica Acta, 900, p1-9 – Featured Article*

**Reading, D.G., Croudace, I.W. & Warwick, P.E. (2015)**

A rapid sample digestion procedure to aid initial nuclear forensics investigations for uranium-bearing ores and concentrates prior to gamma spectrometry.

*Conference Proceedings of the European Safeguards Research and Development Association (ESARDA) 37th Annual Meeting, Manchester UK.*

**Reading, D.G., Croudace, I.W., Warwick, P.E. & Cigliana, K.A. (Accepted Article)**

The accurate characterisation of uranium ore concentrates using high-resolution gamma spectrometry via borate fusion to aid initial nuclear forensic investigations using statistical approaches.

*Journal of Environmental Radioactivity.*

**Croudace, I.W., Warwick, P.E., Reading, D.G. & Russell, B.R. (Accepted Article)**

Analytical challenges for rapid screening of radionuclide contamination in emergency scenarios.

*Trends in Analytical Chemistry. Safety and Security Review.*

**Reading, D.G., Croudace, I.W. & Warwick, P.E. (Due for submission)**

The flux-free preparation of low silica bearing materials using whole-rock iridium strip fusion for trace element determination via laser ablation ICPMS.

*Due for submission to Analytical Chemistry.*

**Reading, D.G., Croudace, I.W. & Warwick, P.E. (In preparation)**

The analysis of rare earth element signatures in uranium ore concentrates as glass beads for laser ablation ICPMS applications in nuclear forensics.

**Reading, D.G., Croudace, I.W., Warwick, P.E. & Taylor, R.N. (In preparation)**

The Uranium Isotopic Composition of Uranium Ore Concentrates Using Double Spike Characterisation to Aid Provenance Determination for a Nuclear Forensics Effort.

**May 2015** European Safeguards Research and Development Association Symposium – 37th Annual Meeting. Manchester, UK.

**Mar 2015** Geochemistry Research in Progress Meeting. Southampton, UK.

**Apr 2014** Co-Ordinating Group on Environmental Radioactivity. Lancaster, UK.

**Sep 2014** RSC Young Researchers Meeting. AWE Aldermaston, UK.

**Apr 2013** Co-Ordinating Group on Environmental Radioactivity. Loughborough, UK.

**Nov 2012** Open meeting with ITU. Karlsruhe, Germany.

**Sep 2012** RSC Radiochemistry Meeting. AWE Aldermaston, UK.

**Apr 2012** Co-Ordinating Group on Environmental Radioactivity. Portsmouth, UK.

## List of References

- Abramowski, T. & Stoyanova, V. (2012). Deep-sea polymetallic nodules: Renewed interest as resources for environmentally sustainable development. In: *12th International Multidisciplinary Scientific GeoConference SGEM 2012*. 2012, pp. 515–521.
- Aggarwal, S.K. (2016). Nuclear forensics : what , why and how ? *Current science*. 110 (5). p.pp. 782–791.
- Agostinelli, S., Allison, J., Amako, K., Apostolakis, J., Araujo, H., Arce, P., Asai, M., Axen, D., Banerjee, S., Barrand, G., Behner, F., Bellagamba, L., Boudreau, J., Broglia, L., Brunengo, A., Burkhardt, H., Chauvie, S., Chuma, J., Chytrcek, R., Cooperman, G., Cosmo, G., Degtyarenko, P., Dell'Acqua, A., Depaola, G., Dietrich, D., Enami, R., Feliciello, A., Ferguson, C., Fesefeldt, H., Folger, G., Foppiano, F., Forti, A., Garelli, S., Giani, S., Giannitrapani, R., Gibin, D., Gómez Cadenas, J.J., González, I., Gracia Abril, G., Greeniaus, G., Greiner, W., Grichine, V., Grossheim, A., Guatelli, S., Gumplinger, P., Hamatsu, R., Hashimoto, K., Hasui, H., Heikkinen, A., Howard, A., Ivanchenko, V., Johnson, A., Jones, F.W., Kallenbach, J., Kanaya, N., Kawabata, M., Kawabata, Y., Kawaguti, M., Kelner, S., Kent, P., Kimura, A., Kodama, T., Kokoulin, R., Kossov, M., Kurashige, H., Lamanna, E., Lampén, T., Lara, V., Lefebvre, V., Lei, F., Liendl, M., Lockman, W., Longo, F., Magni, S., Maire, M., Medernach, E., Minamimoto, K., Mora de Freitas, P., Morita, Y., Murakami, K., Nagamatu, M., Nartallo, R., Nieminen, P., Nishimura, T., Ohtsubo, K., Okamura, M., O'Neale, S., Oohata, Y., Paech, K., Perl, J., Pfeiffer, A., Pia, M.G., Ranjard, F., Rybin, A., Sadilov, S., Di Salvo, E., Santin, G., Sasaki, T., Savvas, N., Sawada, Y., Scherer, S., Sei, S., Sirotenko, V., Smith, D., Starkov, N., Stoecker, H., Sulkimo, J., Takahata, M., Tanaka, S., Tcherniaev, E., Safai Tehrani, E., Tropeano, M., Truscott, P., Uno, H., Urban, L., Urban, P., Verderi, M., Walkden, A., Wander, W., Weber, H., Wellisch, J.P., Wenaus, T., Williams, D.C., Wright, D., Yamada, T., Yoshida, H. & Zschesche, D. (2003). Geant4—a simulation toolkit. *Nuclear Instruments and Methods in Physics Research Section A: Accelerators, Spectrometers, Detectors and Associated Equipment*. [Online]. 506 (3). p.pp. 250–303. Available from: <http://linkinghub.elsevier.com/retrieve/pii/S0168900203013688>. [Accessed: 22 January 2014].

## References

- Albrethson, H., McGinley, F.E. (1982). *Summary History of Domestic Uranium Procurement Under U.S. Atomic Energy Commission Contracts Final Report*.
- Alfredson, P.G. (1980). Australian experience in the production of yellow cake and uranium fluorides. In: *Production of yellow cake and uranium fluorides*. Vienna: IAEA, pp. 149–178.
- Allison, G. (2008). Nuclear Deterance in the Age of Nuclear Terrorism. *Technology Review - MIT*. p.pp. 68–74.
- Anders, E. & Grevesse, N. (1989). Abundances of the elements: Meteoritic and solar. *Geochimica et Cosmochimica Acta*. 53 (1). p.pp. 197–214.
- Badaut, V., Wallenius, M. & Mayer, K. (2009). Anion analysis in uranium ore concentrates by ion chromatography. *Journal of Radioanalytical and Nuclear Chemistry*. [Online]. 280 (1). p.pp. 57–61. Available from: <http://www.springerlink.com/index/10.1007/s10967-008-7404-3>. [Accessed: 29 October 2012].
- Benoit, G. & Hemond, H.F. (1988). Improved methods for the measurement of  $^{210}\text{Po}$ ,  $^{210}\text{Pb}$ , and  $^{226}\text{Ra}$ . *Limnology and Oceanography*. 33. p.pp. 1618–1622.
- Berglund, M. & Wieser, M.E. (2011). Isotopic compositions of the elements 2009 (IUPAC Technical Report). *Pure and Applied Chemistry*. 83 (2). p.pp. 397–410.
- Blake, H. (2011). Wikileaks: uranium bricks and radioactive trains among nuclear terror scares. *The Telegraph*. [Online]. 2 February. Available from: <http://www.telegraph.co.uk/news/worldnews/wikileaks/8296982/WikiLeaks-uranium-bricks-and-radioactive-trains-among-nuclear-terror-scares.html>.
- Bock, R. (1979). *A Handbook of Decomposition Methods in Analytical Chemistry*. London: International Textbook Company Limited.
- Bolivar, J.P., García-Tenorio, R. & García-León, M. (1996). A method for the determination of counting efficiencies in  $\gamma$ -spectrometric measurements with HPGe detectors. *Nuclear Instruments and Methods in Physics Research Section A: Accelerators, Spectrometers, Detectors and Associated Equipment*. [Online]. 382 (3). p.pp. 495–502. Available from:

## References

- <http://linkinghub.elsevier.com/retrieve/pii/S0168900296007905>.
- Boulyga, S.F., Testa, C., Desideri, D. & Becker, J.S. (2001). Optimisation and application of ICP-MS and alpha-spectrometry for determination of isotopic ratios of depleted uranium and plutonium in samples collected in Kosovo. *J. Anal. At. Spectrom.* [Online]. 16 (11). p.pp. 1283–1289. Available from: <http://pubs.rsc.org/en/content/articlehtml/2001/ja/b103178n>.
- Brennecka, G.A., Borg, L.E., Hutcheon, I.D., Sharp, M.A. & Anbar, A.D. (2010). Natural variations in uranium isotope ratios of uranium ore concentrates: Understanding the  $^{238}\text{U}/^{235}\text{U}$  fractionation mechanism. *Earth and Planetary Science Letters*. [Online]. 291 (1-4). p.pp. 228–233. Available from: <http://linkinghub.elsevier.com/retrieve/pii/S0012821X10000579>. [Accessed: 19 November 2012].
- Brokenshire, J. (2014). *How Nuclear Forensics Can Help Us To Tackle Nuclear Terrorism*. [Online]. 2014. The Home Office, UK. Available from: <https://www.gov.uk/government/speeches/how-nuclear-forensics-can-help-us-to-tackle-nuclear-terrorism>. [Accessed: 4 April 2016].
- Brown, R.W. (1977). A sample fusion technique for whole rock analysis with the electron microprobe. *Geochimica et Cosmochimica Acta*. 41 (3). p.pp. 435–438.
- Brown, T.A. (2006). *Confirmatory factor analysis for applied research*. 2nd Ed. New York, USA: Guilford Press.
- Brush, G.J. & Penfield, S.L. (1898). *Manual of Determinative Mineralogy with an Introduction on Blowpipe Analysis*. 15th Ed. New York: John Wiley & Sons.
- Castor, S.B. & Hedrick, J.B. (2001). *Rare Earth Elements*. p.pp. 769–792.
- Claisse, F. (1957). Accurate XRF Analysis Without Internal Standard. *Norelco Reporter III*. 4. p.pp. 3–19, 95–106.
- Claisse, F. & Samson, C. (1962). Heterogeneity effects in X-ray analysis. *Advanced X-ray Analysis*. 5. p.pp. 335–354.
- Croudace, I., Warwick, P., Reading, D. & Russell, B. (n.d.). Recent contributions to the

## References

- rapid screening of radionuclides in emergency responses and nuclear forensics (accepted article). *Trends in Analytical Chemistry*.
- Croudace, I., Warwick, P., Taylor, R. & Dee, S. (1998). Rapid procedure for plutonium and uranium determination in soils using a borate fusion followed by ion-exchange and extraction chromatography. *Analytica Chimica Acta*. [Online]. 371 (2-3). p.pp. 217–225. Available from: <http://linkinghub.elsevier.com/retrieve/pii/S0003267098003535>.
- Croudace, I.W. & Marshall, S. (1991). Determination of rare earth elements and yttrium in nine geochemical reference samples using a novel group separation procedure involving mixed-acid elution ion-exchange chromatography. *Geostandard Newsletter*. 15 (1). p.pp. 139–144.
- Croudace, I.W., Warwick, P.E. & Taylor, R.N. (1997). Borate fusion followed by ion-exchange/extraction chromatography for the rapid determination of plutonium and uranium in environmental materials. In: *Proceedings of NPL Conference 'Rapid Radioanalytical Methods for Emergencies'*. 1997, Teddington, UK.
- Currie, L.A. (1968). Limits for Qualitative Detection and Quantitative Determination. Application to Radiochemistry. *Analytical Chemistry*. 40 (3). p.pp. 586–593.
- Cutshall, N.H., Larsen, I.L. & Olsen, C.R. (1983). Direct Analysis of  $^{210}\text{Pb}$  in Sediment Samples: Self-Absorption Corrections. *Nuclear Instruments and Methods*. (206). p.pp. 309–312.
- Dahlkamp, F. (1993). *Uranium Ore Deposits*. Berlin, Germany: Springer.
- Dalton, J.L. & Bowman, W.S. (1988). *Report 88-3E CUP-2 : A Certified Uranium Ore Concentrate*.
- Dalton, J.L. & Bowman, W.S. (1986). *Report CCRMP 86-2E - CUP-1: A Certified Uranium Reference Ore*.
- DDEP (2016). *Decay Data Evaluation Project - Table of Radionuclides*. [Online]. 2016. Available from: [www.nucleide.org/ddep\\_wg/ddepdata.htm](http://www.nucleide.org/ddep_wg/ddepdata.htm). [Accessed: 4 April 2016].

## References

- Dennis, F., Morgan, G. & Henderson, F. (2007). Dounreay hot particles: the story so far. *Journal of radiological protection : official journal of the Society for Radiological Protection*. [Online]. 27 (3A). p.pp. A3–11. Available from: <http://www.ncbi.nlm.nih.gov/pubmed/17768316>. [Accessed: 11 July 2014].
- Długosz-Lisiecka, M. & Bem, H. (2013). Fast procedure for self-absorption correction for low  $\gamma$  energy radionuclide  $^{210}\text{Pb}$  determination in solid environmental samples. *Journal of Radioanalytical and Nuclear Chemistry*. [Online]. 298 (1). p.pp. 495–499. Available from: <http://link.springer.com/10.1007/s10967-012-2404-8>. [Accessed: 5 July 2013].
- Donard, A., Pottin, A.-C., Pointurier, F. & Pécheyran, C. (2015). Determination of relative rare earth element distributions in very small quantities of uranium ore concentrates using femtosecond UV laser ablation – SF-ICP-MS coupling. *J. Anal. At. Spectrom.* [Online]. 30 (12). p.pp. 2420–2428. Available from: <http://xlink.rsc.org/?DOI=C5JA00309A>.
- Edwards, C.R. & Oliver, A.J. (2000). Uranium processing: A review of current methods and technology. *The Journal of The Minerals, Metals and Materials Society*. [Online]. 52 (9). p.pp. 12–20. Available from: <http://www.springerlink.com/index/10.1007/s11837-000-0181-2>.
- Eggins, S.M. (2003). Laser ablation ICP-MS analysis of geological materials prepared as lithium borate glasses. *Geostand. Newsl.* 27 (2). p.pp. 147–162.
- Enzweilert, J., Potts, P.J. & Jarvis, K.E. (1995). Determination of Platinum , Palladium , Ruthenium and Iridium in Geological Samples by Isotope Dilution Inductively Coupled Plasma Mass Spectrometry Using a Sodium Peroxide Fusion and Tellurium Coprecipitation. *The Analyst*. 120 (May). p.pp. 1391–1396.
- Fahey, A.J., Ritchie, N.W.M., Newbury, D.E. & Small, J.A. (2010). The use of lead isotopic abundances in trace uranium samples for nuclear forensics analysis. *Journal of Radioanalytical and Nuclear Chemistry*. [Online]. 284 (3). p.pp. 575–581. Available from: <http://www.springerlink.com/index/10.1007/s10967-010-0509-5>. [Accessed: 19 November 2012].
- Faye, G.H., Bowman, W.S. & Sutarno, W.S. (1979). *Report 79-4 Uranium Ore BL-5 - A*

## References

### *Certified Reference Material.*

- Fayek, M. & Kyser, T.K. (1997). Characterization of multiple fluid-flow events and rare-earth-element mobility associated with formation of unconformity-type uranium deposits in the Athabasca Basin, Saskatchewan. *Canadian Mineralogist*. 35 (3). p.pp. 627–658.
- Fedorowich, J.S., Richards, J.P., Jain, J.C., Kerrich, R. & Fan, J. (1993). A rapid method for REE and trace-element analysis using laser sampling ICP-MS on direct fusion whole-rock glasses. *Chemical Geology*. [Online]. 106 (3-4). p.pp. 229–249. Available from: <http://linkinghub.elsevier.com/retrieve/pii/000925419390029I>.
- Fisher, S. & Kunin, R. (1957). Use of Ion Exchange Resins for Determination of Uranium in Ores and Solutions. *Analytical Chemistry*. 29 (3). p.pp. 400–402.
- Flynn, W.W. (1968). The determination of low levels of polonium-210 in environmental materials. *Analytica Chimica Acta*. 43. p.pp. 221–227.
- Frimmel, H.E., Schedel, S. & Brätz, H. (2014). Applied Geochemistry Uraninite chemistry as forensic tool for provenance analysis. *Applied Geochemistry*. [Online]. 48. p.pp. 104–121. Available from: <http://dx.doi.org/10.1016/j.apgeochem.2014.07.013>.
- Fritsche, R. & Dahlkamp, F. (1997). Contribution to characteristics of uranium oxides. In: *Assessment of uranium deposit types and resources- a worldwide perspective*. 1997, Vienna: IAEA and OECD Nuclear Energy Agency, p. 253.
- Galindo, C., Mougin, L. & Nourreddine, A. (2007). An improved radiochemical separation of uranium and thorium in environmental samples involving peroxide fusion. *Applied radiation and isotopes : including data, instrumentation and methods for use in agriculture, industry and medicine*. [Online]. 65 (1). p.pp. 9–16. Available from: <http://www.ncbi.nlm.nih.gov/pubmed/16831555>. [Accessed: 4 February 2015].
- Gilmore, G. & Hemingway, J. (1995). *Practical Gamma-Ray Spectrometry*. 1st Ed. Chichester, UK: John Wiley & Sons.
- Gumann, S., Lahaye, Y. & Brey, G. (2003). Iridium-Strip – Rhyolithe enthüllen ihre Details. *Ber Europ Jb Min*. 15 (72).

## References

- Gupta, C.K. & Singh, H. (2003). *Uranium Resource Processing - Secondary Resources*. Berlin, Germany: Springer.
- Han, S.-H., Varga, Z., Krajc6, J., Wallenius, M., Song, K. & Mayer, K. (2013). Measurement of the sulphur isotope ratio ( $^{34}\text{S}/^{32}\text{S}$ ) in uranium ore concentrates (yellow cakes) for origin assessment. *Journal of Analytical Atomic Spectrometry*. [Online]. 28 (12). p.p. 1919. Available from: <http://xlink.rsc.org/?DOI=c3ja50231g>. [Accessed: 26 November 2013].
- Hanlen, R. (2011). Round Robin 3 Exercise After Action and Lessons Learned Report. PNNL-20079. *Pacific Northwest National Laboratory. U.S. Department of Energy, Richland, WA*.
- Harkins, W.D. (1917). The Evolution of the Elements and the Stability of Complex Atoms: A New Periodic System Which Shows A Relation Between The Abundance Of The Elements And The Structure Of The Nuclei Of Atoms. *Journal of the American Chemical Society*. 39 (5). p.pp. 856–879.
- Hausen, D.M. (1998). Characterizing and classifying uranium yellow cakes: A background. *Jom*. [Online]. 50 (12). p.pp. 45–47. Available from: <http://www.springerlink.com/index/10.1007/s11837-998-0307-5>.
- He, Z., Huang, F., Yu, H., Xiao, Y., Wang, F., Li, Q., Xia, Y. & Zhang, X. (2016). A Flux-Free Fusion Technique for Rapid Determination of Major and Trace Elements in Silicate Rocks by LA-ICP-MS. *Geostandards and Geoanalytical Research*. 40 (1). p.pp. 5–27.
- Hinojosa, J.L., Stirling, C.H., Reid, M.R., Moy, C.M. & Wilson, G.S. (2016). Trace metal cycling and  $^{238}\text{U}/^{235}\text{U}$  in New Zealand's fjords: Implications for reconstructing global paleoredox conditions in organic-rich sediments. *Geochimica et Cosmochimica Acta*. 179. p.pp. 89–109.
- Ho Mer Lin, D., Jones, A.E., Goulermas, J.Y., Turner, P., Varga, Z., Fongaro, L., Fanghanel, T. & Mayer, K. (2015). Raman spectroscopy of uranium compounds and the use of multivariate analysis for visualization and classification. *Forensic Science International*. 251. p.pp. 61–68.
- Hussain, N., Kim, G., Church, T.M. & Carey, W. (1996). A Simplified Technique for Analysis

## References

- of  $^{210}\text{Pb}$  in Sediment Samples. *Applied Radiation and Isotopes*. 47 (4). p.p. 473–477.
- Hutcheon, I.D., Kristo, M.J. & Knight, K.B. (2013). Nonproliferation Nuclear Forensics. In: *Uranium - Cradle to Grave*. Winnipeg, pp. 377–394.
- IAEA (2015a). *IAEA Incident and Trafficking Database (ITDB)*. [Online]. Vienna, Austria. Available from: <http://www-ns.iaea.org/downloads/security/itdb-fact-sheet.pdf>.
- IAEA (2015b). *Implementing Guide: Nuclear Forensics in Support of Investigations*. [Online]. Vienna, Austria. Available from: <http://www-pub.iaea.org/books/IAEABooks/10797/Nuclear-Forensics-in-Support-of-Investigations>.
- IAEA (2014). *Incident and Trafficking Database (ITDB)*.
- IAEA (1980). *Significance of Mineralogy in the Development of Flowsheets for Processing Uranium Ores (Technical Reports Series No. 196)*. Vienna.
- IAEA (1993). *Uranium Extraction Technology (Technical Report Series No. 359)*. Vienna, Austria.
- IAEA (1976). Uranium Ore Processing. In: *Proceedings of an Advisory Group Meeting Washington, DC*. 1976, Vienna.
- IAEA (2009). *World Distribution of Uranium Deposits (UDEPO) with Uranium Deposit Classification 2009 (TECDOC-1629)*. Vienna, Austria.
- Jarvis, K.E. (1989). Determination of rare earth elements in geological samples by inductively coupled plasma mass spectrometry. *Journal of Analytical Atomic Spectrometry*. 4 (7). p.p. 563.
- Jarvis, K.E. (1988). Inductively coupled plasma mass spectrometry: A new technique for the rapid or ultra-trace level determination of the rare-earth elements in geological materials. *Chemical Geology*. [Online]. 68 (1-2). p.p. 31–39. Available from: <http://linkinghub.elsevier.com/retrieve/pii/0009254188900848>.
- Jarvis, K.E., Gray, A.L. & Mccurdy, E. (1989). Avoidance of spectral interference on europium in inductively coupled plasma mass spectrometry by sensitive

## References

- measurement of the doubly charged ion. *Journal of Analytical Atomic Spectrometry*. 4 (December). p.pp. 743–747.
- Jochum, K.P. &ENZWEILER, J. (2013). *Reference Materials in Geochemical and Environmental Research*. 2nd Ed. [Online]. Elsevier Ltd. Available from: <http://dx.doi.org/10.1016/B978-0-08-095975-7.01403-0>.
- Jochum, K.P., NOHL, U., HERWIG, K., LAMMEL, E., STOLL, B. & HOFMANN, A.W. (2005). GeoReM: a new geochemical database for reference materials and isotopic standards. *Geostandards and Geoanalytical Research*. 29 (3). p.pp. 333–338.
- Jolliffe, I. (2014). Principal Component Analysis. In: *Wiley StatsRef: Statistics Reference Online*.
- Jurado Vargas, M., Fernández Timón, A., Cornejo Díaz, N. & Perez Sánchez, D. (2002). Monte Carlo simulation of the self-absorption corrections for natural samples in gamma-ray spectrometry. *Applied Radiation and Isotopes*. [Online]. 57 (6). p.pp. 893–8. Available from: <http://www.ncbi.nlm.nih.gov/pubmed/12406634>.
- Keatley, A.C., Scott, T.B., Davis, S., Jones, C.P. & Turner, P. (2015). An investigation into heterogeneity in a single vein-type uranium ore deposit: Implications for nuclear forensics. *Journal of Environmental Radioactivity*. [Online]. 150. p.pp. 75–85. Available from: <http://dx.doi.org/10.1016/j.jenvrad.2015.06.016>.
- Keegan, E., Kristo, M.J., Colella, M., Robel, M., Williams, R., Lindvall, R., Eppich, G., Roberts, S., Borg, L., Gaffney, A., Plaue, J., Wong, H., Davis, J., Loi, E., Reinhard, M. & Hutcheon, I. (2014). Nuclear forensic analysis of an unknown uranium ore concentrate sample seized in a criminal investigation in Australia. *Forensic Science International*. [Online]. 240. p.pp. 111–121. Available from: <http://dx.doi.org/10.1016/j.forsciint.2014.04.004>.
- Keegan, E., Kristo, M.J., Toole, K., Kips, R. & Young, E. (2016). Nuclear Forensics: Scientific Analysis Supporting Law Enforcement and Nuclear Security Investigations. *Analytical Chemistry*. [Online]. 88. p.pp. 1496–1505. Available from: <http://pubs.acs.org/doi/10.1021/acs.analchem.5b02915>.
- Keegan, E., Richter, S., Kelly, I., Wong, H., Gadd, P., Kuehn, H. & Alonso-Munoz, A. (2008).

## References

- The provenance of Australian uranium ore concentrates by elemental and isotopic analysis. *Applied Geochemistry*. [Online]. 23 (4). p.pp. 765–777. Available from: <http://linkinghub.elsevier.com/retrieve/pii/S0883292707003332>. [Accessed: 29 October 2012].
- Keegan, E., Wallenius, M., Mayer, K., Varga, Z. & Rasmussen, G. (2012). Attribution of uranium ore concentrates using elemental and anionic data. *Applied Geochemistry*. [Online]. 27 (8). p.pp. 1600–1609. Available from: <http://linkinghub.elsevier.com/retrieve/pii/S0883292712001321>. [Accessed: 18 October 2012].
- Kennedy, A.K., Bostick, D.A., Hexel, C.R., Smith, R.R. & Giaquinto, J.M. (2013). Non-volatile organic analysis of uranium ore concentrates. *Journal of Radioanalytical and Nuclear Chemistry*. 296 (2). p.pp. 817–821.
- Kitto, M.E. (1991). Determination of photon self-absorption corrections for soil samples. *Applied radiation and isotopes*. 42 (9). p.pp. 835–839.
- Klunder, G.L., Plaue, J.W., Spackman, P.E., Grant, P.M., Lindvall, R.E. & Hutcheon, I.D. (2013). Application of visible/near-infrared reflectance spectroscopy to uranium ore concentrates for nuclear forensic analysis and attribution. *Applied Spectroscopy*. 67 (9). p.pp. 1049–1056.
- Krajčó, J., Varga, Z., Yalcintas, E., Wallenius, M. & Mayer, K. (2014). Application of neodymium isotope ratio measurements for the origin assessment of uranium ore concentrates. *Talanta*. [Online]. 129 (20). p.pp. 499–504. Available from: <http://dx.doi.org/10.1016/j.talanta.2014.06.022>.
- Kristo, M.J. (2012). *Handbook of Radioactivity Analysis*. Third edit. M. F. L. Annunziata (ed.). San Diego: Elsevier.
- Kristo, M.J. & Tumey, S.J. (2013). The state of nuclear forensics. *Nuclear Instruments and Methods in Physics Research Section B: Beam Interactions with Materials and Atoms*. [Online]. 294. p.pp. 656–661. Available from: <http://linkinghub.elsevier.com/retrieve/pii/S0168583X1200554X>. [Accessed: 15 January 2014].

## References

- Kurosawa, M., Shima, K., Ishii, S. & Sasa, K. (2006). Trace Element Analysis of Fused Whole-Rock Glasses by Laser Ablation-ICP-MS and PIXE. *Geostandards and Geoanalytical Research*. [Online]. 30 (1). p.pp. 17–30. Available from: <http://doi.wiley.com/10.1111/j.1751-908X.2006.tb00908.x>.
- L'annunziata, M.F. (2012). *Handbook of radioactivity analysis*. San Diego: Elsevier Science.
- Lach, P., Mercadier, J., Dubessy, J., Boiron, M.C. & Cuney, M. (2013). In situ quantitative measurement of rare earth elements in uranium oxides by laser ablation-inductively coupled plasma-mass spectrometry. *Geostandards and Geoanalytical Research*. 37 (3). p.pp. 277–296.
- Lee, H.M., Hong, G.H., Baskaran, M., Kim, S.H. & Kim, Y.I.L.L. (2014). Evaluation of plating conditions for the recovery of <sup>210</sup>Po on a Ag planchet. *Applied Radiation and Isotopes*. [Online]. 90. p.pp. 170–176. Available from: <http://dx.doi.org/10.1016/j.apradiso.2014.03.025>.
- Lentz, D.R. (1996). U, Mo, and REE mineralization in the late-tectonic granitic pegmatites, southwestern Grenville province, Canada. *Ore Geology Reviews*. 11. p.pp. 197–227.
- Lin, M., Zhao, Y., Zhao, L., Li, L., Wang, F., Zhu, L., Hu, X. & Ning, W. (2015). Tracing origins of uranium ore concentrates (UOCs) by multidimensional statistical analysis of rare-earth impurities. *J. Anal. At. Spectrom.* [Online]. 30 (3). p.pp. 396–402. Available from: <http://xlink.rsc.org/?DOI=C4JA00354C>.
- Lodders, K. (2003). *SOLAR SYSTEM ABUNDANCES AND CONDENSATION TEMPERATURES OF THE ELEMENTS Katharina Lodders*. p.pp. 1220–1247.
- May, M., Davis, J. & Jeanloz, R. (2006). Preparing for the worst. *Nature*. 443. p.pp. 907–908.
- Mayer, K., Wallenius, M. & Fanghänel, T. (2007). Nuclear forensic science - From cradle to maturity. *Journal of Alloys and Compounds*. [Online]. 444-445. p.pp. 50–56. Available from: <http://linkinghub.elsevier.com/retrieve/pii/S0925838807003659>. [Accessed: 5 October 2012].
- Mayer, K., Wallenius, M. & Ray, I. (2005). Nuclear forensics - a methodology providing

## References

- clues on the origin of illicitly trafficked nuclear materials. *The Analyst*. [Online]. 130 (4). p.pp. 433–41. Available from: <http://www.ncbi.nlm.nih.gov/pubmed/15776151>. [Accessed: 5 October 2012].
- Mayer, K., Wallenius, M. & Varga, Z. (2013). Nuclear forensic science: Correlating measurable material parameters to the history of nuclear material. *Chemical Reviews*. 113. p.pp. 884–900.
- Mckay, A.D. & Miezeitis, Y. (2001). *Australia's Uranium Resources, Geology and Development of Deposits*.
- McMahon, C.A., Fegan, M.F., Wong, J., Long, S.C., Ryan, T.P. & Colgan, P.A. (2004). Determination of self-absorption corrections for gamma analysis of environmental samples: comparing gamma-absorption curves and spiked matrix-matched samples. *Applied Radiation and Isotopes*. [Online]. 60 (2-4). p.pp. 571–7. Available from: <http://www.ncbi.nlm.nih.gov/pubmed/14987706>. [Accessed: 5 July 2013].
- Mercadier, J., Cuney, M., Lach, P., Boiron, M.-C., Bonhoure, J., Richard, A., Leisen, M. & Kister, P. (2011). Origin of uranium deposits revealed by their rare earth element signature. *Terra Nova*. [Online]. 23 (4). p.pp. 264–269. Available from: <http://doi.wiley.com/10.1111/j.1365-3121.2011.01008.x>. [Accessed: 19 November 2012].
- Moody, K., Hutcheon, I. & Grant, P. (2005). *Nuclear Forensic Analysis*. Boca Raton, FL: Taylor & Francis.
- Mutua, J.-M. (2015). Uranium yellowcake trafficking incidents in Africa. *African Security Review*. [Online]. 24 (2). p.pp. 162–189. Available from: <http://www.tandfonline.com/doi/full/10.1080/10246029.2015.1034737>.
- Nehring, F., Jacob, D.E., Barth, M.G. & Foley, S.F. (2007). Laser-ablation ICP-MS analysis of siliceous rock glasses fused on an iridium strip heater using MgO dilution. *Microchimica Acta*. [Online]. 160 (1-2). p.pp. 153–163. Available from: <http://link.springer.com/10.1007/s00604-007-0819-7>. [Accessed: 15 July 2014].
- Nguyen, C.T. & Zsigrai, J. (2006). Gamma-spectrometric uranium age-dating using intrinsic efficiency calibration. *Nuclear Instruments and Methods in Physics Research, Section*

## References

- B: Beam Interactions with Materials and Atoms*. 243. p.pp. 187–192.
- Nguyen, C.T., Zsigrai, J. & Lakosi, L. (2009). Characterization of uranium-bearing material by passive non-destructive gamma spectrometry. In: *7th Conference on Nuclear and particle Physics*. 2009, Sharm El-Sheikh, Egypt, pp. 413–424.
- Nicholls, I.A. (1974). A Direct Fusion Method of Preparing Silicate Rock Glasses for Energy-Dispersive Electron Microprobe Analysis. *Chemical Geology*. 14. p.pp. 151–157.
- NTI (2012a). *2011 Illicit Trafficking Incidents*. [Online]. 2012. Nuclear Threat Initiative. Available from:  
[http://www.nti.org/media/pdfs/2011\\_illicit\\_trafficking\\_incidents\\_2.pdf?\\_=1370293383](http://www.nti.org/media/pdfs/2011_illicit_trafficking_incidents_2.pdf?_=1370293383). [Accessed: 27 April 2016].
- NTI (2012b). *Namibia: 170 kg of natural uranium stolen from Rossing Mine*. [Online]. 2012. Available from: <http://www.nti.org/analysis/articles/namibia-170-kg-natural-uranium-stolen-rossing-mine/>. [Accessed: 27 April 2016].
- Oddo, G. (1914). Die Molekularstruktur der radioaktiven Atome. *Zeitschrift für anorganische Chemie*. 87 (1). p.pp. 253–268.
- Oliver, N.H.S., Pearson, P.J., Holcombe, R.J. & Ord, A. (1999). Mary Kathleen metamorphic-hydrothermal uranium - rare-earth element deposit: ore genesis and numerical model of coupled deformation and fluid flow. *Australian Journal of Earth Science*. 46. p.pp. 467–484.
- Organisation for Economic Co-Operation and Development, IAEA & Nuclear Energy Agency (2014). *Uranium 2014: Resources, Production and Demand*. NEA no. 7209.
- Parsa, B. (1992). A Sequential radiochemical procedure for isotopic analysis of uranium and thorium in soil. *Journal of Radioanalytical and Nuclear Chemistry*. 157 (1). p.pp. 65–73.
- Pearce, N.J.G., Perkins, W.T., Westgate, J.A., Gorton, M.P., Jackson, S.E., Neal, C.R. & Chenery, S.P. (1997). A compilation of new and published major and trace element data for NIST SRM 610 and NIST SRM 612 glass reference materials. *Geostandards Newsletter*. 21 (1). p.pp. 115–144.

## References

- Pilleyre, T., Sanzelle, S., Miallier, D., Faïn, J. & Courtine, F. (2006). Theoretical and experimental estimation of self-attenuation corrections in determination of  $^{210}\text{Pb}$  by  $\alpha$ -spectrometry with well Ge detector. *Radiation Measurements*. [Online]. 41 (3). p.pp. 323–329. Available from: <http://linkinghub.elsevier.com/retrieve/pii/S1350448704002586>. [Accessed: 5 July 2013].
- Pirrie, D., Butcher, A.R., Power, M.R., Gottlieb, P. & Miller, G.L. (2004). Rapid quantitative mineral and phase analysis using automated scanning electron microscopy (QemSCAN); potential applications in forensic geoscience. *Geological Society, London, Special Publications*. [Online]. 232 (1). p.pp. 123–136. Available from: <http://sp.lyellcollection.org/cgi/doi/10.1144/GSL.SP.2004.232.01.12>. [Accessed: 5 October 2012].
- Pirrie, D. & Rollinson, G.K. (2011). Unlocking the applications of automated mineral analysis. *Geology Today*. [Online]. 27 (6). p.pp. 226–235. Available from: <http://doi.wiley.com/10.1111/j.1365-2451.2011.00818.x>.
- Plaue, J.W., Klunder, G.L., Hutcheon, I.D. & Czerwinski, K.R. (2013). Near infrared reflectance spectroscopy as a process signature in uranium oxides. *Journal of Radioanalytical and Nuclear Chemistry*. 296 (1). p.pp. 551–555.
- Prohaska, T., Hann, S., Latkoczy, C. & Stingeder, G. (1999). Determination of rare earth elements U and Th in environmental samples by inductively coupled plasma double focusing sectorfield mass spectrometry (ICP-SMS). *Journal of Analytical Atomic Spectrometry*. 14 (1). p.pp. 1–8.
- Proulx, M. (1997). *The uranium mining industry of the Bancroft Area: An environmental history and heritage assessment*. Trent Univeristy, California, USA.
- Rafter, T.A. (1950). Sodium peroxide decomposition of minerals in platinum vessels. *The Analyst*. [Online]. 75 (894). p.p. 485. Available from: <http://xlink.rsc.org/?DOI=an9507500485>.
- Reading, D.G., Croudace, I.W. & Warwick, P.E. (n.d.). A novel nuclear forensics tool: rapid production of flux-free fusion beads for the rapid analysis of lanthanides in suspect materials by LA-ICPMS (submitted article). *Analytical Chemistry*.

## References

- Reading, D.G., Croudace, I.W., Warwick, P.E. & Britton, R. (2015). A Rapid Dissolution Procedure to Aid Initial Nuclear Forensics Investigations of Chemically Refractory Compounds and Particles Prior to Gamma Spectrometry. *Analytica Chimica Acta*. 900. p.pp. 1–9.
- Reading, D.G., Croudace, I.W., Warwick, P.E. & Cigliana, K.A. (2016). Applying multivariate statistics to discriminate uranium ore concentrate geolocations using (radio)chemical data in support of nuclear forensic investigations. *Journal of Environmental Radioactivity*. 162-163. p.pp. 172–181.
- Reid, J.E., Longerich, H.P., Forsythe, L. & Jenner, G.A. (1999). Determination of Zr and Hf in a Flux-Free Fusion of Whole Rock Samples using Laser Ablation Inductively Coupled Plasma-Mass Spectrometry ( LA-ICP-MS ) with Isotope Dilution Calibration. *Geostandard Newsletter*. 23 (2). p.pp. 149–155.
- Reynolds, H.S., Ram, R., Charalambous, F. a., Antolasic, F., Tardio, J. & Bhargava, S. (2010). Characterisation of a uranium ore using multiple X-ray diffraction based methods. *Minerals Engineering*. [Online]. 23 (9). p.pp. 739–745. Available from: <http://linkinghub.elsevier.com/retrieve/pii/S0892687510001391>. [Accessed: 21 January 2013].
- Richter, S., Alonso, a, De Bolle, W., Wellum, R. & Taylor, P.D.. (1999). Isotopic ‘fingerprints’ for natural uranium ore samples. *International Journal of Mass Spectrometry*. [Online]. 193 (1). p.pp. 9–14. Available from: <http://linkinghub.elsevier.com/retrieve/pii/S1387380699001025>.
- Richter, S., Eykens, R., Kühn, H., Aregbe, Y., Verbruggen, a. & Weyer, S. (2010). New average values for the n(238U)/n(235U) isotope ratios of natural uranium standards. *International Journal of Mass Spectrometry*. [Online]. 295 (1-2). p.pp. 94–97. Available from: <http://linkinghub.elsevier.com/retrieve/pii/S1387380610001879>. [Accessed: 26 November 2012].
- Robel, M., Kristo, M. & Heller, M. (2009). Nuclear forensic inferences using iterative multidimensional statistics. In: *Institute of Nuclear Materials Management 50th Annual Meeting*,. [Online]. 2009, Tuscon, AZ, USA. Available from: <https://e-reports-ext.llnl.gov/pdf/374432.pdf>.

## References

- Robinson, P., Townsend, a T., Zongshou, Y. & Münker, C. (1999). Determination of scandium, yttrium and rare earth elements in rocks by high-resolution inductively coupled plasma-mass spectrometry. *Geostandards Newsletter*. 23 (Potts). p.pp. 31–46.
- Rowson, J. & Nguyen, T. (1987). Case Studies of the Chemical Precipitation Processes at the Cluff Lake Mining Uranium Mill. In: *Proceedings of the International Symposium on Crystallization and Precipitation*. 1987, Toronto, Canada: Pergamon Press.
- Salbu, B., Krekling, T., Oughton, D.H., Kashparov, V.A., Brand, T.L. & Day, J.P. (1994). Hot Particles in Accidental Releases From Chernobyl and Windscale Nuclear Installations. *The Analyst*. 119 (January). p.pp. 125–130.
- San Miguel, E.G., Perez-Moreno, J.P., Bolivar, J.P., Garcia-Tenorio, R. & Martin, J.E. (2002). <sup>210</sup>Pb determination by gamma spectrometry in voluminal samples ( cylindrical geometry ). *Nuclear Instruments and Methods in Physics Research Section A: Accelerators, Spectrometers, Detectors and Associated Equipment*. 493. p.pp. 111–120.
- Sandalls, F.J., Segal, M.G. & Victorova, N. (1993). Hot Particles from Chernobyl : A Review. *Journal of Environmental Radioactivity*. 18 (April 1986). p.pp. 5–22.
- Seim, H.J., Morris, R.J. & Frew, D.W. (1957). Rapid Routine Method for Determination of Uranium in Ores. *Analytical Chemistry*. 29 (3). p.pp. 443–446.
- Sill, C.W., Puphal, K.W. & Hindman, F.D. (1974). Simultaneous determination of alpha-emitting nuclides of radium through californium in soil. *Analytical Chemistry*. [Online]. 46 (12). p.pp. 1725–1737. Available from: <http://pubs.acs.org/doi/abs/10.1021/ac60348a021>.
- Sima, O. & Dovlete, C. (1997). Matrix Effects in the Activity Measurement of Environmental Samples Implementation of Specific Corrections in a Gamma-ray Spectrometry Analysis Program. *Applied Radiation and Isotopes*. 48 (1). p.pp. 59–69.
- Sirven, J.-B., Pailloux, A., M'Baye, Y., Coulon, N., Alpettaz, T. & Gossé, S. (2009). Towards the determination of the geographical origin of yellow cake samples by laser-induced breakdown spectroscopy and chemometrics. *Journal of Analytical Atomic*

## References

- Spectrometry*. [Online]. 24 (4). p.p. 451. Available from:  
<http://xlink.rsc.org/?DOI=b821405k>. [Accessed: 5 October 2012].
- Smith, C.W. & Steger, H.F. (1983). *Radium-226 in Certified Uranium Reference Ores DL-1a, BL-4a, DH-1a and BL-5*.
- Smith, C.W. & Steger, H.F. (1984). *Report 84-11e - Lead-210 in Certified Uranium Reference Ores DL-1a, BL-4a, DH-1a and BL-5*.
- Smith, D.K. & Niemeyer, S. (2004). International Technical Working Group Cooperation to Counter Illicit Nuclear Trafficking. In: *3rd Eurasian Conference on Nuclear Science and its Application*. 2004, Tashkent, Uzbekistan: Lawrence Livermore National Laboratory.
- Smith, L.I. (2002). *A tutorial on Principal Components Analysis*. [Online]. Available from:  
<http://www.mendeley.com/research/computational-genome-analysis-an-introduction-statistics-for-biology-and-health/>.
- Smith, L.L., Crain, J.S., Yaeger, J.S., Horwitz, E.P., Diamond, H. & Chiarizia, R. (1995). Improved Separation Method for Determining Actinides in Soil Samples. *Journal of Radioanalytical and Nuclear Chemistry*. 194 (1). p.p. 151–156.
- Stanley, F.E. (2012). A beginner's guide to uranium chronometry in nuclear forensics and safeguards. *Journal of Analytical Atomic Spectrometry*. [Online]. 27 (11). p.p. 1821. Available from: <http://xlink.rsc.org/?DOI=c2ja30182b>. [Accessed: 26 November 2013].
- Stanley, F.E., Stalcup, A.M. & Spitz, H.B. (2013). A brief introduction to analytical methods in nuclear forensics. *Journal of Radioanalytical and Nuclear Chemistry*. [Online]. 295 (2). p.p. 1385–1393. Available from:  
<http://www.springerlink.com/index/10.1007/s10967-012-1927-3>. [Accessed: 22 October 2012].
- Stewart, J.A., Gutjahr, M., Pearce, F., Swart, P.K. & Foster, G.L. (2015). Boron during meteoric diagenesis and its potential implications for Marinoan snowball Earth  $\delta^{11}\text{B}$ -pH excursions. *Geology*. 43 (7). p.p. 627–630.
- Stirling, C.H., Andersen, M.B., Potter, E.-K. & Halliday, A.N. (2007). Low-temperature

## References

- isotopic fractionation of uranium. *Earth and Planetary Science Letters*. [Online]. 264 (1-2). p.pp. 208–225. Available from:  
<http://linkinghub.elsevier.com/retrieve/pii/S0012821X07006000>. [Accessed: 1 December 2014].
- Stoll, B., Jochum, K.P., Herwig, K., Amini, M., Flanz, M. & Kreuzburg, B. (2007). An Automated Iridium-Strip Heater for LA-ICP-MS Bulk Analysis of Geological Samples. *Geostandards and Geoanalytical Research*. 32 (1). p.pp. 5–26.
- Švedkauskaitė-LeGore, J., Rasmussen, G., Abousahl, S. & Belle, P. (2008). Investigation of the sample characteristics needed for the determination of the origin of uranium-bearing materials. *Journal of Radioanalytical and Nuclear Chemistry*. [Online]. 278 (1). p.pp. 201–209. Available from:  
<http://www.springerlink.com/index/10.1007/s10967-007-7215-y>. [Accessed: 4 February 2013].
- Švedkauskaitė-Le Gore, J. (2008). *Development and validation of a method for origin determination of uranium-bearing material*. Vilnius University.
- Tabachnick, B.G. & Fidell, L.S. (2013). *Using Multivariate Statistics*. 6th Ed. Harlow, UK: Pearson Education Limited.
- Talmadge, C. (2007). Deterring a Nuclear 9/11. *The Washington Quarterly*. [Online]. 30 (2). p.pp. 21–34. Available from:  
<http://www.tandfonline.com/doi/abs/10.1162/wash.2007.30.2.21>. [Accessed: 15 January 2014].
- Taylor, R.N., Croudace, I.W., Warwick, P.E. & Dee, S.J. (1998). Precise and rapid determination of  $^{238}\text{U}$   $^{235}\text{U}$  and uranium concentration in soil samples using thermal ionisation mass spectrometry. *Chemical Geology*.
- Tissot, F.L.H. & Dauphas, N. (2015). Uranium isotopic compositions of the crust and ocean: Age corrections, U budget and global extent of modern anoxia. *Geochimica et Cosmochimica Acta*. 167. p.pp. 113–143.
- U.S. Environmental Protection Agency (2014). *Rapid Method for Sodium Hydroxide / Sodium Peroxide Fusion of Radioisotope Thermoelectric Generator Materials in*

## References

### *Water and Air Filter Matrices Prior to Plutonium Analyses for Environmental Remediation Following Radiological Incidents.*

- Uvarova, Y. a., Kyser, T.K., Geagea, M.L. & Chipley, D. (2014). Variations in the uranium isotopic compositions of uranium ores from different types of uranium deposits. *Geochimica et Cosmochimica Acta*. [Online]. 146. p.pp. 1–17. Available from: <http://linkinghub.elsevier.com/retrieve/pii/S0016703714005924>. [Accessed: 1 December 2014].
- Varga, Z., Katona, R., Stefánka, Z., Wallenius, M., Mayer, K. & Nicholl, A. (2010a). Determination of rare-earth elements in uranium-bearing materials by inductively coupled plasma mass spectrometry. *Talanta*. [Online]. 80 (5). p.pp. 1744–9. Available from: <http://www.ncbi.nlm.nih.gov/pubmed/20152406>. [Accessed: 5 October 2012].
- Varga, Z., Ozturk, B., Meppen, M., Mayer, K., Wallenius, M. & Apostolidis, C. (2011a). Characterization and classification of uranium ore concentrates (yellow cakes) using infrared spectrometry. *Radiochimica Acta*. 99 (12). p.pp. 807–813.
- Varga, Z. & Surányi, G. (2009). Detection of previous neutron irradiation and reprocessing of uranium materials for nuclear forensic purposes. *Applied radiation and isotopes : including data, instrumentation and methods for use in agriculture, industry and medicine*. [Online]. 67 (4). p.pp. 516–22. Available from: <http://www.ncbi.nlm.nih.gov/pubmed/19179085>. [Accessed: 5 October 2012].
- Varga, Z., Wallenius, M. & Mayer, K. (2010b). Origin assessment of uranium ore concentrates based on their rare-earth elemental impurity pattern. *Radiochimica Acta*. [Online]. 98 (12). p.pp. 771–778. Available from: <http://www.oldenbourg-link.com/doi/abs/10.1524/ract.2010.1777>. [Accessed: 15 January 2013].
- Varga, Z., Wallenius, M., Mayer, K. & Hrncsek, E. (2011b). Alternative method for the production date determination of impure uranium ore concentrate samples. *Journal of Radioanalytical and Nuclear Chemistry*. [Online]. 290 (2). p.pp. 485–492. Available from: <http://www.springerlink.com/index/10.1007/s10967-011-1233-5>. [Accessed: 22 October 2012].
- Varga, Z., Wallenius, M., Mayer, K., Keegan, E. & Millet, S. (2009). Application of lead and strontium isotope ratio measurements for the origin assessment of uranium ore

## References

- concentrates. *Analytical chemistry*. [Online]. 81 (20). p.pp. 8327–34. Available from: <http://www.ncbi.nlm.nih.gov/pubmed/19824713>.
- Venturini, L. & Vanin, V.R. (1993). HPGe detector efficiency calibration for extended sources in the 50–1400 keV energy range. *Applied Radiation and Isotopes*. 44 (7). p.pp. 999–1002.
- Wacker, J.F. (2011). ' *Proposed Framework for National Nuclear Forensics Libraries and International Directories, Version 1 Approved by the ITWG Executive Committee, 06 June 2011*. (June).
- Wallenius, M., Mayer, K. & Ray, I. (2006). Nuclear forensic investigations: two case studies. *Forensic science international*. [Online]. 156 (1). p.pp. 55–62. Available from: <http://www.ncbi.nlm.nih.gov/pubmed/16410154>. [Accessed: 19 March 2013].
- Wallenius, M., Morgenstern, a, Apostolidis, C. & Mayer, K. (2002). Determination of the age of highly enriched uranium. *Analytical and bioanalytical chemistry*. [Online]. 374 (3). p.pp. 379–84. Available from: <http://www.ncbi.nlm.nih.gov/pubmed/12373381>. [Accessed: 29 October 2012].
- Wallenius, W., Mayer, K. & Varga, Z. (2014). Procedures and Techniques for Nuclear Forensics Investigations. In: *IAEA-TECDOC-1730: Application of Nuclear Forensics in Combating Illicit Trafficking of Nuclear and Other Radioactive Material*. Vienna: IAEA, pp. 20–24.
- Weyer, S., Anbar, A.D., Gerdes, A., Gordon, G.W., Algeo, T.J. & Boyle, E.A. (2008). Natural fractionation of  $^{238}\text{U}/^{235}\text{U}$ . *Geochimica et Cosmochimica Acta*. 72 (2). p.pp. 345–359.
- Williams, B.R.W. & Gaffney, A.M. (2011). *Th-  $^{234}\text{U}$  model ages of some uranium standard reference materials*. 35. p.pp. 31–35.
- Williams, R.W., Gaffney, A.M. & Kristo, M.J. (2009).  *$^{230}\text{Th}$ - $^{234}\text{U}$  Model-Ages of Some Uranium Standard Reference Materials*.
- Wilson, P.D. (1997). *The Nuclear Fuel Cycle - From Ore to Waste*. Oxford: Oxford University Press.

## References

- World Nuclear Association (2013). *The Global Nuclear Fuel Market: Supply and Demand 2013-2030*. I. Emsley (ed.). World Nuclear University Press.
- World Nuclear Association (2015). *Uranium Markets*. [Online]. 2015. Available from: <http://www.world-nuclear.org/info/Nuclear-Fuel-Cycle/Uranium-Resources/Uranium-Markets/>. [Accessed: 16 March 2015].
- Yu, Z., Norman, M.D. & Robinson, P. (2003). Major and trace element analysis of silicate rocks by XRF and laser ablation ICP-MS using lithium borate fused glasses: Matrix effects, instrument response and results for international reference materials. *Geostandards Newsletter*. 27. p.pp. 67–89.
- Zaitseva, L. & Hand, K. (2003). Nuclear Smuggling Chains: Suppliers, Intermediaries, and End-Users. *American Behavioral Scientist*. [Online]. 46 (6). p.pp. 822–844. Available from: <http://abs.sagepub.com/cgi/doi/10.1177/0002764202239177>. [Accessed: 20 November 2013].
- Zhu, L., Liu, Y., Hu, Z., Hu, Q., Tong, X., Zong, K., Chen, H. & Gao, S. (2013). Simultaneous Determination of Major and Trace Elements in Fused Volcanic Rock Powders Using a Hermetic Vessel Heater and LA-ICP-MS. *Geostandards and Geoanalytical Research*. 37 (2). p.pp. 207–229.